NASA CONTRACTOR REPORT

NASA CR-1226

EVALUATION OF MAGNETIC MATERIALS FOR STATIC INVERTERS AND CONVERTERS

by R. M. Frost, R. E. McVay, and D. M. Pavlovic

Prepared by
WESTINGHOUSE ELECTRIC CORPORATION
Lima, Ohio
for Lewis Research Center

NATIONAL AERONAUTICS AND SPACE ADMINISTRATION • WASHINGTON, D. C. • FEBRUARY 1969

NASA CR-1226

EVALUATION OF MAGNETIC MATERIALS FOR STATIC INVERTERS AND CONVERTERS

By R. M. Frost, R. E. McVay, and D. M. Pavlovic

Prepared under Contract No. NAS 3-2792 by
WESTINGHOUSE ELECTRIC CORPORATION
Lima, Ohio

for Lewis Research Center

NATIONAL AERONAUTICS AND SPACE ADMINISTRATION

For sale by the Clearinghouse for Federal Scientific and Technical Information
Springfield, Virginia 22151 – CFSTI price $3.00

ABSTRACT

Magnetic materials for use in static inverters and converters were tested under dc excitation and under 400 to 3200 Hz square-wave voltage excitation. Materials evaluated included: 4%Mo-79%Ni-17%Fe, 50%Ni-50%Fe, magnetically annealed 49%Co-2%V-49%Fe, singly and doubly grain-oriented silicon steel, the latter both stress-relief annealed and magnetic field annealed. Magnetization curves, hysteresis loops, core loss and apparent power were determined for temperatures from -55° to +250° C; constant current flux reset data were obtained at room ambient. The effects of both vacuum exposure at 250° C and several conventional processing steps on magnetic properties were evaluated.

PREFACE

The work described herein was done at the Aerospace Electrical Division, Westinghouse Electric Corporation, under NASA Contract NAS3-2792. Mr. Francis Gourash, Space Power Systems Division, NASA-Lewis Research Center, was the Project Manager for NASA. The entire program, "Parallel Operation of Static Inverters and Converters and Evaluation of Magnetic Materials," is described in five reports:

"Inverter-Converter Parallel Operation" defines and experimentally verifies the circuit conditions that must exist for operating static inverters and static converters in parallel (NASA CR-1224).

"Inverter-Converter Automatic Paralleling and Protection" defines and experimentally verifies the electrical control and protection circuits necessary for isolating faulted inverters and converters from a parallel system while maintaining continuity of high-quality electric power to load equipment (NASA CR-1225).

"Evaluation of Magnetic Materials for Static Inverters and Converters" defines the magnetic characteristics of improved materials for magnetic components as applied in advanced static inverters or static converters (NASA CR-1226).

"Load Programmers, Static Switches, and Annunciator for Inverters and Converters" assesses the characteristics of static electrical switches for both ac and dc systems, defines the characteristics of a load programmer for maintaining power to the critical system loads, and provides an annunciator function for displaying inverter and/or converter operating conditions (NASA CR-72454).

"Parallel Operation of Static Inverters and Converters and Evaluation of Magnetic Materials" is the summary report (NASA CR-72455).

CONTENTS

EVALUATION OF MAGNETIC MATERIALS FOR STATIC INVERTERS AND CONVERTERS

by R.M. Frost, R.E. McVay, D.M. Pavlovic

SUMMARY

A program was conducted to study materials for use in static inverters and converters. This program included a literature survey of conductor materials, a series of tests on magnetic alloys and the evaluation of one transformer design.

The materials evaluated were square hysteresis loop 4%Mo-79%Ni-17%Fe; grain oriented 50%Ni-50%Fe; magnetic field annealed 49%Co-2%V-49%Fe; doubly grain oriented silicon steel; and singly grain oriented silicon steel.

Tests were conducted at -55° to 250° C to determine dc magnetic properties; ac magnetic properties at 400 to 3200 Hz using square wave excitation; and, at room ambient only, constant current flux reset properties at 400 to 3200 Hz using square wave excitation. Degradation of magnetic properties resulting from normal factory processing and effects of vacuum at 250° C were evaluated. The data obtained from these tests are described and potential uses for the materials are discussed.

Transformers for an inverter were built from singly grain oriented and doubly grain oriented silicon steel and tested. These tests show that inverter efficiency was improved by use of the doubly grain oriented material.

INTRODUCTION

The design of lightweight, highly efficient static inverters and converters has been seriously hampered by the lack of suitable data on the behavior of commonly used materials when excited with square wave power.

The objective of this program was to obtain suitable information and test data to improve the performance of static inverters and converters.

Tests were conducted with square wave excitation to evaluate two thicknesses of available types of core materials, to determine: the CCFR (Constant Current Flux Reset) properties at room temperature at 400 to 3200 Hz; ac (400 to 3200 Hz), and dc magnetic

properties at -55° C, room temperature and 250° C; degradation of magnetic properties resulting from normal factory processing; and effects of high vacuum at 250° C.

The materials evaluated were 49%Co-2%V-49%Fe alloy, magnetic field annealed; doubly grain oriented silicon steel, both with and without magnetic field anneal; singly grain oriented silicon steel from two vendors; square hysteresis loop 4%Mo-79%Ni-17%Fe alloy, from two vendors; and grain oriented 50%Ni-50%Fe alloy from two vendors.

The test results and data should enable a designer using square wave excitation to select suitable materials to minimize losses when operating at various induction levels and frequencies.

The tests made in this program with square wave excitation are unique in that they represent the first comprehensive compilation of data using a square wave form of voltage instead of a sinusoidal wave form of voltage. The formation of a square wave requires the use of the odd harmonic powers 1, 3, 5, 7, 9, 11, etc. The test equipment used in this program was designed to measure through the 15th harmonic to provide the utmost in accuracy.

The square wave tests represented the actual operating conditions of aerospace equipment where dc power must be inverted to ac power and square wave voltages are generated.

Conductors and conductor systems suitable for use in static inverters and converters are described in Appendix A.

Test transformers for inverter application using singly and doubly grain oriented silicon steel are described in Appendix B.

NOMENCLATURE

Symbols Used in Magnetic Testing

B	Normal induction, magnetic induction, or magnetic flux density
B_m	Maximum induction in a hysteresis loop
B_r	Residual induction
B_s	Saturation induction
H	Magnetizing force, magnetic field strength

H_m	Magnetizing force, maximum
H_c	Coercive force
H_{c_s}	Coercivity
$\Delta L/L$	Magnetostriction
P_a	Apparent power
$P_{a(B;f)}$	Apparent power, specific
$P_{a,sq}$	Apparent power, specific, square wave
P_c	Total core loss
$P_{c(B;f)}$	Core loss, specific
$P_{c,sq}$	Core loss, specific, square wave
P_h	Normal hysteresis core loss
P_e	Normal eddy current core loss
SCM	Symmetrically Cyclically Magnetized
μ	Normal permeability
μ_Δ	Incremental permeability
μ_m	Maximum permeability
μ_o	Initial permeability

Definitions of Terms Used in Magnetic Testing

Apparent Power, P_a. - The product (volt-amperes) of the rms exciting current and the applied rms terminal voltage in an electric circuit containing inductive impedance. The components of this impedance due to the winding are linear, while the components due to the magnetic core are nonlinear.

Apparent Power, Specific, $P_{a(B;f)}$. - The value of the apparent power divided by the active mass of the specimen (volt-amperes

per unit mass) taken at a specified maximum value of cyclically varying induction, B, and at a specified frequency, f.

Apparent Power, Specific, Square Wave, $P_{a,sq}$. - The specific apparent power obtained when the cyclically varying induction is nonsinusoidal with time, but follows a square wave form.

Coercive Force, H_c. - The dc magnetizing force at which the magnetic induction is zero when the material is in a symmetrically cyclically magnetized condition.

Coercivity, H_{cs}. · The maximum value of coercive force.

Core Loss (Total), P_c. - The active power (watts) expended in a magnetic circuit in which there is a cyclically alternating induction, normally sinusoidal.

Core Loss, Specific, $P_{c(B;f)}$. - The active power (watts) expended per unit mass of magnetic material in which there is a cyclically varying induction of a specified maximum value, B, at a specified frequency, f.

Core Loss, Specific, Square Wave, $P_{c,sq}$. - The specific core loss obtained when the cyclically varying induction is nonsinusoidal with time, but follows a square wave form.

Eddy Current Loss, Normal, P_e. - That portion of the core loss which is due to induced currents circulating in the magnetic material subject to a symmetrically cyclically magnetized excitation.

Hysteresis Loss, Normal, P_h. - The power expended in a ferromagnetic material, as a result of hysteresis, when the material is subjected to a symmetrically cyclically magnetized excitation.

Induction, Maximum, B_m. - The maximum value of B in a dc hysteresis loop. The tip of this loop has the magnetostatic coordinates H_m, B_m which exist simultaneously.

Induction, Normal, B. - The maximum induction in a magnetic material that is in a symmetrically cyclically magnetized condition.

Induction, Residual, B_r. - The magnetic induction corresponding to zero magnetizing force in a magnetic material that is

in a symmetrically cyclically magnetized condition.

Induction, Saturation, B_s. - The maximum intrinsic induction possible in a material.

Magnetizing Force (Magnetic Field Strength), H. - That magnetic vector quantity at a point in a magnetic field which measures the ability of electric currents or magnetized bodies to produce a magnetic induction at the given point.

Magnetizing Force, Maximum, H_m. - The maximum value of H in a hysteresis loop.

Magnetostriction, $\Delta L/L$. - The change in length per unit length of a body which results from magnetization.

Permeability, Incremental, μ_Δ. - The ratio of a cyclic change in magnetic induction to the corresponding cyclic change in magnetizing force when the mean induction differs from zero.

Permeability, Initial, μ_o. - The limiting value approached by the normal permeability as the applied magnetizing force, H, is reduced to zero.

Permeability, Maximum, μ_m. - The maximum value of normal permeability for a given material.

Permeability, Normal, μ. - The ratio of the normal induction to the corresponding magnetizing force.

Symmetrically Cyclically Magnetized, SCM. - A magnetic material is in a SCM condition when, under the influence of a magnetizing force that varies cyclically between two equal positive and negative limits, its successive hysteresis loops or flux-current loops are both identical and symmetrical with respect to the origin of the axes.

NOTE: Definitions of additional terms may be found in ASTM Designation A340-65 or later revisions.

Symbols Used in CCFR Testing of Toroidal Magnetic Amplifier Cores

AT Same as H_1

B_m Peak induction or peak flux density

$2B_m$	Maximum flux density swing
B_r	Residual induction or residual flux density
$B_m - B_r$	Squareness
$\frac{B_r}{B_m}$	Squareness ratio
ΔB	Delta induction or delta flux density
ΔB_0	Delta induction, fixed
ΔB_1	Delta induction, fixed
ΔB_2	Delta induction, fixed
CCFR	Constant current flux reset
DAT	Same as ΔH
G	Gain
H_m	Peak magnetizing force
H_0	Magnetizing force, dependent
H_1	Magnetizing force, dependent
H_2	Magnetizing force, dependent
ΔH	Incremental magnetizing force
SAT	Same as B_m
T	Same as $\frac{B_r}{B_m}$

Definitions Used in CCFR Testing of Toroidal Magnetic Amplifier Cores

Constant Current Flux Reset, CCFR. - This test employs an excitation current consisting of half-wave sine current pulses

of sufficient and constant magnitude to drive the core flux into positive saturation. A direct-current magnetizing force of adjustable magnitude is applied to the core so as to reset the magnetic flux away from positive saturation during the intervals between pulses of excitation current. The resultant cyclic flux change is measured by means of a sensitive flux voltmeter connected to a separate pickup winding on the core.

The test provides a means for measurement of core magnetic properties under conditions which approximate the operating conditions in several types of self-saturating magnetic amplifier circuits. An understanding of the symbols and definitions is materially aided by reference to the sketch below. It shows the transfer curve for a magnetic core operating in a self-saturating magnetic amplifier circuit and several of the associated pertinent parameters. The individual values of ΔB for a given material, and the corresponding dependent values of H, are different for each material, but are specified for it in terms of its natural magnetic limiting values.

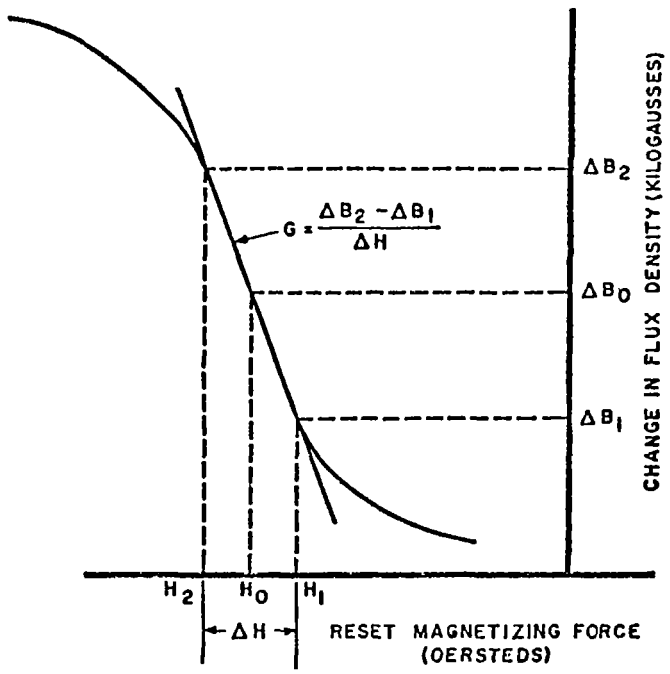

Test points for the constant-current flux reset core test method.

Flux Density Swing, Maximum; $2B_m$. - The maximum flux density swing equal to the absolute total value of positive and negative peak induction or $2B_m$. ($2B_m$ = 2 SAT)

Gain, G. - $G = \frac{\Delta B_2 - \Delta B_1}{\Delta H}$, a measure of loop steepness in terms of incremental permeability.

Induction, Delta (Delta Flux Density); ΔB. - Delta induction is the change in induction (flux density) when a core is in a SCM condition.

Induction, Fixed Delta; ΔB_1, ΔB_0, ΔB_2. -

(1) ΔB_1 - delta induction equal to one third of $2B_m$, maximum flux density swing.

(2) ΔB_0 - delta induction equal to one half of $2B_m$, maximum flux density swing.

(3) ΔB_2 - delta induction equal to two thirds of $2B_m$, maximum flux density swing.

Induction, Residual (Residual Flux Density), B_r. - Residual induction as measured in this test is the magnetic induction at which the magnetizing force is zero while the material is cyclically magnetized with a half-wave sinusoidal magnetizing force of a specified peak magnitude. (This definition differs from the standard definition which requires SCM conditions.)

Induction, Peak (Peak Flux Density), B_m. - Peak induction is the magnetic induction corresponding to the peak applied magnetizing force. The peak induction will usually be slightly less than the true saturation. (B_m = SAT)

Magnetizing Force, Dependent; H_1, H_0, H_2. -

(1) H_1 - The dc reset magnetizing force required to produce a cyclic change of induction ΔB_1 (H_1 = AT).

(2) H_0 - The dc reset magnetizing force required to produce a cyclic change of induction ΔB_0 (H_0 = AT + 1/2 DAT).

(3) H_2 - The dc reset magnetizing force required to produce a cyclic change of induction ΔB_2 (H_2 = AT + DAT).

Magnetizing Force, Incremental; ΔH. - The incremental change in magnetizing force equal to $H_2 - H_1$. (ΔH = DAT)

Magnetizing Force, Peak; H_m. - Peak magnetizing force is the maximum value of applied magnetomotive force per mean length of path of the core.

Squareness; $B_m - B_r$. - The delta B induction change between the peak induction, B_m, and the residual induction, B_r.

Squareness Ratio; $\frac{B_r}{B_m}$. - The ratio of residual induction, B_r, over peak induction, B_m

$$\frac{B_r}{B_m} = 1 - \left(\frac{B_m - B_r}{B_m}\right) = T$$

Definitions of General Magnetic Terms

Anisotropy. - A characteristic of a material in which several properties or any property shows a variation with different directions inside the material.

Anisotropy (Magnetic). - A material having different magnetic properties in different directions within it has magnetic anisotropy. The magnetic energy of a crystal depends on the direction of spontaneous magnetization and is a minimum along the "easy direction." The types of anisotropy usually considered are magnetocrystalline, magnetostrictive, shape, and thermomagnetic.

Atomic Ordering. - A process which transforms the crystal structure of a solid solution from one of random distribution of the atoms of different elements to available lattice sites to one of regular repetitive pattern occupation of the available lattice sites by the atoms of the different elements in the solid solution.

Base Line Property. - Those initial magnetic, physical or mechanical properties that are normally present at room temperature, i.e., saturation induction, thermal expansion, tensile strength.

Critical Temperature. - The temperature at which a change in crystal structure, phase or physical properties occurs under constant pressure conditions.

Curie Temperature. - The temperature above which a ferromagnetic material loses its spontaneous magnetism.

Disordered Structure. - The crystal structure of a solid solution in which the atoms of different elements are randomly distributed with respect to the available lattice sites.

Domain, Ferromagnetic. - A small region, in ferromagnetic materials, where the atomic magnetic moments are all aligned parallel to one another. The material within the domain is magnetized to intrinsic saturation.

Domain Wall (Bloch Wall). - The boundary between adjacent domains of different magnetization vectors in which the electron spins of adjacent atoms in the wall are slightly changed in direction so as to effect, across a large number of atoms, the complete change in magnetization vectors between adjacent domains. The Bloch wall width is determined by the individual ferromagnetic material and is a discrete width. The energy of the wall is variable depending upon the angle between adjacent domains and the crystallographic plane of the wall.

Doubly grain Oriented Silicon Steel. - See later definition and description under Oriented Silicon-Iron.

Field. - A region in space where there is a tendency for anything which can interact with the particular type of field to experience a force.

Field, Magnetic. - A region in space where anything having a magnetic moment experiences a force tending to align its magnetic moment in the direction of the maximum field gradient. A magnetic material experiences a magnetizing force tending to increase the number or size of magnetic domains aligned with the direction of the magnetic field. Inside the material the summation of these individual increases represents the total change in magnetic induction or magnetic flux density.

Isotropic. - Having the same properties in all directions.

Magnetic Field Annealing (MFA). - The thermal treatment of a magnetic material in such a way and with such a temperature cycle that, during the cooling process, when the temperature is below the Curie temperature of the material, a magnetic field is present. This treatment does not change the grain structure but does align the magnetic domains in a direction parallel to the field.

Ordering Temperature. - The temperature at which atomic ordering occurs.

Ordered Structure. - The crystal structure of a solid solution in which the atoms of different elements occupy the available lattice sites in a regular repetitive (ordered) pattern (a super lattice imposed on the normal solute lattice).

Oriented Silicon-Iron. - Ordinary iron or steel consists of an assemblage of tiny grains (crystals) with irregular boundaries, but with a regular body-centered crystal structure with orientation which is constant within a grain, but which varies in a random fashion from grain to grain. Grain oriented silicon-iron consists of grains having the same basic body-centered cubic structure, but as a result of previous cold work and subsequent recrystallization during annealing, the growth of the grains has been induced to produce a structure which is very nearly alike from grain to grain. A principal crystallographic direction of the body centered cube is lined up with the direction of cold rolling of the iron. This type of steel usually contains about 3 to 3-1/4% silicon, since this composition seems to give the best response in the recrystallization process. Singly grain oriented and doubly grain oriented material have been produced with as little as 0.5% silicon and as high as 6.5% silicon.

The sketch below shows the principal crystallographic directions of the silicon-iron cube and their corresponding magnetization curves. The [001] direction corresponds to any edge of the cube. The [011] direction corresponds to the diagonal of a face of the cube and the [111] direction corresponds to the diagonal through the center of the body and through opposite

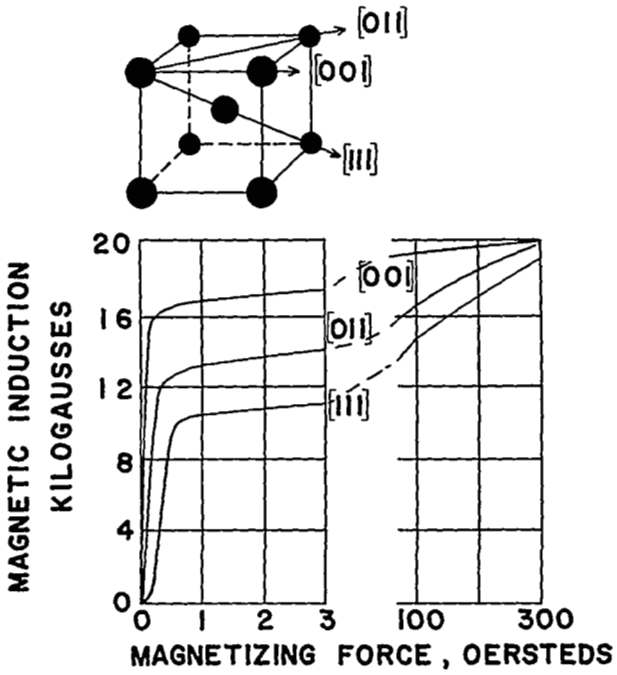

Magnetic Properties of 3.8% Si-Fe Single Crystals

corners of the cube. The corresponding magnetization curves indicate the [001] or cube edge, CE, direction is the easiest direction of magnetization. The [011] direction is intermediate and the [111] direction is the most difficult. From the sketch it is clear that an advantage would result if the cube edge direction could be lined up in the direction in which magnetic flux is to pass in any piece of apparatus.

Below are sketches showing the relationship between the silicon-iron cube and its crystallographic directions and planes with respect to the plane and rolling direction of the steel sheet.

The sketch below shows the (100) plane in the plane of the sheet and cube edges, CE, lined up both parallel and transverse to the direction of rolling. This is known as "cube texture" material, sometimes spoken of as "doubly grain oriented" or DGO. The only other principal direction in the plane of the sheet is the [011] direction or face diagonal, FD, which occurs at 45° to either of the cube edge, CE, directions.

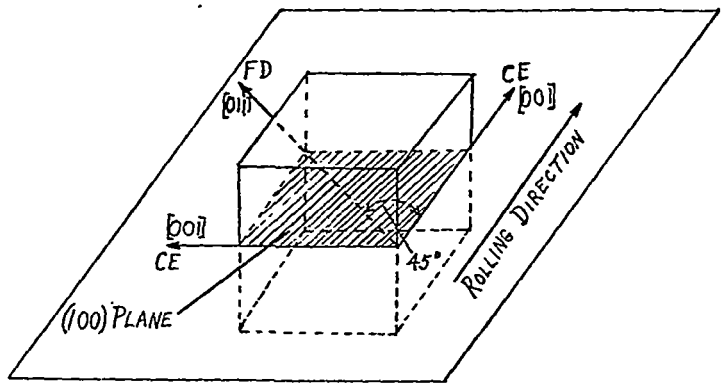

Relation of the Iron Cube to the Plane and Rolling Direction of the Steel Sheet in Cube Texture Orientation

The following sketch shows the cubic crystal with the (110) plane in the plane of the sheet and the cube edge or [001] direction parallel to the rolling direction. Transverse to the rolling direction is the face diagonal, FD, [011] which is the second most difficult direction of magnetization and at an angle of 55° to the rolling direction is the [111] direction or body diagonal, BD. This material is variously known as "Goss texture," or "singly grain oriented" silicon steel, or SGO.

Resistivity, Electrical ρ. - This is defined by the relation $R = \rho \frac{L}{A}$, where R is resistance, L is the length of the specimen and A is its area in the same system of units. For example,

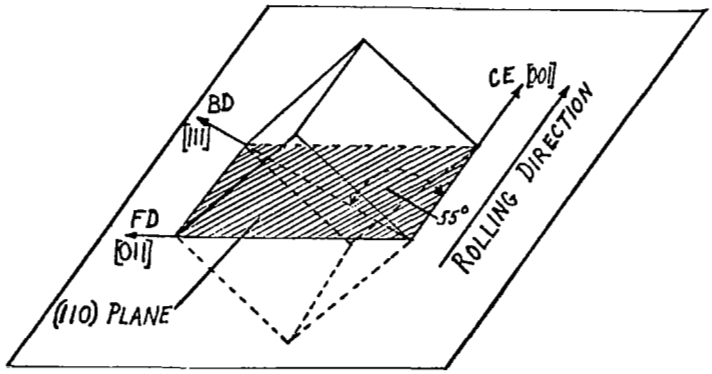

Relation of the Iron Cube to the Plane and Rolling Direction of the Steel Sheet in Cube-on-Edge Orientation

ρ has the units of ohm centimeters.

Resistivity, Interlaminar, R_s. - Interlaminar resistivity is defined by the equation $R = R_s \frac{S}{A}$, where A is the blank area, R is the stack resistance, and S is the number of blanks in the stack. In the metric system R_s has the units of ohms centimeters squared per lamination.

Rowland Ring. - A continuous ring of magnetic material of uniform radial width and cross-sectional area with no joints or welds. The ratio of its mean diameter to its radial width is ten to one or greater.

Singly Grain Oriented Silicon Steel. - See section above on Oriented Silicon-Iron.

Square Hysteresis Loop Material. - This is a term which has developed in the industry referring to a magnetic material having a reasonably rectangular dc hysteresis loop. Such a loop shows very sharp points of inflection or abrupt changes in the slope of the magnetization curve near the approach to saturation and on the demagnetization curve shortly after the point of residual induction has been passed.

Stress Relief Anneal (SRA). - Thermal treatment to reduce residual stresses, followed by a cooling rate which minimizes development of new stresses, leaving the material in a nearly stress-free condition.

Structure Sensitive Properties. - The properties that are structure sensitive in magnetic materials are permeability (μ), coercive force (H_c), and hysteresis loss (P_h). The factors that affect these properties are composition, impurities, strain,

temperature, crystal structure and crystal orientation.

MATERIALS EVALUATED

The magnetic materials for this program were selected on the basis of being those commonly used in static inverter and converter circuits. The magnetic materials evaluated are described below. The physical and mechanical properties are shown in table I.

Square Hysteresis Loop 4%Mo-79%Ni-17%Fe

After a special heat treatment this alloy exhibits square hysteresis loop properties. The molybdenum addition increases the electrical resistivity and magnetic permeability as well as oxidation resistance of this alloy. There is evidence of atomic ordering in this alloy.

This material is characterized by slightly higher coercive force than the alloy would have when annealed to produce maximum permeability rather than maximum rectangularity of the hysteresis loop.

Grain Oriented 50%Ni-50%Fe

This is an alloy of 50%Ni and 50%Fe which develops a strong orientation in the rolling direction after annealing strip, cold reduced 98%. The material has a face-centered cubic structure with the cube edge direction [001] both in the rolling direction and perpendicular to it and the cube face plane (100) in the material plane. The basic orientation is the same as in doubly grai oriented silicon steel except that the alloy has a face-centered cubic structure rather than a body-centered cubic structure.

Magnetic Field Annealed 49%Co-2%V-49%Fe Alloy

This material is magnetically annealed by applying a field of 6 to 10 oersteds during cooling to create rectangularity in the hysteresis loop. The purity of raw materials, alloy preparation, mechanical processing, and annealing are very carefully controlled to keep elements such as sulfur, carbon, nitrogen, and oxygen as low as possible.

The annealing temperature is below the alpha-gamma phase transition and above the ordering region and cooled at a rate of 3° C/min. This optimum cooling rate prevents atomic ordering created by slower cooling rates. The atomic ordering reduces

Table I. - Physical and Mechanical Properties of Magnetic Materials Evaluated

Material	Density (g/cc)	Tensile Strength (psi)		Compressive Strength (psi)		Thermal Expansion (in/in/°C)	Chemical Composition	Crystalline Structure & Orientation	Electrical Resistivity ρ (microhm-cm)	Curie Points (°C)
		Longitudinal	Transverse	Longitudinal	Transverse					
Square Hysteresis Loop 4%Mo-79%Ni-17%Fe	8.74					12.9×10^{-6} -70° to 200°	79% Ni 4% Mo Bal. Fe	fcc Isotropic	58	460
Grain Oriented 50%Ni-50%Fe	8.25	55,000 Annealed				10×10^{-6} 0° to 500°	50% Ni 50% Fe	fcc [001] in direction of rolling (100) in plane of material	45	500
Magnetic Field Annealed 49%Co-2%V-49%Fe	8.20					9.9×10^{-6} 20° to 100°	49% Co 2% V 49% Fe	bcc Ordered structure 70-80%	26	940
Singly Grain Oriented Silicon Steel	7.65	51,500 Annealed	59,600 Annealed				3.25% Si Bal. Fe	bcc Singly Grain Oriented, [001] in direction of rolling, (110) in material plane	50	750
Doubly Grain Oriented Silicon Steel	7.65	40,200 Annealed	40,200 Annealed	37,120 Annealed		12.7×10^{-6} 20°	3.00% Si Bal. Fe	bcc [001] in direction of rolling, (110) in plane of material. Doubly grain oriented.	48.5 at 22.2°C 78.0 at 371°C 87.5 at 482°C	757

Table I. - Continued

Material	Magneto-Striction $\Delta L/L$	Saturation Induction, B_S (kG)	Initial Permeability μ_0	Incremental Permeability μ_Δ	Maximum Permeability μ_m	Coercivity H_{cs}, Oersteds	Hysteresis Loss, Normal P_h (ergs/cm^3/Hz)
Square Hysteresis Loop 4%Mo-79%Ni-17%Fe	0.6×10^{-6} at 6 kG Longitu-dinal	8	25,000		500,000	0.2-0.4 2 mil	
Grain Oriented 50%Ni-50%Fe		16	500		100,000 200,000	0.04-0.2 2 mil	500 at B_m ~15 kG
Magnetic Field Annealed 49%Co-2%V-49%Fe	66×10^{-6} at 24 kG Longitu-dinal	24	2,500		66,000 80,000	0.15-0.35 2 mil	
Singly Grain Oriented Silicon Steel	25×10^{-6} at 20 kG Longitu-dinal	20	1,000 2 and 4 mil		15,000(2 mil) 20,000(4 mil)	0.4 to 0.7 2 and 4 mil	
Doubly Grain Oriented Silicon Steel	25×10^{-6} at 20.3 kG	20.3	4,000		30,000 50,000	0.05 to 1.5	

ductility and has a detrimental effect on the magnetic quality of the material. A faster cooling rate introduces thermal strains that harmfully affect the magnetic properties.

The vanadium addition slows down the rate of atomic ordering. It increases the resistivity but decreases somewhat the intrinsic saturation of the alloy.

Singly Grain Oriented Silicon Steel

Singly grain oriented silicon steel (3.25%Si, balance Fe) has a cube edge direction [001], the easy direction of magnetization, in the rolling direction of the material and the face diagonal plane (110) in the plane of the material.

Doubly Grain Oriented Silicon Steel, With and Without Magnetic Field Anneal

A doubly grain oriented silicon steel (3%Si, balance Fe) has a cube edge direction [001], the easy direction of magnetization, in both the rolling and cross-rolling direction, and the cube face plane (100) in the plane of the material.

The silicon addition increases the initial permeability and resistivity, but decreases the intrinsic saturation of the steel.

SAMPLE DESCRIPTION AND TESTS CONDUCTED

General Magnetic Tests

Core Descriptions. - The materials evaluated, thickness and sample configurations are as follows:

Material	Thickness, Inches	No. of Samples	Sample Core Configuration
Square Hysteresis Loop 79%Ni-4%Mo-17%Fe Alloy, (Two Vendors)	0.002	3	Toroid, Tape Wound
	0.004	3	Toroid, Tape Wound
Grain Oriented 50%Ni-50%Fe Alloy, (Two Vendors)	0.002	3	Toroid, Tape Wound
	0.004	3	Toroid, Tape Wound
Magnetic Field Annealed 49%Co-2%V-49%Fe Alloy	0.002	3	Toroid, Tape Wound
	0.004	3	Rowland Ring Lamination

Material	Thickness, Inches	No. of Samples	Sample Core Configuration
Singly Grain Oriented Silicon Steel (Vendor No. 1)	0.002 0.004	3 3	Toroid, Tape Wound Toroid, Tape Wound
Doubly Grain Oriented Silicon Steel (Stress Relief Annealed)	0.002 0.006	3 3	Toroid, Tape Wound Double Window Punched Laminations
Doubly Grain Oriented Silicon Steel (Magnetic Field Annealed	0.002 0.006	3 3	Toroid, Tape Wound Double Window Punched Laminations

The material used to make the tape wound toroids was coated with magnesium oxide for interlaminar insulation except that 0.002-inch doubly grain oriented silicon steel was coated with aluminum oxide. The thickness of the magnesium oxide coating, assuming no reaction with the steel surface, was approximately 0.03 mil.

The Rowland ring laminations and double window laminations were coated with aluminum orthosphosphate for interlaminar insulation. The coating was approximately 0.007-mil thick.

The Rowland ring lamination drawing is shown in figure 1. The double window lamination drawing is shown in figure 2. All samples weighed approximately one pound.

The annealing treatments for the various magnetic materials were as follows:

Material	Annealing Treatment
Square Hysteresis Loop, 4%Mo-79%Ni-17%Fe Alloy, (Two Vendors)	1160°C, 4 hrs.; cool @ 5° C/min. Dry hydrogen atmosphere
Grain Oriented 50%Ni-50%Fe Alloy, Vendor No. 1	1175° C, 4 hrs.; Dry hydrogen atmosphere, Furnace cool to 900° C, air quench.
Grain Oriented 50%Ni-50%Fe Alloy, Vendor No. 2	1040° C, 1.5 hrs.; cool @ 7.5° C/min, Dry hydrogen atmosphere
Magnetic Field Annealed 49%Co-2%V-49%Fe Alloy	850° C, 2 hrs.; cool 3° C/min., Dry hydrogen atmosphere, Field
Singly Grain Oriented Silicon Steel	800° C, 1 hr.; Dry hydrogen atmosphere

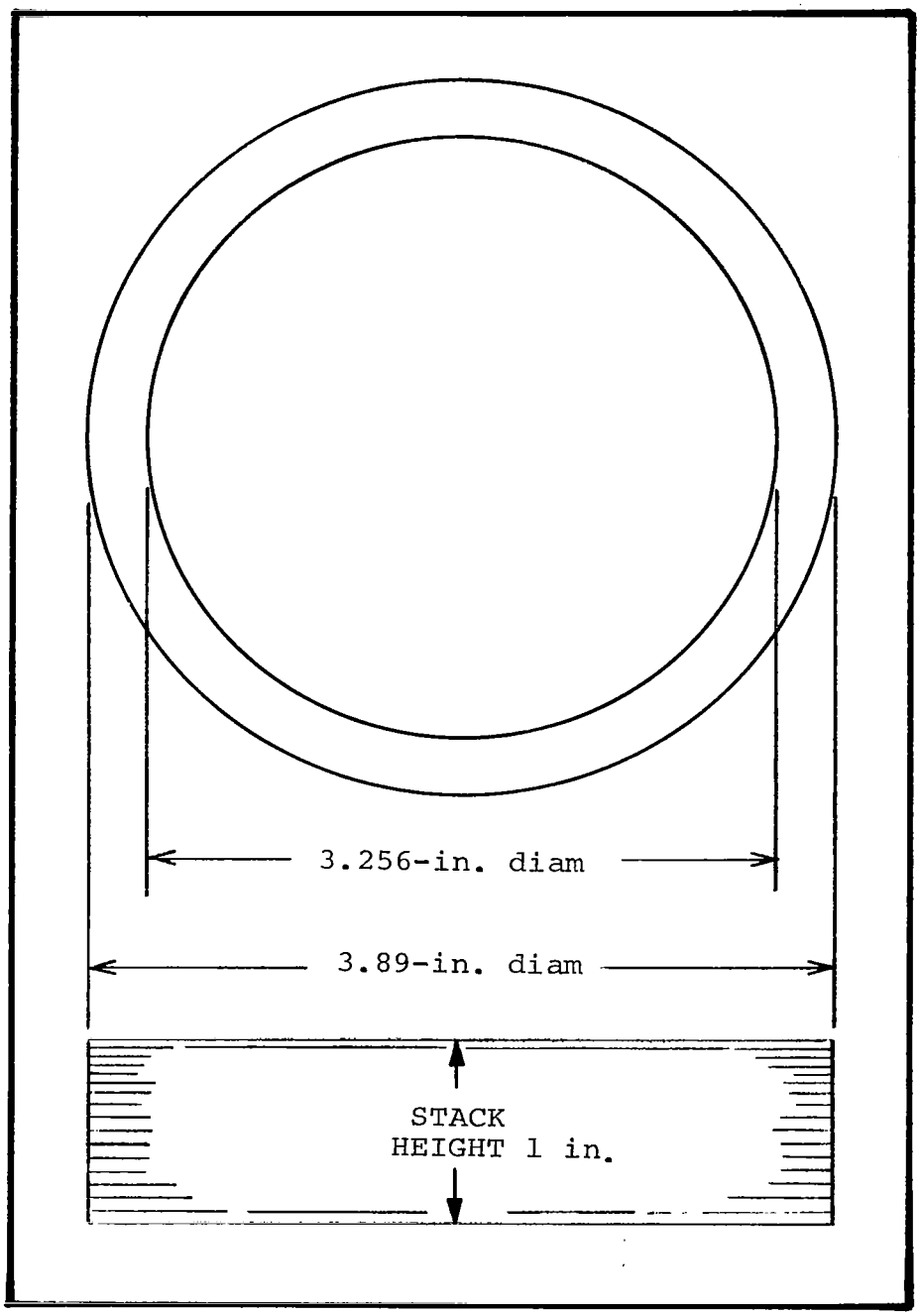

Figure 1. - Rowland Ring Lamination

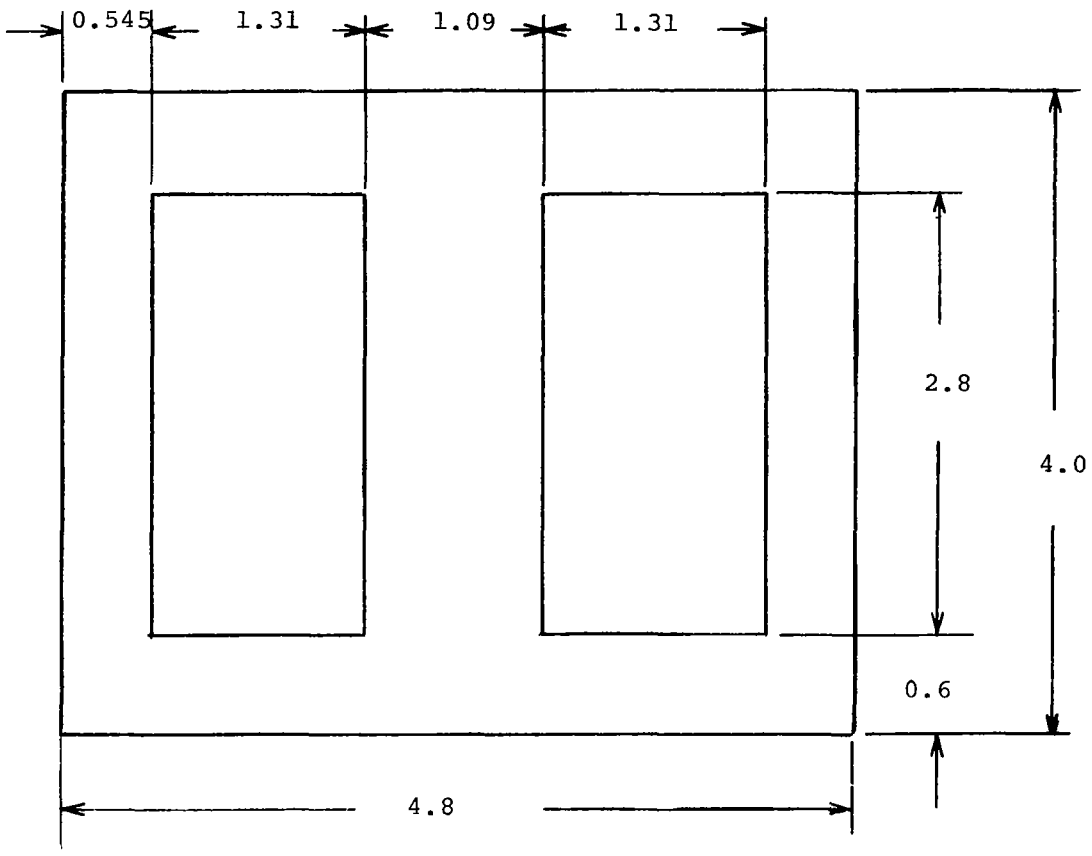

Figure 2. - Double Window Lamination

Material	Annealing Treatment
Doubly Grain Oriented Silicon Steel	900° C, 1.5 hr.; Dry hydrogen atmosphere, Furnace cool

After annealing, all cores were enclosed in anodized aluminum core boxes with a glass epoxy insert to provide a break in the electrical path. The core boxes were insulated with an epoxy with a minimum voltage breakdown of 1,000 volts rms at 60 Hz. The core boxes were silicone oil filled and hermetically sealed after inserting the cores. A typical sealed round core box is shown in figure 3. A typical sealed double window core box is shown in figure 4.

The following magnetic property tests were conducted using the equipment and procedures described in Appendix C.

CCFR Testing. - CCFR (Constant Current Flux Reset) tests were conducted on 2 cores of each material at room ambient temperature. Tests were conducted at 800, 1600, and 3200 Hz using square wave excitation. In addition, tests were conducted on 3 cores of each material at 400 Hz using both sine and square wave excitation. The properties determined were T, Br, AT, DAT, SAT, and G.

DC Testing. - Tests were conducted on two thicknesses of each type of material at -55° C, room ambient temperature and 250° C to obtain dc magnetization curves and dc hysteresis loops.

AC Testing. - Tests were conducted using square wave excitation on two thicknesses of each type of material to determine 400, 800, 1600, and 3200 Hz total core loss, apparent power and ac hysteresis loops. Tests were conducted at -55° C, room ambient temperature and 250° C.

Additional experimental problems encountered in preparing specimens for testing and the solutions of those problems are treated in Appendix D.

Degradation Testing

The degradation tests were designed to evaluate the detrimental magnetic effects, if any, of some of the normal factory processing steps. The following materials were tested for the following condition:

Material and Form	Process Variable Steps
0.004-inch Square Hysteresis Loop, 4%Mo-79%Ni-17%Fe Alloy, Vendor No. 1, tape wound in	Enclosed in an unsealed core box with windings on the core box

Figure 3. - Round Toroid Sealed Core Box

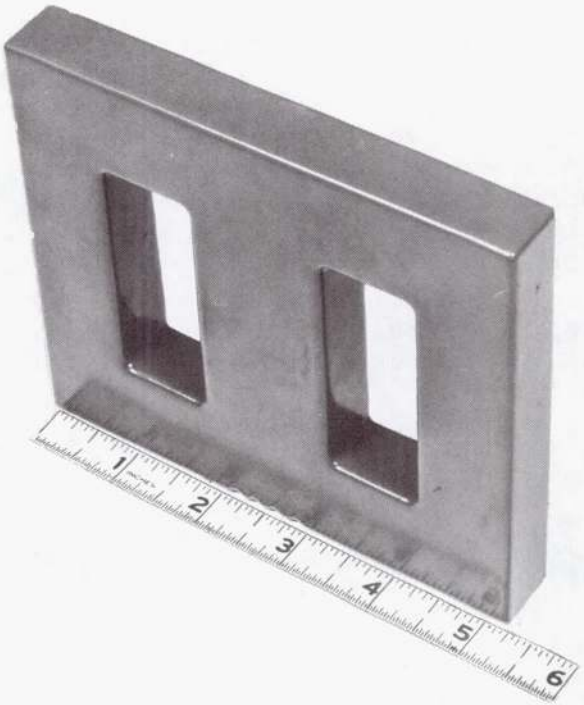

Figure 4. - Double Window Sealed Core Box

Material and Form	Process Variable Steps
square form, magnesium oxide interlaminar insulation	Windings directly on unprotected core
	Core bonded with varnish
	Core cut to make two C-cores and banded to make a square core again
	Core dipped in varnish and baked to cure varnish
0.004-inch single grain oriented silicon steel, Vendor No. 1, tape wound in square form, magnesium oxide interlaminar insulation	Enclosed in an unsealed core box with windings on the core box
	Windings directly on unprotected core
	Core bonded with varnish
	Core cut to make two C-cores and banded to make a square core again
	Core dipped in varnish and baked to cure varnish
0.006-inch doubly grain oriented silicon steel, double window laminations, magnetic field annealed, aluminum orthophosphate interlaminar insulation	Only center leg enclosed with a core box, windings only on center leg
	Windings directly on center leg of laminations and laminations bonded
	Laminations dipped in varnish and baked to cure varnish

Material	Process Variable Steps
0.006-inch doubly grain oriented silicon steel, double window laminations, stress relief annealed, aluminum orthophosphate interlaminar insulation	Only center leg enclosed with a core box, windings only on center leg Windings directly on center leg of laminations and laminations bonded Laminations dipped in varnish and baked to cure varnish
Magnetically annealed 0.004-inch 49%Co-2%V-49%Fe Alloy, tape wound as circle, magnesium oxide interlaminar insulation	Enclosed in an unsealed core box with windings on the core box Windings directly on unprotected core Core coated by fluidizing
0.004-inch grain oriented, 50%Ni-50%Fe Alloy, Vendor No. 1, tape wound as circle magnesium oxide interlaminar insulation	Enclosed in an unsealed core box with windings on the core box Windings directly on unprotected core Core coated by fluidizing

The materials were annealed as described on page 18.

The bonding procedure used was one vacuum and two room-pressure impregnations with a clear silicone varnish followed by baking four hours at 204° C.

The "dip and bake" procedure used was one vacuum impregnation with a clear silicone varnish followed by baking for six hours at 265° C.

The "fluidizing" was accomplished by dipping cores preheated

to approximately 500° F in an air agitated bath of epoxy resin powder. The coated cores were then cured at 400° F for four hours.

The cores were tested to determine dc magnetization properties and total core loss using square wave excitation at 400 and 3200 Hz following each operation.

Vacuum Exposure Testing

Two series of tests were conducted to determine the effect of exposure of magnetic materials for 1000 hours at 250° C in a vacuum in the range of 1.4×10^{-5} to 7×10^{-6} torr.

The first series was the evaluation of fully processed cores similar to those used in the factory processing tests.

The materials evaluated are as follows:

Material and Form	Processing
0.004-inch Square Hysteresis Loop, 4%Mo-79%Ni-17%Fe Alloy, tape wound in square form, magnesium oxide interlaminar insulation	Core cut to make two C-cores and banded to make a square core again. Core dipped in varnish and baked to cure varnish
0.004-inch Singly Grain Oriented Silicon Steel, Vendor No. 1, tape wound in square form, magnesium oxide interlaminar insulation	Core cut to make two C-cores and banded to make a square core again. Core dipped in varnish and baked to cure varnish
0.006-inch Doubly Grain Oriented Silicon Steel, double window laminations, stress relief annealed, aluminum orthophosphate interlaminar insulation	Laminations dipped in varnish and baked to cure varnish
0.006-inch Doubly Grain Oriented Silicon steel, double window laminations, magnetic field annealed, aluminum orthophosphate interlaminar insulation	Laminations dipped in varnish and baked to cure varnish

The cores were tested at room ambient temperature to obtain total core loss using square wave excitation at 400 Hz. Tests were conducted prior to vacuum treatment, after 500 hours, and after 1000 hours exposure. The weight of cores prior to and after 500 and 1000 hours exposure was determined.

The second series was conducted to determine the effect of vacuum on laminations that had been coated with aluminum orthophosphate but not impregnated or in contact with any windings.

The materials tested were as follows:

Material

0.006-inch Square Hysteresis Loop, 4%Mo-79%Ni-17%Fe Alloy, Vendor No. 1
0.004-inch Square Hysteresis Loop, 4%Mo-79%Ni-17%Fe Alloy, Vendor No. 2
0.004-inch Singly Grain Oriented Silicon Steel, Vendor No. 1
0.004-inch, 49%Co-2%V-49%Fe Alloy (Magnetic Field Annealed)
0.006-inch, 49%Co-2%V-49%Fe Alloy (Magnetic Field Annealed)
0.006-inch, Doubly Grain Oriented Silicon Steel (Stress relief annealed)
0.006-inch, Singly Grain Oriented Silicon Steel, Vendor No. 2
0.006-inch, Grain Oriented, 50%Ni-50%Fe Alloy, Vendor No. 2
0.004-inch, Grain Oriented 50%Ni-50%Fe Alloy, Vendor No. 1

The materials were evaluated in the form of round Rowland rings and as round blanks insulated with aluminum orthophosphate.

The Rowland Rings were banded as shown in figure 5. The plates were loaded to 150 pounds prior to bonding. Clamps were removed prior to core loss testing.

The cores were tested at room ambient temperature after 500 and 1000 hours at 250° C in a vacuum in the range of 10^{-6} torr.

The blanks were exposed as loose blanks. The average interlamination resistance and weight were determined prior to exposure and after 1000 hours exposure.

DATA AND TECHNICAL DISCUSSION

Test Results

Data Presentation. - The data obtained in the "General Magnetic Tests" for each material thickness, core configuration, and heat treatment were reviewed and curves representative of the

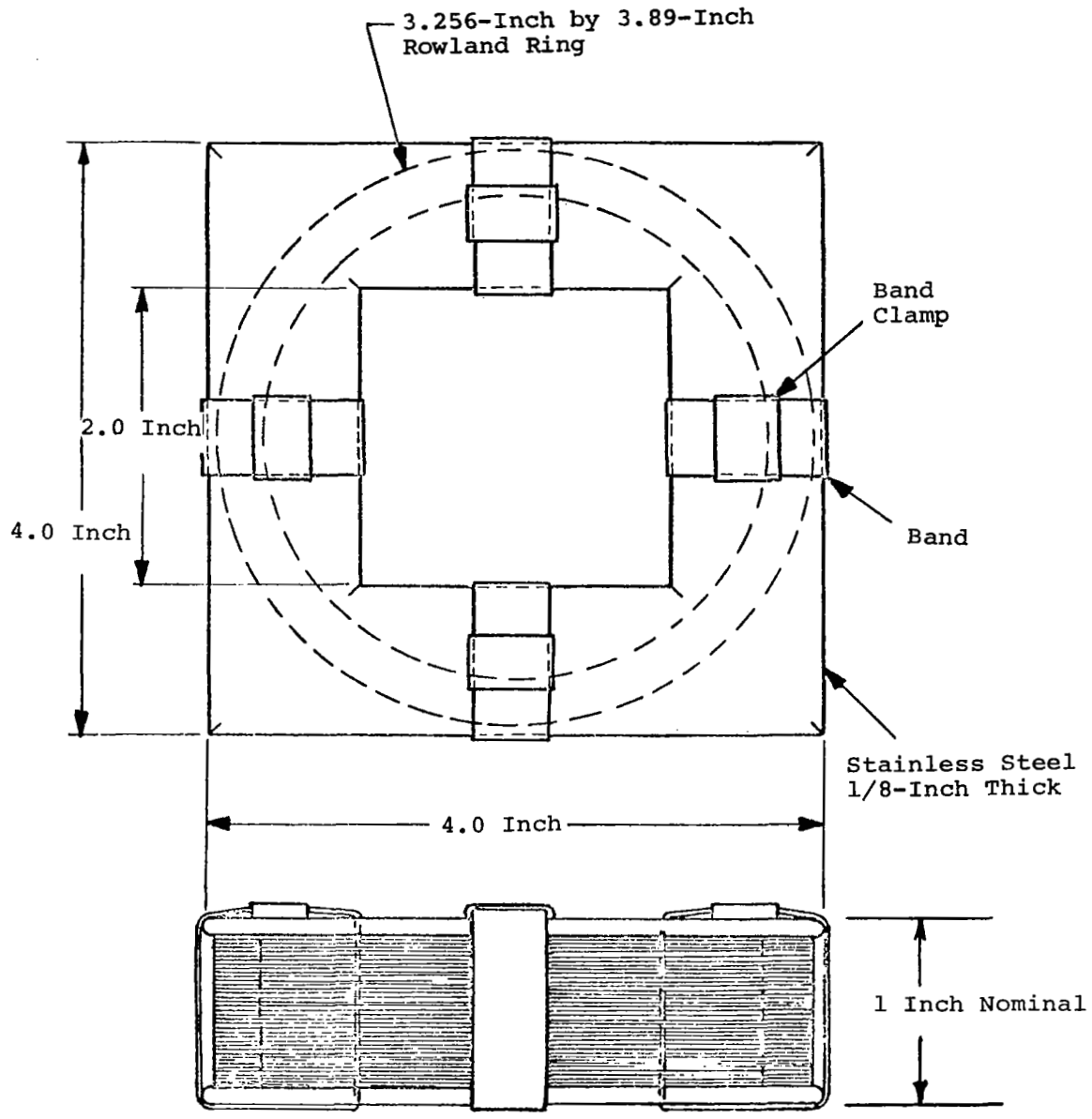

Figure 5. - Clamping Arrangement for Rowland Rings Vacuum Testing

various properties were prepared and are presented below. The data from the "Degradation Testing" and "Vacuum Exposure Testing" are presented in their entirety. For purposes of brevity the following short designations are used.

Designation	Complete Description
SHL 4Mo-79NiFe	Square Hysteresis Loop 4%Mo-79%Ni-17%Fe
GO 50Ni-Fe	Grain Oriented 50%Ni-50%Fe
MFA 2V-CoFe	Magnetic Field Annealed 49%Co-2%V-49%Fe
SGO Si Steel	Singly Grain Oriented Silicon Steel
DGO Si Steel	Doubly Grain Oriented Silicon Steel
SRA	Stress Relief Anneal
MFA	Magnetic Field Anneal
DW	Double Window

Square Hysteresis Loop 4%Mo-79%Ni-17%Fe: Two tape thicknesses were evaluated: 0.002-inch and 0.004-inch. Although these two gauges show some, rather slight, differences in properties, they follow the same pattern of property change with frequency and temperature.

DC Magnetization Curves: Figure 6 displays dc magnetization curves at temperatures of -55° C, room ambient, and 250° C for the 0.004-inch and 0.002-inch tapes. The temperature has a considerable effect on the dc magnetization of this material because of the relatively low Curie temperature of this composition. For instance, in the 0.002-inch core the flux density corresponding to a field of 10 oersteds increases from 7.5 kG at room temperature to 9.5 kG at -55° C, and then decreases to 5.6 kG with an increase in temperature to 250° C. The 0.004-inch material displays the same temperature pattern except that the values are somewhat different; for instance, the flux density at 10 oersteds increased from 7.4 kG at room temperature to 8.3 kG at -55° C and decreased to 5.8 kG at 250° C.

DC Hysteresis Loops: The dc hysteresis loops for the 0.002-inch material at -55° C, room ambient, and 250° C are shown on figure 7. The loops follow the typical pattern in response to the change in temperature.

AC Core Loss Curves: Figures 8 and 9 depict the core loss of 0.004-inch and 0.002-inch-tape thicknesses, respectively, as

a function of both square wave frequencies of 400 to 3200 Hz and temperatures of -55° C, room ambient, and 250° C. The temperature effect was not as pronounced in core loss as in the dc properties. For instance, between 1 and 7 kG which covers the useful induction range for this material, the losses at -55° C did not differ much from those at room temperature. However, the pattern changes at 250° C. A considerable drop occurs in core loss up to a flux level of 4.5 kG; but from this point on, due to a decrease in saturation induction, there is a rapid increase toward higher core loss values with increasing induction.

The 0.002-inch material shows a considerably lower core loss than the 0.004-inch material. For instance, at a flux density of 6 kG, the 0.002-inch tape displays a room temperature 400 Hz core loss of 0.18 watts/lb versus 0.27 watts/lb for the 0.004-inch tape.

AC Apparent Power Curves: AC apparent power curves for both gauges are shown on figures 10 and 11 that display exciting volt-amperes at -55° C, room ambient, and 250° C for 400 to 3200 Hz. As expected, the curves follow the typical patterns of change in response to changes in frequency and temperature.

AC Hysteresis Loops: AC hysteresis loops for both gauges at -55° C, room ambient, and 250° C are shown on figures 12 through 17 for 400 to 3200 Hz. As expected, the loops broaden with increasing frequency. No loop distortion was observed in response to changes of either frequency or temperature.

CCFR Properties: The CCFR properties of both gauges are shown on figures 18 and 19 for 400 to 3200 Hz. There are some differences in the AT and DAT values between the two gauges. The 0.002-inch material displays a DAT value of 0.005 oersteds at 400 Hz; this property increases to 0.023 oersteds at 3200 Hz. The AT value of the same material was 0.030 oersteds at 400 Hz and 0.052 oersteds at 3200 Hz. The DAT value of the 0.004-inch material was approximately four times greater at 400 Hz, but only 25% greater at 3200 Hz. There was quite a difference in gain, amounting to 9.5×10^5 at 400 Hz in the 0.002-inch material versus 4.35×10^5 in the 0.004-inch material. As the frequency increases to 3200 Hz, the former material showed a gain decrease to 2.5×10^5 whereas the latter material dropped in gain to 0.55×10^5.

Grain Oriented 50%Ni-50%Fe. - Two tape thicknesses were evaluated: 0.002-inch and 0.004-inch.

DC Magnetization Curves: DC magnetization curves for both gauges at -55° C, room ambient, and 250° C are shown on figure 20. The effect of temperature on the dc magnetization properties of this material follows the conventional pattern; its magnitude is between those of Si-Steels and 4Mo-79NiFe. The thicker material has a somewhat higher dc permeability at higher inductions at all

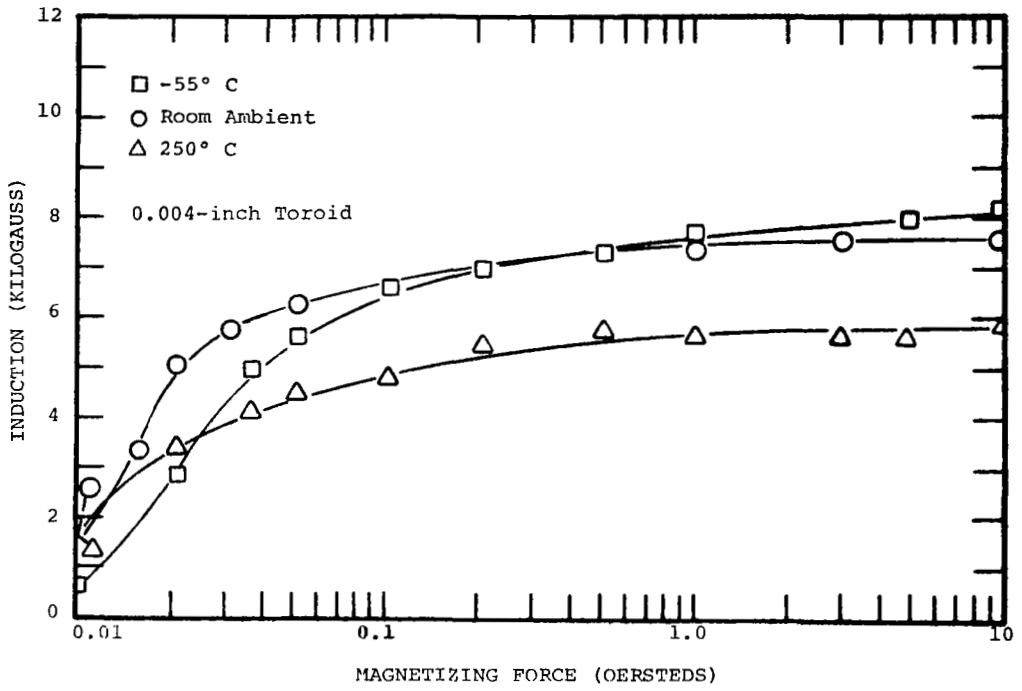

(a)

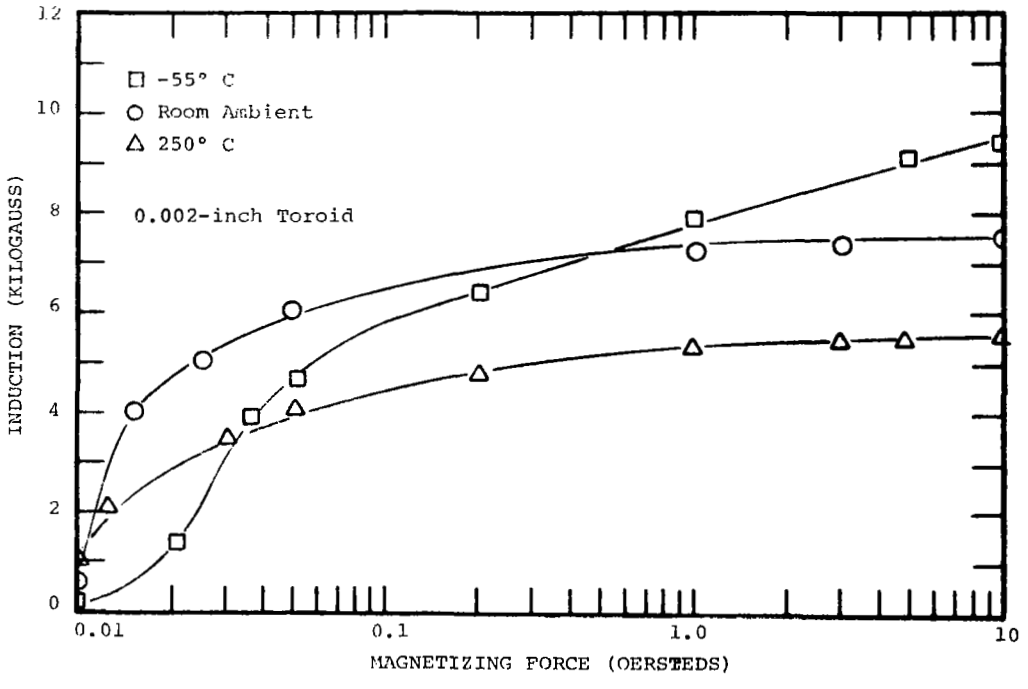

(b)

Figure 6. - DC Magnetization, 0.004- and 0.002-Inch 4%Mo-79%Ni-17%Fe Toroid, Square Loop

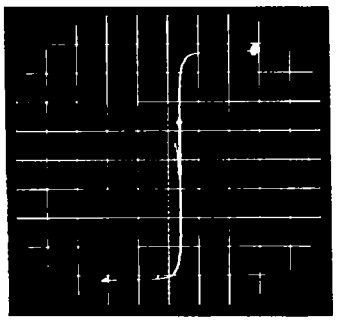

B = 2 kG/div

H = 2 Oe/div

T = -55° C

(a)

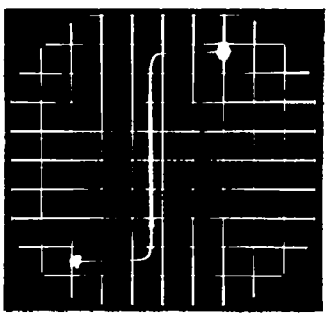

B = 2 kG/div

H = 2 Oe/div

T = Room Ambient

(b)

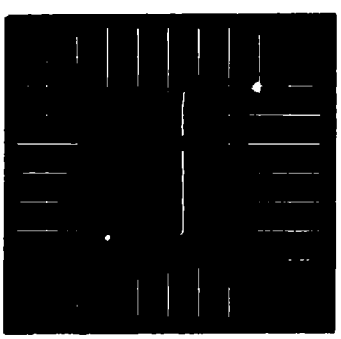

B = 2 kG/div

H = 2 Oe/div

T = 250° C

(c)

Figure 7.- DC Hysteresis Loop, 0.002-Inch 4%Mo-79%Ni-17%Fe, Square Loop

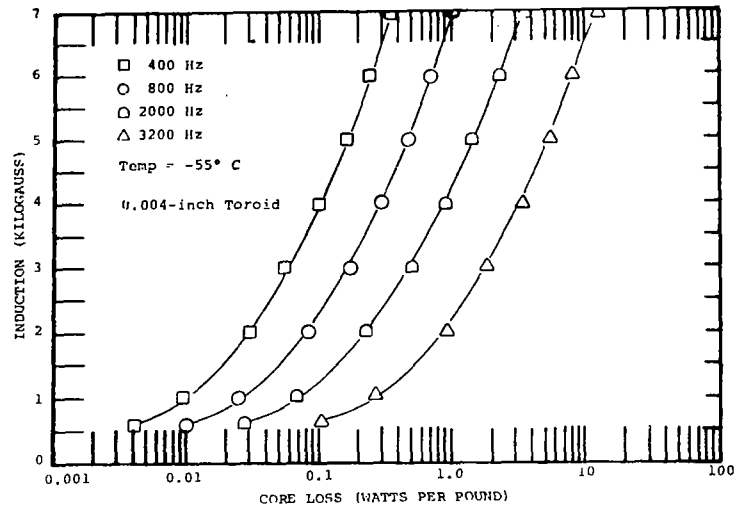

(a)

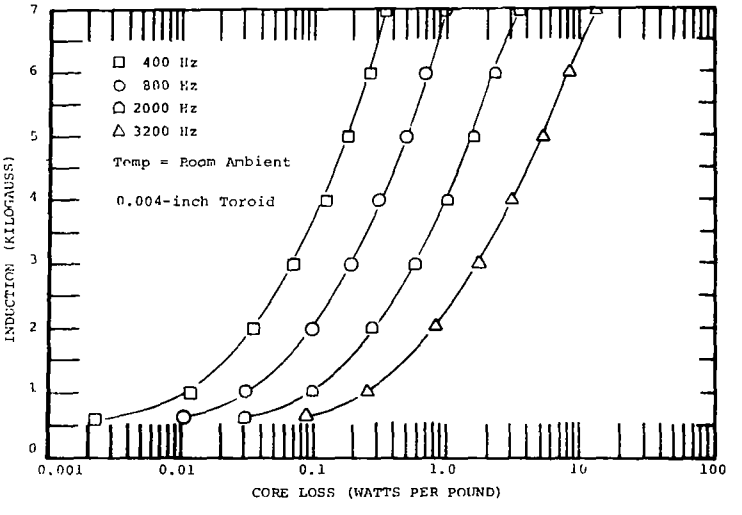

(b)

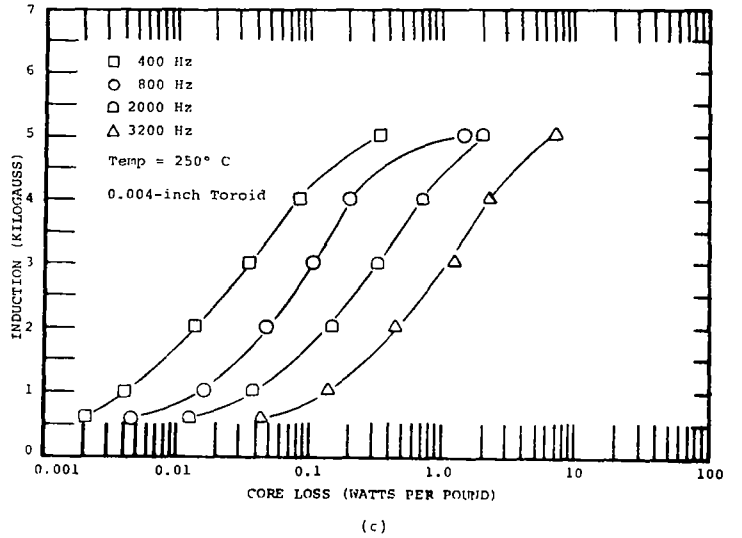

(c)

Figure 8. - $P_{c,\ sq,}$ Total Core Loss vs Induction and Frequency, 0.004-Inch 4%Mo-79%Ni-17%Fe Toroid, Square Loop

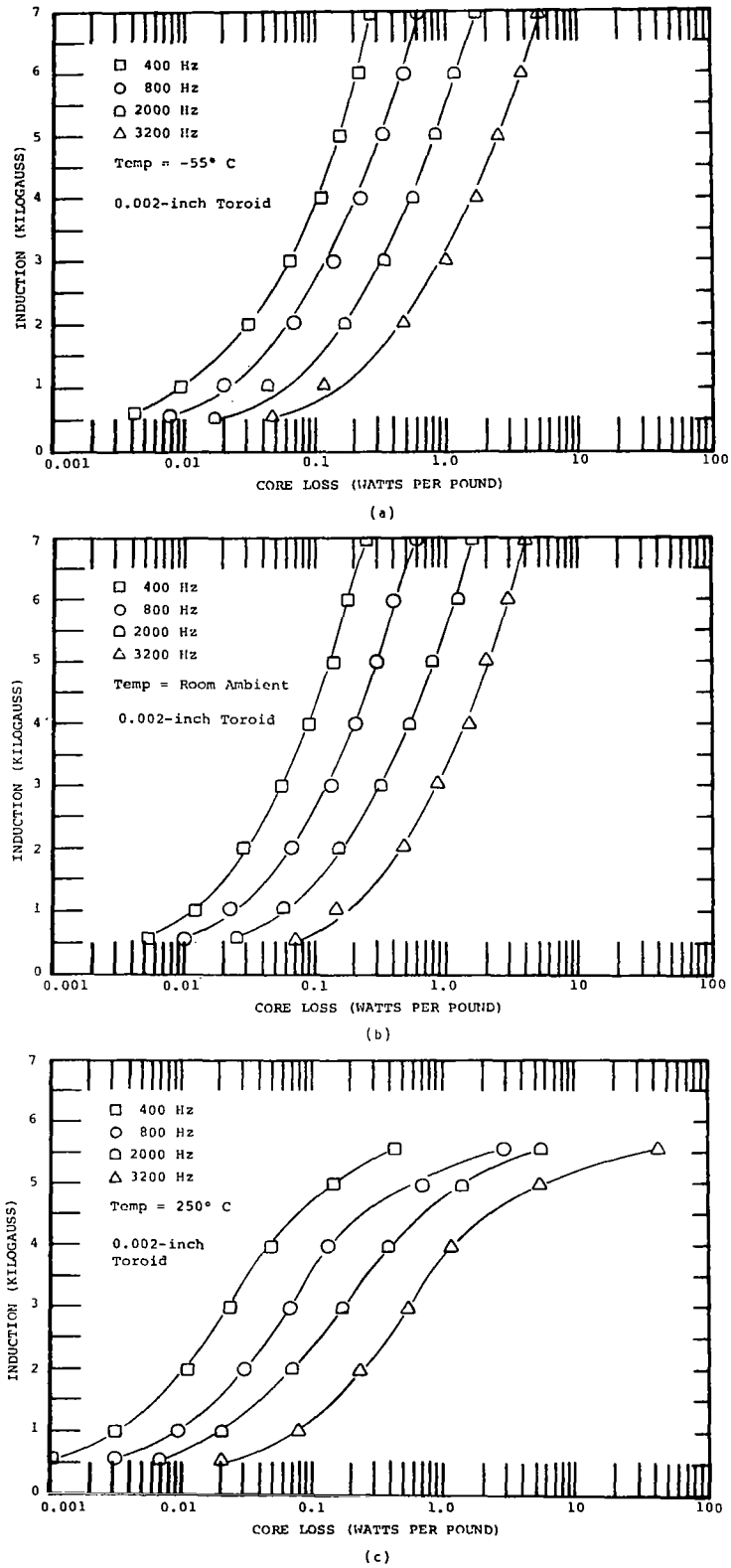

Figure 9. - $P_{c, sq,}$ Total Core Loss vs Induction and Frequency, 0.002-Inch 4%Mo-79%Ni-17%Fe Toroid, Square Loop

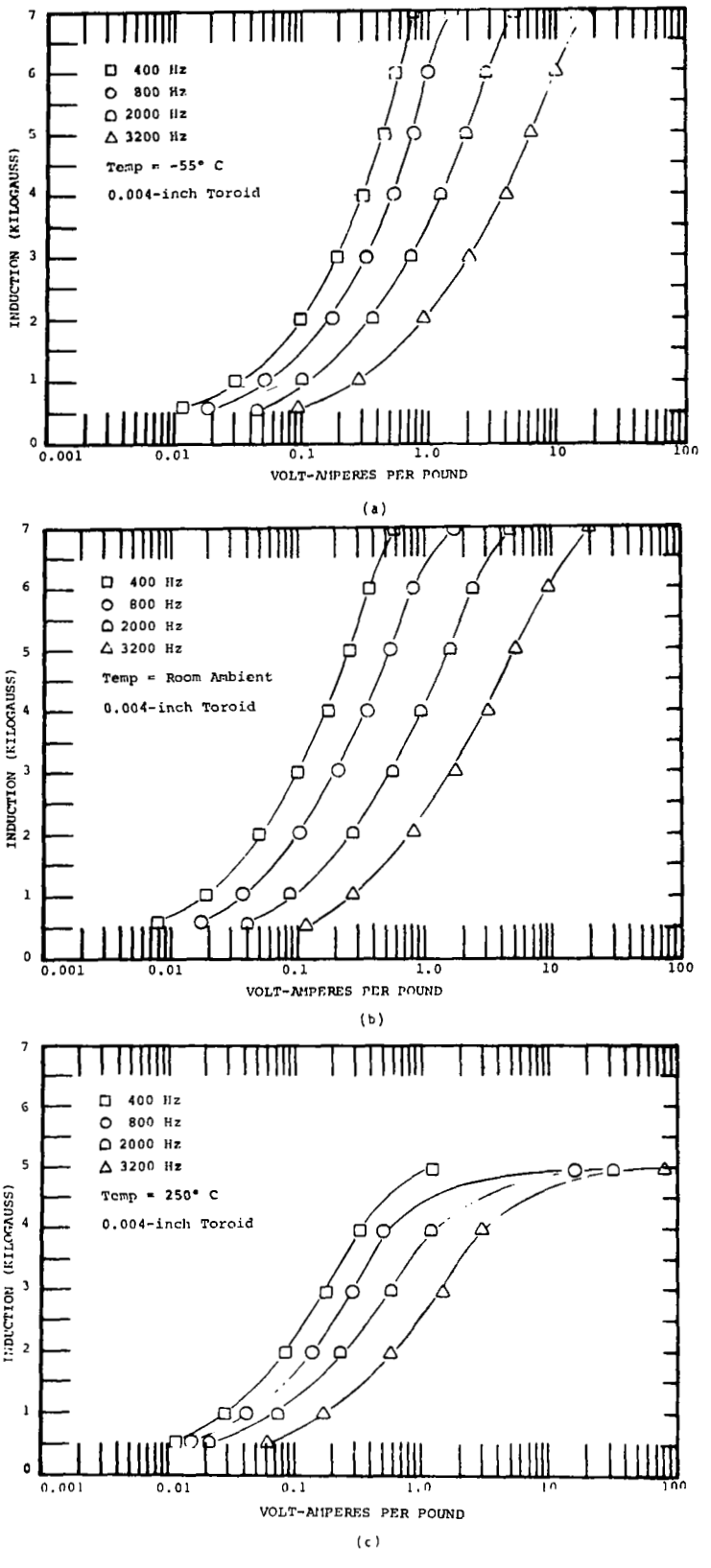

Figure 10. - $P_{a,\ sq}$, Apparent Power vs Induction and Frequency, 0.004-Inch 4%Mo-79%Ni-17%Fe Toroid, Square Loop

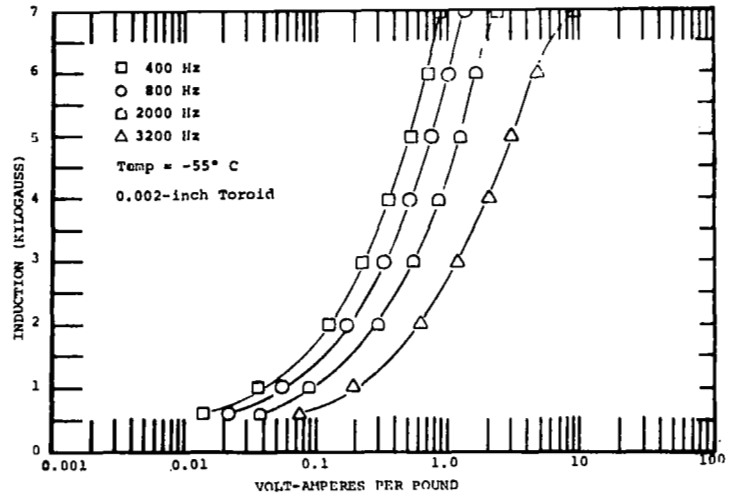

(a)

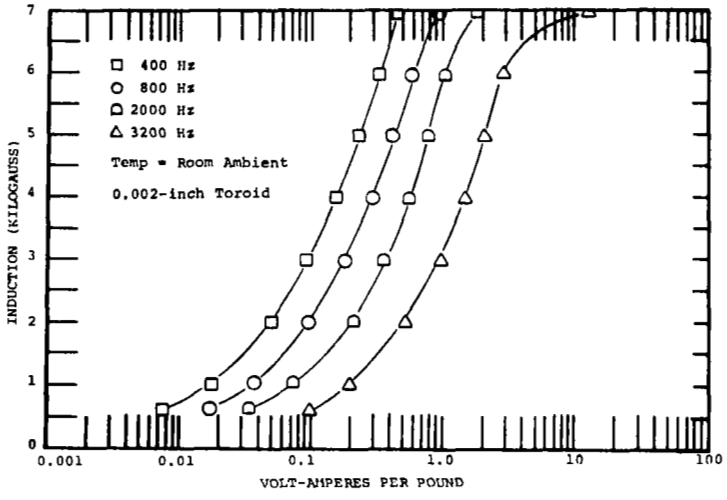

(b)

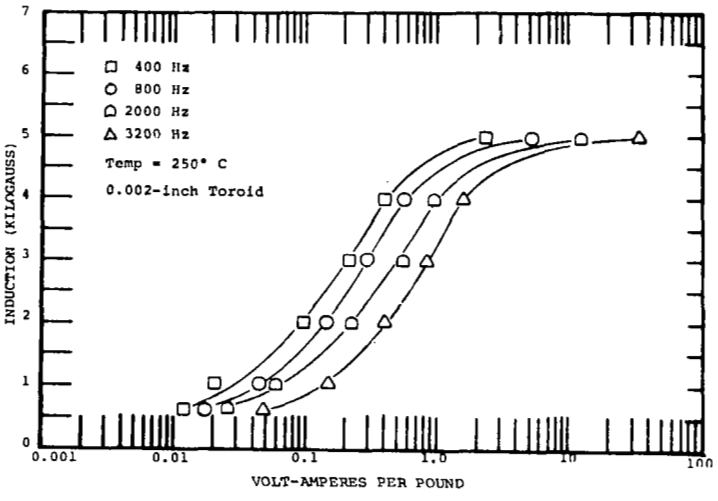

(c)

Figure 11. - $P_{a,\ sq,}$ Apparent Power vs Induction and Frequency, 0.002-Inch 4%Mo-79%Ni-17%Fe Toroid, Square Loop

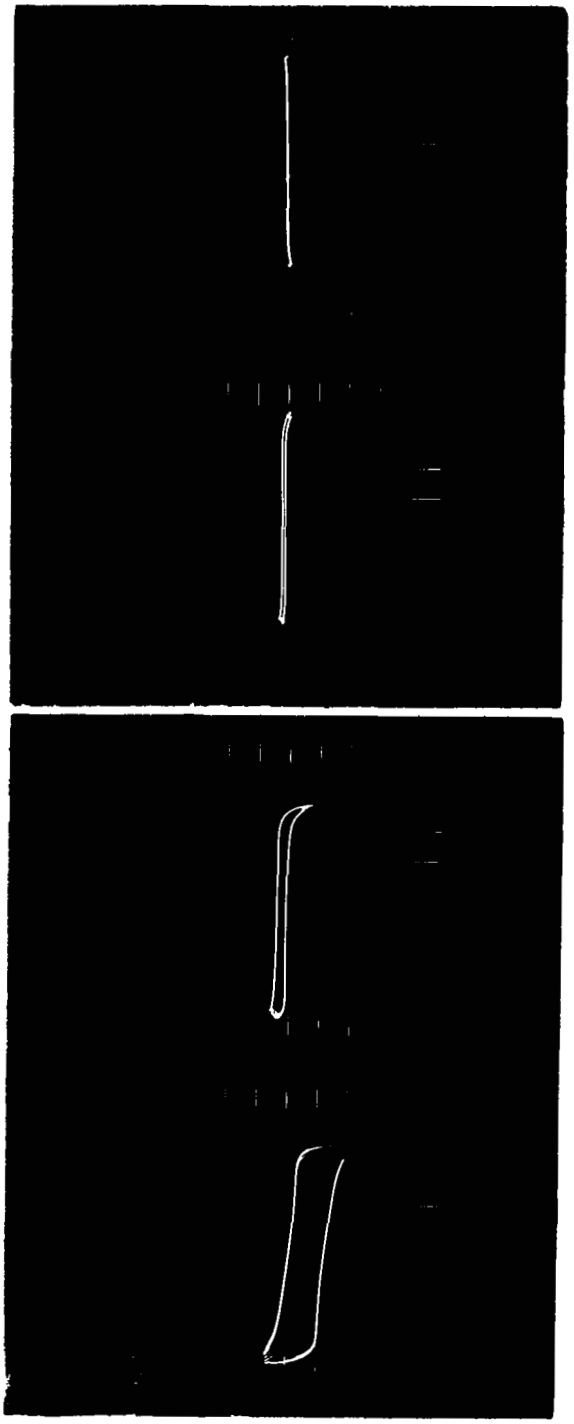

(a) f = 400 Hz
B = 2 kG/div
H = 2.5 Oe/div

(b) f = 800 Hz
B = 2 kG/div
H = 2.5 Oe/div

(c) f = 1600 Hz
B = 2 kG/div
H = 2.5 Oe/div

(d) f = 3200 Hz
B = 2 kG/div
H = 2.5 Oe/div

Figure 12. - AC Hysteresis Loop, Square Wave Excitation, 400, 800, 1600, and 3200 Hz, 0.004-Inch 4%Mo-79%Ni-17%Fe Toroid, Square Loop, -55° C

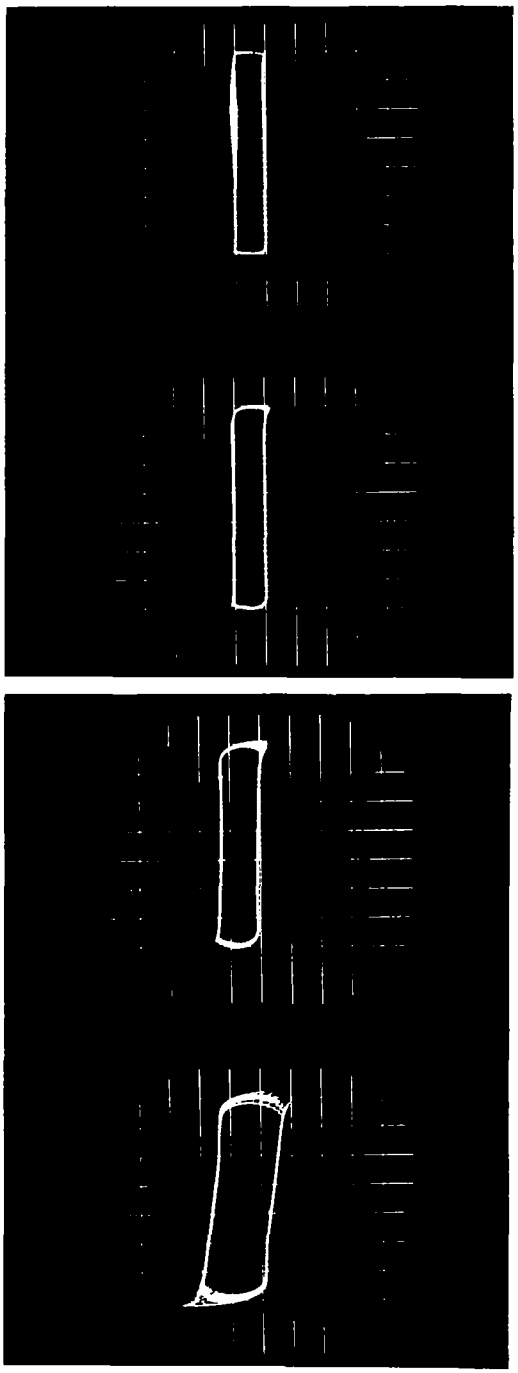

(a) f = 400 Hz
B = 2 kG/div
H = 2.5 Oe/div

(b) f = 800 Hz
B = 2 kG/div
H = 2.5 Oe/div

(c) f = 1600 Hz
B = 2 kG/div
H = 2.5 Oe/div

(d) f = 3200 Hz
B = 2 kG/div
H = 2.5 Oe/div

Figure 13.- AC Hysteresis Loop, Square Wave Excitation, 400, 800, 1600, and 3200 Hz, 0.004-Inch 4%Mo-79%Ni-17%Fe Toroid, Square Loop, Room Ambient

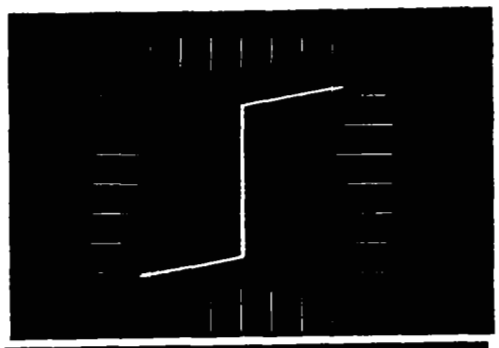

(a) f = 400 Hz
B = 2 kG/div
H = 100 Oe/div

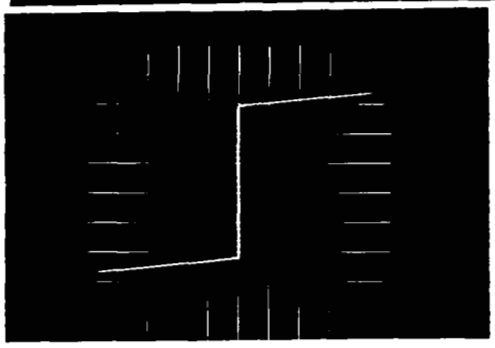

(b) f = 800 Hz
B = 2 kG/div
H = 50 Oe/div

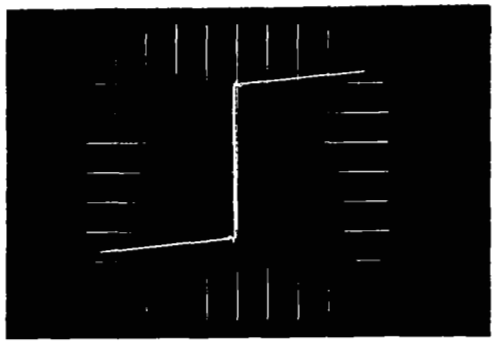

(c) f = 1600 Hz
B = 2 kG/div
H = 50 Oe/div

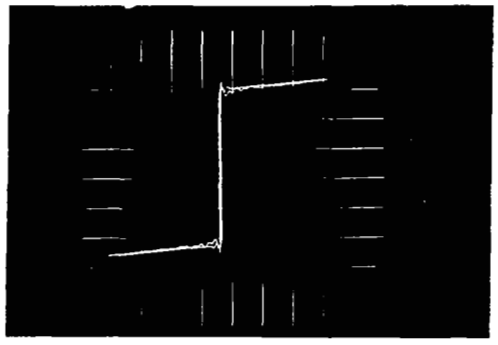

(d) f = 3200 Hz
B = 2 kG/div
H = 50 Oe/div

Figure 14.- AC Hysteresis Loop, Square Wave Excitation, 400, 800, 1600, and 3200 Hz, 0.004-Inch 4%Mo-79%Ni-17%Fe Toroid, Square Loop, 250° C

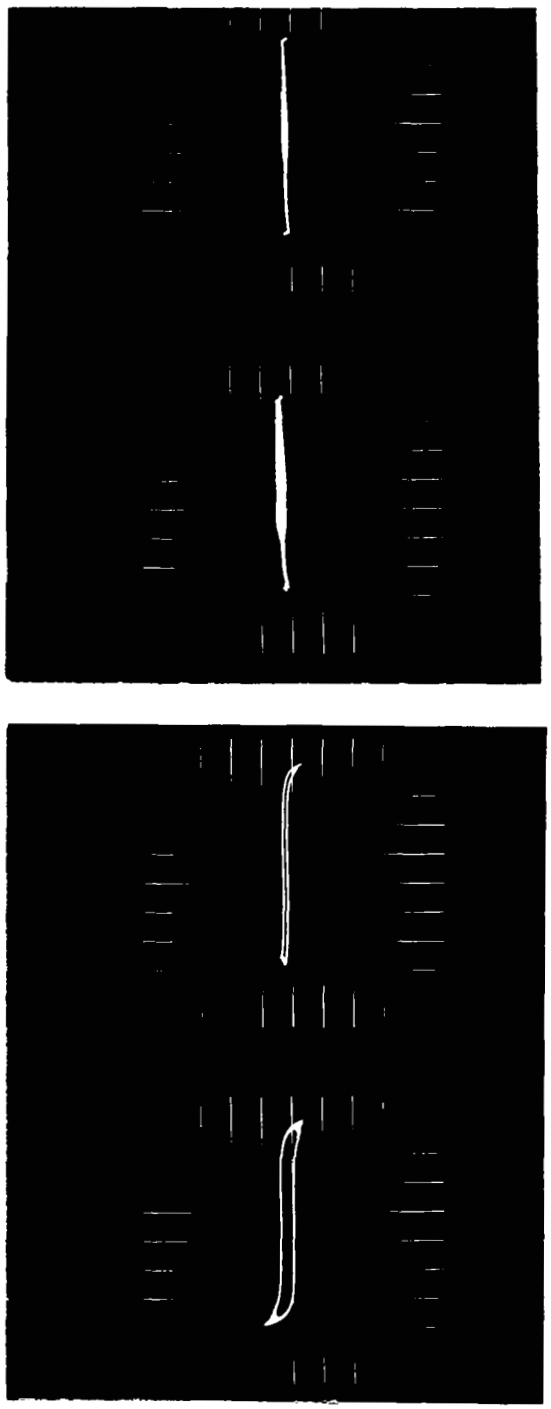

(a) f = 400 Hz
B = 2 kG/div
H = 2.5 Oe/div

(b) f = 800 Hz
B = 2 kG/div
H = 2.5 Oe/div

(c) f = 1600 Hz
B = 2 kG/div
H = 2.5 Oe/div

(d) f = 3200 Hz
B = 2 kG/div
H = 2.5 Oe/div

Figure 15.– AC Hysteresis Loop, Square Wave Excitation, 400, 800, 1600, and 3200 Hz, 0.002-Inch 4%Mo-79%Ni-17%Fe Toroid, Square Loop, -55° C

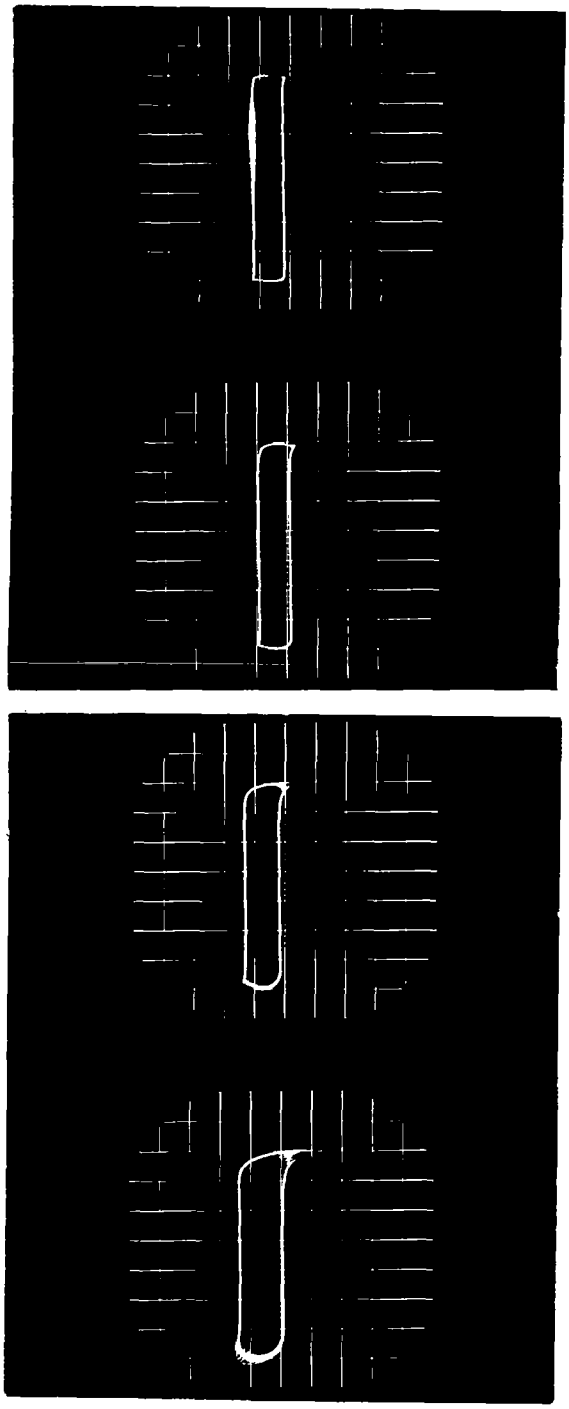

(a) f = 400 Hz
B = 2 kG/div
H = 2.5 Oe/div

(b) f = 800 Hz
B = 2 kG/div
H = 2.5 Oe/div

(c) f = 1600 Hz
B = 2 kG/div
H = 2.5 Oe/div

(d) f = 3200 Hz
B = 2 kG/div
H = 2.5 Oe/div

Figure 16.- AC Hysteresis Loop, Square Wave Excitation, 400, 800, 1600, and 3200 Hz, 0.002-Inch 4%Mo-79%Ni-17%Fe Toroid, Square Loop, Room Ambient

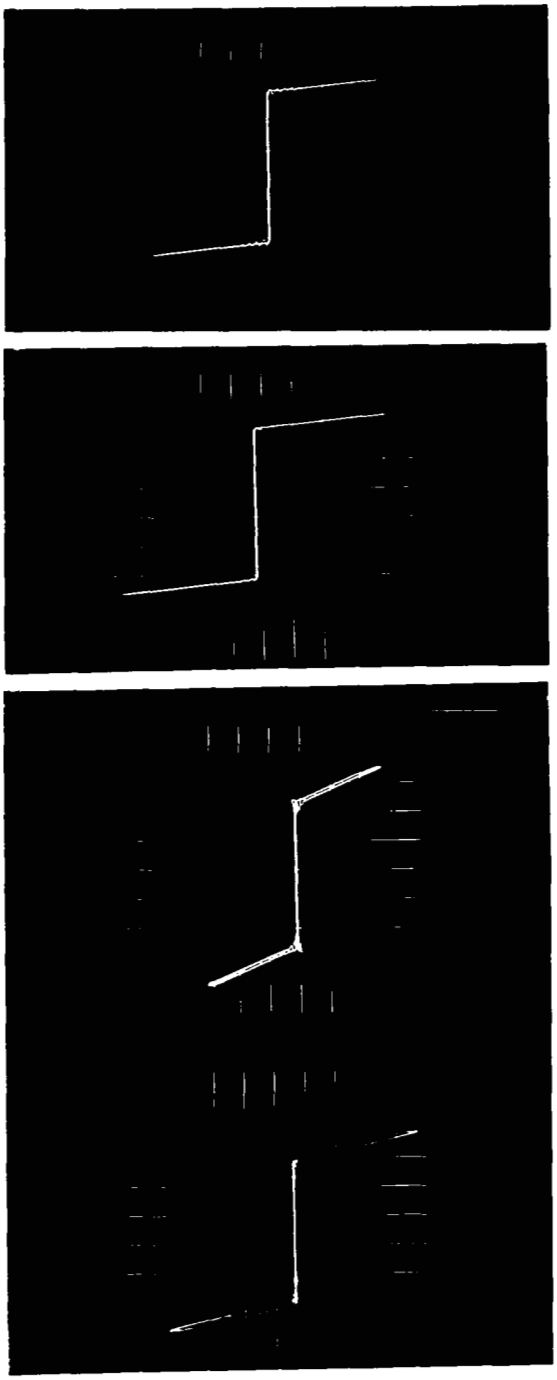

(a) f = 400 Hz
B = 2 kG/div
H = 50 Oe/div

(b) f = 800 Hz
B = 2 kG/div
H = 50 kG/div

(c) f = 1600 Hz
B = 2 kG/div
H = 250 Oe/div

(d) f = 3200 Hz
B = 2 kG/div
H = 250 Oe/div

Figure 17.- AC Hysteresis Loop, Square Wave Excitation, 400, 800, 1600, and 3200 Hz, 0.002-Inch 4%Mo-79%Ni-17%Fe Toroid, Square Loop, 250° C

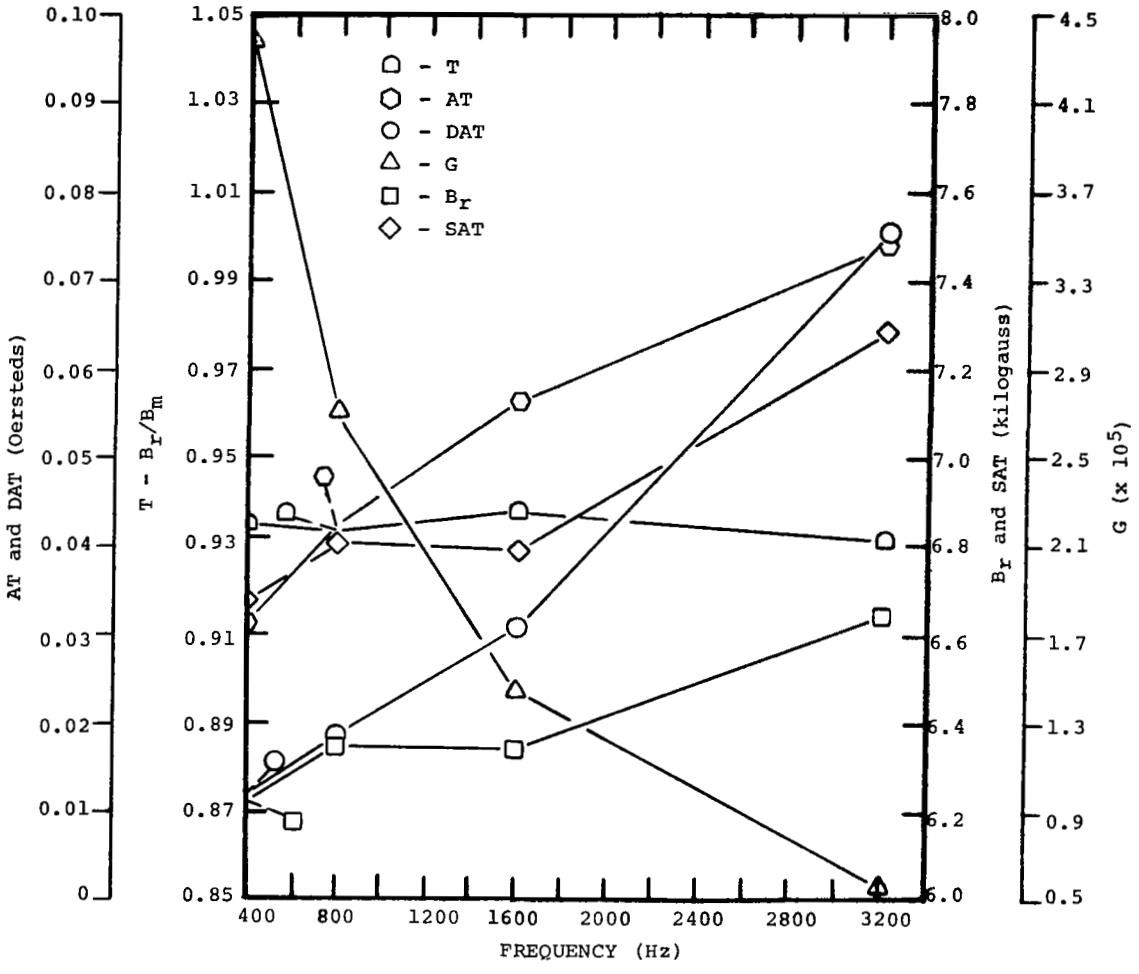

Figure 18. - CCFR Properties, 0.004-Inch 4%Mo-79%Ni-17%Fe Toroid, Square Loop, Room Ambient

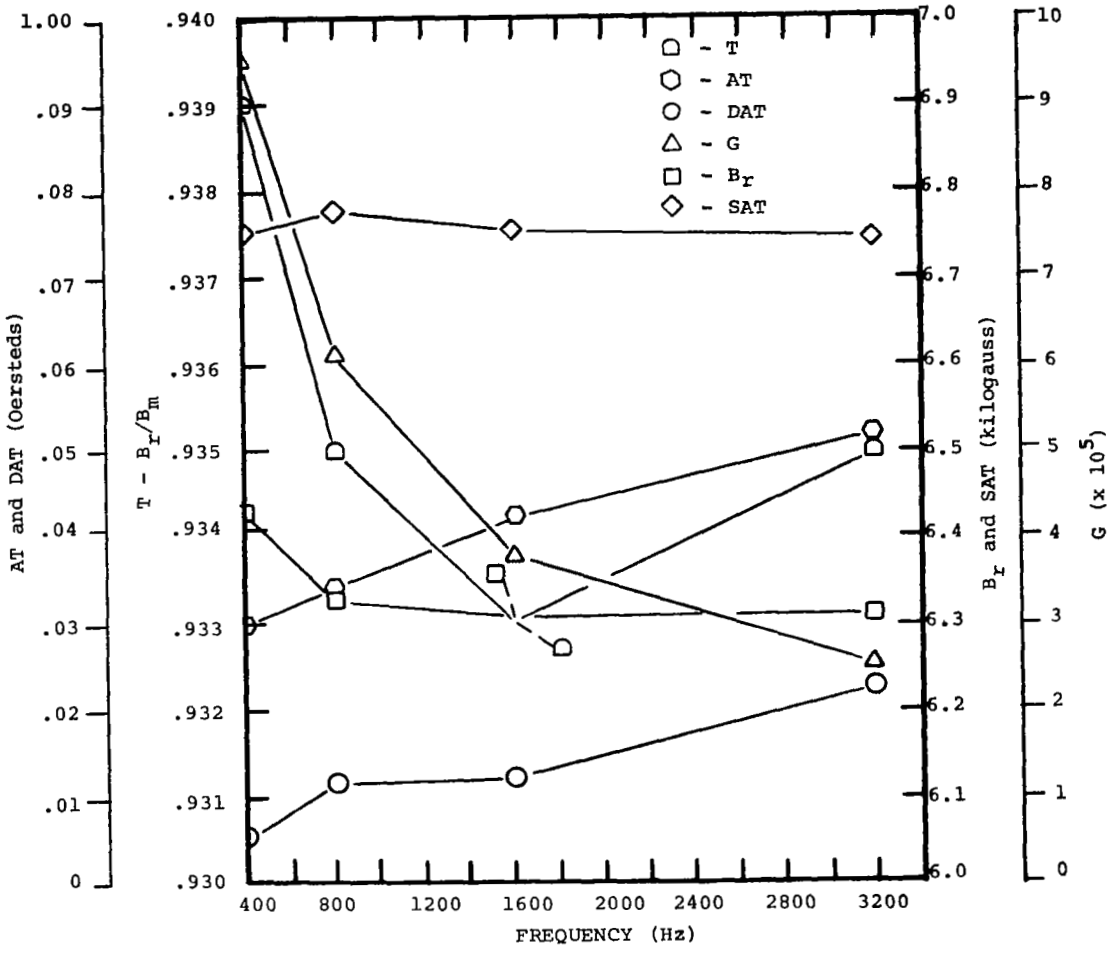

Figure 19. - CCFR Properties, 0.002-Inch 4%Mo-79%Ni-17%Fe Toroid, Square Loop, Room Ambient

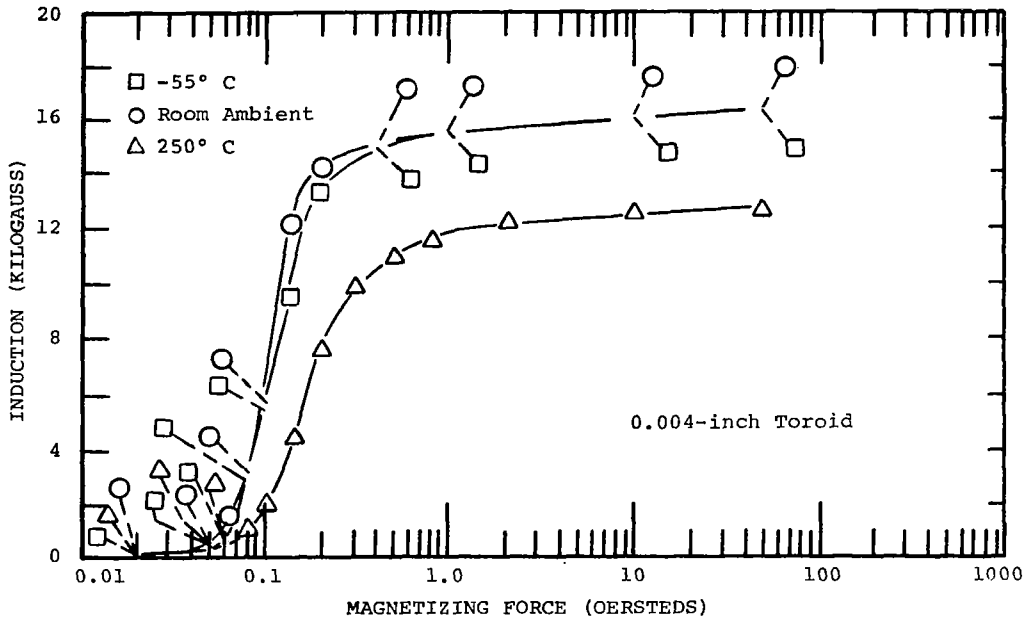

(a)

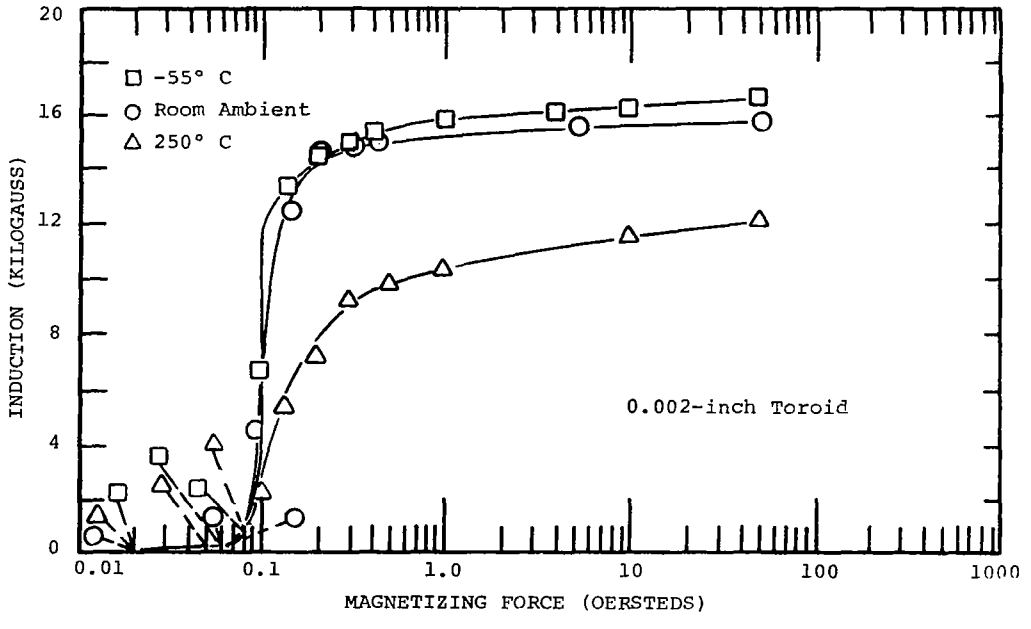

(b)

Figure 20. - DC Magnetization, 0.004- and 0.002-Inch 50%Ni-50%Fe Toroid, Grain Oriented

temperatures applied. For the magnetization forces of 10 and 100 oersteds, the corresponding flux densities are 16.1 and 16.4 kG for the 0.004-inch material versus 15.7 and 15.8 kG for the 0.002-inch material.

DC Hysteresis Loops: Figure 21 displays dc hysteresis loops for the 0.002-inch material as a function of temperature. All three loops show a high degree of rectangularity.

AC Core Loss Curves: AC core loss curves for both gauges at -55° C, room ambient, and 250° C are shown in figures 22 and 23 that display losses at 400 to 3200 Hz. The core loss at 10 kG and 400 Hz amounts to 1.3 watts/pound for the thinner material and 1.9 watts/pound for the 0.004-inch material. As the induction increases to 15 kG, the 400 Hz core loss at room temperature amounts to 2.3 watts/pound for the thinner material and 3.1 watts/pound for the thicker material. The change in core loss with temperature is considerably less pronounced than in the SHL 4Mo-79NiFe toroids. There is a slight increase in core loss, especially at 400 Hz, as the temperature is lowered to -55° C. The reverse pattern applies for lower inductions when the temperature is increased to 250° C. At high inductions there is a considerable increase in core loss.

AC Apparent Power Curves: AC apparent power curves for both gauges are shown on figures 24 and 25 that display exciting-volt amperes at -55° C, room ambient, and 250° C for 400 to 3200 Hz. The curves follow the conventional temperature pattern.

AC Hysteresis Loops: AC hysteresis loops for both geometries at -55° C, room ambient, and 250° C for 400 to 3200 Hz are shown in figures 26 through 31. The curves show no distortion and, as expected, the loops widen in response to an increase in frequency.

CCFR Properties: The CCFR properties of both gauges are shown on figures 32 and 33 for 400 to 3200 Hz. By comparison the 0.004-inch material showed a somewhat higher SAT value, 15.27 kG at 400 Hz as compared to 15.07 kG for the 0.002-inch material. As the frequency increases to 3200 Hz there is only a slight change in the SAT value for both materials. The same pattern applies to B_r, being 15.2 kG for the 0.004-inch material and 14.93 kG for the 0.002-inch material, both at 400 Hz. The T value is about the same for both materials, 0.99; this property shows only a slight change with an increase in frequency. The gain was 4.25×10^5 for the 0.004-inch material versus 5.0×10^5 for the 0.002-inch material. Both gauges show a considerably steep decrease in gain with an increase in frequency to 3200 Hz, the 0.004-inch material to a value of 0.875×10^5.

Magnetic-Field Annealed 49%Co-2%V-49%Fe Alloy. - Two gauges of magnetic-field annealed 49%Co-2%V-49%Fe alloy were evaluated:

toroids wound from 0.002-inch tape and cores assembled from punched 0.004-inch Rowland ring laminations.

DC Magnetization Curves: DC magnetization curves for both gauges at -55° C, room ambient, and 250° C are shown in figure 34. The toroid displays considerably higher permeabilities at high inductions than the Rowland ring core because of a greater degree of domain orientation in the tape-wound core (better response to magnetic annealing). This difference in the degree of domain orientation brings about a difference in the magnetic properties of the two gauges when tested at the same temperature. As the temperature of the toroids changes, the pattern of change in the magnetic properties displays a trend opposite to that shown by other core materials tested in this program. As compared with the magnetic properties at room temperature, the flux densities of the toroid at 1 and 10 oersteds decrease at -55° C and increase at 250° C. On the other hand, the pattern of change with temperature of the magnetization curve of the laminated ring resembles a typical soft-magnetic alloy.

DC Hysteresis Loops: The dc hysteresis loops for the 0.002-inch thickness at -55° C, room ambient, and 250° C are shown on figure 35. The loops display a high degree of rectangularity and show no distortion.

AC Core Loss Curves: AC core loss curves for both gauges and temperatures of -55° C, room ambient, and 250° C are shown in figures 36 and 37 that display losses at 400 to 3200 Hz. In spite of a greater thickness, the ring core (figure 36) shows lower losses at lower inductions and lower frequencies than the tape-wound toroid (figure 37); the opposite situation applies at higher inductions and especially at higher frequencies. The reason for this behavior is the high anomalous loss of a highly domain-oriented structure. However, as will be discussed elsewhere in this report, the domain-oriented structure responds to square wave excitation with a decrease in core loss especially at higher frequencies.

AC Apparent Power Curves: AC apparent power curves for both gauges are shown on figures 38 and 39 that display exciting-volt amperes at -55° C, room ambient, and 250° C for 400 to 3200 Hz. As in core loss, the ring core (figure 38) displays lower apparent power values at lower inductions and lower frequencies.

AC Hysteresis Loops: AC hysteresis loops for both gauges at -55° C, room ambient, and 250° C are shown on figures 40 through 45 for 400 to 3200 Hz. The toroids (figures 43, 44, and 45) show somewhat higher rectangularity. At higher frequencies both cores show some distortion.

CCFR Properties: The CCFR properties for both gauges are shown on figures 46 and 47 for frequencies of 400 to 3200 Hz.

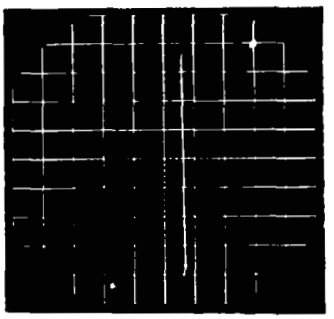

B = 4 kG/div

H = 10 Oe/div

T = -55° C

(a)

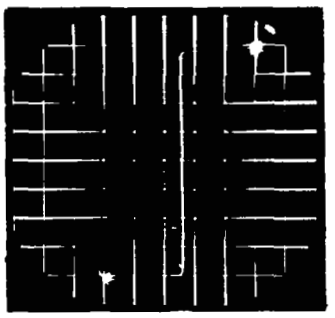

B = 4 kG/div

H = 10 Oe/div

T = Room Ambient

(b)

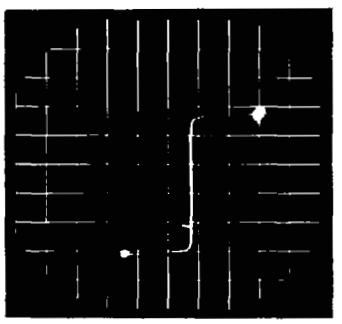

B = 5 kG/div

H = 10 kG/div

T = 250° C

(c)

Figure 21.- DC Hysteresis Loop, 0.002-Inch 50%Ni-50%Fe Toroid

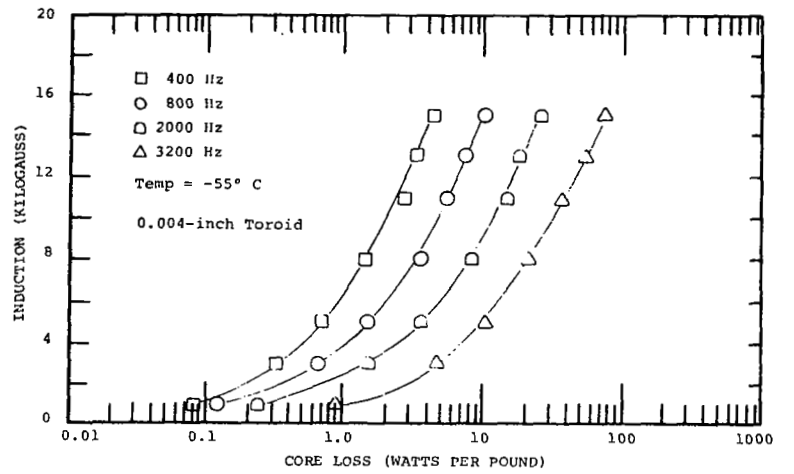

(a)

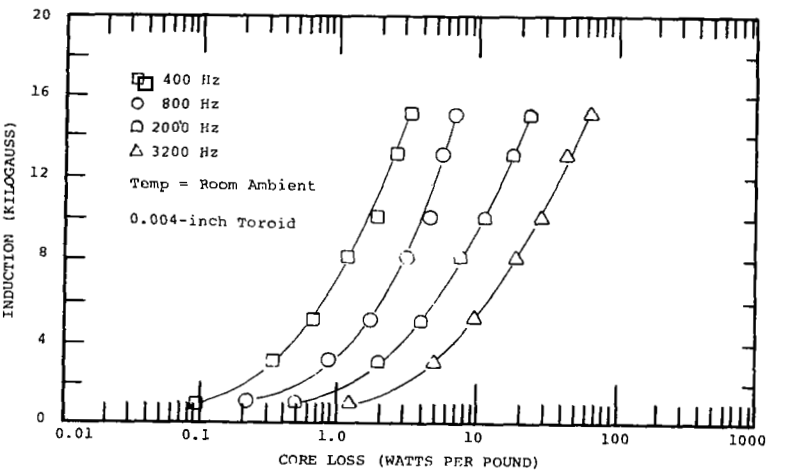

(b)

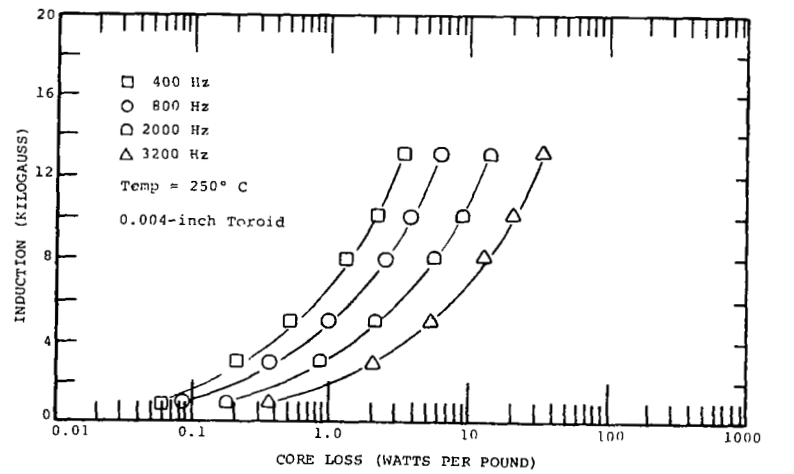

(c)

Figure 22. - $P_{c,\ sq,}$ Total Core Loss vs Induction and Frequency, 0.004-Inch 50%Ni-50%Fe Toroid Grain Oriented

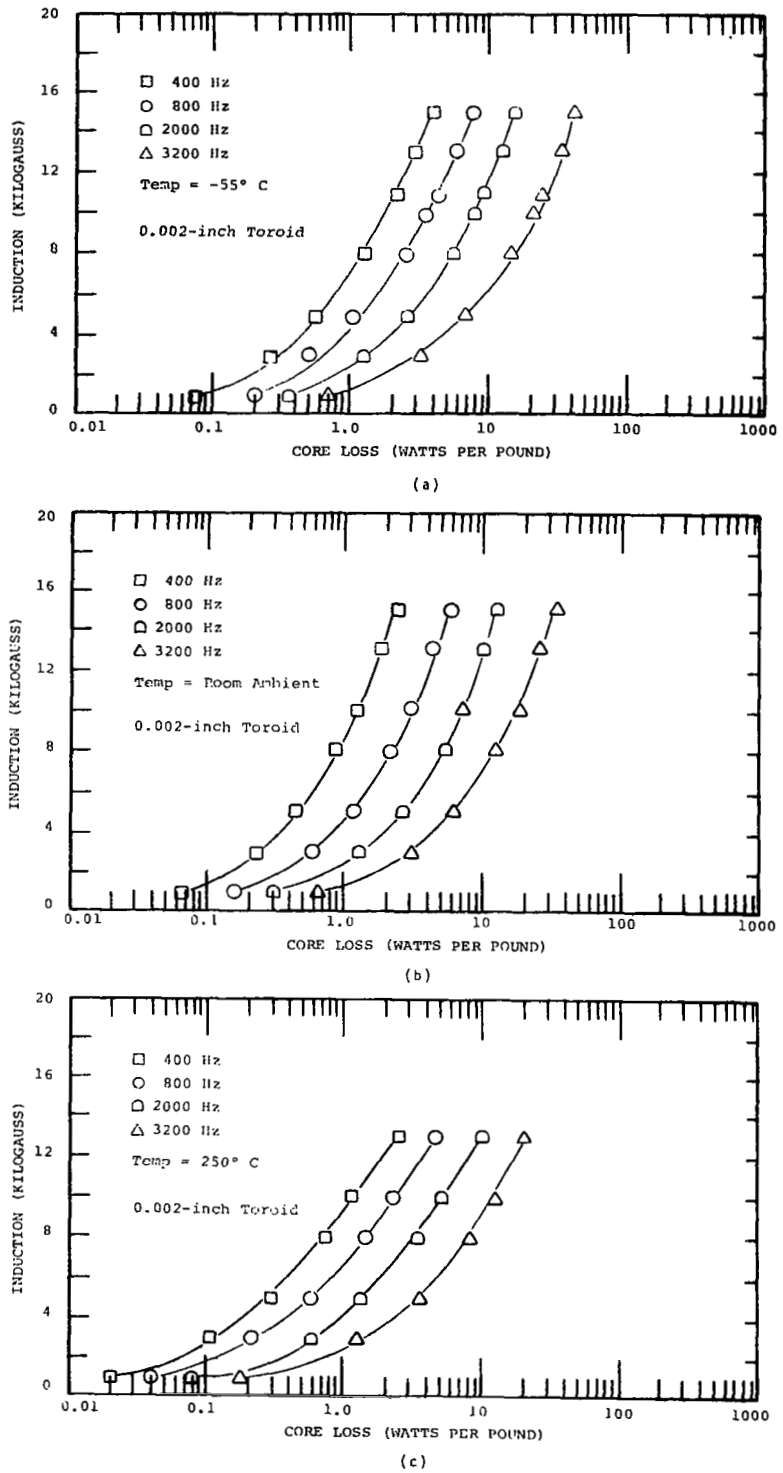

Figure 23. - $P_{c,\ sq,}$ Total Core Loss vs Induction and Frequency, 0.002-Inch 50%Ni-50%Fe Toroid, Grain Oriented

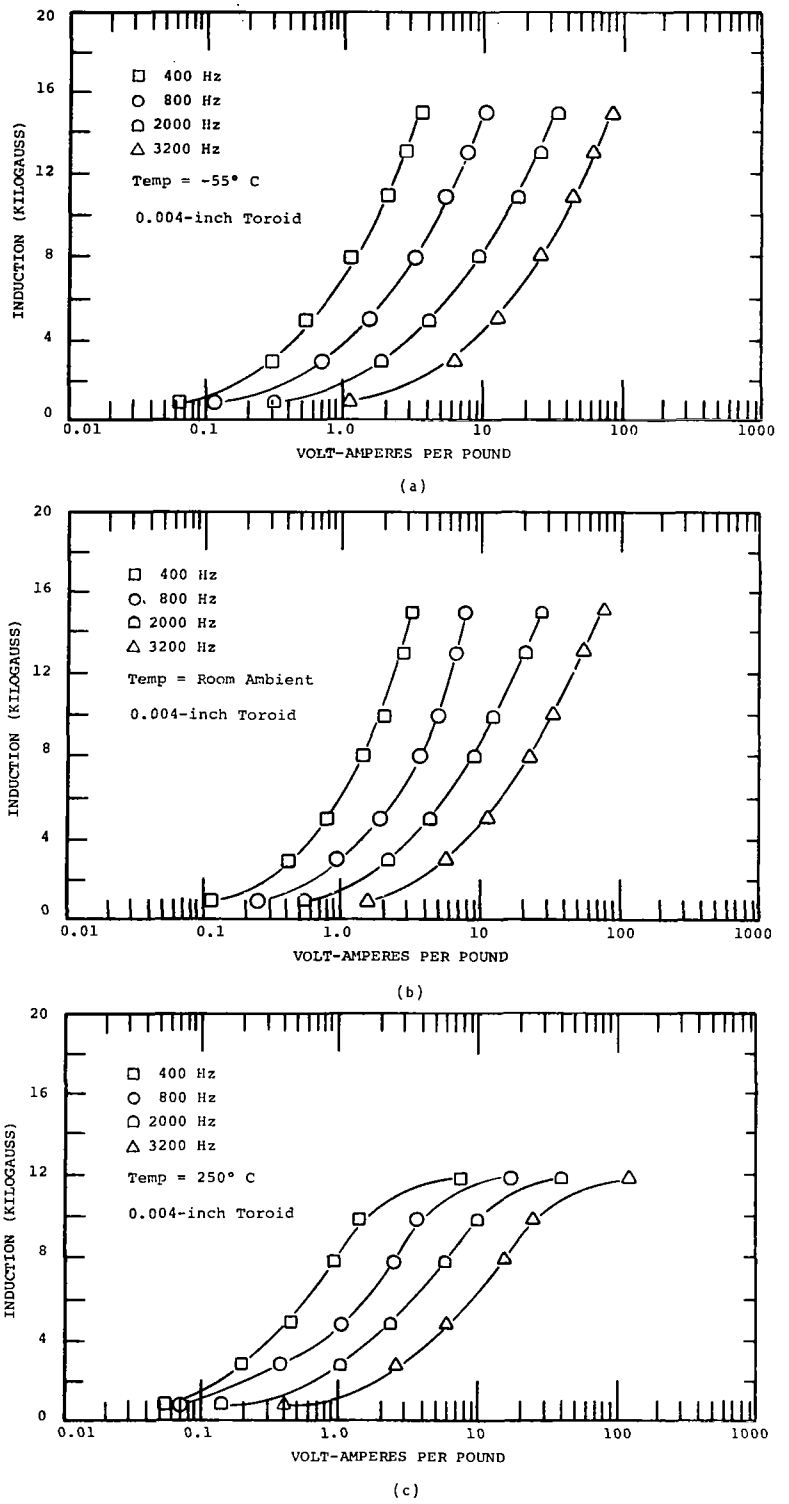

Figure 24. - $P_{a,\ sq,}$ Apparent Power vs Induction and Frequency, 0.004-Inch 50%Ni-50%Fe Toroid, Grain Oriented

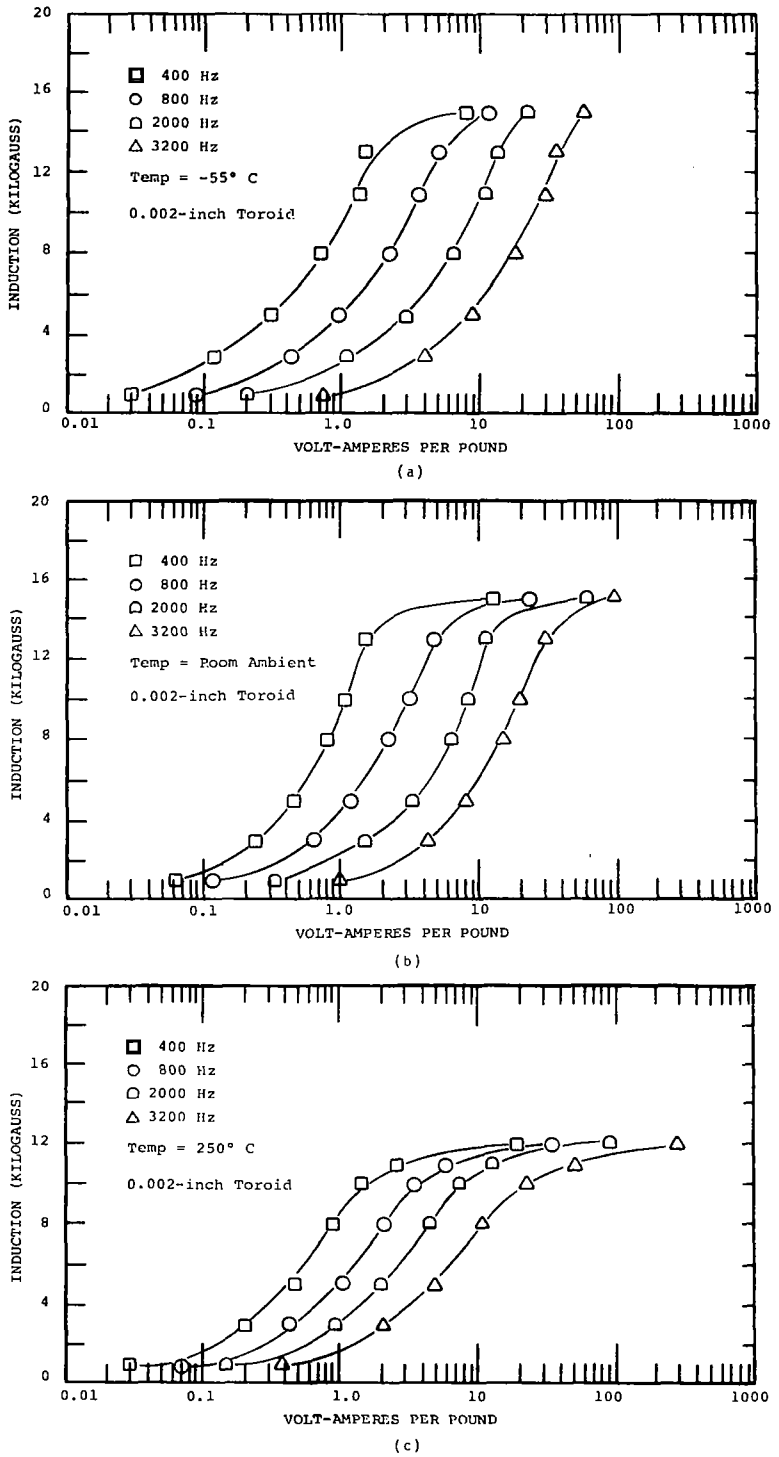

Figure 25. - $P_{a,\ sq,}$ Apparent Power vs Induction and Frequency, 0.002-Inch 50%Ni-50%Fe Toroid, Grain Oriented

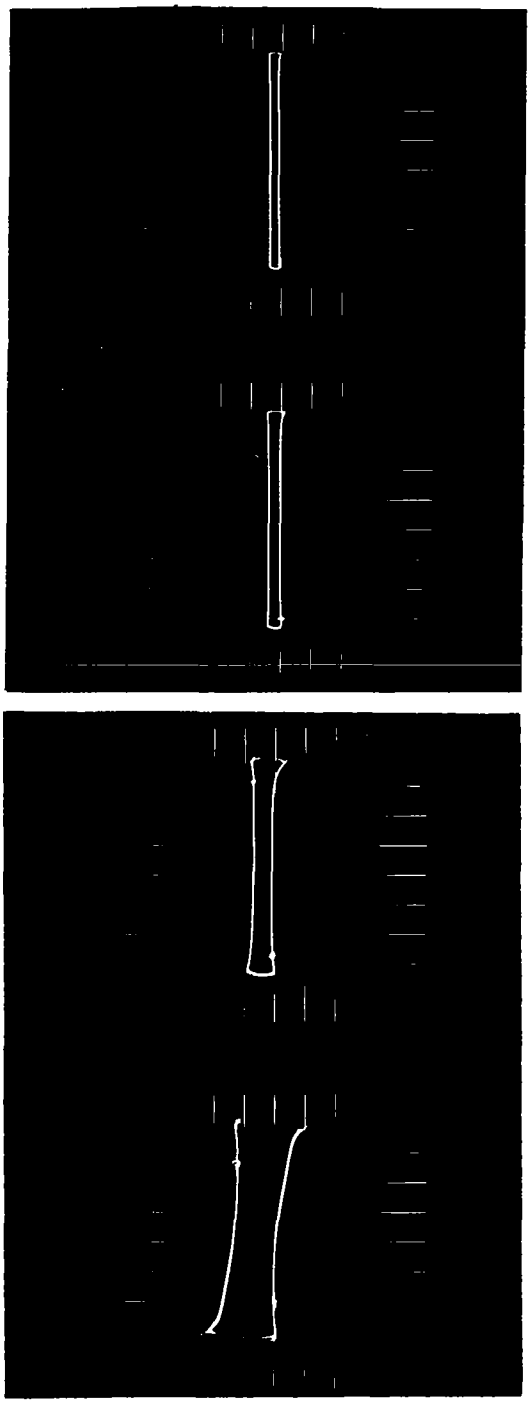

(a) f = 400 Hz
B = 4 kG/div
H = 5 Oe/div

(b) f = 800 Hz
B = 4 kG/div
H = 5 Oe/div

(c) f = 1600 Hz
B = 4 kG/div
H = 5 Oe/div

(d) f = 3200 Hz
B = 4 kG/div
H = 5 Oe/div

Figure 26.– AC Hysteresis Loop, Square Wave Excitation, 400, 800, 1600, and 3200 Hz, 0.004-Inch 50%Ni-50%Fe Toroid, Grain Oriented, -55° C

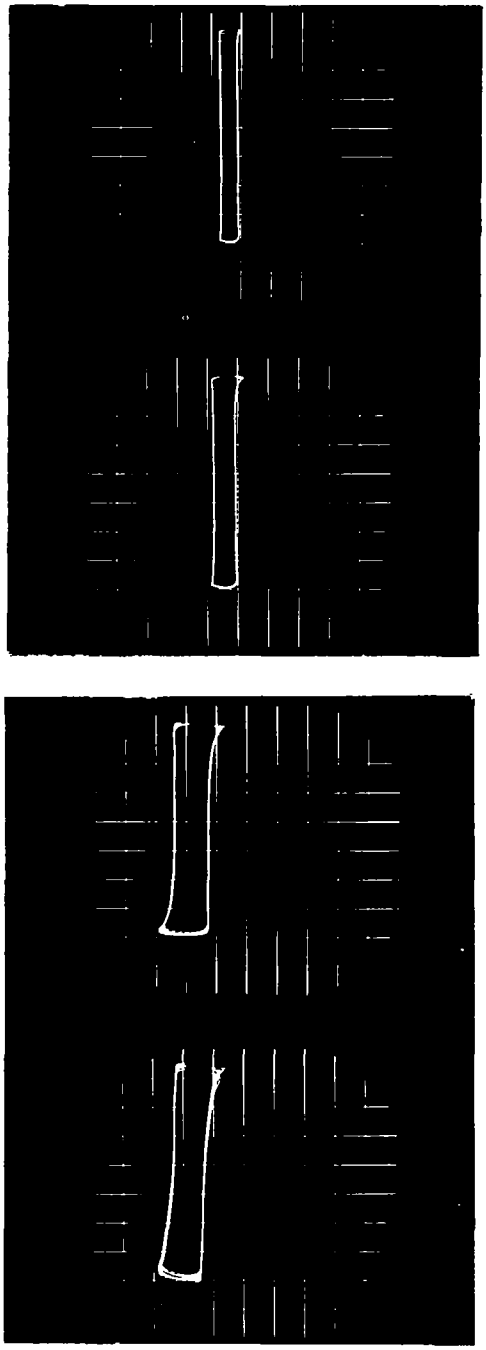

(a) f = 400 Hz
B = 4 kG/div
H = 2.5 Oe/div

(b) f = 800 Hz
B = 4 kG/div
H = 2.5 Oe/div

(c) f = 1600 Hz
B = 4 kG/div
H = 2.5 Oe/div

(d) f = 3200 Hz
B = 4 kG/div
H = 6.25 Oe/div

Figure 27.- AC Hysteresis Loop, Square Wave Excitation, 400, 800, 1600, and 3200 Hz, 0.004-Inch 50%Ni-50%Fe Toroid, Grain Oriented, Room Ambient

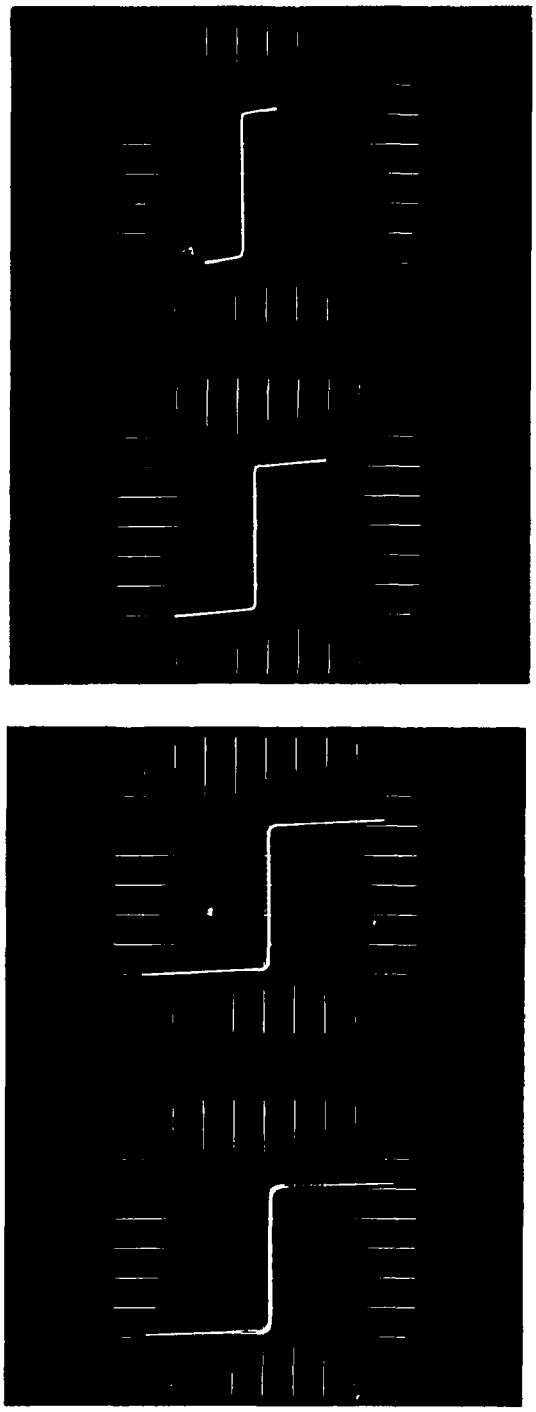

(a) f = 400 Hz
B = 5 kG/div
H = 100 Oe/div

(b) f = 800 Hz
B = 5 kG/div
H = 100 Oe/div

(c) f = 1600 Hz
B = 5 kG/div
H = 100 Oe/div

(d) f = 3200 Hz
B = 5 kG/div
H = 100 Oe/div

Figure 28.- AC Hysteresis Loop, Square Wave Excitation, 400, 800, 1600, and 3200 Hz, 0.004-Inch 50%Ni-50%Fe Toroid, Grain Oriented, 250° C

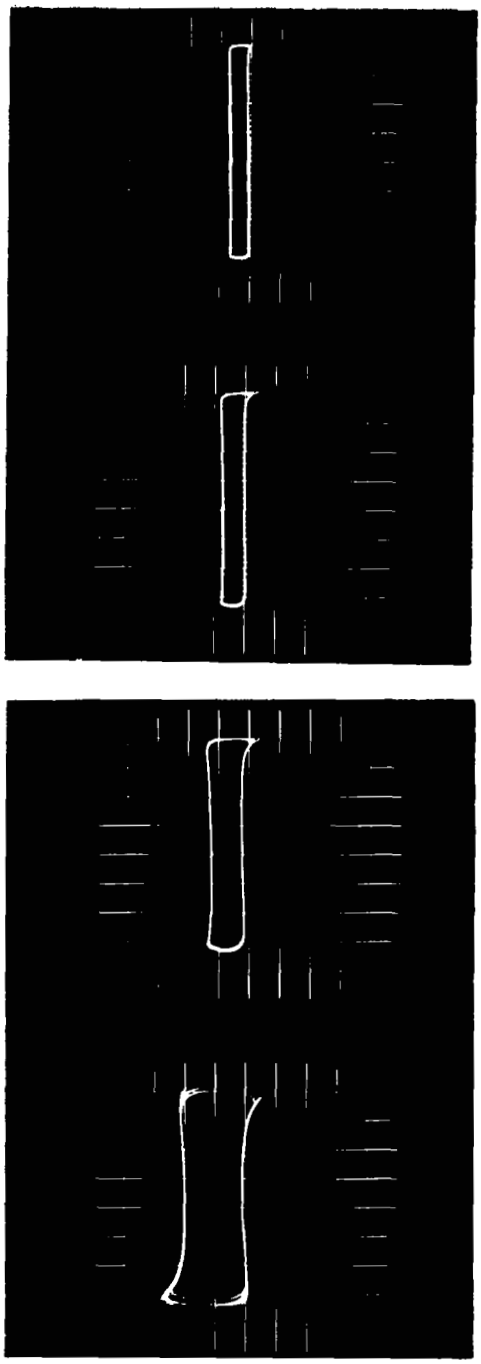

(a) f = 400 Hz
B = 4 kG/div
H = 2.5 Oe/div

(b) f = 800 Hz
B = 4 kG/div
H = 2.5 Oe/div

(c) f = 1600 Hz
B = 4 kG/div
H = 2.5 Oe/div

(d) f = 3200 Hz
B = 4 kG/div
H = 2.5 Oe/div

Figure 29. - AC Hysteresis Loop, Square Wave Excitation, 400, 800, 1600, and 3200 Hz, 0.002-Inch 50%Ni-50%Fe Toroid, Grain Oriented, -55° C

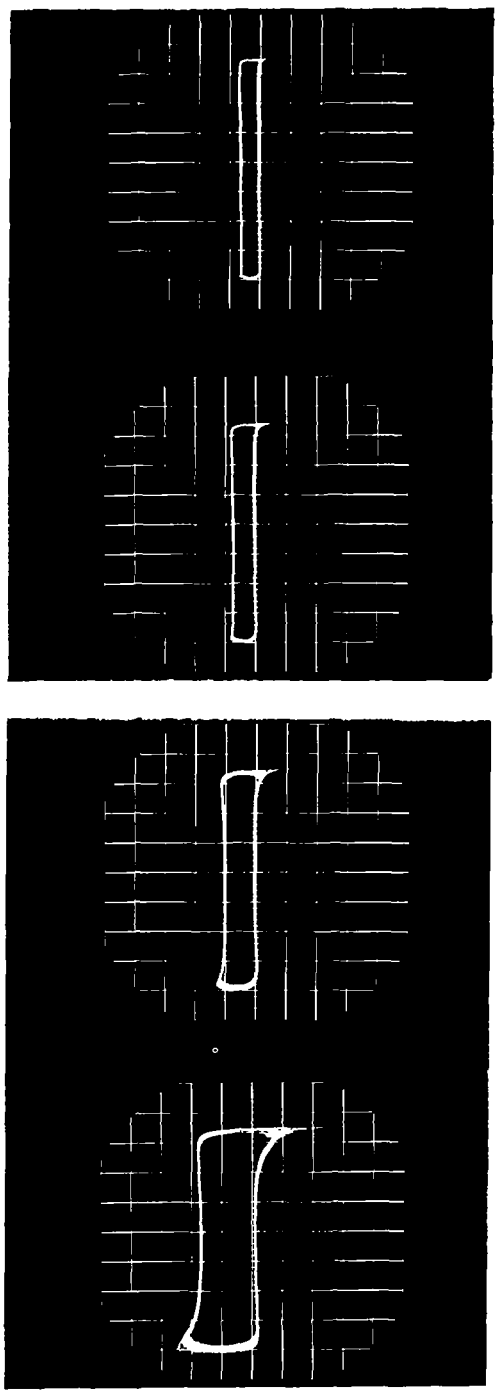

(a) f = 400 Hz
B = 4 kG/div
H = 2.5 Oe/div

(b) f = 800 Hz
B = 4 kG/div
H = 2.5 Oe/div

(c) f = 1600 Hz
B = 4 kG/div
H = 2.5 Oe/div

(d) f = 3200 Hz
B = 4 kG/div
H = 2.5 Oe/div

Figure 30. - AC Hysteresis Loop, Square Wave Excitation, 400, 800, 1600, and 3200 Hz, 0.002-Inch 50%Ni-50%Fe Toroid, Grain Oriented, Room Ambient

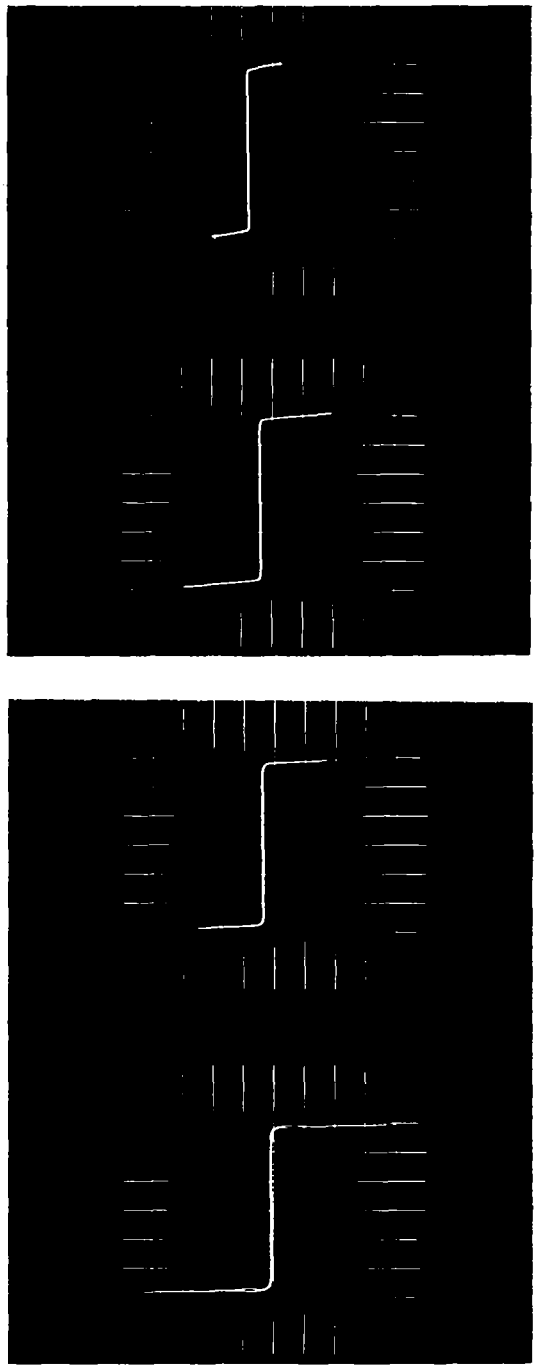

(a) f = 400 Hz
B = 4 kG/div
H = 100 Oe/div

(b) f = 800 Hz
B = 4 kG/div
H = 100 Oe/div

(c) f = 1600 Hz
B = 4 kG/div
H = 100 Oe/div

(d) f = 3200 Hz
B = 4 kG/div
H = 100 Oe/div

Figure 31. - AC Hysteresis Loop, Square Wave Excitation, 400, 800, 1600, and 3200 Hz, 0.002-Inch 50%Ni-50%Fe Toroid, Grain Oriented, 250° C

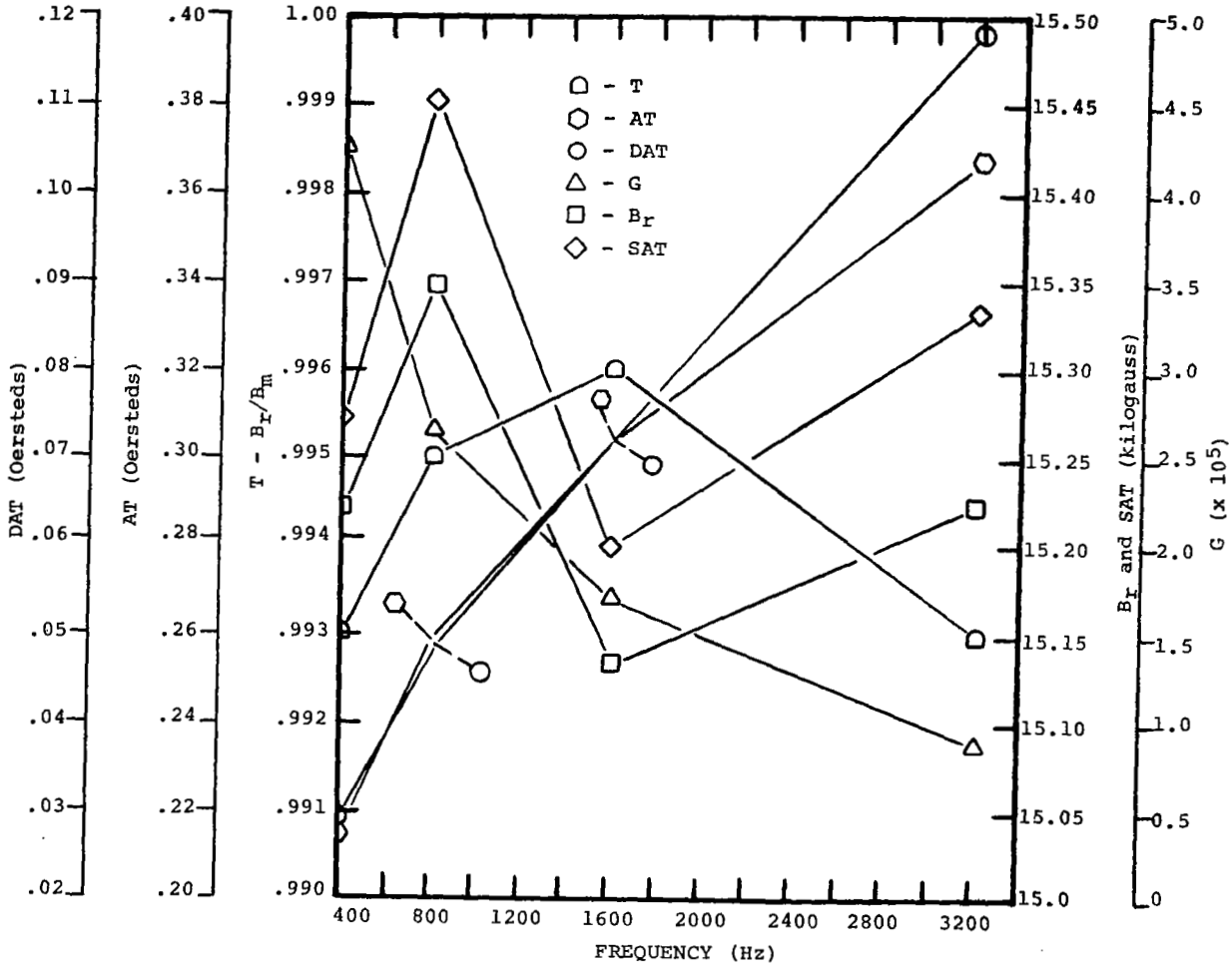

Figure 32. - CCFR Properties, 0.004-Inch 50%Ni-50%Fe Toroid, Grain Oriented, Room Ambient

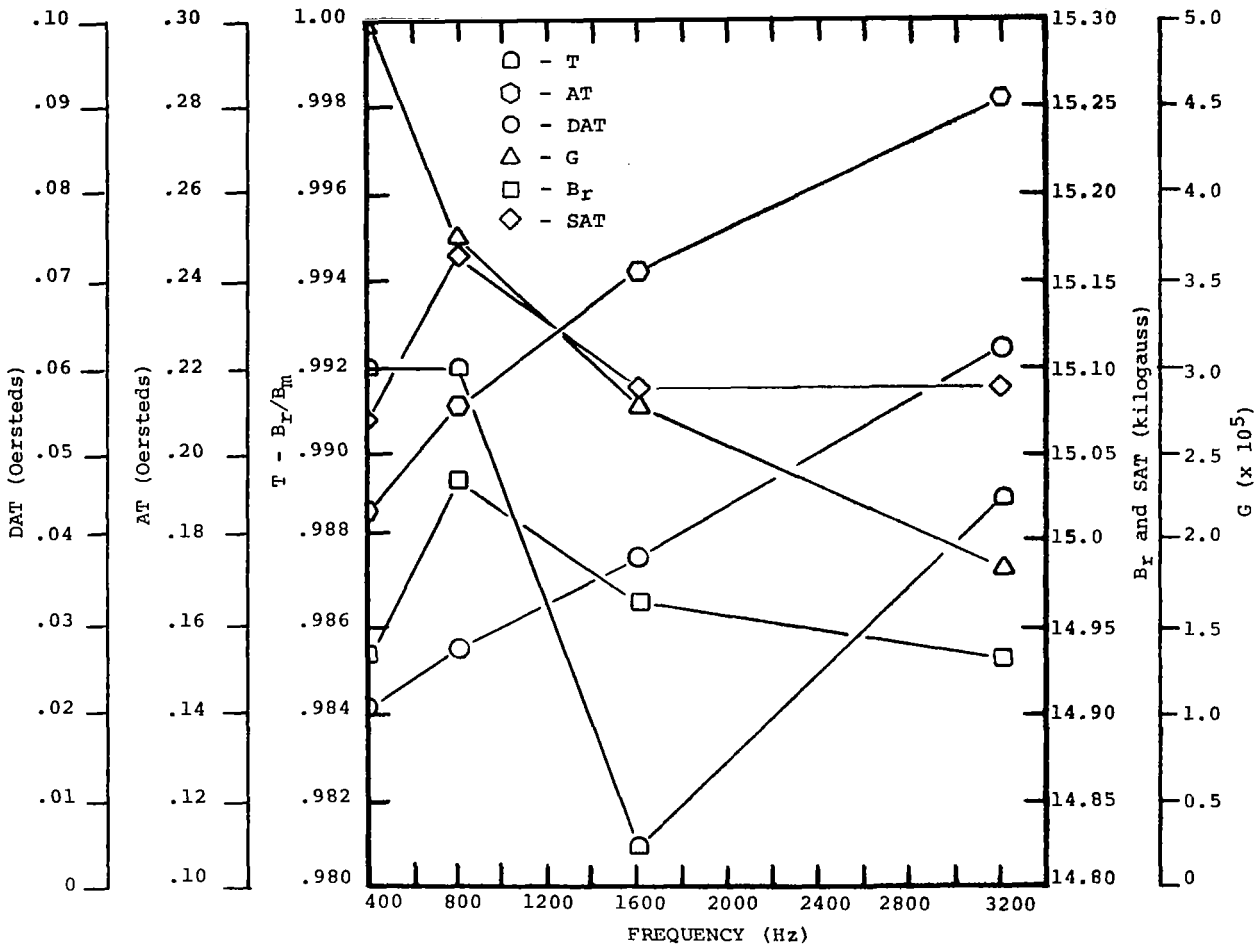

Figure 33. - CCFR Properties, 0.002-Inch 50%Ni-50%Fe Toroid, Grain Oriented, Room Ambient

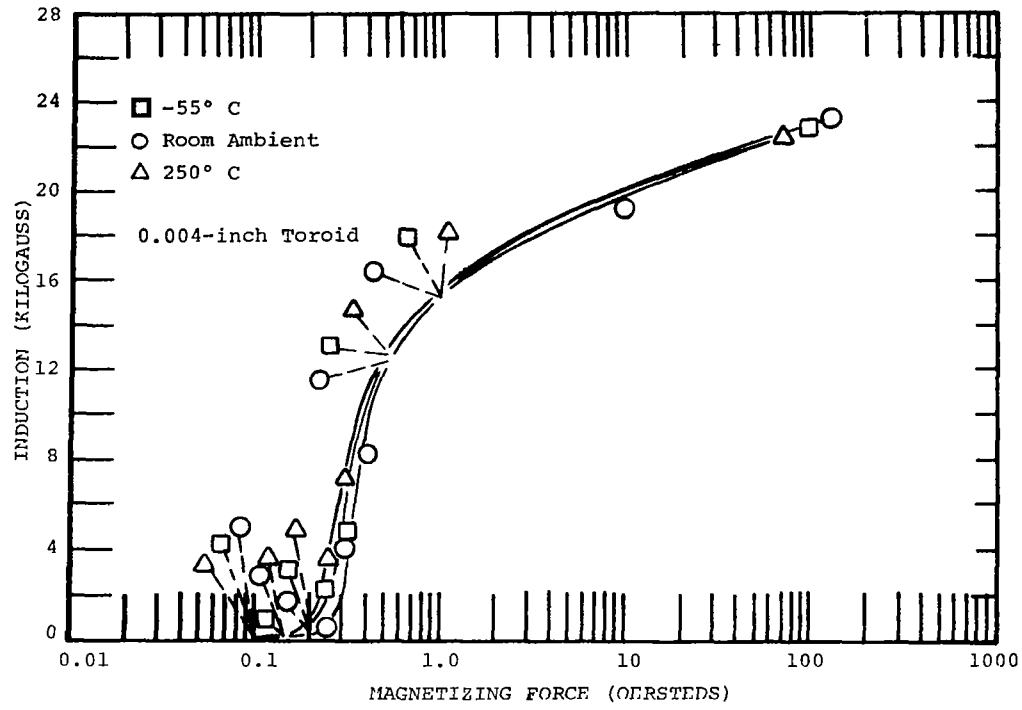

(a)

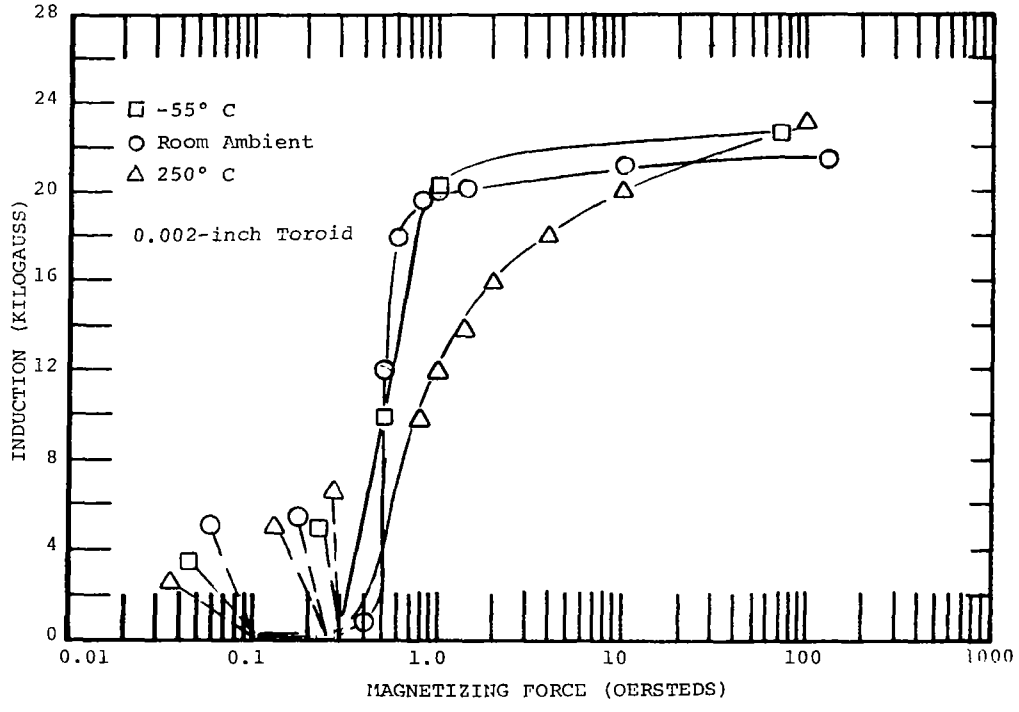

(b)

Figure 34. - DC Magnetization, 0.004- and 0.002-Inch 49%Co-2%V-49%Fe Toroid, Magnetic Field Annealed

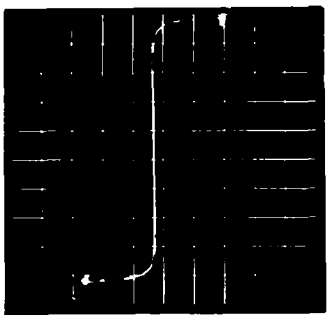

B = 5 kG/div

H = 20 Oe/div

T = -55° C

(a)

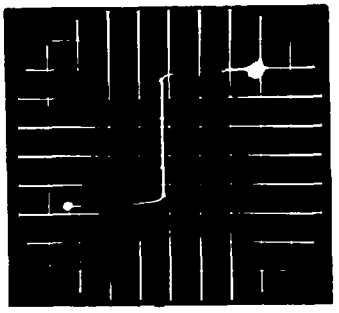

B = 10 kG/div

H = 20 Oe/div

T = Room Ambient

(b)

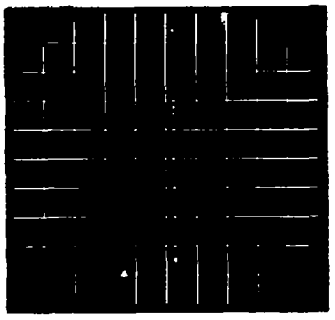

B = 5 kG/div

H = 20 Oe/div

T = 250° C

(c)

Figure 35.- DC Hysteresis Loop, 0.002-Inch 49%Co-2%V-49%Fe Toroid, Magnetic Field Annealed

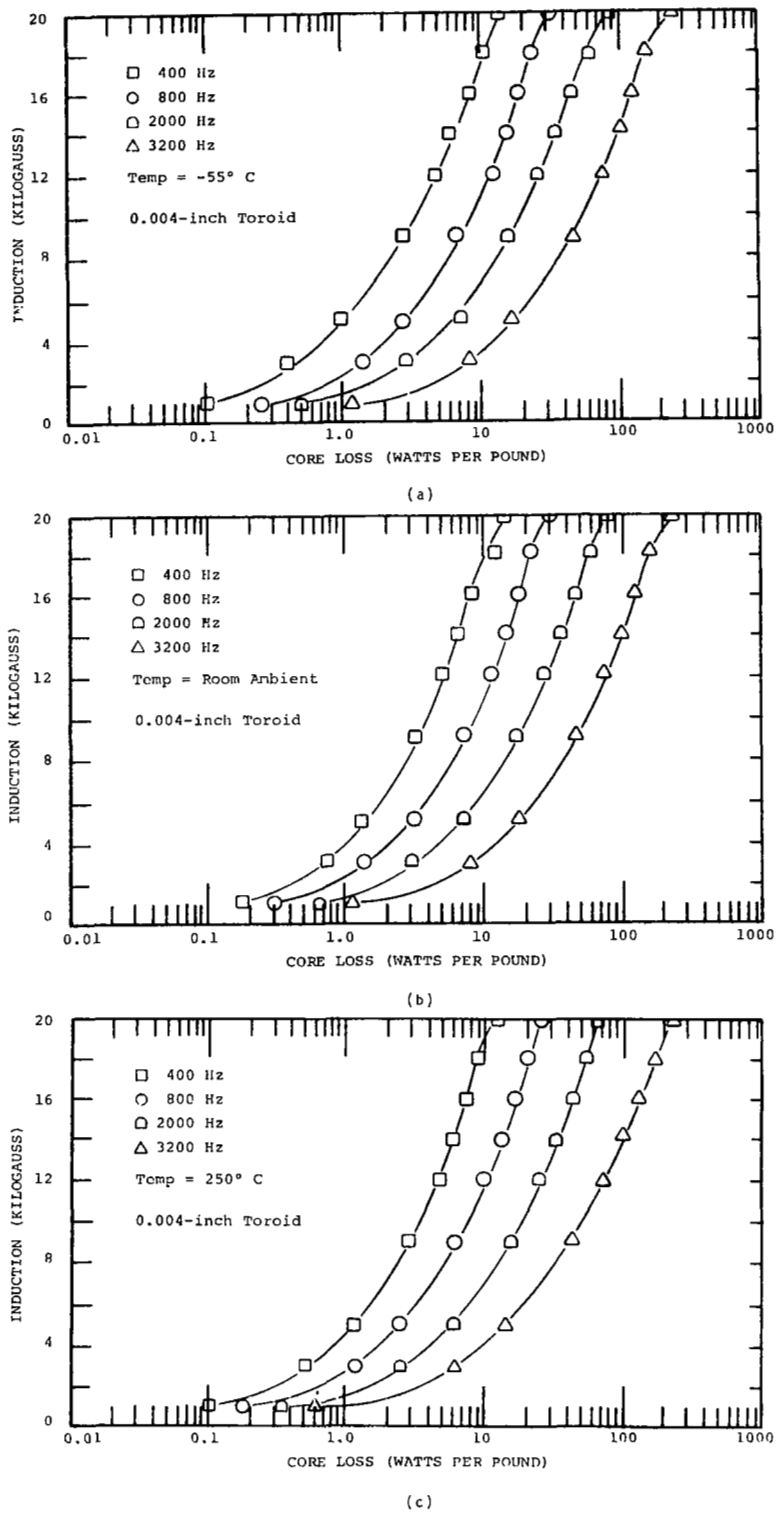

Figure 36. - $P_{c,\ sq,}$ Total Core Loss vs Induction and Frequency, 0.004-Inch 49%Co-2%V-49%Fe Rowland Ring, Magnetic Field Annealed

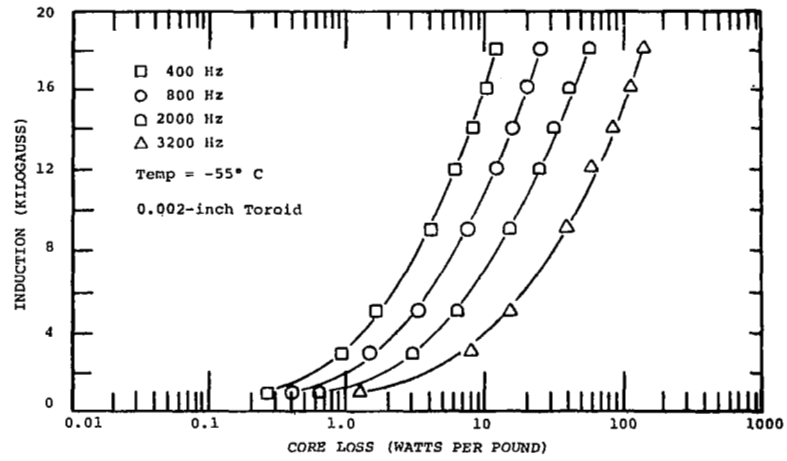

(a)

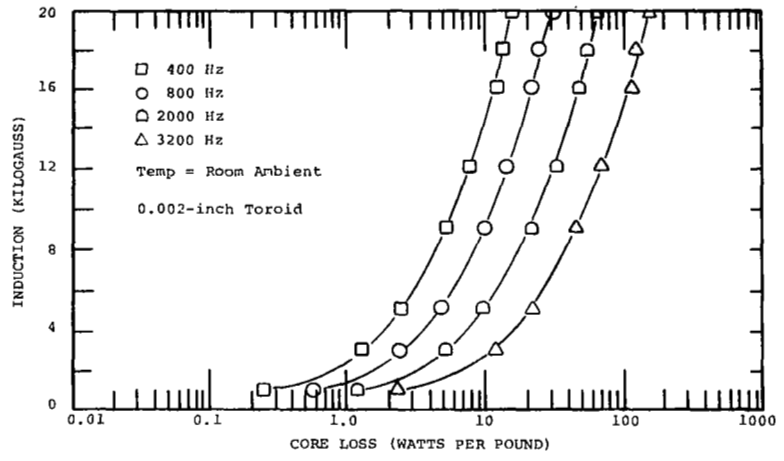

(b)

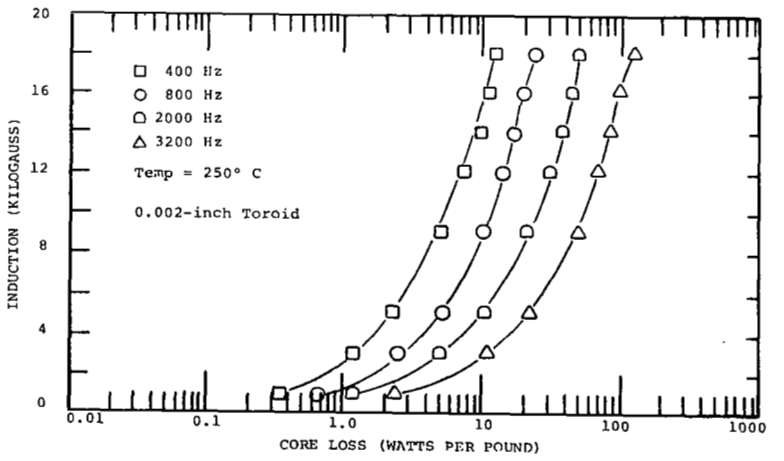

(c)

Figure 37. - $P_{c, sq,}$ Total Core Loss vs Induction and Frequency, 0.002-Inch 49%Co-2%V-49%Fe Toroid, Magnetic Field Annealed

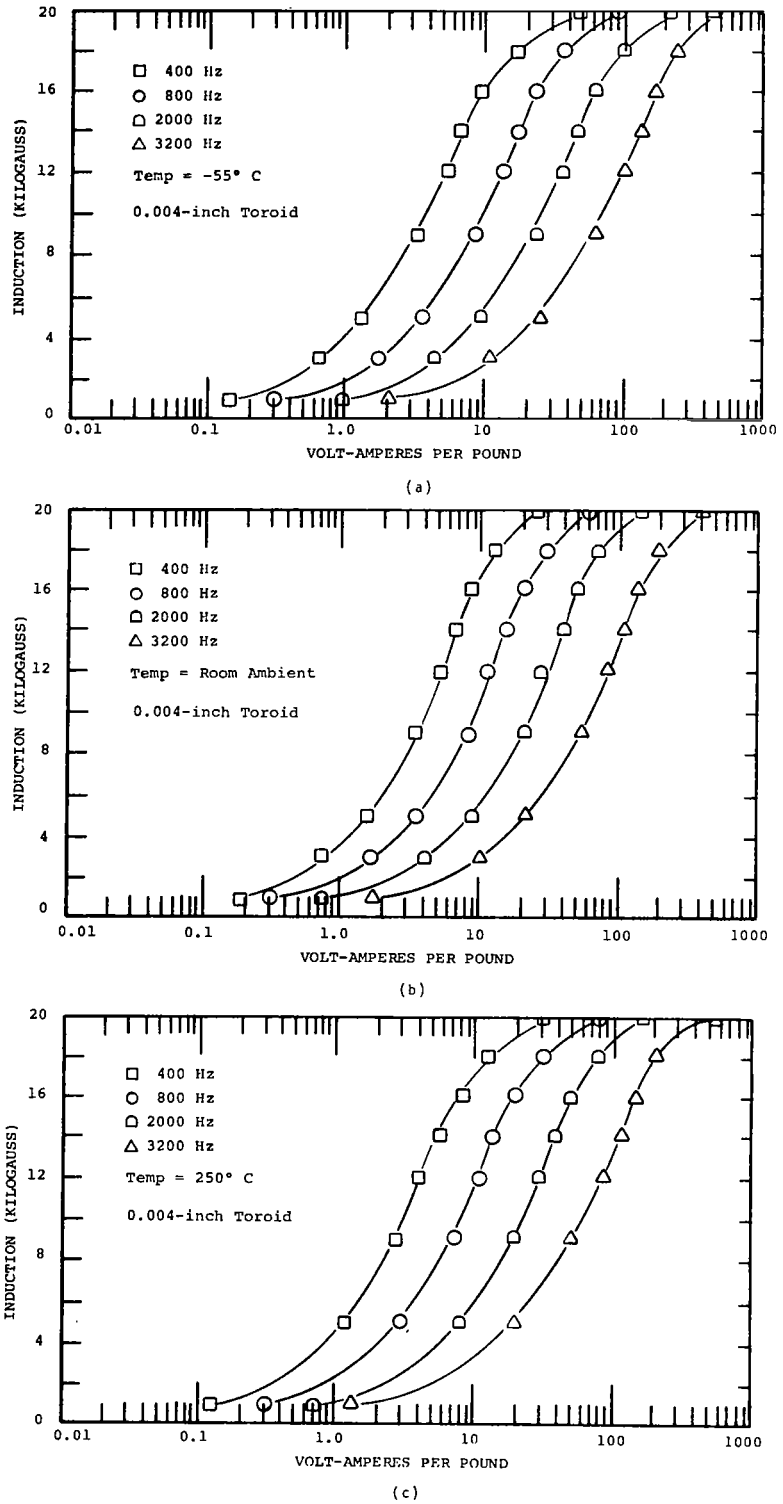

Figure 38. - $P_{a,\ sq,}$ Apparent Power vs Induction and Frequency, 0.004-Inch 49%Co-2%V-49%Fe Rowland Ring, Magnetic Field Annealed

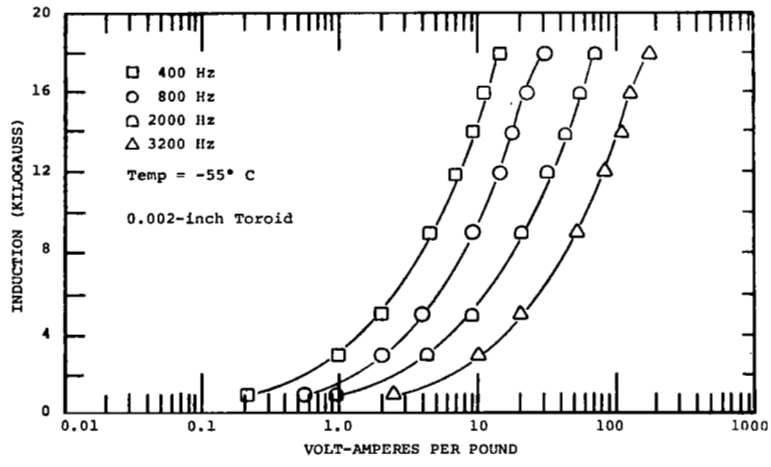

(a)

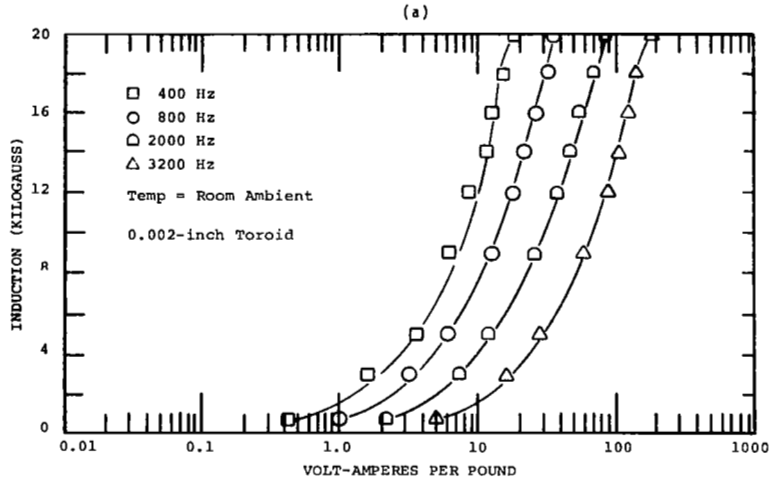

(b)

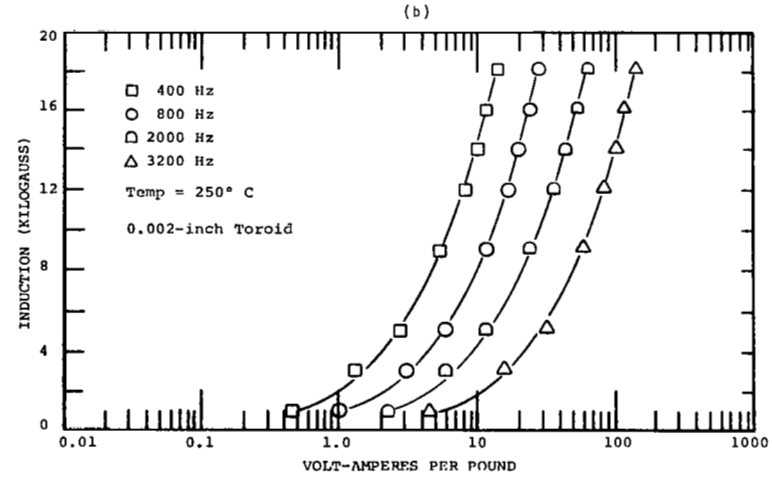

(c)

Figure 39. - $P_{a,\ sq,}$ Apparent Power vs Induction and Frequency, 0.002-Inch Toroid, Magnetic Field Annealed

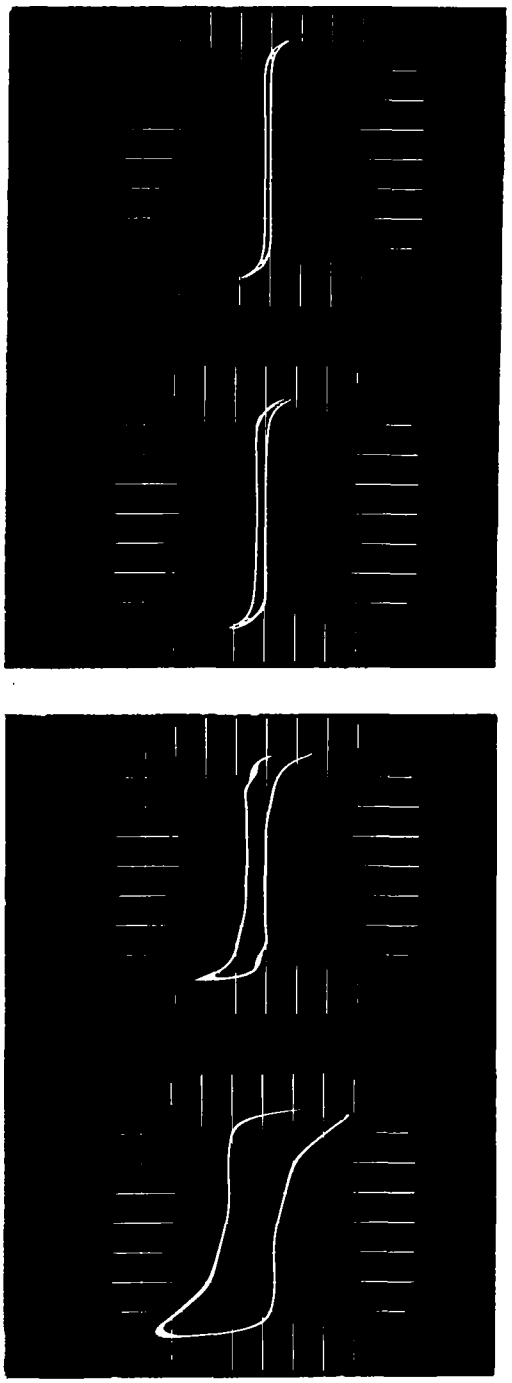

(a) f = 400 Hz
B = 5 kG/div
H = 10 Oe/div

(b) f = 800 Hz
B = 5 kG/div
H = 10 Oe/div

(c) f = 1600 Hz
B = 5 kG/div
H = 10 Oe/div

(d) f = 3200 Hz
B = 5 kG/div
H = 10 Oe/div

Figure 40.— AC Hysteresis Loop, Square Wave Excitation, 400, 800, 1600, and 3200 Hz, 0.004-Inch 49%Co-2%V-49%Fe Rowland Ring, Magnetic Field Annealed, -55° C

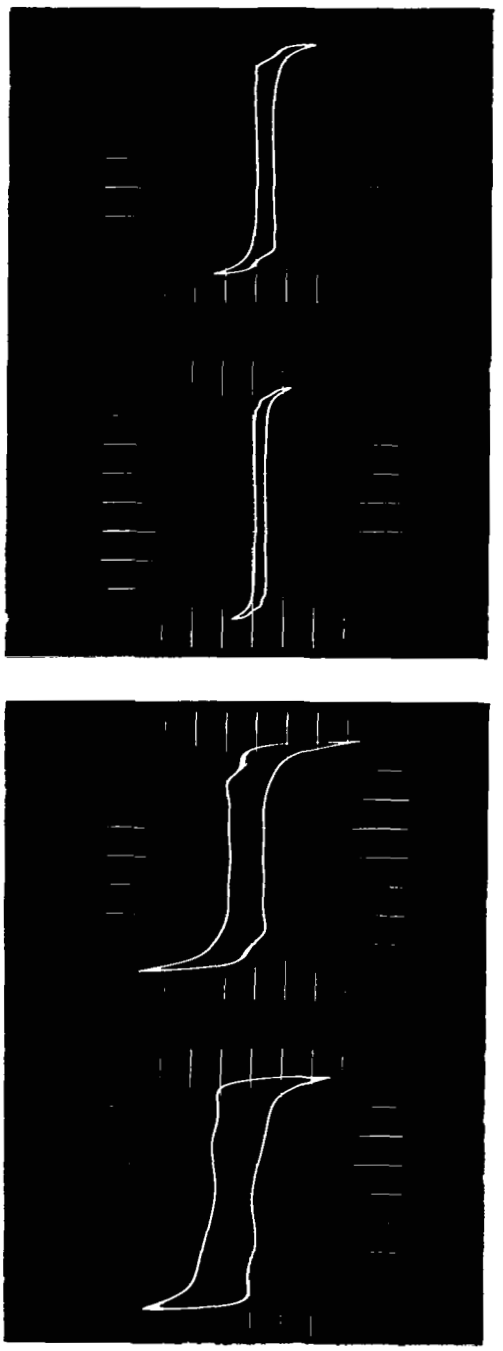

(a) f = 400 Hz
B = 5 kG/div
H = 5 Oe/div

(b) f = 800 Hz
B = 5 kG/div
H = 5 Oe/div

(c) f = 1600 Hz
B = 5 kG/div
H = 5 Oe/div

(d) f = 3200 Hz
B = 5 kG/div
H = 10 Oe/div

Figure 41. - AC Hysteresis Loop, Square Wave Excitation, 400, 800, 1600, and 3200 Hz, 0.004-Inch 49%Co-2%V-49%Fe Rowland Ring, Magnetic Field Annealed, Room Ambient

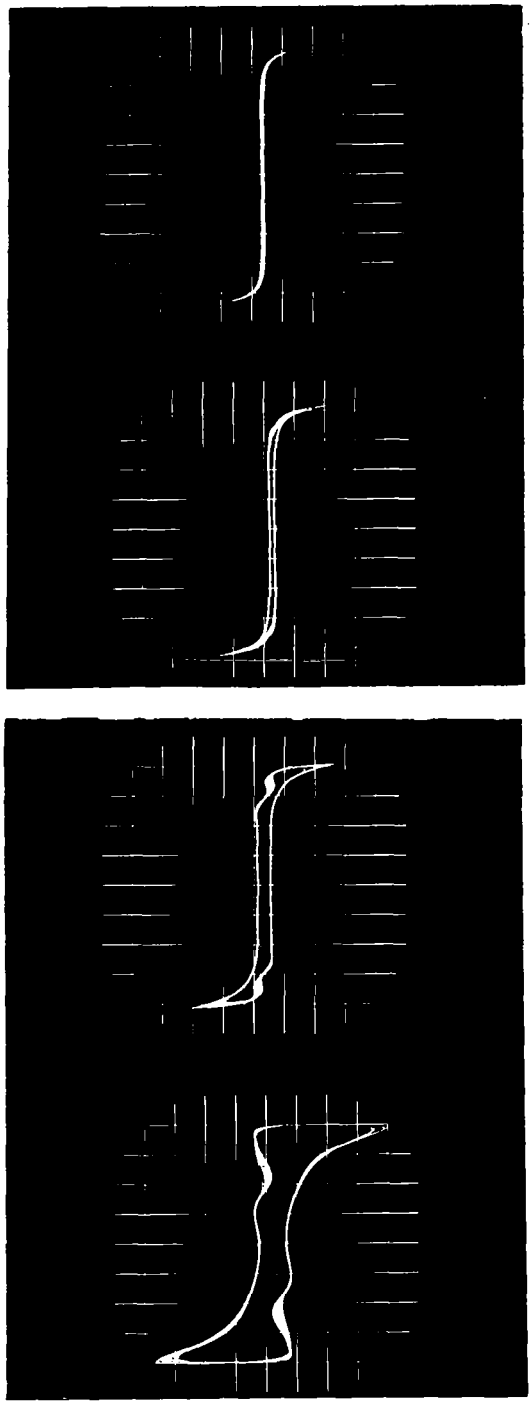

(a) f = 400 Hz
B = 5 kG/div
H = 10 Oe/div

(b) f = 800 Hz
B = 5 kG/div
H = 10 Oe/div

(c) f = 1600 Hz
B = 5 kG/div
H = 10 Oe/div

(d) f = 3200 Hz
B = 5 kG/div
H = 10 Oe/div

Figure 42. - AC Hysteresis Loop, Square Wave Excitation, 400, 800, 1600, and 3200 Hz, 0.004-Inch 49%Co-2%V-49%Fe Rowland Ring, Magnetic Field Annealed, 250° C

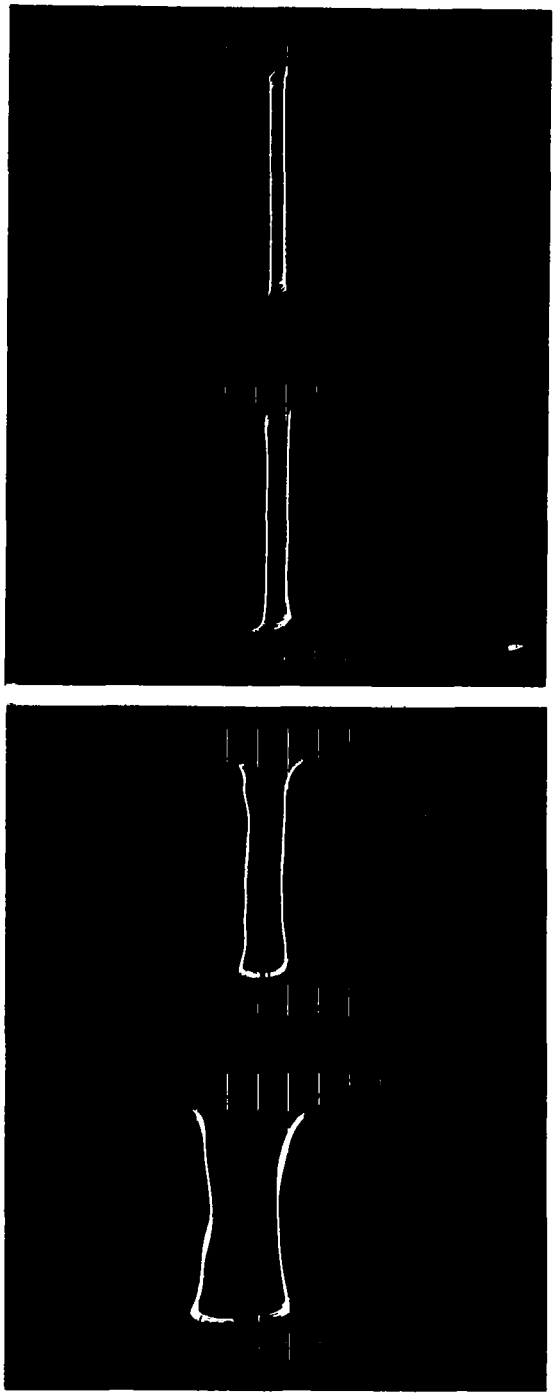

(a) f = 400 Hz
B = 5 kG/div
H = 5 Oe/div

(b) f = 800 Hz
B = 5 kG/div
H = 5 Oe/div

(c) f = 1600 Hz
B = 5 kG/div
H = 5 Oe/div

(d) f = 3200 Hz
B = 5 kG/div
H = 5 Oe/div

Figure 43. - AC Hysteresis Loop, Square Wave Excitation, 400, 800, 1600, and 3200 Hz, 0.002-Inch 49%Co-2%V-49%Fe Toroid, Magnetic Field Annealed, -55° C

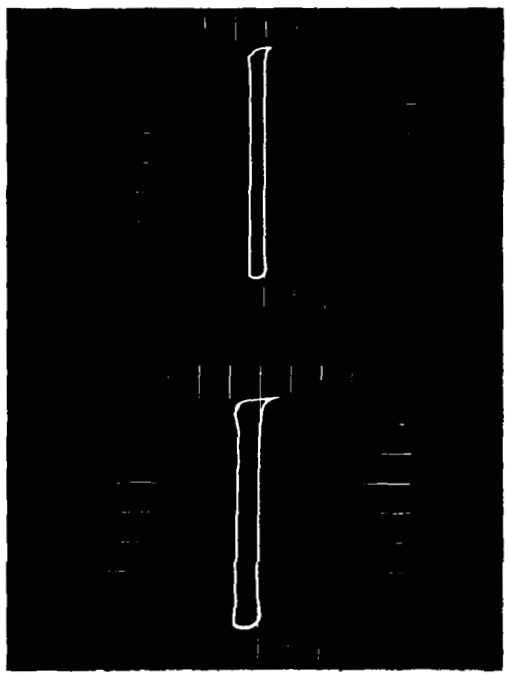

(a) f = 400 Hz
B = 5 kG/div
H = 5 Oe/div

(b) f = 800 Hz
B = 5 kG/div
H = 5 Oe/div

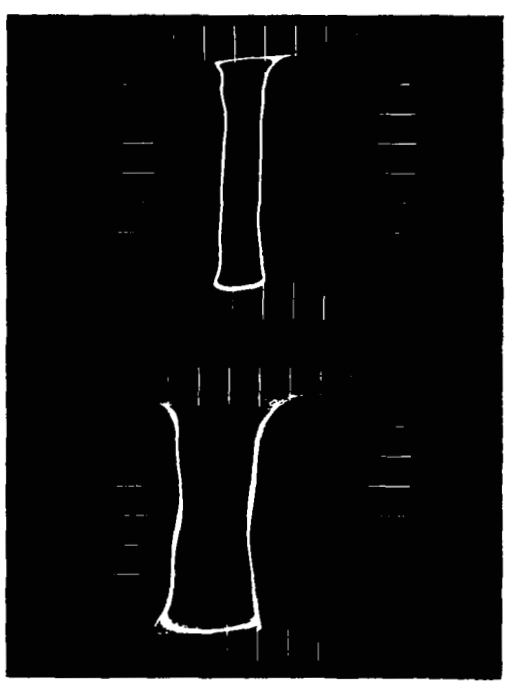

(c) f = 1600 Hz
B = 5 kG/div
H = 5 Oe/div

(d) f = 3200 Hz
B = 5 kG/div
H = 5 Oe/div

Figure 44. - AC Hysteresis Loop, Square Wave Excitation, 400, 800, 1600, and 3200 Hz, 0.002-Inch 49%Co-2%V-49%Fe Toroid, Magnetic Field Annealed, Room Ambient

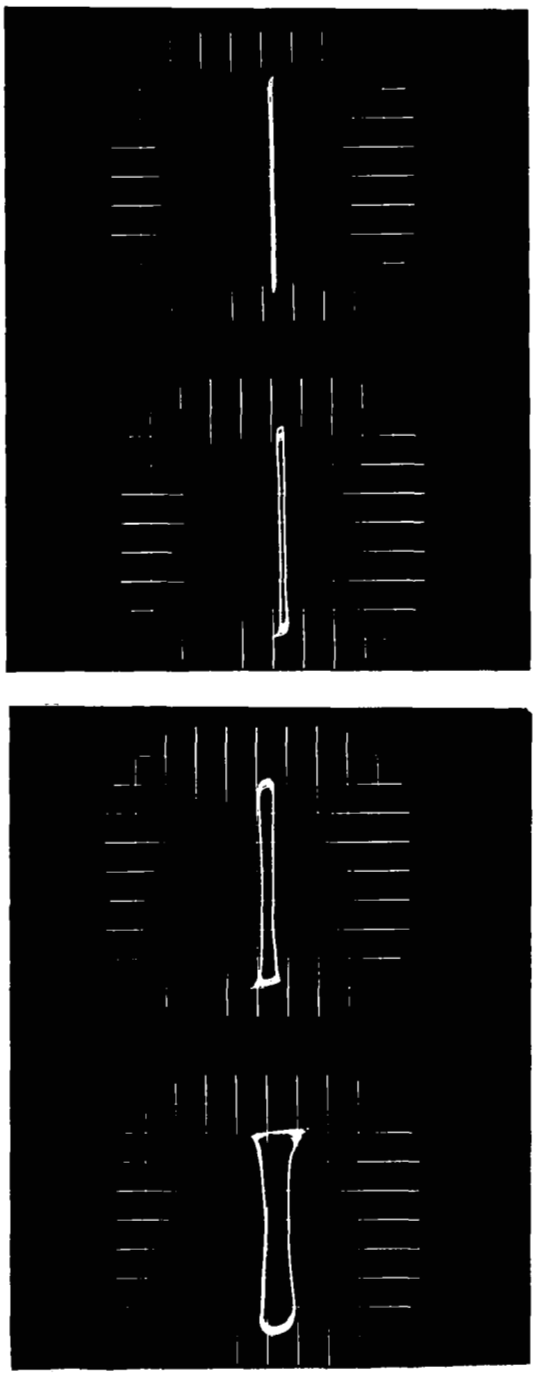

(a) f = 400 Hz
B = 5 kG/div
H = 10 Oe/div

(b) f = 800 Hz
B = 5 kG/div
H = 10 Oe/div

(c) f = 1600 Hz
B = 5 kG/div
H = 10 Oe/div

(d) f = 3200 Hz
B = 5 kG/div
H = 10 Oe/div

Figure 45. - AC Hysteresis Loop, Square Wave Excitation, 400, 800, 1600, and 3200 Hz, 0.002-Inch 49%Co-2%V-49%Fe Toroid, Magnetic Field Annealed, 250° C

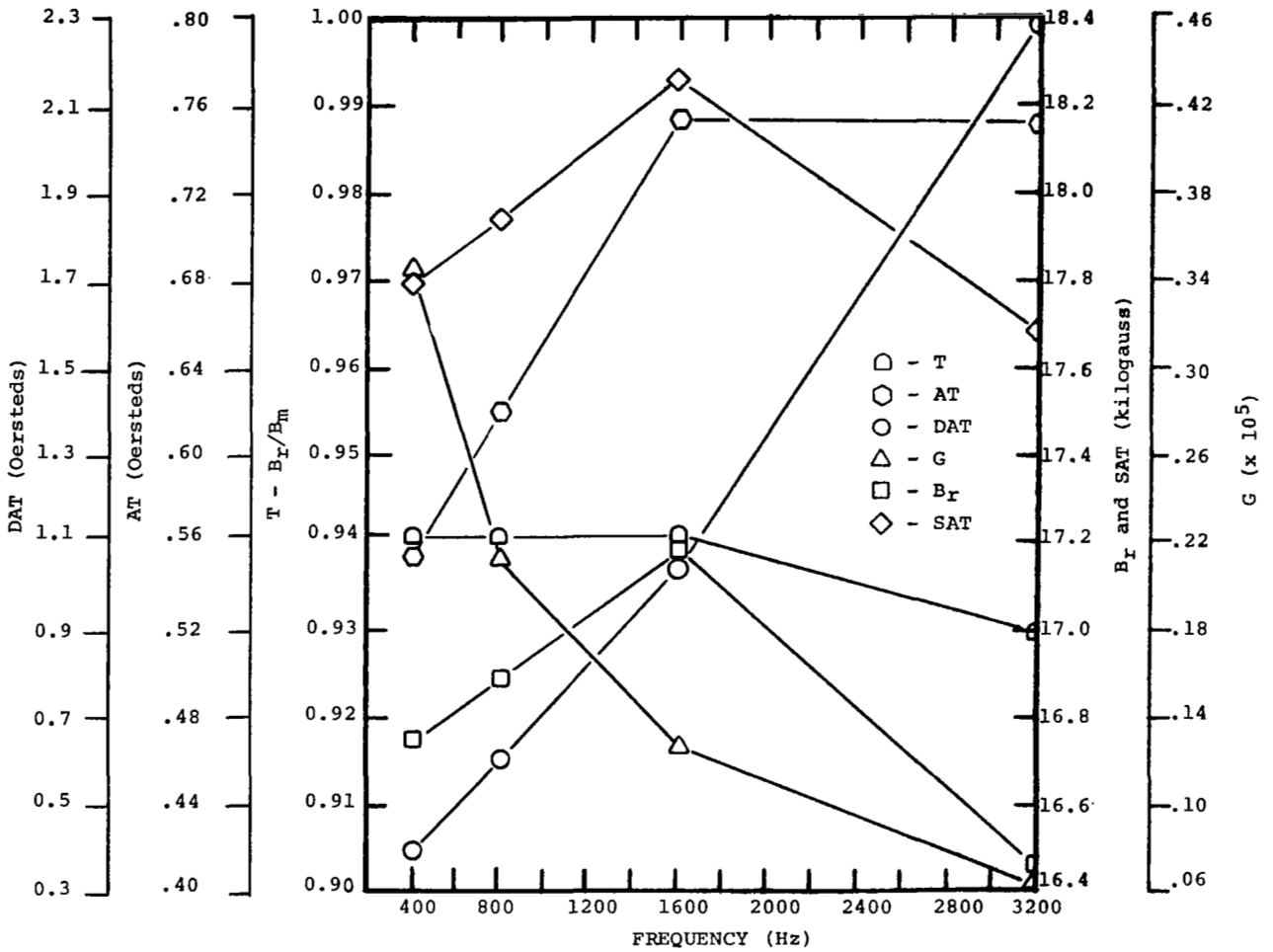

Figure 46. - CCFR Properties, 0.004-Inch 49%Co-2%V-49%Fe Rowland Ring, Magnetic Field Annealed, Room Ambient

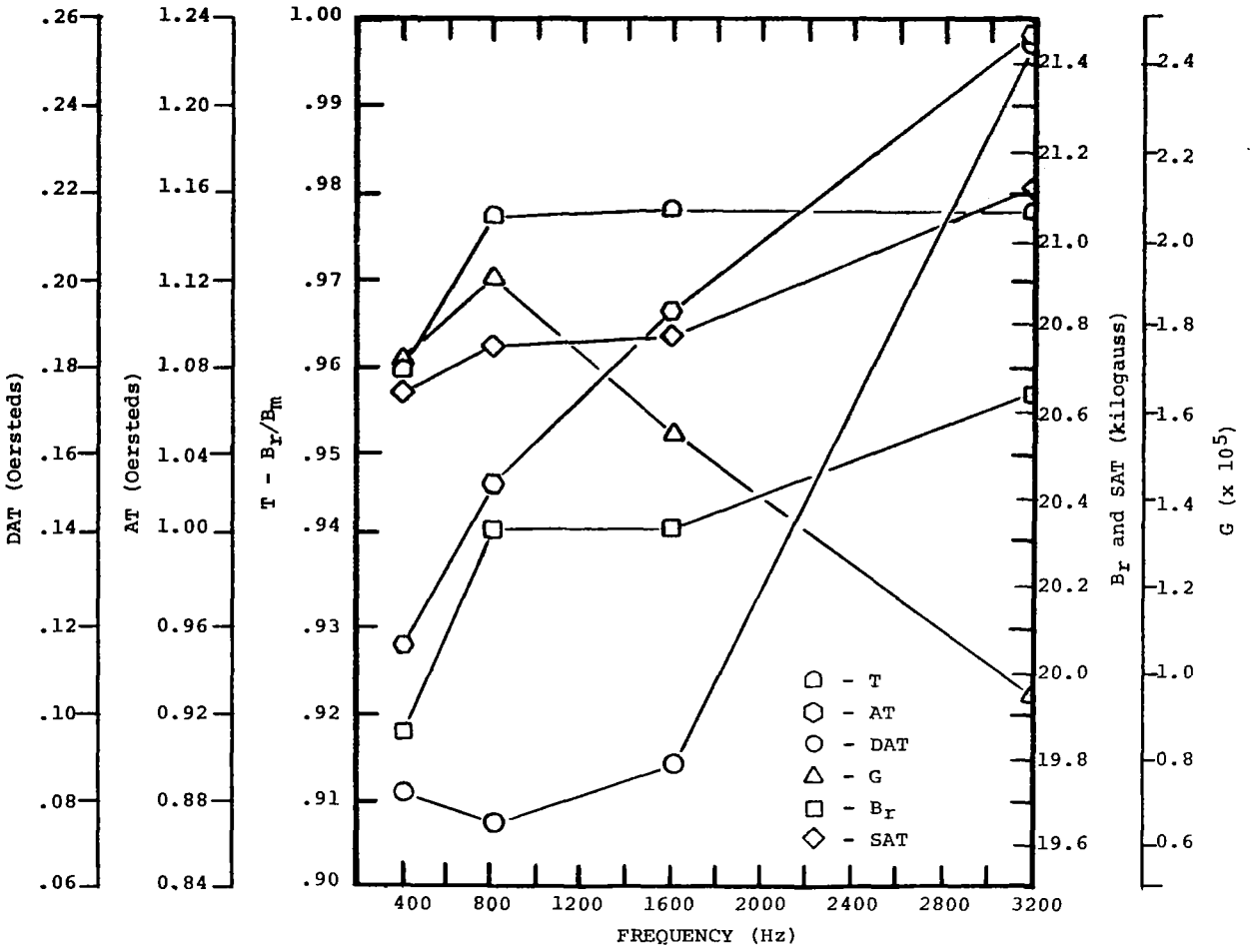

Figure 47. - CCFR Properties, 0.002-Inch 49%Co-2%V-49%Fe Toroid, Magnetic Field Annealed Room Ambient

The AT and DAT values of both the laminated ring and the toroid increase with frequency reflecting the fact that the magnetization loop widens with increased frequency. Another consequence of this increase in loop width is a drop in gain which shows a decrease in the toroid from 1.7×10^5 to 0.94×10^5 and from 1.75×10^5 to 0.3×10^5 in the laminated ring. The SAT and B_r values show some variations with frequency; in the toroid, SAT increased from 20.65 kG at 400 Hz to 21.12 kG at 3200 Hz, and B_r from 19.86 to 20.64 kG. As expected, both SAT and B_r are considerably higher in the toroid than in the laminated ring core. The loop rectangularity of the toroid is high which is reflected in a high T value, 0.98, of this material. This value compares favorably with a T value of 0.94 for the laminated ring.

Singly Grain Oriented Silicon Steel. - Two tape thicknesses were evaluated: 0.002-inch and 0.004-inch.

DC Magnetization Curves: DC magnetization curves for both gauges at -55° C, room ambient, and 250° C are shown in figure 48. Both thicknesses respond to a change in temperature in the conventional manner. The 0.004-inch-tape toroid is somewhat superior in dc magnetic properties to the 0.002-inch-tape toroid.

DC Hysteresis Loops: The dc hysteresis loops for the 0.002-inch thickness at -55° C, room ambient, and 250° C are shown on figure 49. The loops display considerable rectangularity and no distortion.

AC Core Loss Curves: AC core loss curves for both gauges and temperatures of -55° C, room ambient, and 250° C are shown in figures 50 and 51 that display losses at 400 to 3200 Hz. There is only a small increase in core loss as the tape gauge is increased from 0.002-inch to 0.004-inch; for instance, at 15 kG and room temperature the core loss amounted to 6.8 watts/pound and 7.5 watts/pound for 0.002- and 0.004-inch tapes, respectively.

AC Apparent Power Curves: AC apparent power curves for both gauges are shown on figures 52 and 53 that display exciting volt-amperes at -55° C, room ambient, and 250° C for 400 to 3200 Hz. The volt-ampere values are similar in both gauges; for instance, at 15 kG and room temperature, the apparent power amounted to 7.9 and 8.2 volt-amperes/pound for 0.002- and 0.004-inch tapes, respectively.

AC Hysteresis Loops: AC hysteresis loops for both gauges at -55° C, room ambient, and 250° C are shown on figures 54 through 59 for 400 to 3200 Hz. All of the loops widened with increasing frequency and showed no distortion.

CCFR Properties: The CCFR properties for both gauges are shown on figures 60 and 61. In comparing the two tape thicknesses, the 0.004-inch material displayed a higher 400 Hz SAT value, 16.05 versus 15.1 kG for the 0.002-inch material, as well as a higher 400 Hz B_r value, 15.68 versus 14.83 kG for the 0.002-inch material. However, as the frequency increases both gauges approach at 3200 Hz the same level for both properties, 15.2 kG for SAT and 14.9 kG for B_r. The difference in magnetic quality between these two gauges is probably based on the greater degree of cube-on-edge texture perfection of the 0.004-inch material. There are only slight differences between these two gauges in the other CCFR properties. The T value for both gauges is 0.98.

Doubly Grain Oriented Silicon Steel. - Two different core geometries were evaluated: toroids wound from 0.002-inch tape and cores assembled from 0.006-inch double window (DW) punched laminations. Both geometries were evaluated in the stress relief annealed (SRA) and magnetic field annealed (MFA) condition.

DC Magnetization Curves: DC magnetization curves for both geometries and annealing treatments at -55° C, room ambient, and 250° C are shown in figures 62 and 63.

The dc curves for the 0.002-inch toroids both SRA (figure 62) and MFA (figure 63) show the usual pattern of change with temperature. For instance, in figure 63, the curves show at -55° C as compared to 250° C a decrease in permeability between 0.1 oersted and 1.0 oersted, but an increase in permeability for the fields above 1.0 oersted. The flux density at 10 oersteds is 18.4 kG for -55° C and 18.0 kG for the room ambient curve. At 100 oersteds, the corresponding flux density values are 19.5 and 19 kG. At 250° C the pattern is reversed; there is an increase in permeability between 0.1 oersted and 1.0 oersted and a decrease in permeability above 1.0 oersted.

DC Hysteresis Loops: The dc hysteresis loops for 0.002-inch toroids at -55° C, room ambient, and 250° C are shown in figures 64 and 65. Both the SRA (figure 64) and the MFA (figure 65) display rectangular loops without distortion.

AC Core Loss Curves: AC core loss curves for both geometries and annealing treatments at -55° C, room ambient, and 250° C are shown in figure 66, 67, 68, and 69, that display losses at 400 to 3200 Hz.

The core loss values of the MFA (figures 68 and 69) material are either identical or similar to those of the SRA (figures 66 and 67) material. At -55° C, the core loss of the MFA material is somewhat higher and at 250° C somewhat lower than that of the SRA toroids.

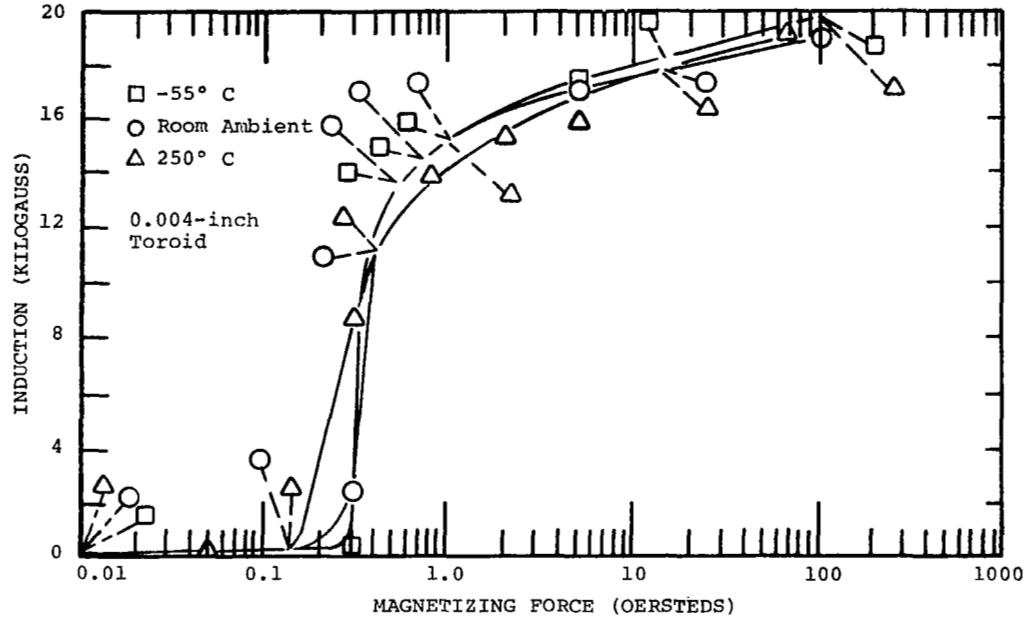

(a)

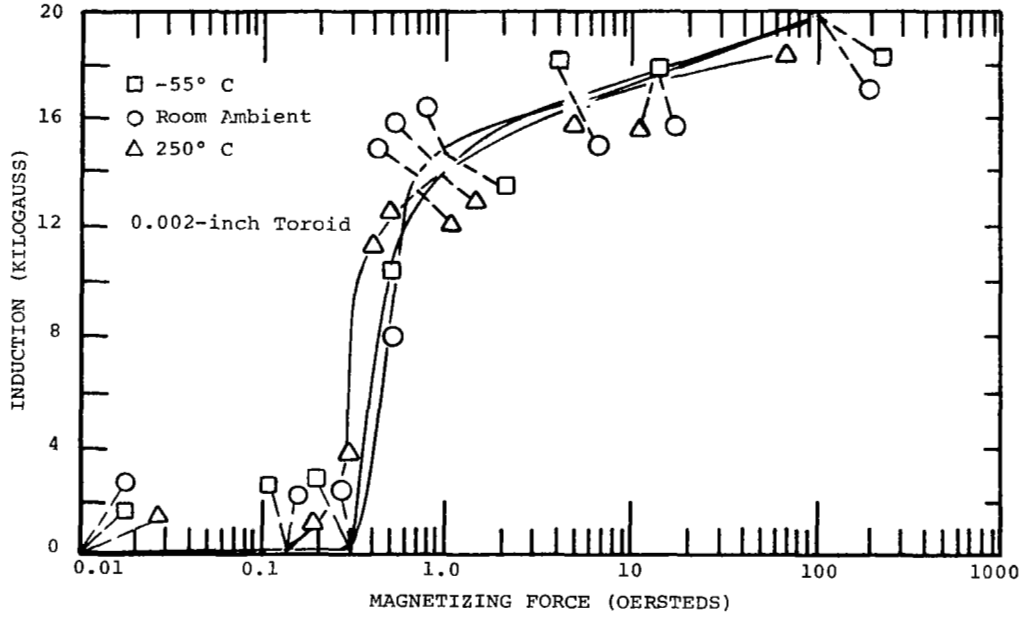

(b)

Figure 48. - DC Magnetization, 0.004- and 0.002-Inch Singly Grain Oriented Silicon Steel Toroid

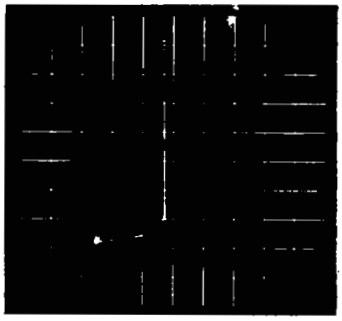

B = 5 kG/div

H = 20 Oe/div

T = -55° C

(a)

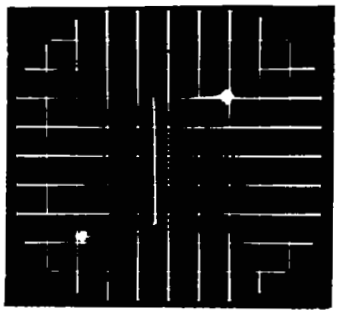

B = 8 kG/div

H = 20 Oe/div

T = Room Ambient

(b)

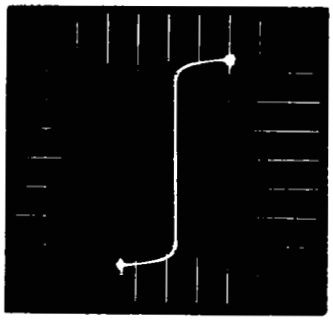

B = 5 kG/div

H = 20 Oe/div

T = 250° C

(c)

Figure 49.- DC Hysteresis Loop, 0.002-Inch Singly Grain Oriented Silicon Steel Toroid

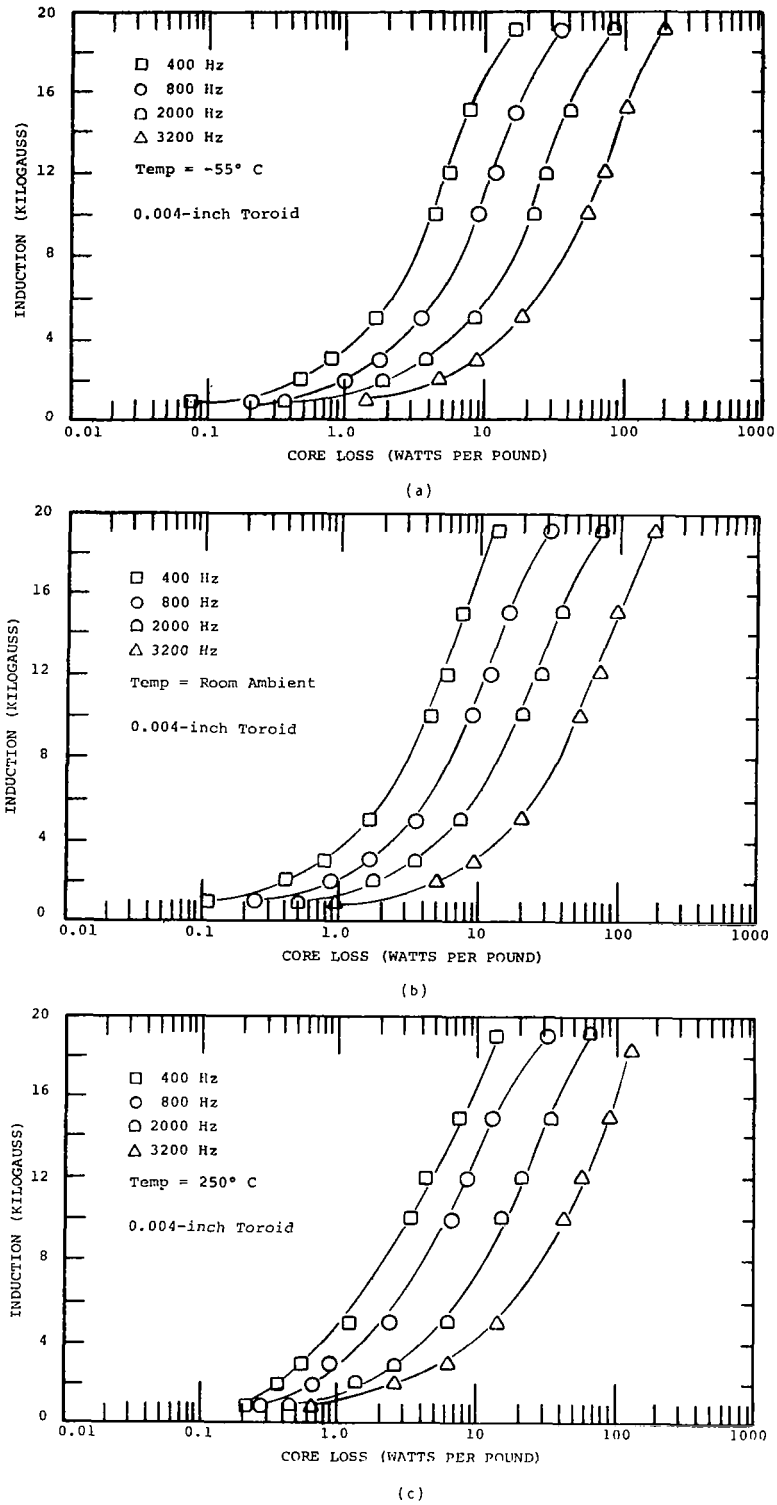

Figure 50. - $P_{c, sq,}$ Total Core Loss vs Induction and Frequency, 0.004-Inch Singly Grain Oriented Silicon Steel Toroid

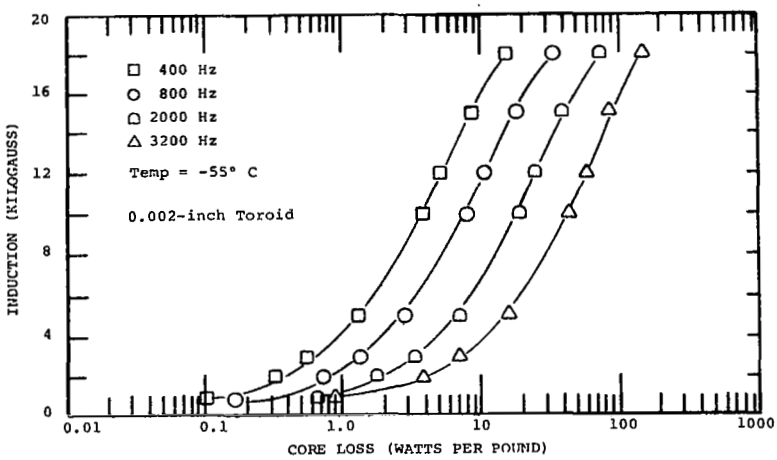

(a)

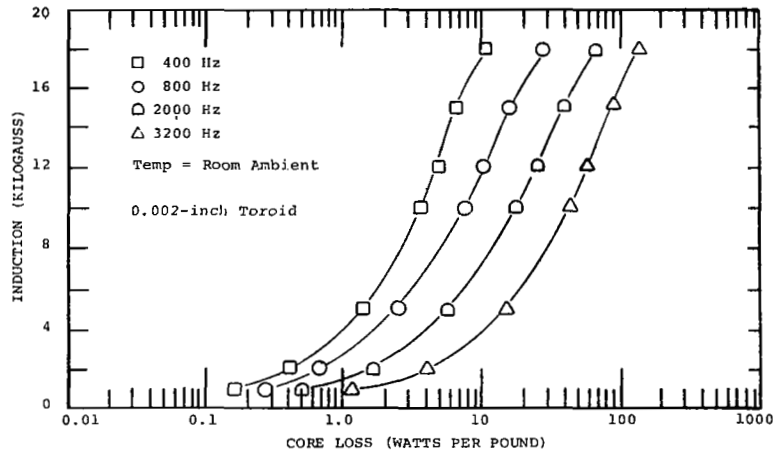

(b)

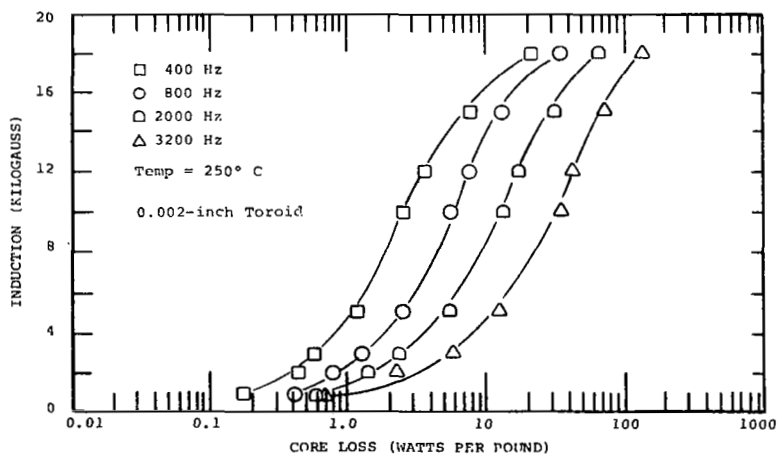

(c)

Figure 51. - $P_{c,\ sq,}$ Total Core Loss vs Induction and Frequency, 0.002-Inch Singly Grain Oriented Silicon Steel Toroid

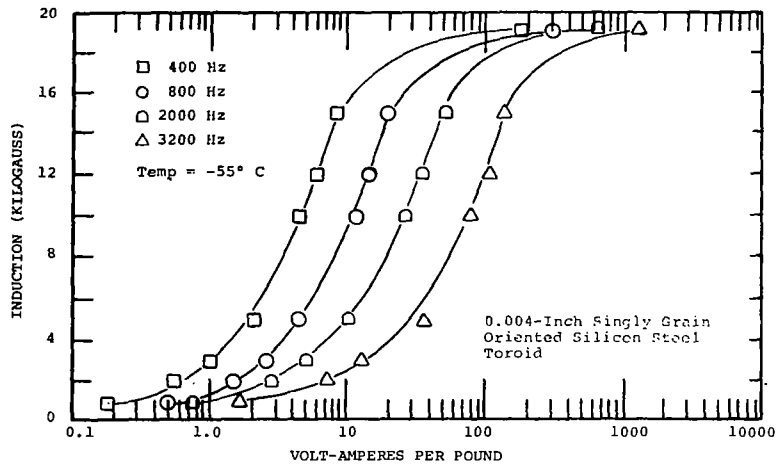

(a)

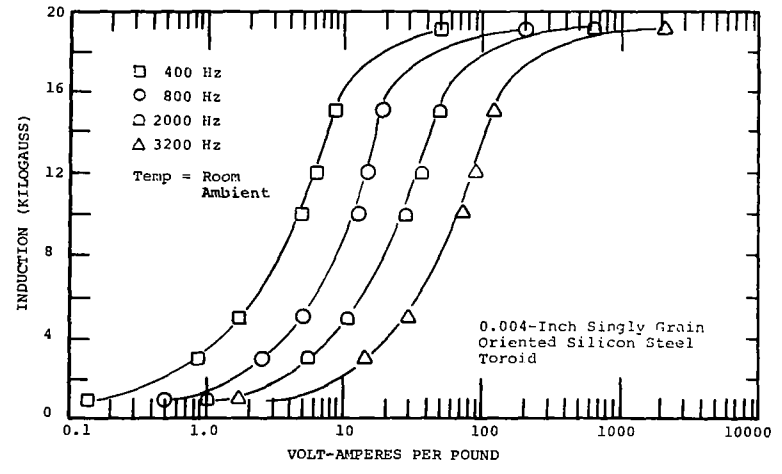

(b)

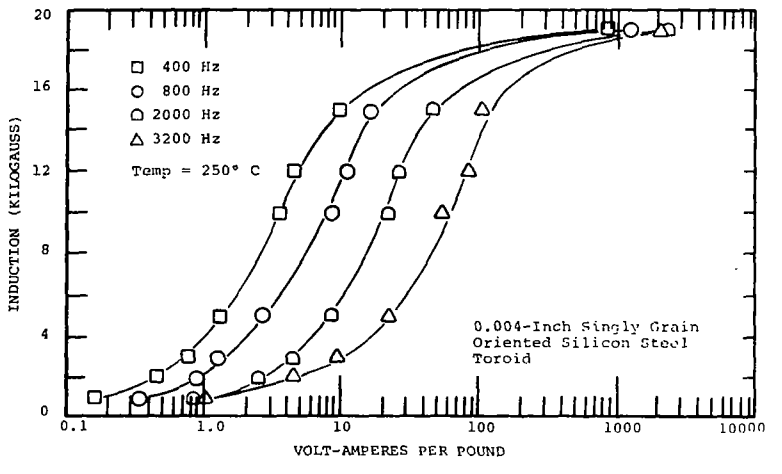

(c)

Figure 52. - $P_{a,\ sq,}$ Apparent Power vs Induction and Frequency, 0.004-Inch Singly Grain Oriented Silicon Steel Toroid

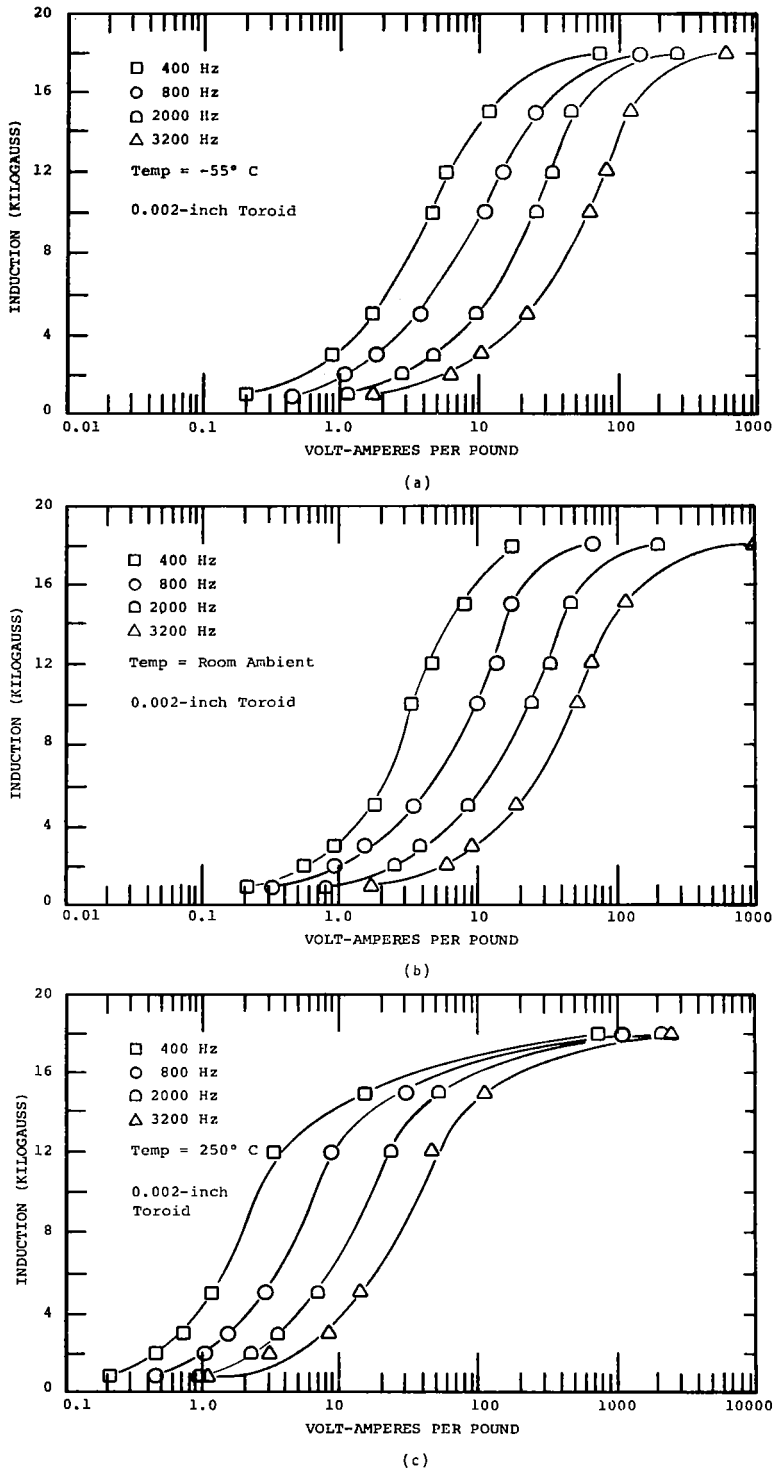

Figure 53. - $P_{a,\ sq,}$ Apparent Power vs Induction and Frequency, 0.002-Inch Singly Grain Oriented Silicon Steel Toroid

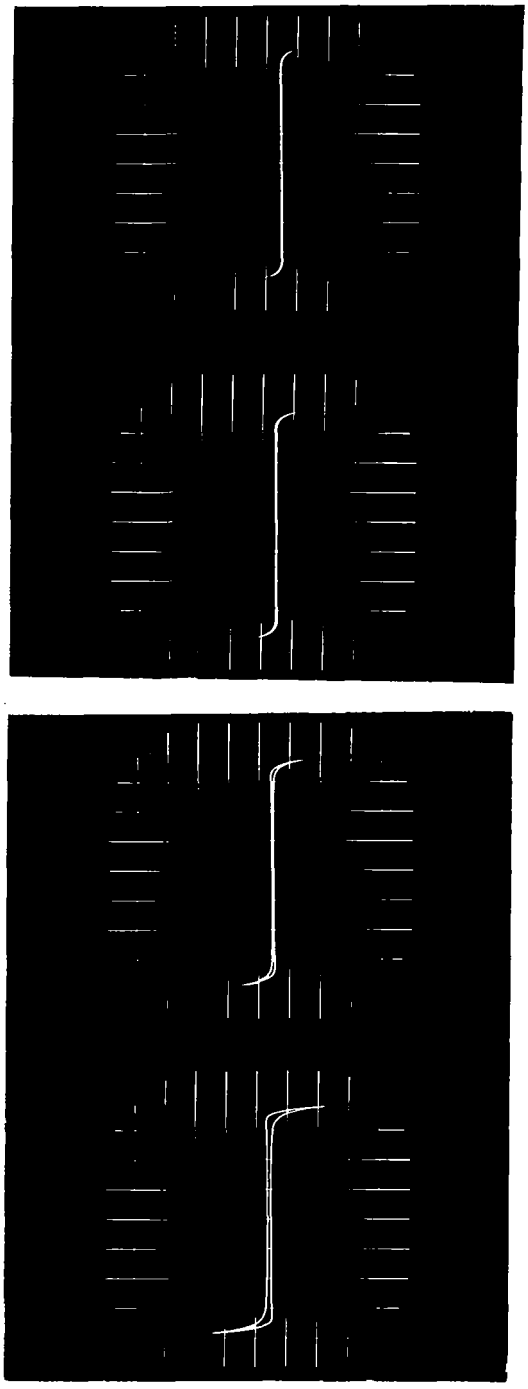

(a) f = 400 Hz
B = 5 kG/div
H = 100 Oe/div

(b) f = 800 Hz
B = 5 kG/div
H = 100 Oe/div

(c) f = 1600 Hz
B = 5 kG/div
H = 100 Oe/div

(d) f = 3200 Hz
B = 5 kG/div
H = 100 Oe/div

Figure 54. - AC Hysteresis Loop, Square Wave Excitation, 400, 800, 1600, and 3200 Hz, 0.004-Inch Singly Grain Oriented Silicon Steel Toroid, -55° C

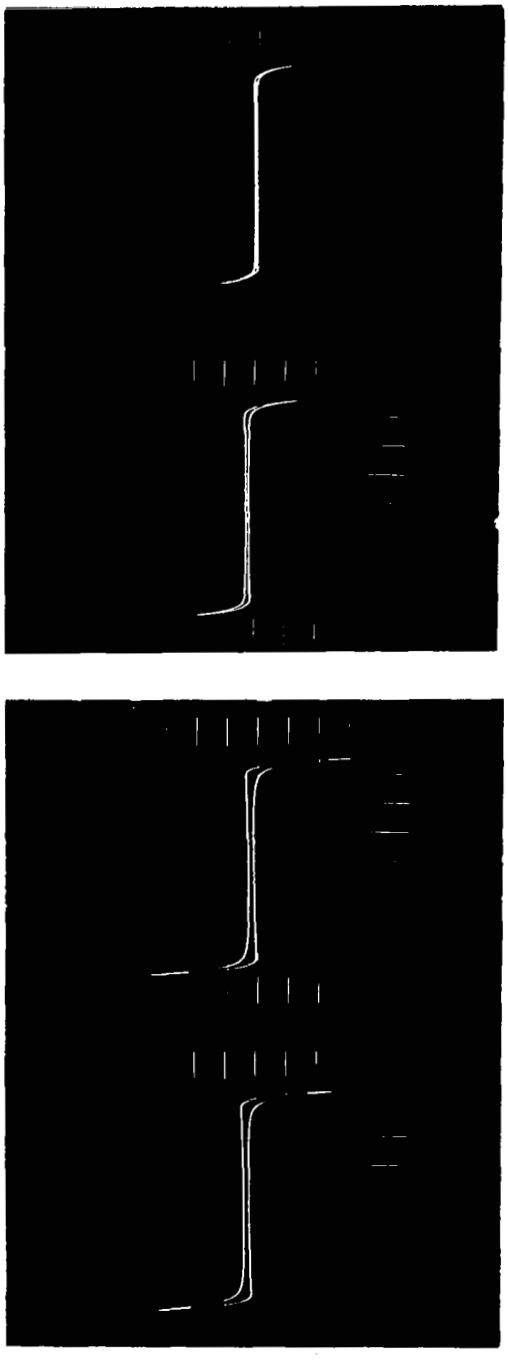

(a) f = 400 Hz
B = 5 kG/div
H = 25 Oe/div

(b) f = 800 Hz
B = 5 kG/div
H = 25 Oe/div

(c) f = 1600 Hz
B = 5 kG/div
H = 25 Oe/div

(d) f = 3200 Hz
B = 5 kG/div
H = 62.5 Oe/div

Figure 55. - AC Hysteresis Loop, Square Wave Excitation, 400, 800, 1600, and 3200 Hz, 0.004-Inch Singly Grain Oriented Silicon Steel Toroid, Room Ambient

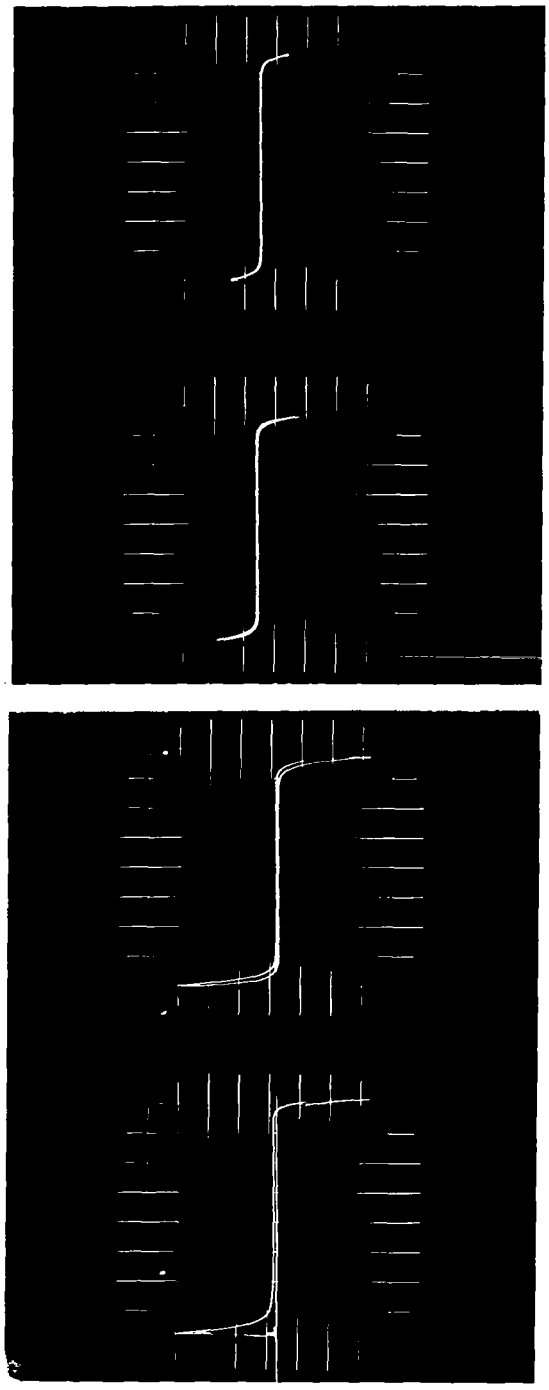

(a) f = 400 Hz
B = 5 kG/div
H = 100 Oe/div

(b) f = 800 Hz
B = 5 kG/div
H = 100 Oe/div

(c) f = 1600 Hz
B = 5 kG/div
H = 100 Oe/div

(d) f = 3200 Hz
B = 5 kG/div
H = 100 Oe/div

Figure 56. - AC Hysteresis Loop, Square Wave Excitation, 400, 800, 1600, and 3200 Hz, 0.004-Inch Singly Grain Oriented Silicon Steel Toroid, 250° C

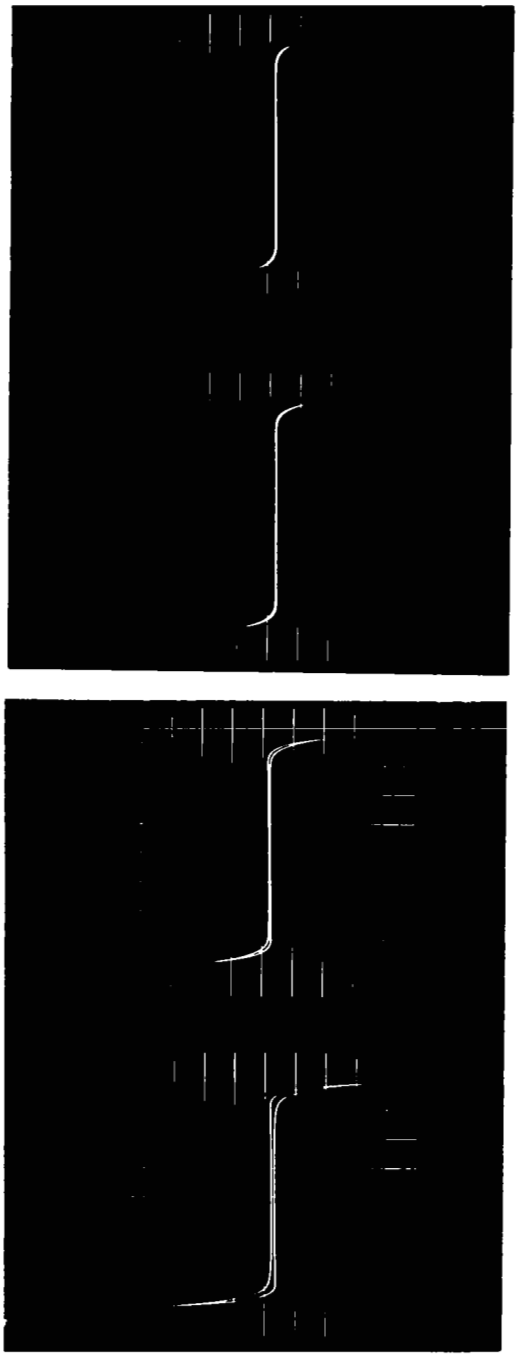

(a) f = 400 Hz
B = 50 kG/div
H = 100 Oe/div

(b) f = 800 Hz
B = 50 kG/div
H = 100 Oe/div

(c) f = 1600 Hz
B = 5 kG/div
H = 100 Oe/div

(d) f = 3200 Hz
B = 5 kG/div
H = 100 Oe/div

Figure 57. - AC Hysteresis Loop, Square Wave Excitation, 400, 800, 1600, and 3200 Hz, 0.002-Inch Singly Grain Oriented Silicon Steel, -55° C

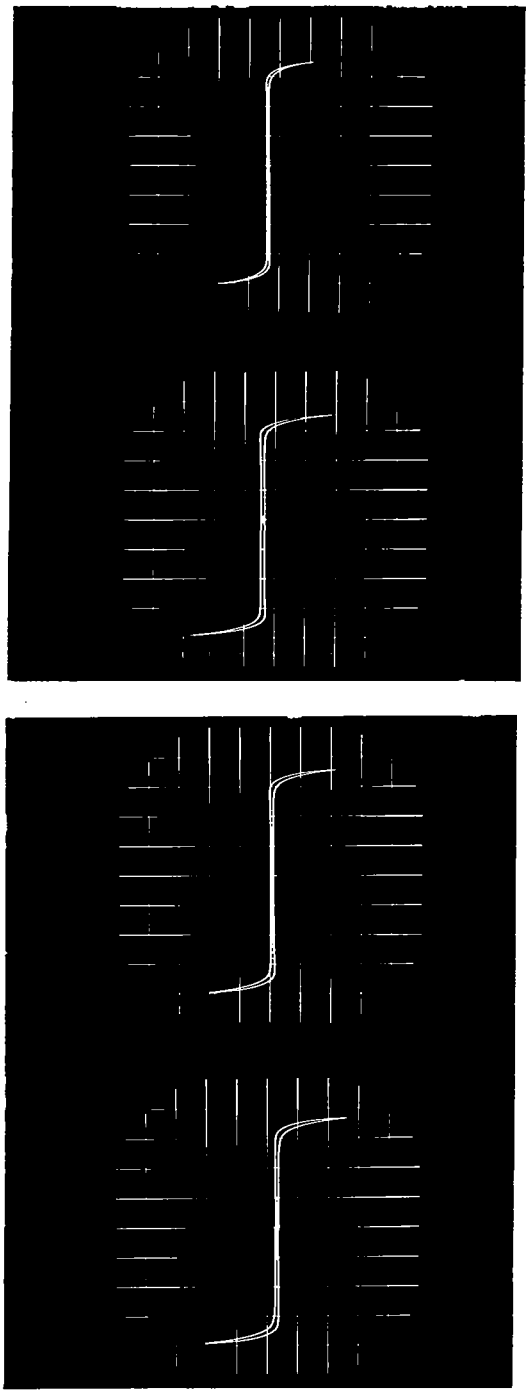

(a) f = 400 Hz
B = 5 kG/div
H = 25 Oe/div

(b) f = 800 Hz
B = 5 kG/div
H = 25 Oe/div

(c) f = 1600 Hz
B = 5 kG/div
H = 62.5 Oe/div

(d) f = 3200 Hz
B = 5 kG/div
H = 125 Oe/div

Figure 58. - AC Hysteresis Loop, Square Wave Excitation, 400, 800, 1600, and 3200 Hz, 0.002-Inch Singly Grain Oriented Silicon Steel, Room Ambient

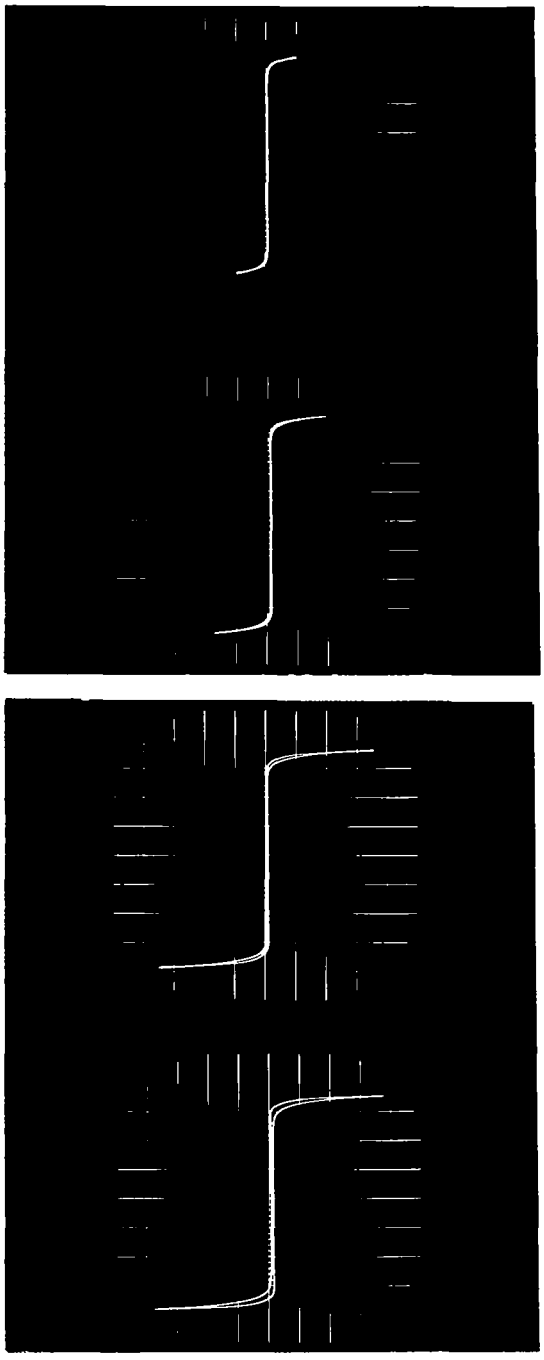

(a) f = 400 Hz
B = 5 kG/div
H = 100 Oe/div

(b) f = 800 Hz
B = 5 kG/div
H = 100 Oe/div

(c) f = 1600 Hz
B = 5 kG/div
H = 100 Oe/div

(d) f = 3200 Hz
B = 5 kG/div
H = 100 Oe/div

Figure 59.- AC Hysteresis Loop, Square Wave Excitation, 400, 800, 1600, and 3200 Hz, 0.002-Inch Singly Grain Oriented Silicon Steel, 250° C

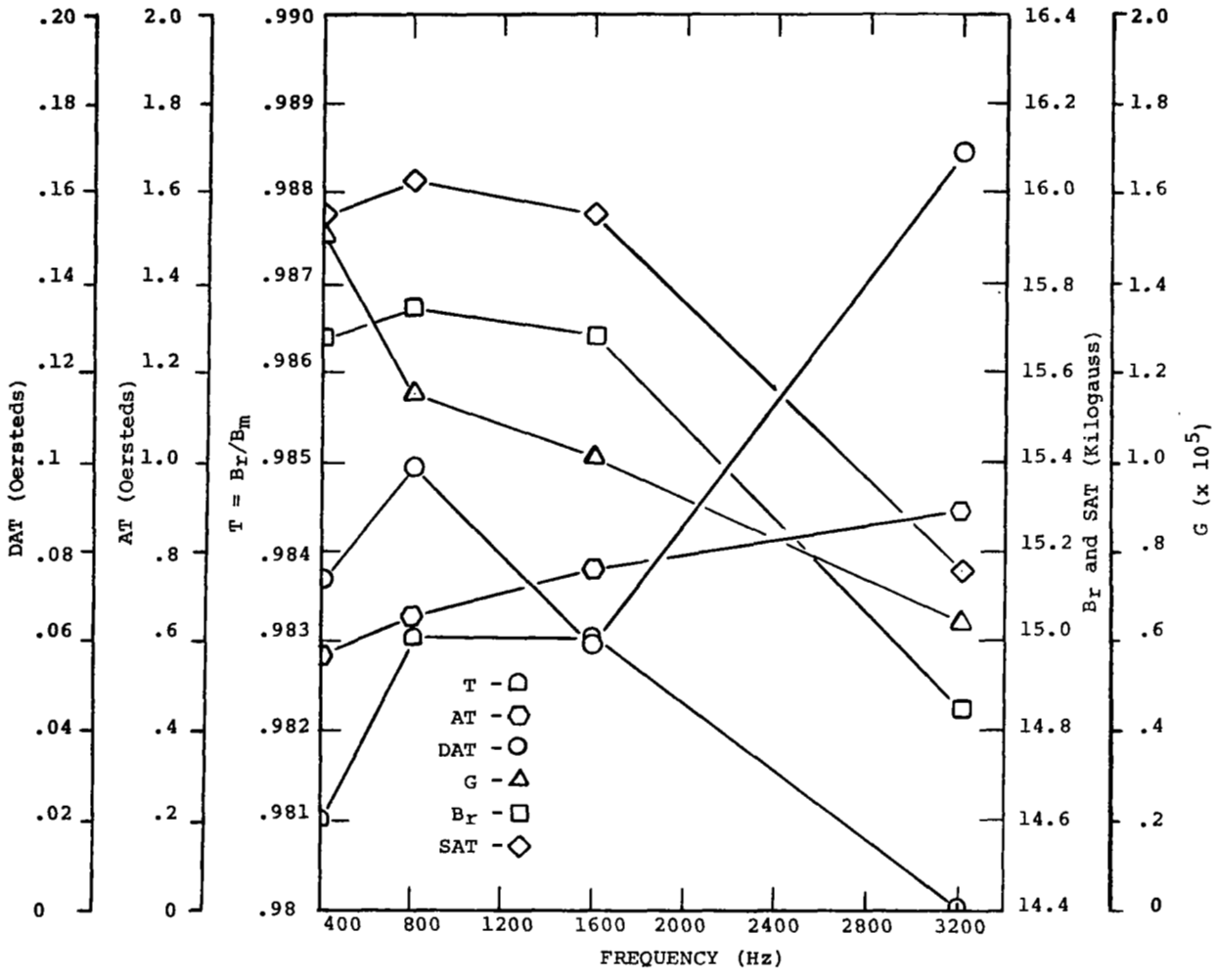

Figure 60. - CCFR Properties, 0.004 Inch Singly Oriented Silicon Steel, Toroids, Room Ambient

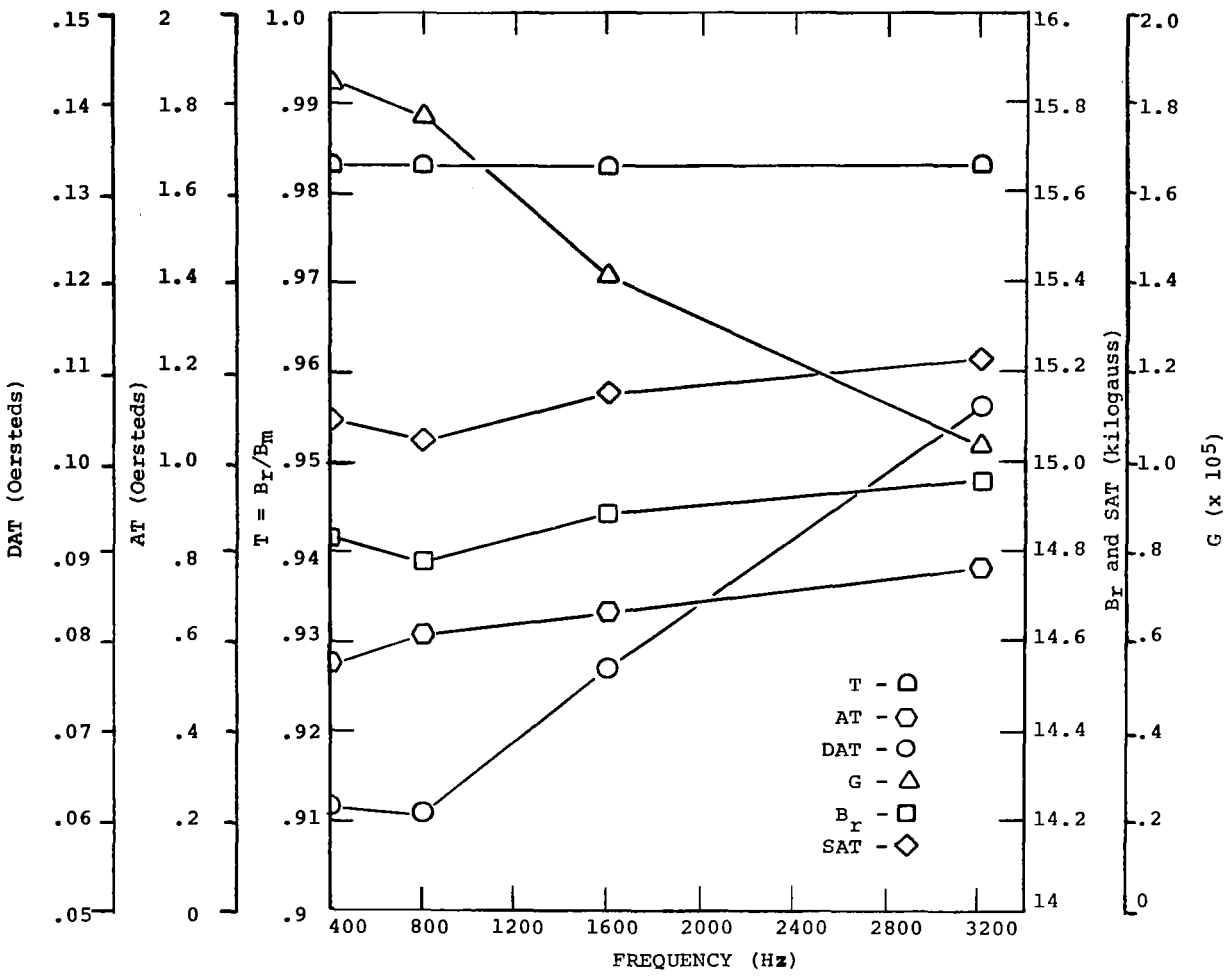

Figure 61. - CCFR Properties, 0.002-Inch Singly Oriented Silicon Steel, Toroids, Room Ambient

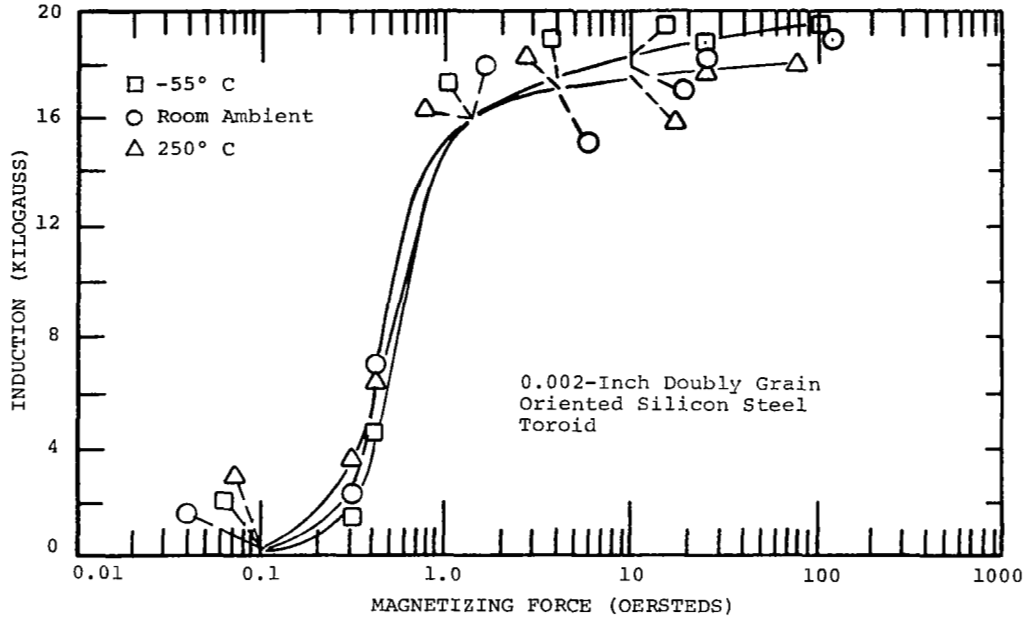

(a)

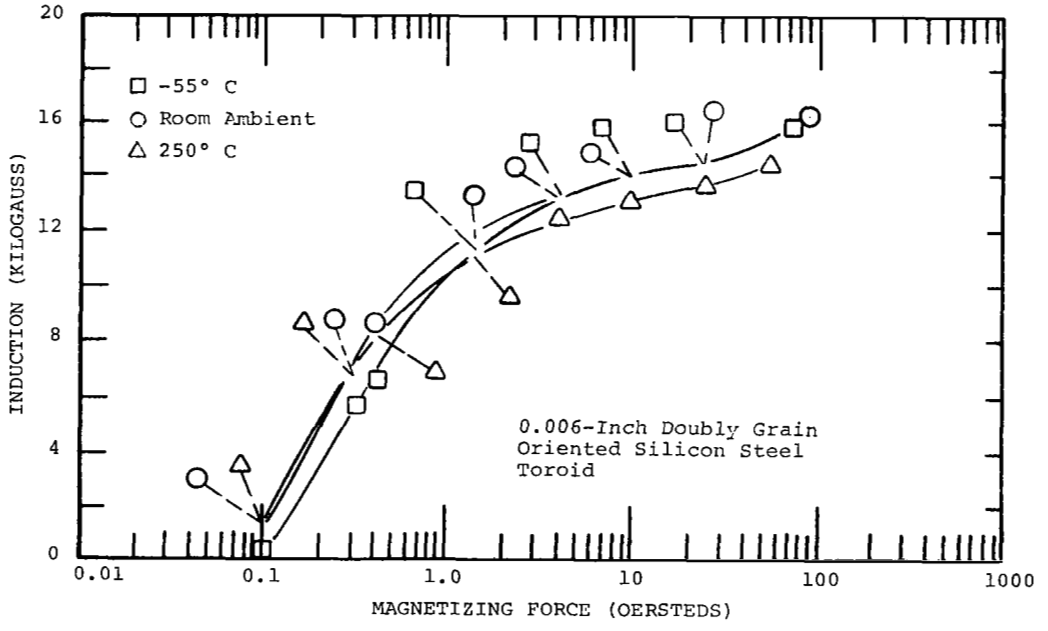

(b)

Figure 62. - DC Magnetization, 0.002- and 0.006-Inch Doubly Grain Oriented Silicon Steel Toroid, Stress Relief Annealed

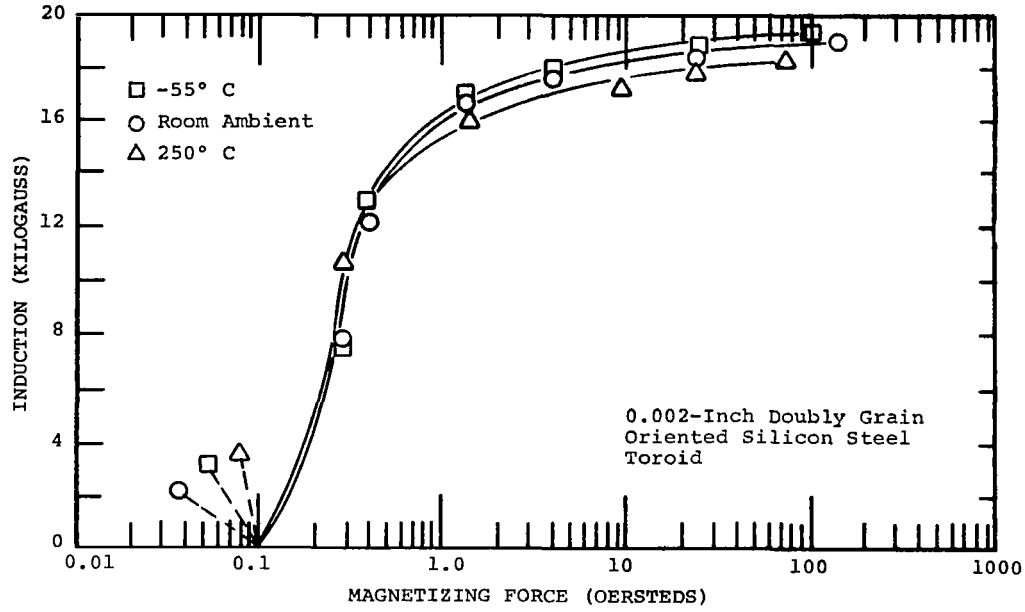

(a)

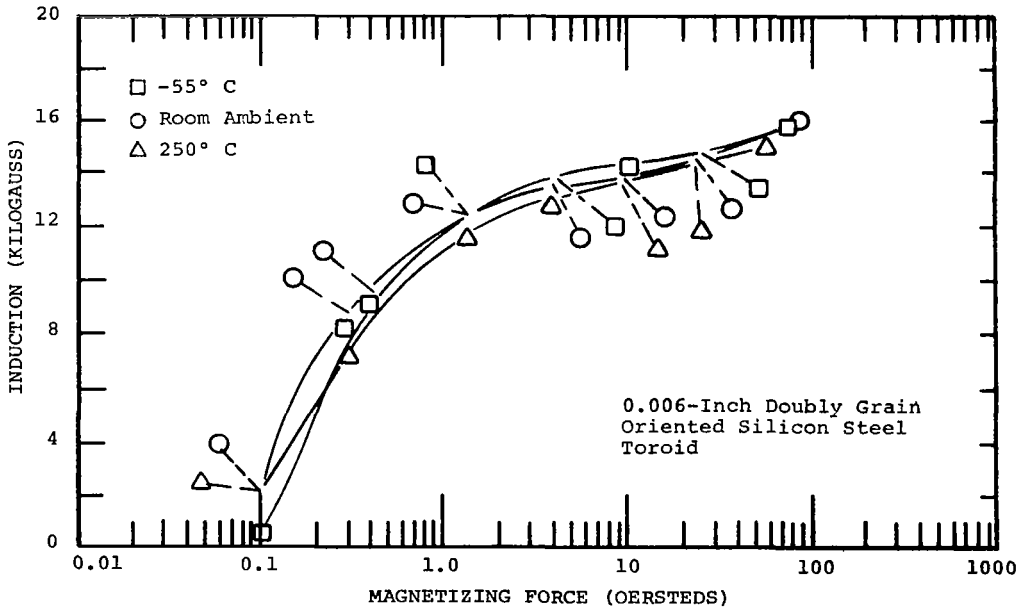

(b)

Figure 63. - DC Magnetization, 0.002- and 0.006-Inch Doubly Grain Oriented Silicon Steel Toroid, Magnetic Field Annealed

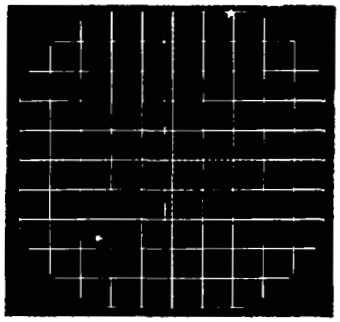

B = 5 kG/div

H = 20 Oe/div

T = -55° C

(a)

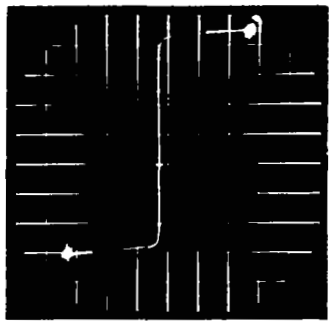

B = 5 kG/div

H = 20 Oe/div

T = Room Ambient

(b)

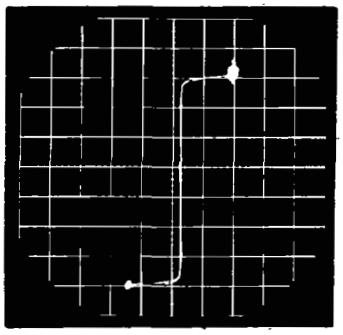

B = 5 kG/div

H = 20 Oe/div

T = 250° C

(c)

Figure 64.- DC Hysteresis Loop, 0.002-Inch Doubly Grain Oriented Silicon Steel Toroid, Stress Relief Annealed

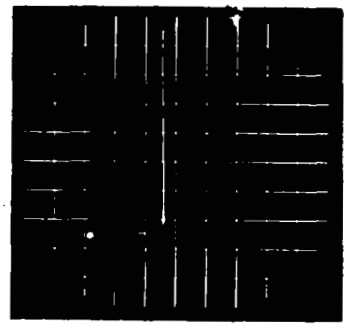

B = 5 kG/div

H = 20 Oe/div

T = -55° C

(a)

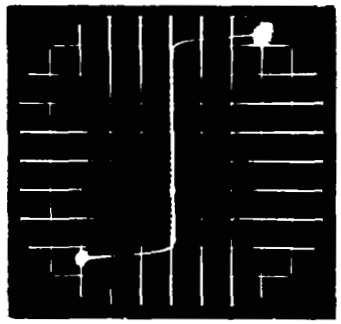

B = 5 kG/div

H = 20 Oe/div

T = Room Ambient

(b)

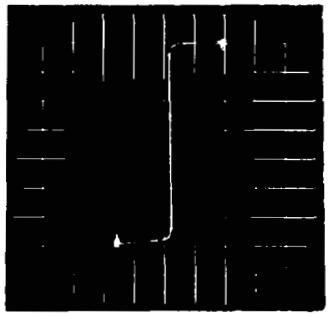

B = 5 kG/div

H = 20 Oe/div

T = 250° C

(c)

Figure 65. — DC Hysteresis Loop, 0.002-Inch Doubly Grain Oriented Silicon Steel, Magnetic Field Annealed

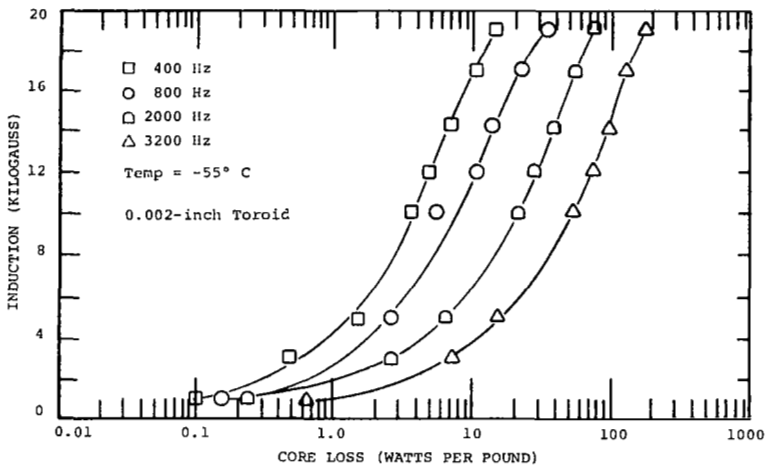

(a)

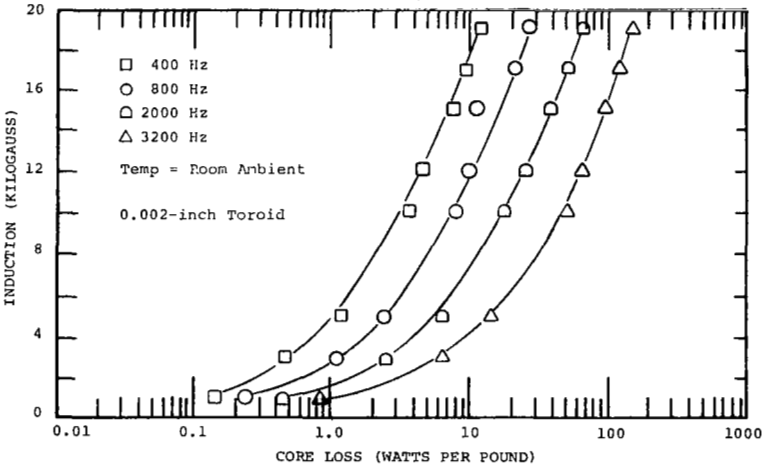

(b)

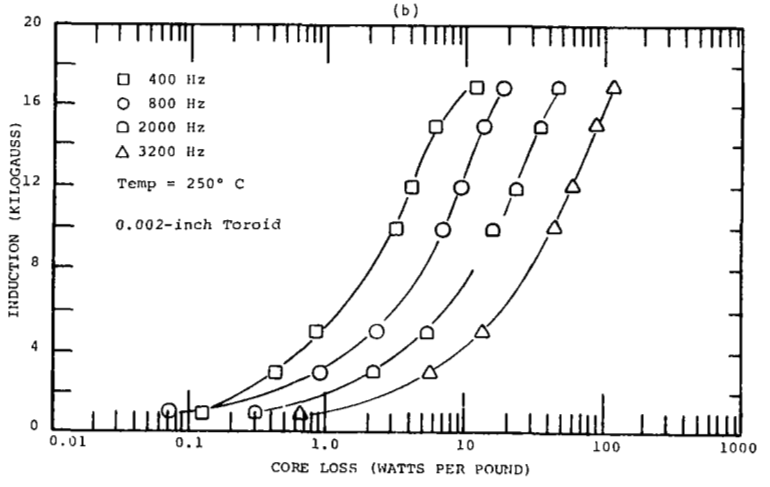

(c)

Figure 66. - $P_{c,\ sq,}$ Total Core Loss vs Induction and Frequency, 0.002-Inch Doubly Grain Oriented Silicon Steel Toroid Stress Relief Annealed

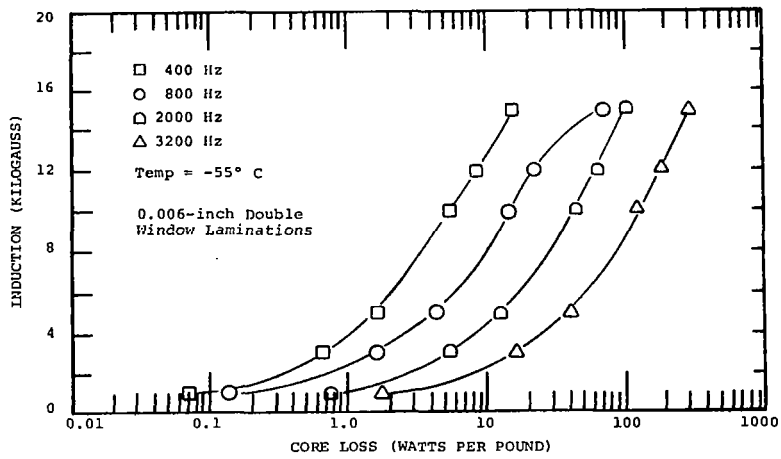

(a)

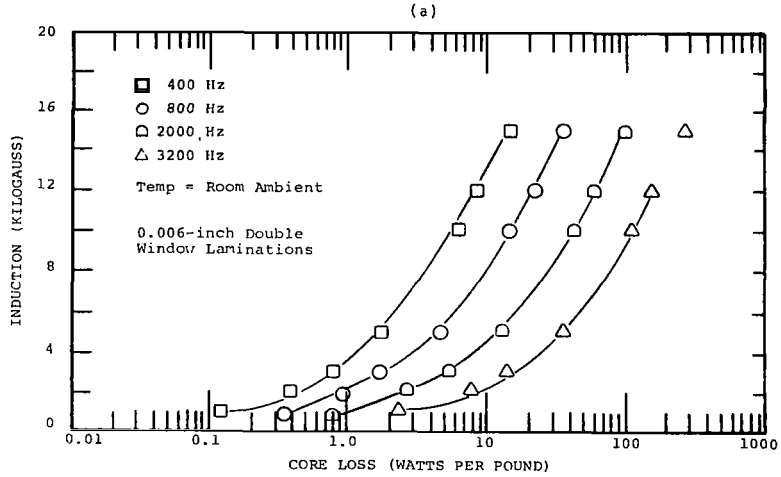

(b)

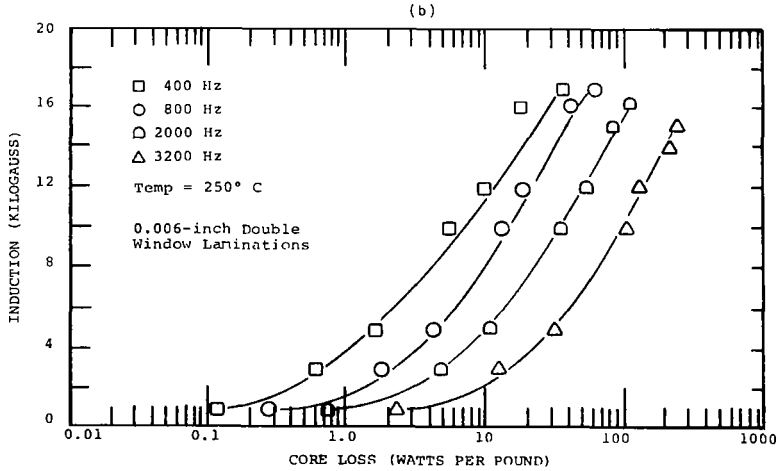

(c)

Figure 67. - $P_{c,\ sq,}$ Total Core Loss vs Indution and Frequency, 0.006-Inch Doubly Grain Oriented Silicon Steel Toroid Double Window, Stress Relief Annealed

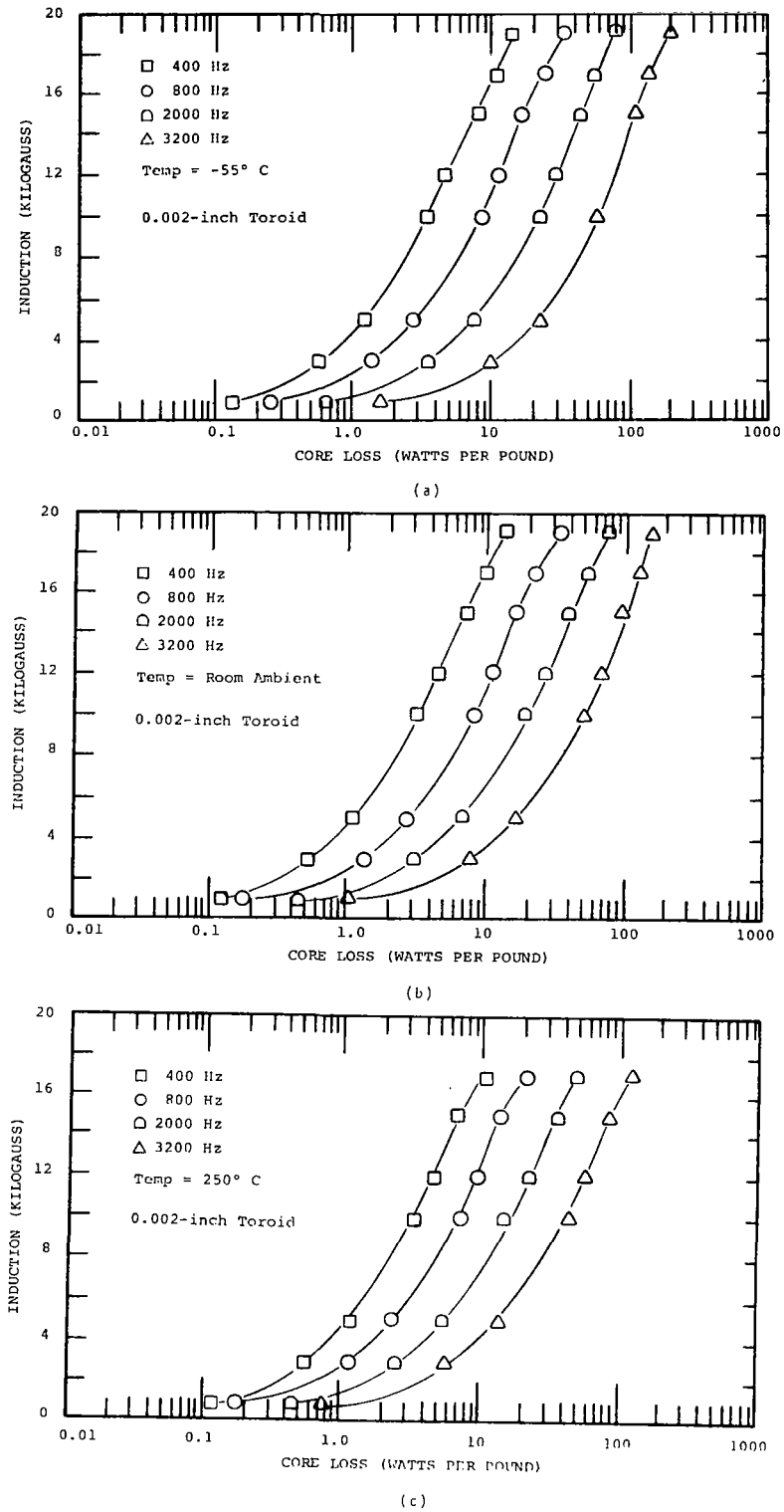

Figure 68. - $P_{c,\ sq,}$ Total Core Loss vs Induction and Frequency, 0.002-Inch Doubly Grain Oriented Silicon Steel Toroid Magnetic Field Annealed

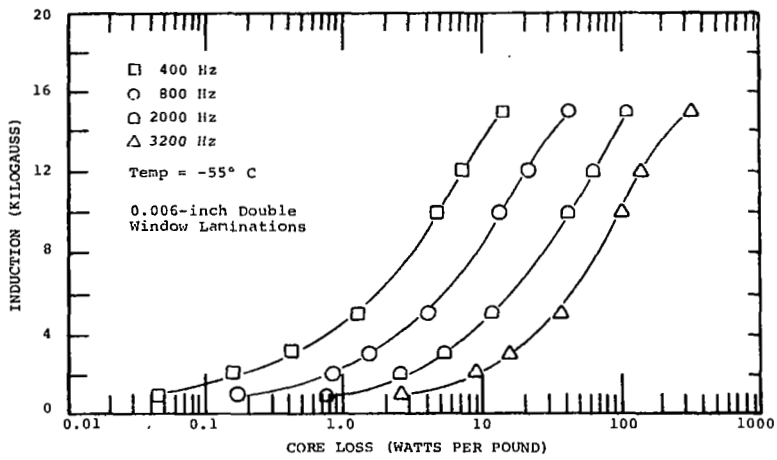

(a)

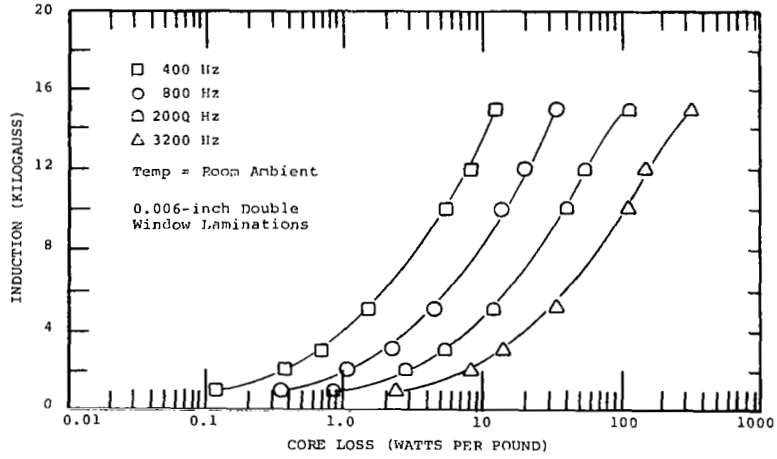

(b)

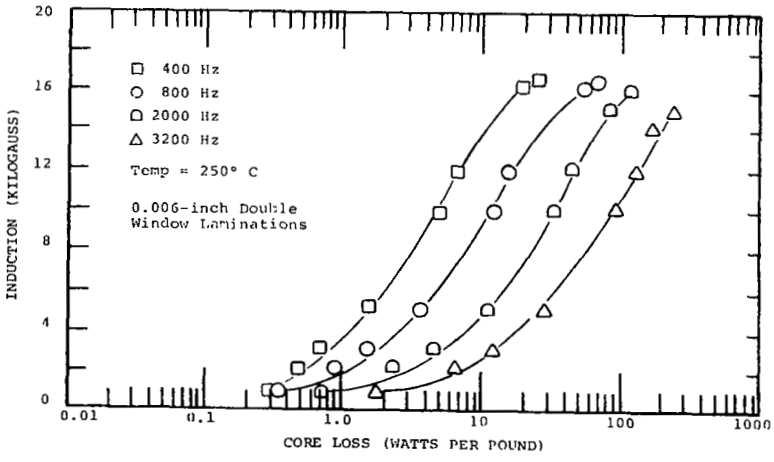

(c)

Figure 69. - $P_{c,\ sq,}$ Total Core Loss vs Induction and Frequency, 0.006-Inch Doubly Grain Oriented Silicon Steel Toroid Magnetic Field Annealed

The 400 Hz core loss values of the SRA toroid are 3.8 watts/pound and about 7 watts/pound for 10 and 15 kG, respectively. An increase in temperature lowers the core loss. The core loss follows the typical change in pattern as the temperature is increased to 250° C or decreased to -55° C.

As compared with the core loss value of sinusoidally excited toroids,[2] the core loss of square-wave excited toroids is lower at frequencies of 1600 and 3200 Hz. This difference increased with increasing frequency.

Double window cores follow the usual pattern of change with temperature. The dc magnetic properties of the cores are inferior to those of the toroids, thus reflecting the presence at the window corners of the less favorable direction of magnetization (cube face diagonal) in the the plane of double window laminations. The MFA (figure 63) as compared to the SRA (figure 62) brought about only a slight improvement in the dc magnetic properties of the double window core.

AC Apparent Power Curves: AC apparent power curves for both geometries and annealing treatments are shown on figures 70, 71, 72, and 73, that display apparent power at -55° C, room ambient, and 250° C for 400 to 3200 Hz. The same relative pattern observed for core loss applies to the apparent power (exciting VA) values up to flux densities of 15 kG. Above this induction level, the exciting VA values increase at a considerably steeper rate at both room ambient and 250° C as compared to -55° C. At 250° C, however, there is a considerable increase in exciting VA values at all inductions tested, especially at those of 15 kG and above.

AC Hysteresis Loops: AC hysteresis loops for both geometries at -55° C, room ambient, and 250° C for 400 to 3200 Hz are shown in figures 80 through 85 for SRA and figures 74 through 79 for SRA and figures 80 through 85 for MFA. The loops are practically the same for different annealing treatments. All loops are rectangular but the double window cores display a lower induction for the same drive compared to the toroids. The double window cores also show a somewhat wider loop.

CCFR Properties: The CCFR properties of both geometries and annealing treatments are shown on figures 86 through 89 for 400 to 3200 Hz.

In the CCFR properties of the SRA material the T value stayed fairly constant over the frequency range amounting to 0.897 to 0.929. A slight increase in B_r and SAT with frequency took place; the B_r values were 14.6 and 14.95 kG for 400 and 3200 Hz respectively, and correspondingly 16.3 and 16.4 kG for SAT. In the same frequency range, the gain decreased from 0.75×10^5 to

0.47×10^5. Both AT and DAT values increased with an increase in frequency; AT from 0.38 oersteds for 400 Hz to 0.6 oersteds for 3200 Hz; and DAT, correspondingly, from 0.15 to 0.25 oersteds.

The MFA grade, as compared to the SRA grade, shows an increase in the T value to 0.97. This property remains almost constant over the frequency range applied. The SAT value of the MFA grade was 16.57 kG at 400 Hz; it increases to 16.73 kG at 3200 Hz. Both the AT and DAT values were lower than those of the SRA grade, but their rate of increase with frequency was about the same. The AT value increases from 0.5 oersted at 400 Hz to 0.8 oersted at 3200 Hz, and the DAT value from 0.06 to 0.14 oersted for the same frequency range. The B_r value of this grade, 16.15 kG, was considerably higher than that of the SRA grade, and it shows a slight increase to 16.3 kG as the frequency is increased to 3200 Hz. The gain of this grade was twice that of the SRA grade; it amounted to 1.65×10^5 at 400 Hz and decreased to 0.85×10^5 at 3200 Hz.

Degradation Testing. - Degradation tests included dc magnetization and core loss determination after each step in a sequence of potentially damaging actions to the core such as core winding, bonding, dip-and-bake or fluidizing and core cutting. The results obtained are shown in figures 90 through 101. The conditions generated by core boxing, bonding, and dipping-and-baking were used on DGO Si Steel double-window cores SRA (figures 90 and 91) or MFA (figures 92 and 93). The bonding as well as the dip-and-bake operation decrease dc permeability below 10 oersteds, especially in the MFA double-window core of DGO Si steel. In core loss tests, this harmful effect is already apparent at inductions above 10 kG for 400 Hz and above 5 kG for 3200 Hz.

In addition a five-step degradation schedule (wound without protection, in core box, as bonded, as cut, as dip-and-bake) was applied to SGO Si Steel square tape-wound core (figures 94 and 95) and SHL 4Mo-79NiFe square tape-wound core (figures 96 and 97); whereas a three-step degradation schedule (wound without protection in core-box, as fluidize-coated) was applied to GO 50NiFe toroid (figures 98 and 99) and MFA 2V-CoFe toroid (figures 100 and 101). In the five-step operation, the core cutting showed the maximum damaging effect on the dc properties of both SGO Silicon Steel and SHL 4Mo-79NiFe cores. The subsequent dip-and-bake operation brought about slight additional damaging of the dc properties. By comparison the changes induced by core winding, boxing and bonding were minor in the GO 50NiFe toroid but somewhat more pronounced in SHL 4Mo-79NiFe. The five steps had considerably less effect on core loss than on the dc properties, although the trend was generally the same. Fluidized coating brings about a decrease of 5 to 50% in dc permeability at fields below one oersted in GO 50NiFe toroids (figure 98) and of 5 to 15% over a wide field range in the MFA 2V-CoFe toroid (figure 100), but has only a minor effect on the core loss of both materials (figures 99 and 100).

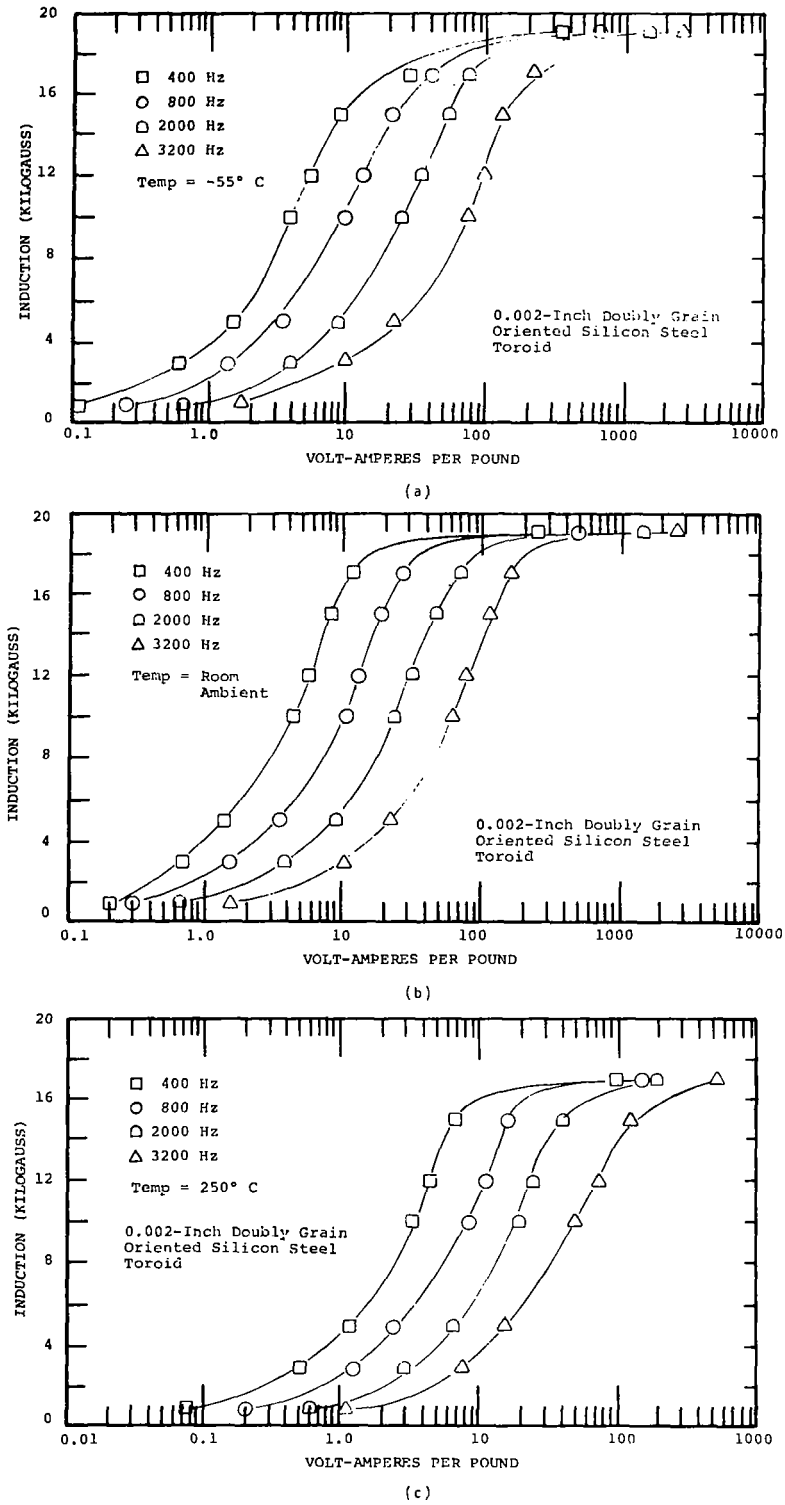

Figure 70. - $P_{a,\ sq,}$ Apparent Power vs Induction and Frequency, 0.002-Inch Doubly Grain Oriented Silicon Steel Toroid, Stress Relief Annealed

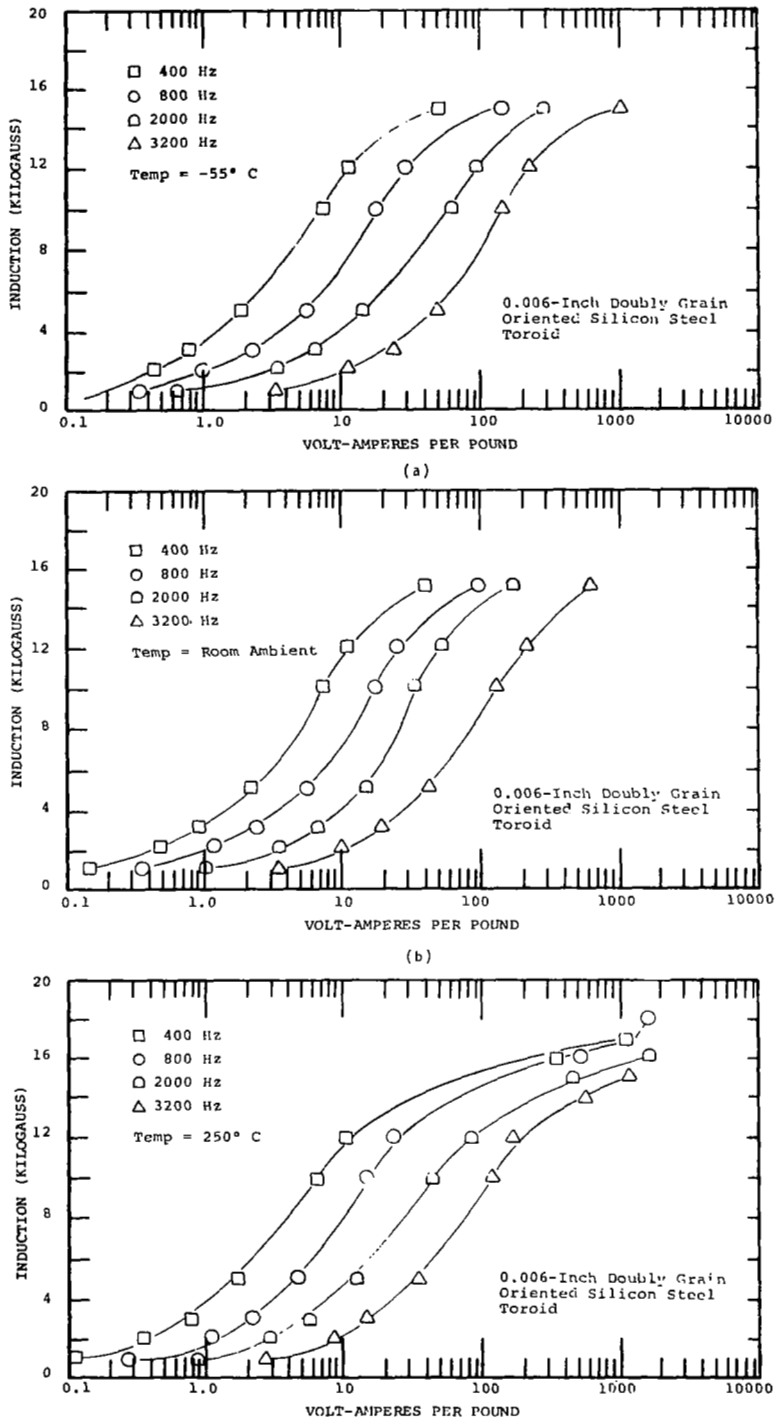

Figure 71. - $P_{a,\ sq,}$ Apparent Power vs Induction and Frequency, 0.006-Inch Doubly Grain Oriented Silicon Steel Double Window, Stress Relief Annealed

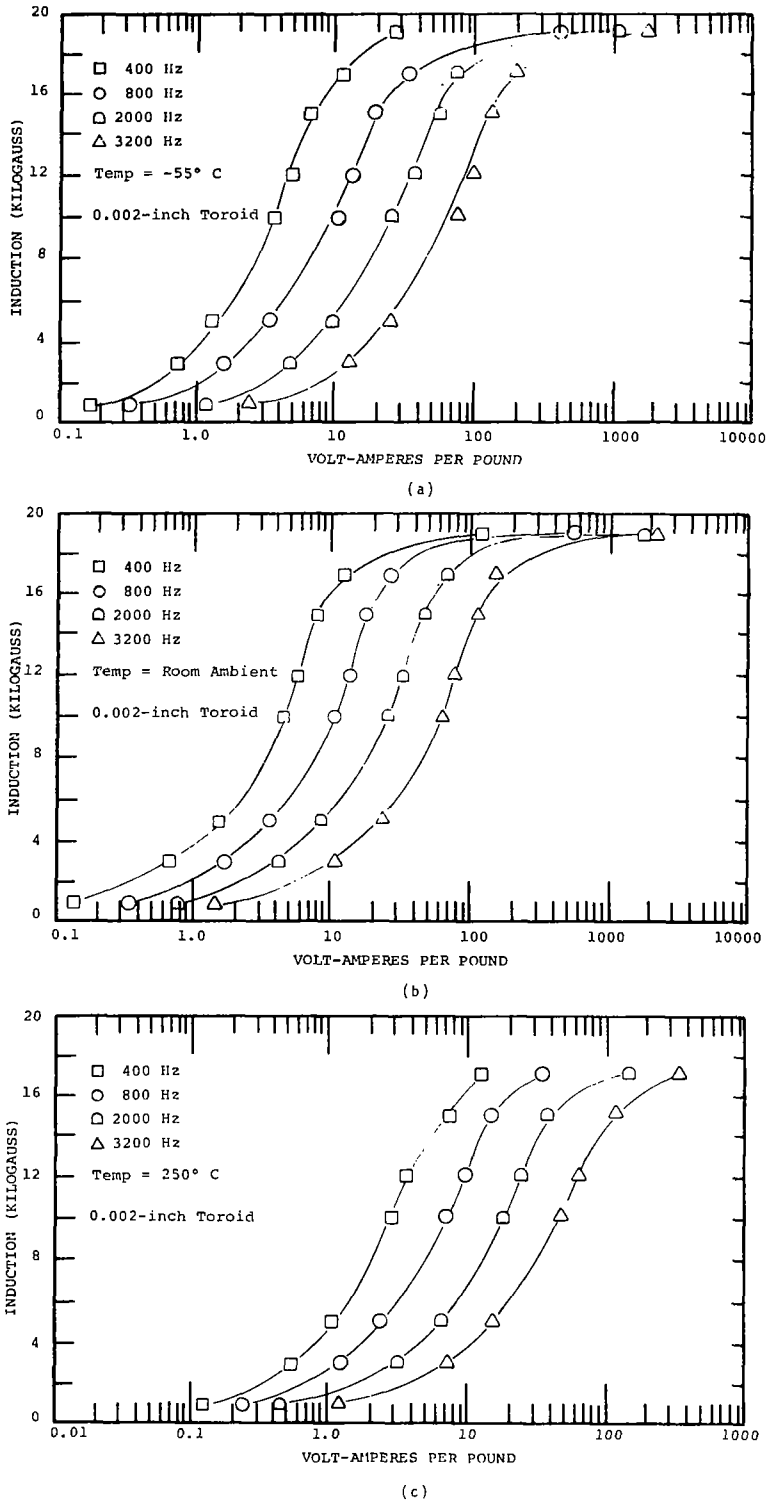

Figure 72. - $P_{a,\ sq,}$ Apparent Power vs Induction and Frequency, 0.002-Inch Doubly Grain Oriented Silicon Steel Toroid, Magnetic Field Annealed

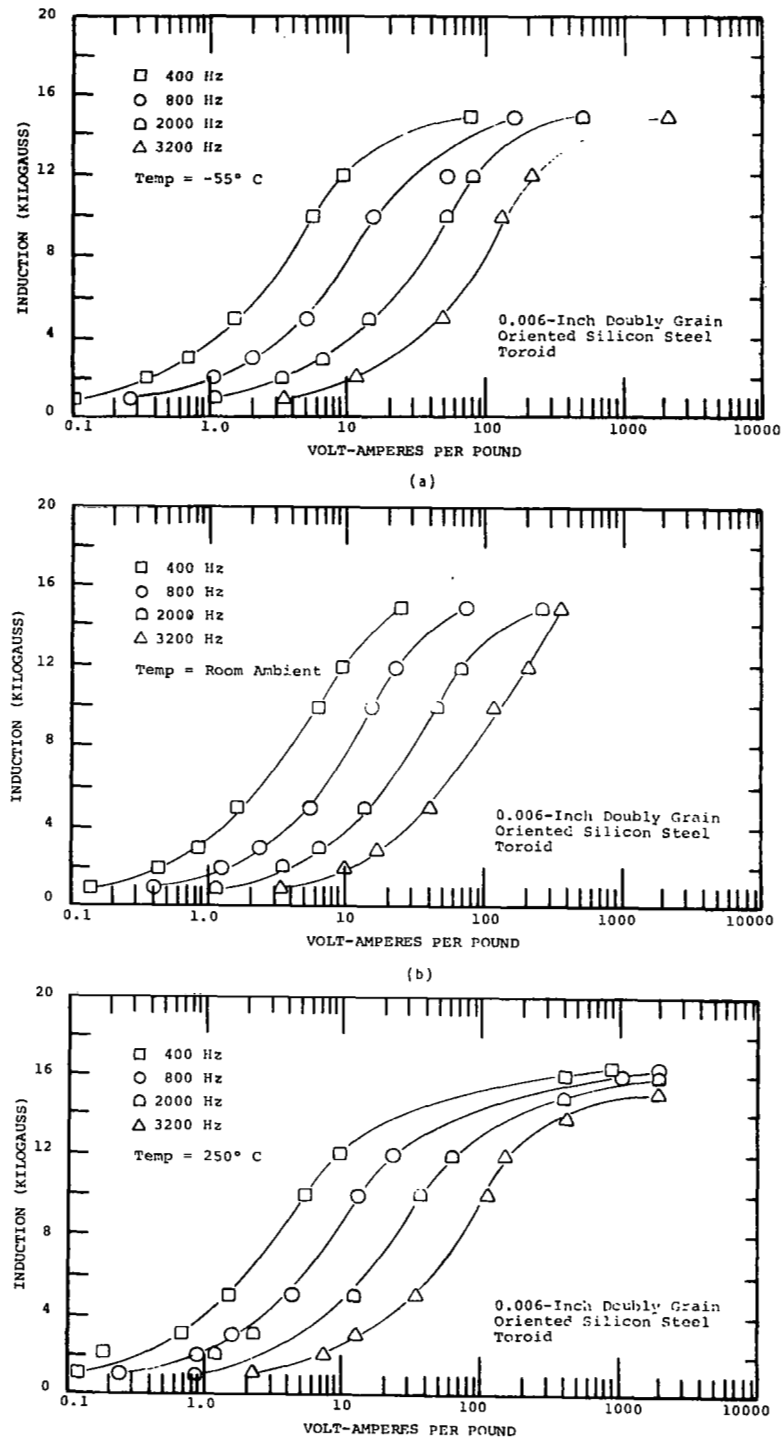

Figure 73. - $P_{a,\ sq,}$ Apparent Power vs Induction and Frequency 0.006-Inch Doubly Grain Oriented Silicon Steel Double Window, Magnetic Field Annealed

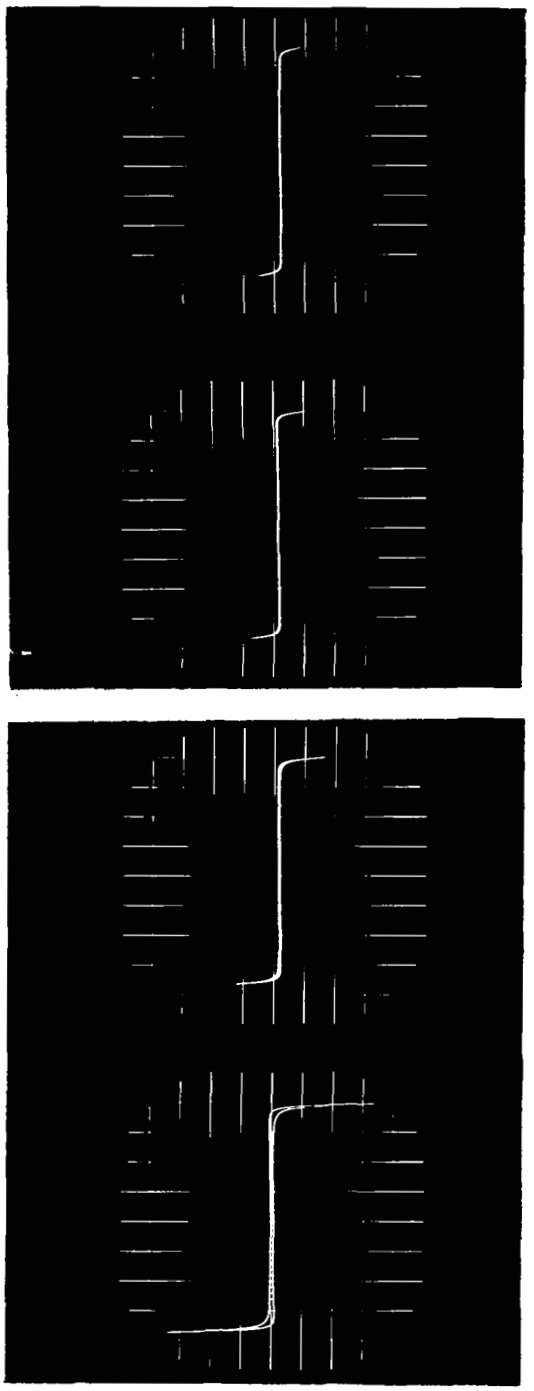

(a) f = 400 Hz
B = 5 kG/div
H = 100 Oe/div

(b) f = 800 Hz
B = 5 kG/div
H = 100 Oe/div

(c) f = 1600 Hz
B = 5 kG/div
H = 100 Oe/div

(d) f = 3200 Hz
B = 5 kG/div
H = 100 Oe/div

Figure 74. - AC Hysteresis Loop, Square Wave Excitation, 400, 800, 1600, and 3200 Hz, 0.002-Inch Doubly Grain Oriented Silicon Steel Toroid, Stress Relief Annealed, -55° C

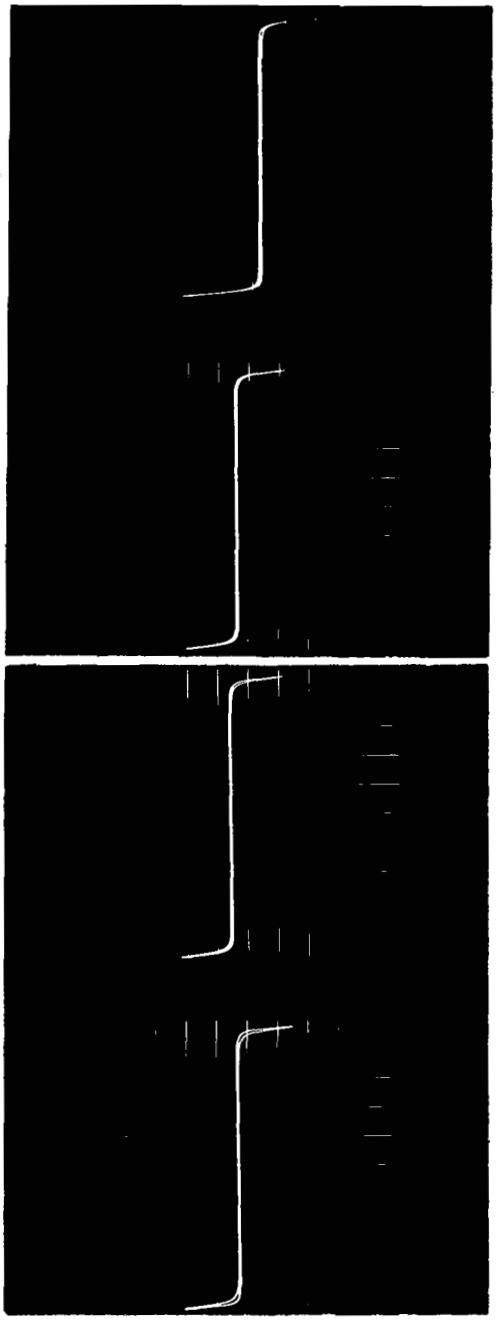

(a) f = 400 Hz
B = 4 kG/div
H = 25 Oe/div

(b) f = 800 Hz
B = 4 kG/div
H = 62.5 Oe/div

(c) f = 1600 Hz
B = 4 kG/div
H = 125 Oe/div

(d) f = 3200 Hz
B = 4 kG/div
H = 250 Oe/div

Figure 75. - AC Hysteresis Loop, Square Wave Excitation, 400, 800, 1600, and 3200 Hz, 0.002-Inch Doubly Grain Oriented Silicon Steel Toroid, Stress Relief Annealed, Room Ambient

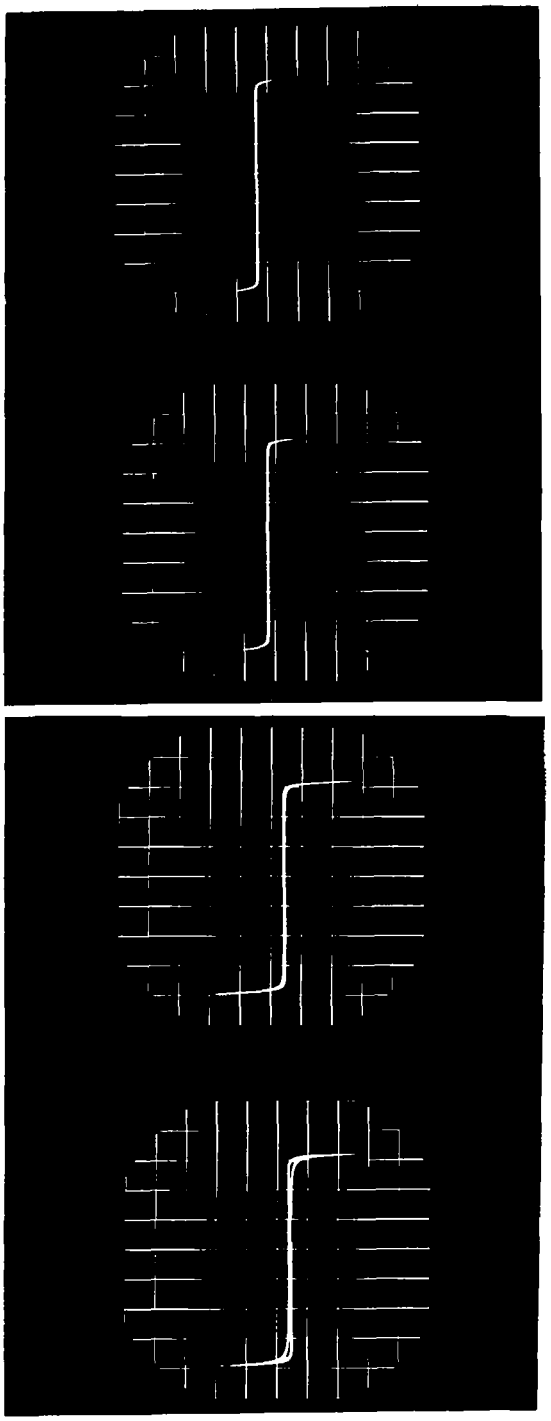

(a) f = 400 Hz
B = 5 kG/div
H = 100 Oe/div

(b) f = 800 Hz
B = 5 kG/div
H = 100 Oe/div

(c) f = 1600 Hz
B = 5 kG/div
H = 100 Oe/div

(d) f = 3200 Hz
B = 5 kG/div
H = 100 Oe/div

Figure 76. - AC Hysteresis Loop, Square Wave Excitation, 400, 800, 1600, and 3200 Hz, 0.002-Inch Doubly Grain Oriented Silicon Steel Toroid, Stress Relief Annealed, 250° C

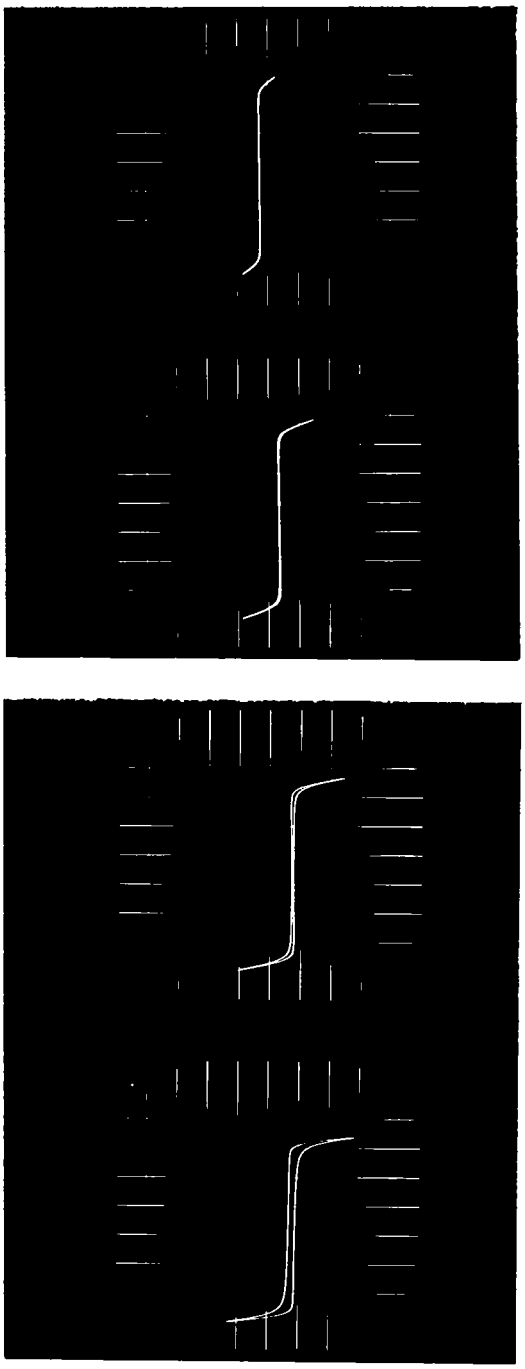

(a) f = 400 Hz
B = 5 kG/div
H = 100 Oe/div

(b) f = 800 Hz
B = 5 kG/div
H = 100 Oe/div

(c) f = 1600 Hz
B = 5 kG/div
H = 100 Oe/div

(d) f = 3200 Hz
B = 5 kG/div
H = 100 Oe/div

Figure 77. - AC Hysteresis Loop, Square Wave Excitation, 400, 800, 1600, and 3200 Hz, 0.006-Inch Doubly Grain Oriented Silicon Steel Toroid, Double Window Stress Relief Annealed, -55° C

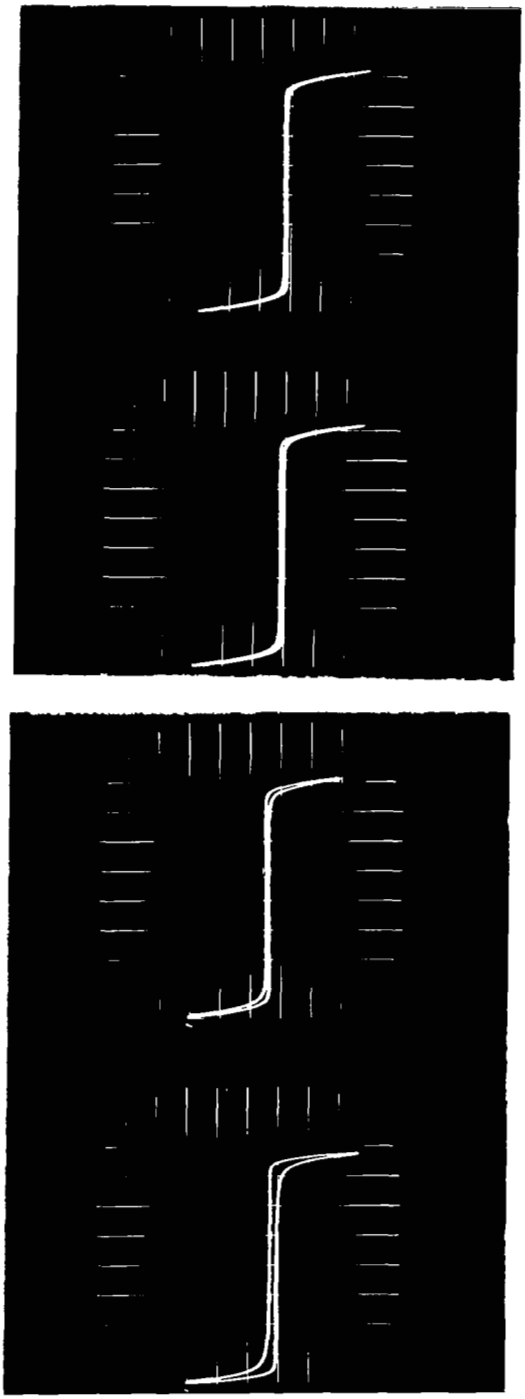

(a) f = 400 Hz
B = 4 kG/div
H = 25 Oe/div

(b) f = 800 Hz
B = 4 kG/div
H = 25 Oe/div

(c) f = 1600 Hz
B = 4 kG/div
H = 100 Oe/div

(d) f = 3200 Hz
B = 4 kG/div
H = 100 Oe/div

Figure 78. - AC Hysteresis Loop, Square Wave Excitation, 400, 800, 1600, and 3200 Hz, 0.006-Inch Doubly Grain Oriented Silicon Steel Toroid, Double Window Stress Relief Annealed, Room Ambient

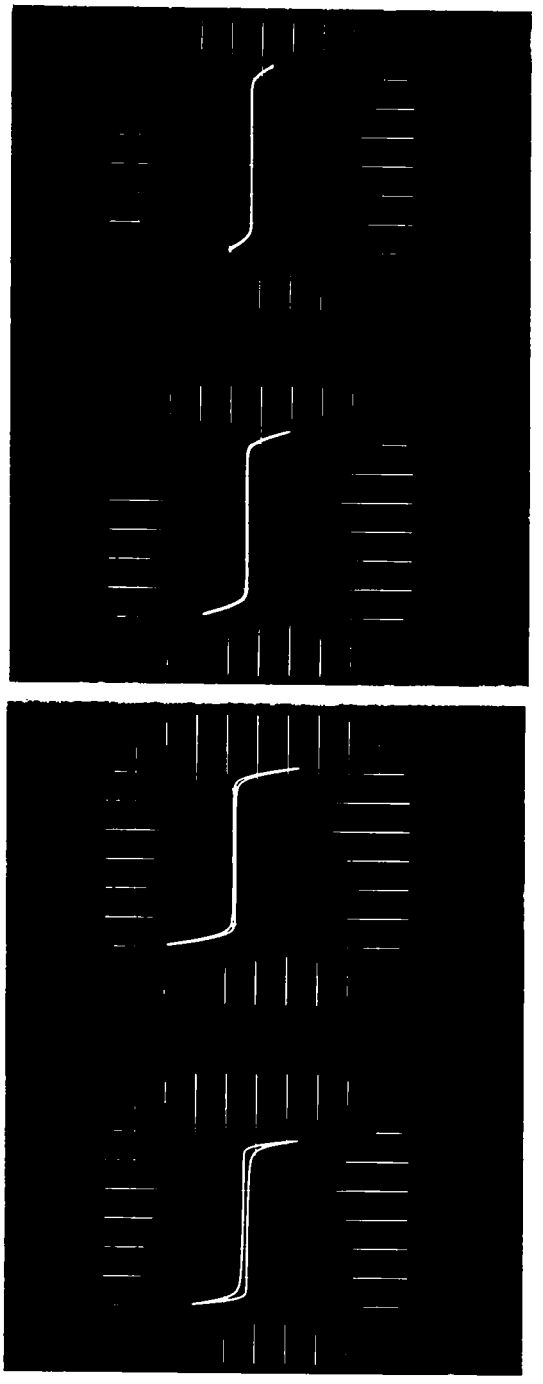

(a) f = 400 Hz
B = 5 kG/div
H = 100 Oe/div

(b) f = 800 Hz
B = 5 kG/div
H = 100 Oe/div

(c) f = 1600 Hz
B = 5 kG/div
H = 100 Oe/div

(d) f = 3200 Hz
B = 5 kG/div
H = 100 Oe/div

Figure 79. - AC Hysteresis Loop, Square Wave Excitation, 400, 800, 1600, and 3200 Hz, 0.006-Inch Doubly Grain Oriented Silicon Steel Toroid, Double Window Stress Relief Annealed, 250° C

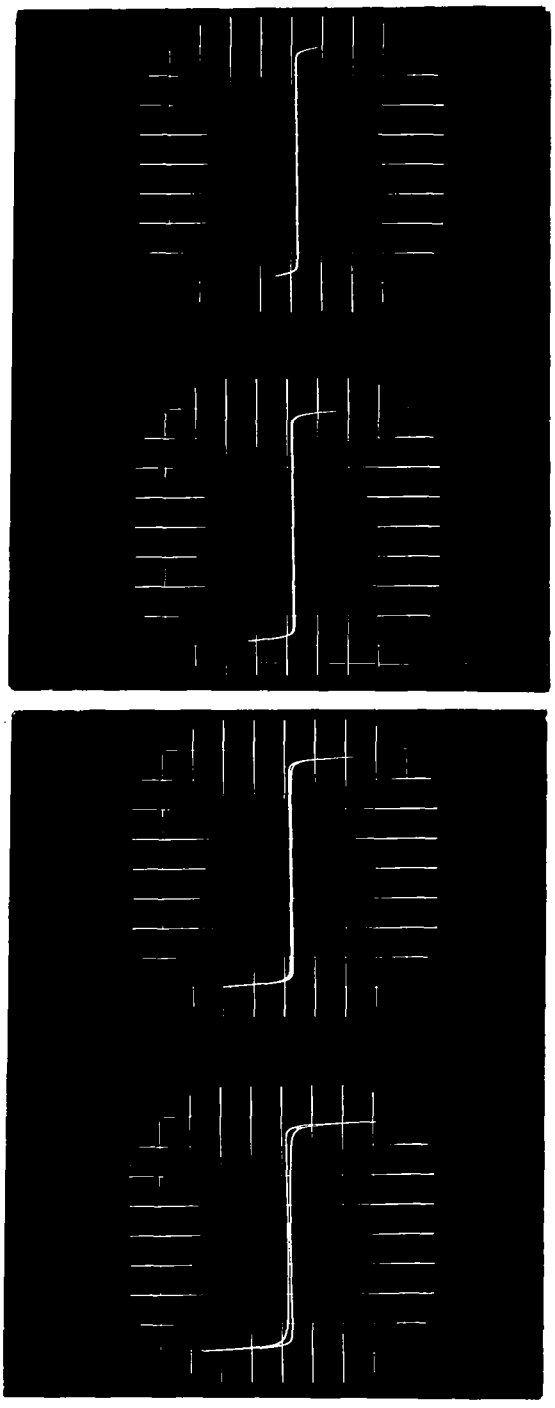

(a) f = 400 Hz
B = 5 kG/div
H = 100 Oe/div

(b) f = 800 Hz
B = 5 kG/div
H = 100 Oe/div

(c) f = 1600 Hz
B = 5 kG/div
H = 100 Oe/div

(d) f = 3200 Hz
B = 5 kG/div
H = 100 Oe/div

Figure 80. - AC Hysteresis Loop, Square Wave Excitation, 400, 800, 1600, and 3200 Hz, 0.002-Inch Doubly Grain Oriented Silicon Steel Toroid, Magnetic Field Annealed, -55° C

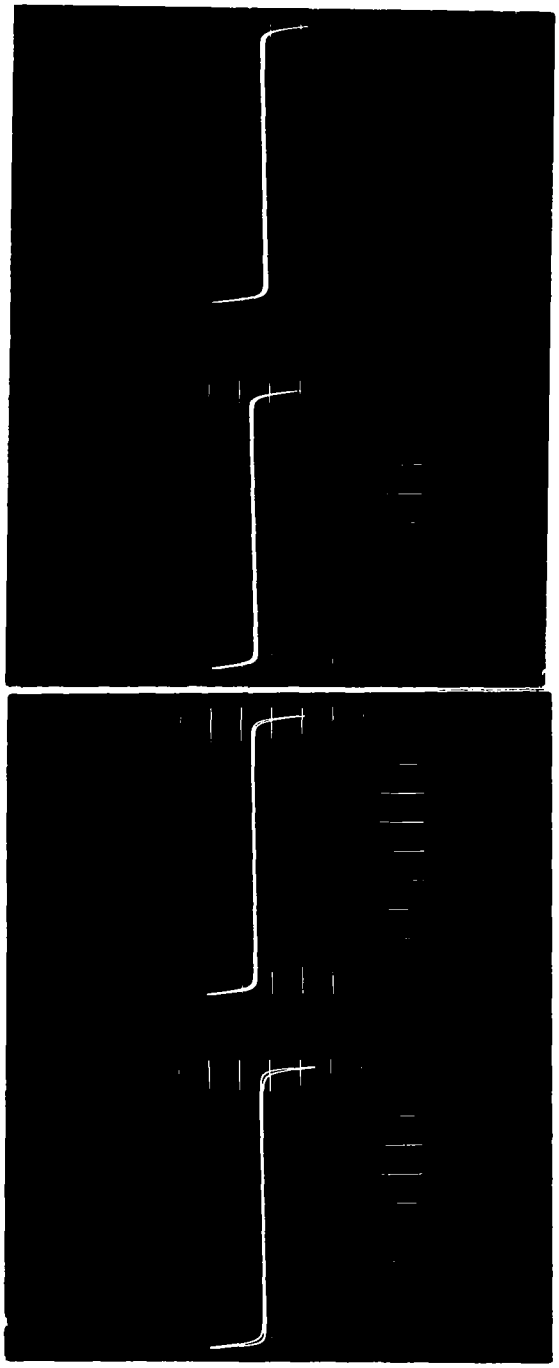

(a) f = 400 Hz
B = 4 kG/div
H = 25 Oe/div

(b) f = 800 Hz
B = 4 kG/div
H = 25 Oe/div

(c) f = 1600 Hz
B = 4 kG/div
H = 62.5 Oe/div

(d) f = 3200 Hz
B = 4 kG/div
H = 250 Oe/div

Figure 81. - AC Hysteresis Loop, Square Wave Excitation, 400, 800, 1600, and 3200 Hz, 0.002-Inch Doubly Grain Oriented Silicon Steel Toroid, Magnetic Field Annealed, Room Ambient

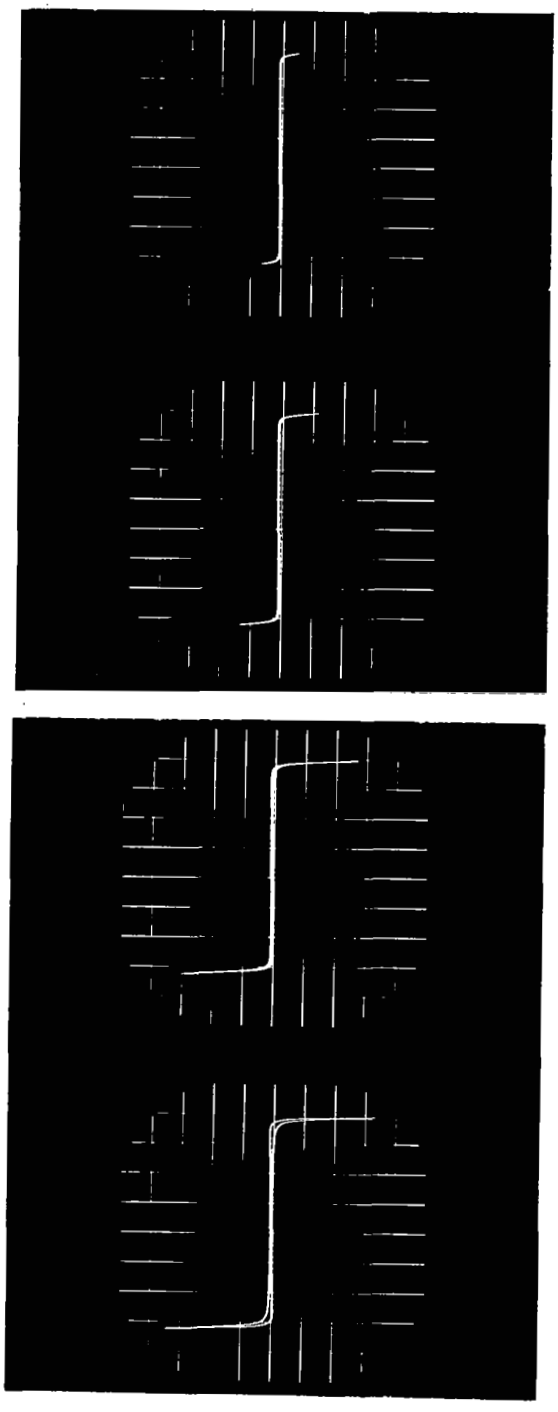

(a) f = 400 Hz
B = 5 kG/div
H = 100 Oe/div

(b) f = 800 Hz
B = 5 kG/div
H = 100 Oe/div

(c) f = 1600 Hz
B = 5 kG/div
H = 100 Oe/div

(d) f = 3200 Hz
B = 5 kG/div
H = 100 Oe/div

Figure 82. - AC Hysteresis Loop, Square Wave Excitation, 400, 800, 1600, and 3200 Hz, 0.002-Inch Doubly Grain Oriented Silicon Steel Toroid, Magnetic Field Annealed, 250° C

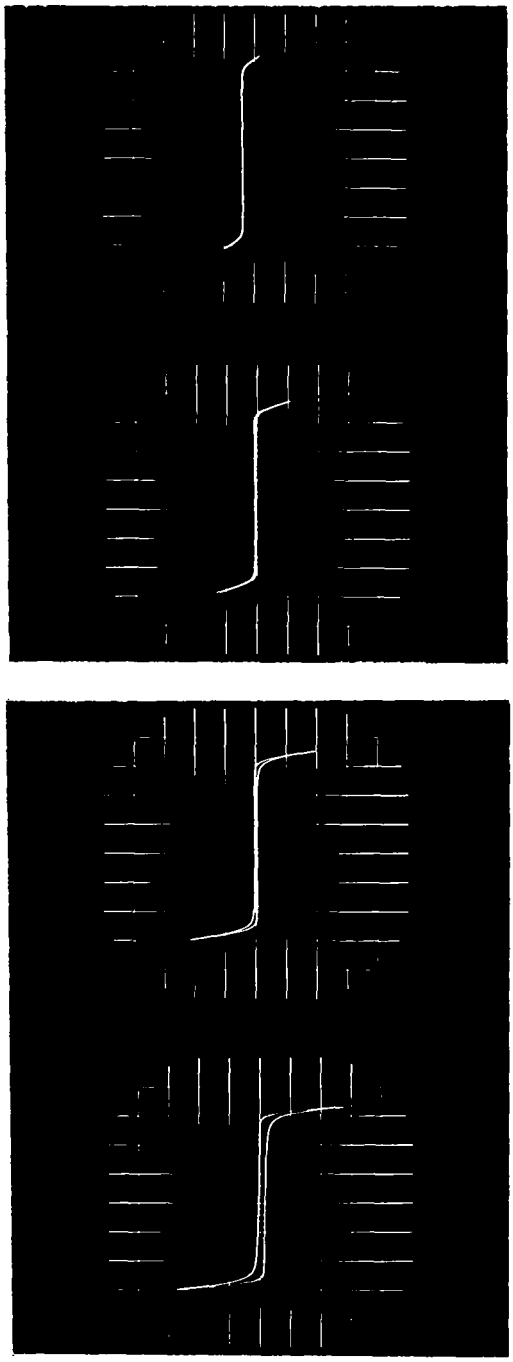

(a) f = 400 Hz
B = 5 kG/div
H = 100 Oe/div

(b) f = 800 Hz
B = 5 kG/div
H = 100 Oe/div

(c) f = 1600 Hz
B = 5 kG/div
H = 100 Oe/div

(d) f = 3200 Hz
B = 5 kG/div
H = 100 Oe/div

Figure 83. - AC Hysteresis Loop, Square Wave Excitation, 400, 800, 1600, and 3200 Hz, 0.006-Inch Doubly Grain Oriented Silicon Steel Toroid, Double Window Magnetic Field Annealed, -55° C

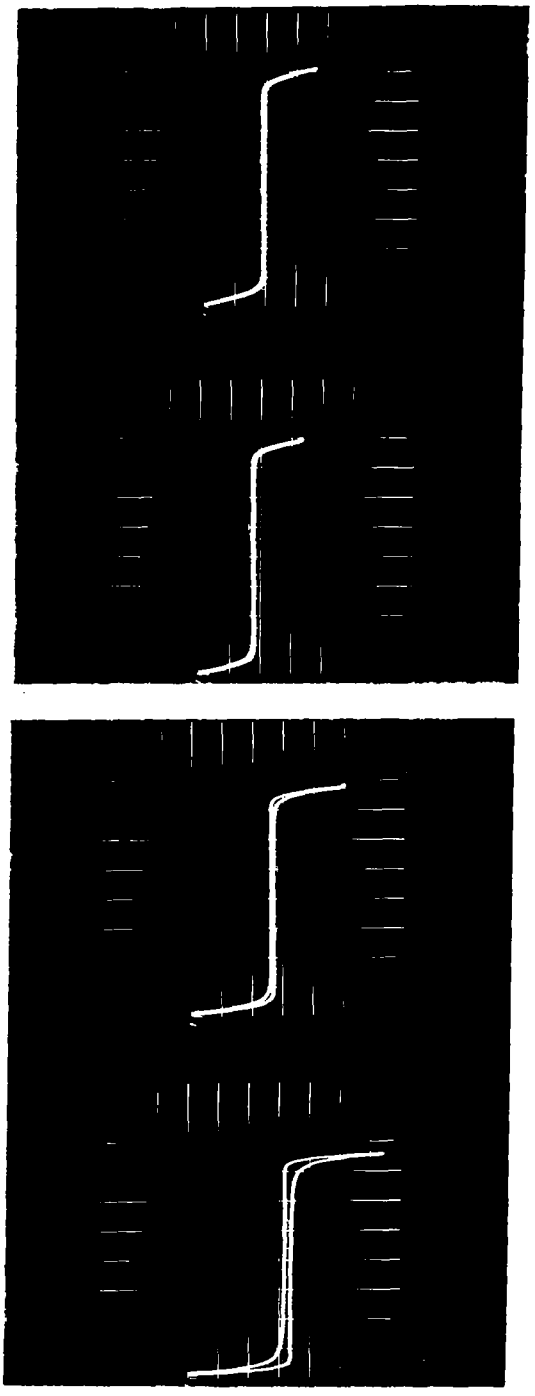

(a) f = 400 Hz
B = 4 kG/div
H = 50 Oe/div

(b) f = 800 Hz
B = 4 kG/div
H = 100 Oe/div

(c) f = 1600 Hz
B = 4 kG/div
H = 100 Oe/div

(d) f = 3200 Hz
B = 4 kG/div
H = 100 Oe/div

Figure 84. - AC Hysteresis Loop, Square Wave Excitation, 400, 800, 1600, and 3200 Hz, 0.006-Inch Doubly Grain Oriented Silicon Steel Toroid, Double Window Magnetic Field Annealed, Room Ambient

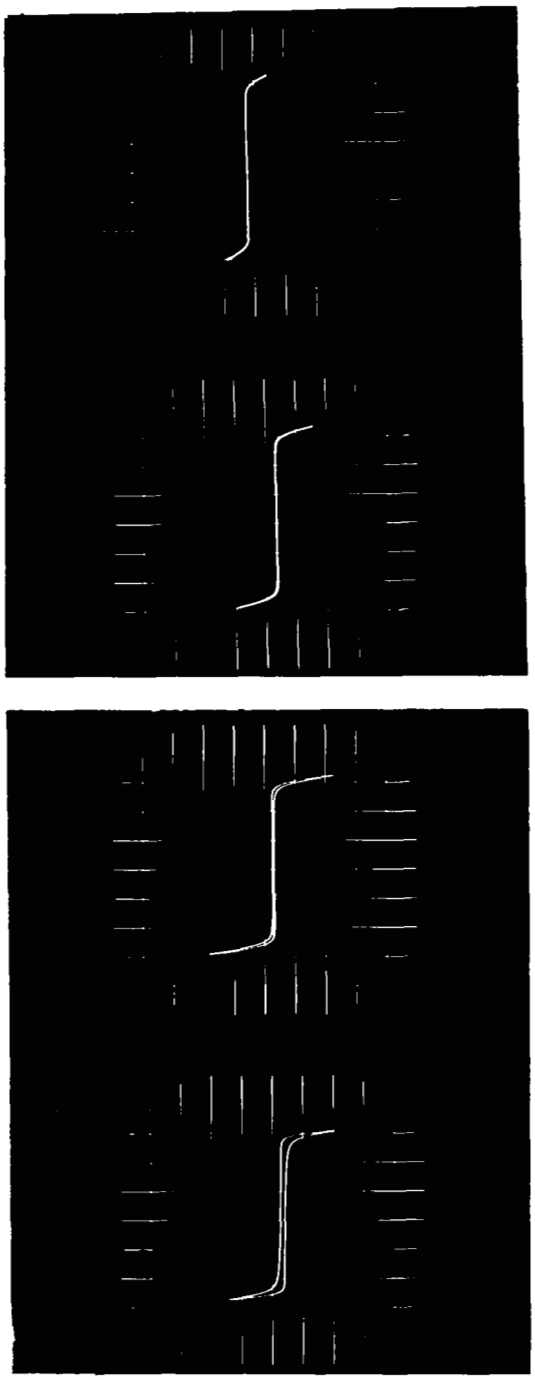

(a) f = 400 Hz
B = 5 kG/div
H = 100 Oe/div

(b) f = 800 Hz
B = 5 kG/div
H = 100 Oe/div

(c) f = 1600 Hz
B = 5 kG/div
H = 100 Oe/div

(d) f = 3200 Hz
B = 5 kG/div
H = 100 Oe/div

Figure 85. - AC Hysteresis Loop, Square Wave Excitation, 400, 800, 1600, and 3200 Hz, 0.006-Inch Doubly Grain Oriented Silicon Steel Toroid, Double Window Magnetic Field Annealed, 250° C

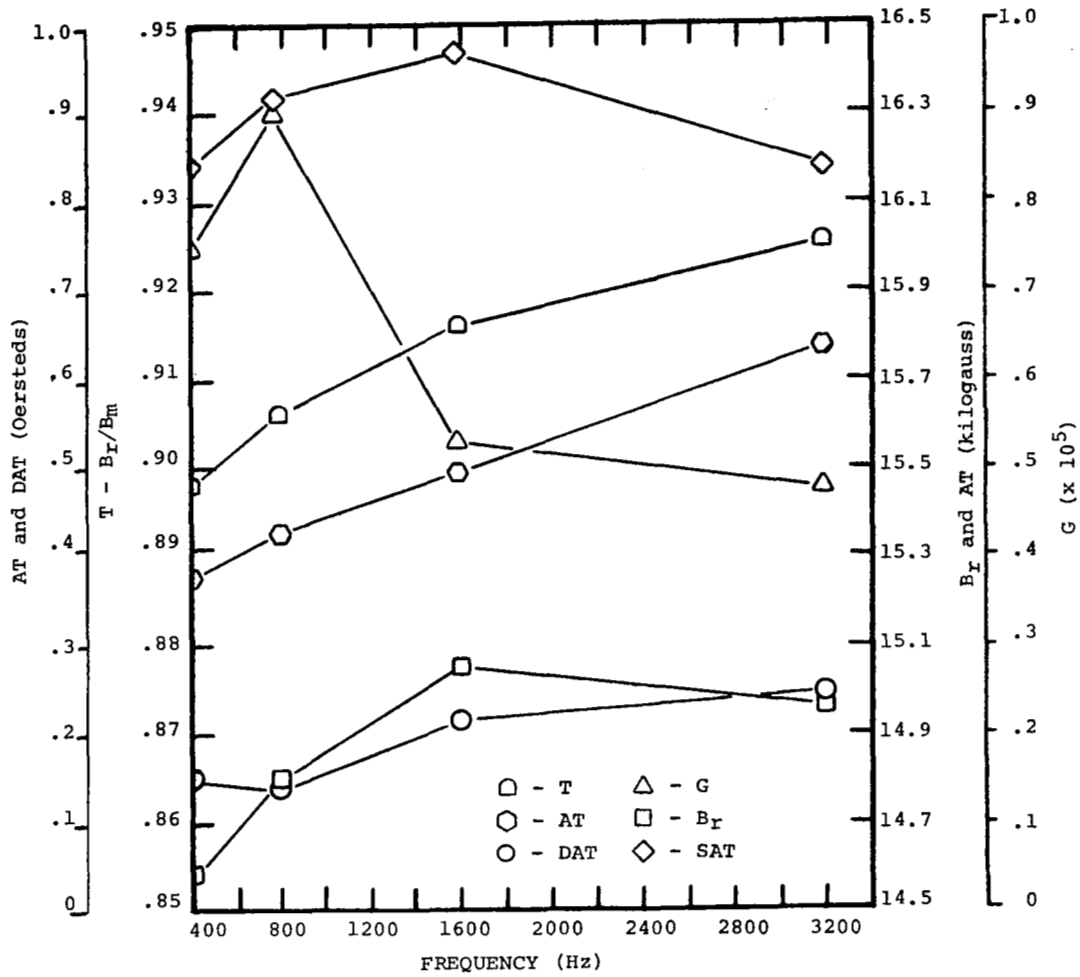

Figure 86. - CCFR Properties, 0.002-Inch Doubly Grain Oriented Silicon Steel, Double Window, Stress Relief Annealed, Room Ambient

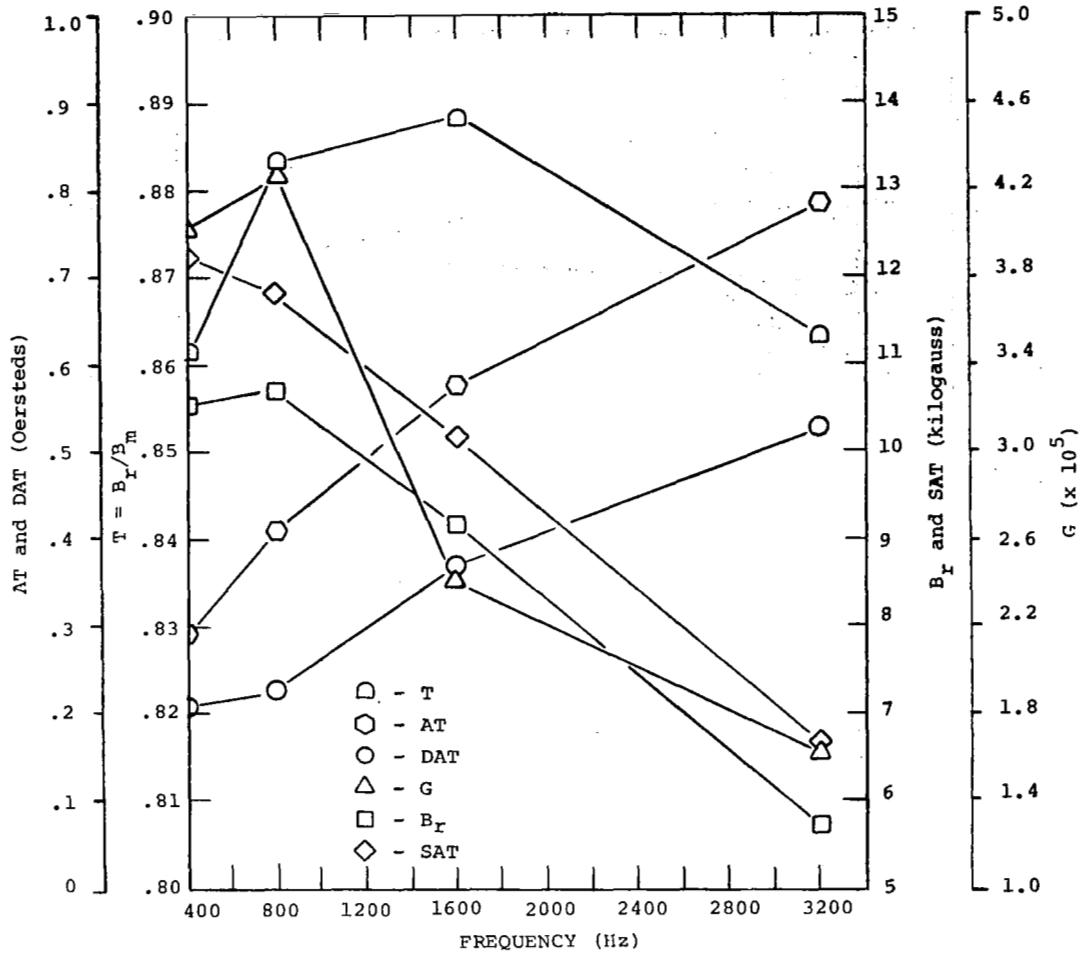

Figure 87. - CCFR Properties, 0.006-Inch Doubly Grain Oriented Silicon Steel, Double Window, Stress Relief Annealed, Room Ambient

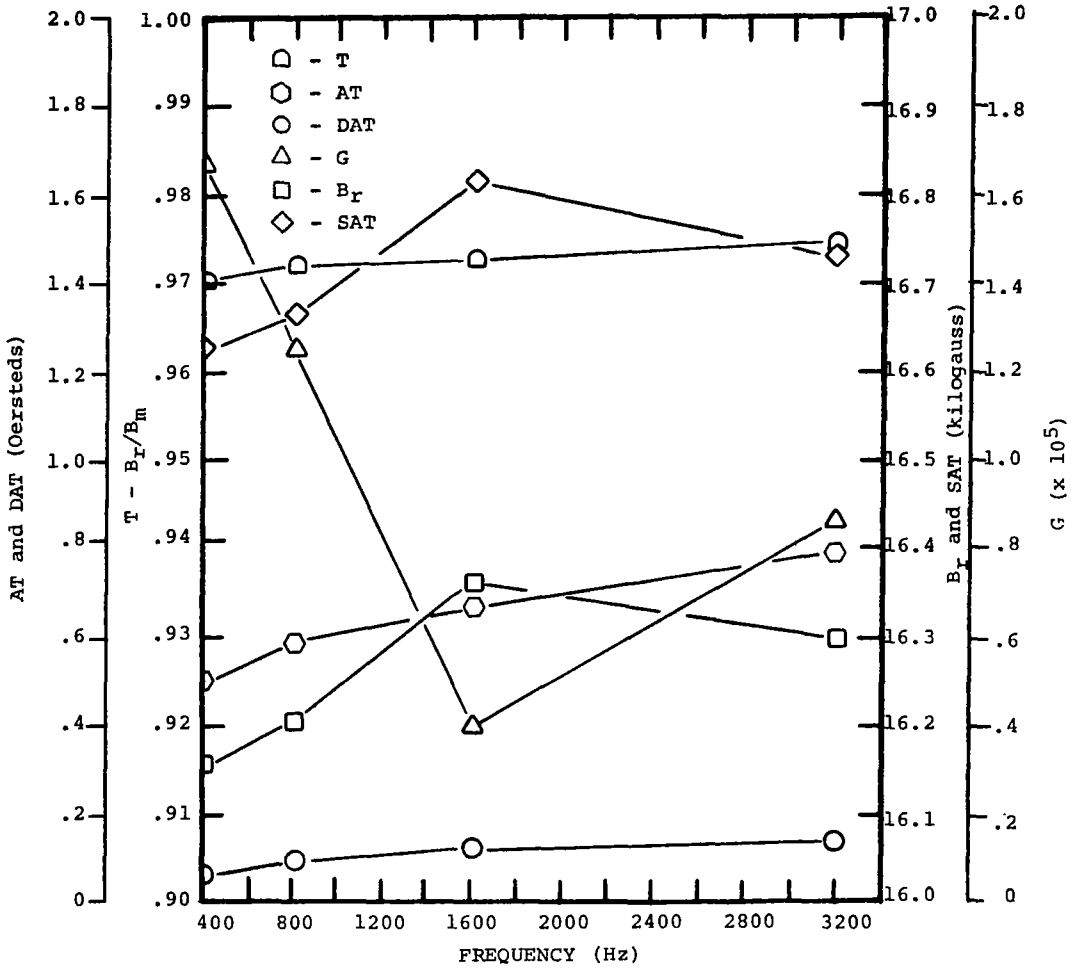

Figure 88. - CCFR Properties, 0.002-Inch Doubly Grain Oriented Silicon Steel, Double Window, Magnetic Field Annealed, Room Ambient

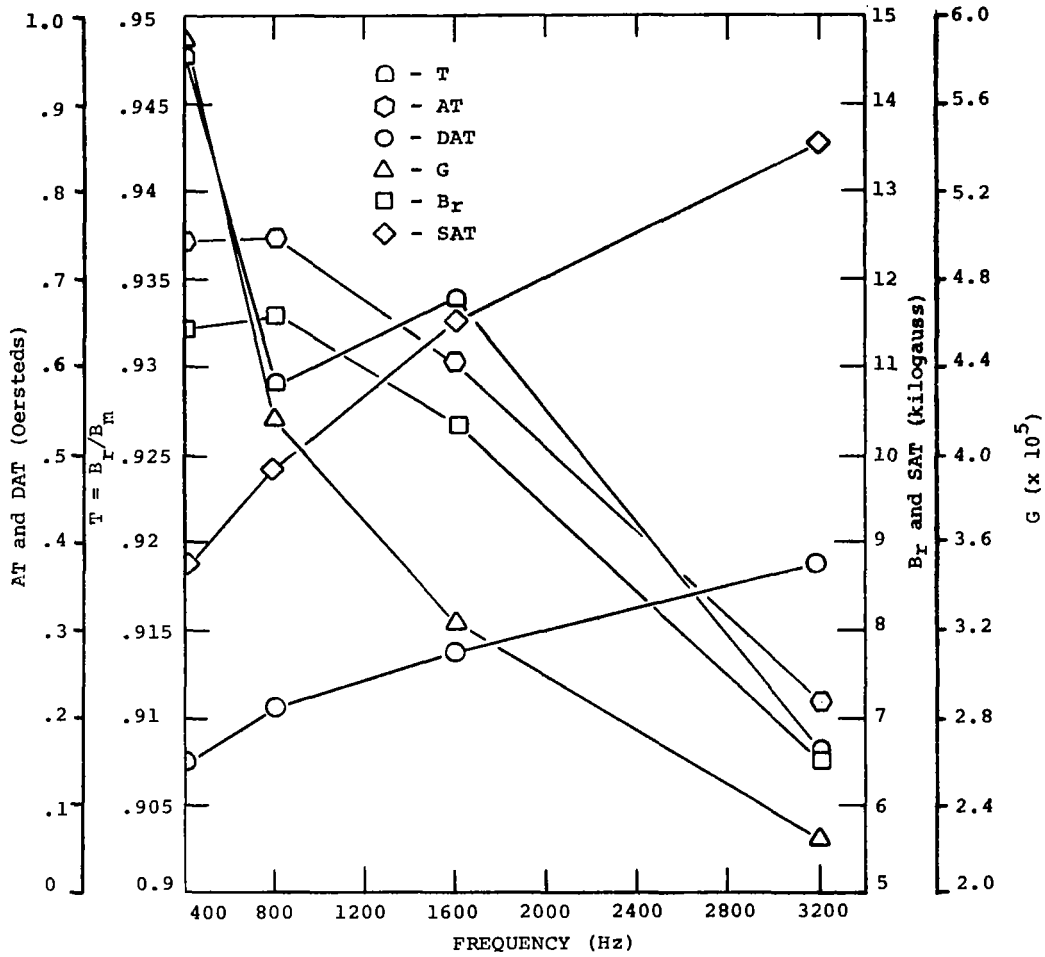

Figure 89. - CCFR Properties, 0.006-Inch Doubly Grain Oriented Silicon Steel, Double Window, Magnetic Field Annealed, Room Ambient

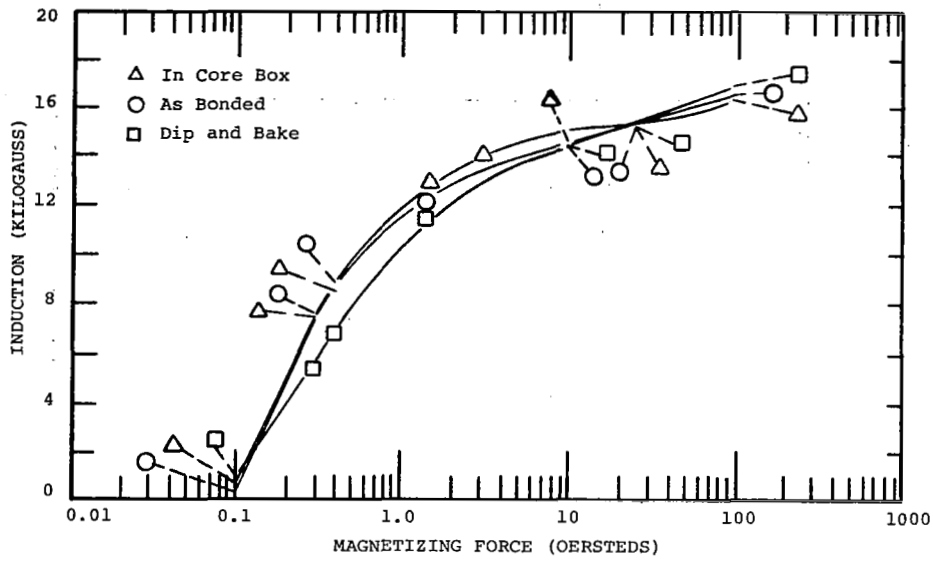

Figure 90. - Degradation Test, DC Magnetization, 0.006-Inch Doubly Grain Oriented Silicon Steel, Double Window, Stress Relief Annealed, Core 2, Room Ambient. Processing Variables: In Core Box, As Bonded, and Dip and Bake

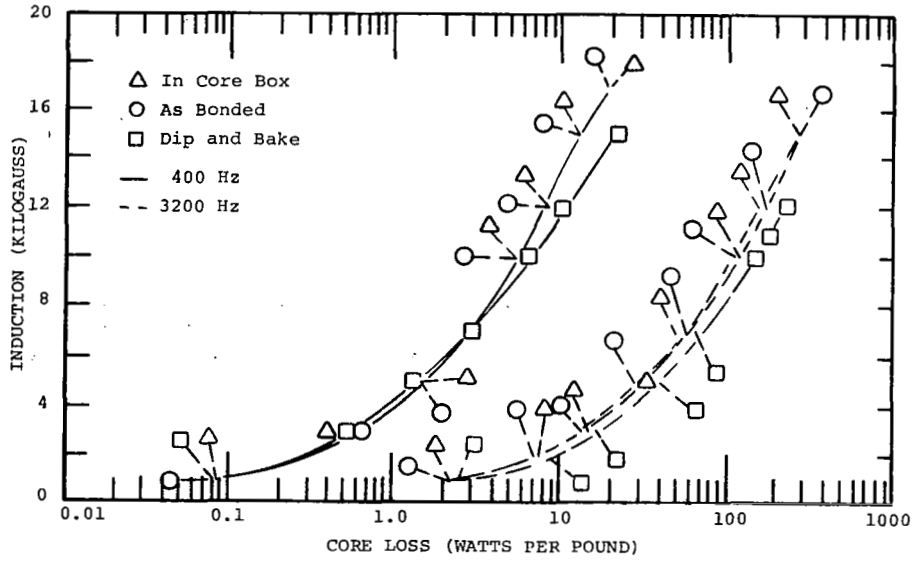

Figure 91. - Degradation Test, $P_{c,\ sq,}$ Total Core Loss, 0.006-Inch Doubly Grain Oriented Silicon Steel, Double Window, Stress Relief Annealed, Core 2, Room Ambient. Processing Variables: In Core Box, As Bonded, and Dip and Bake

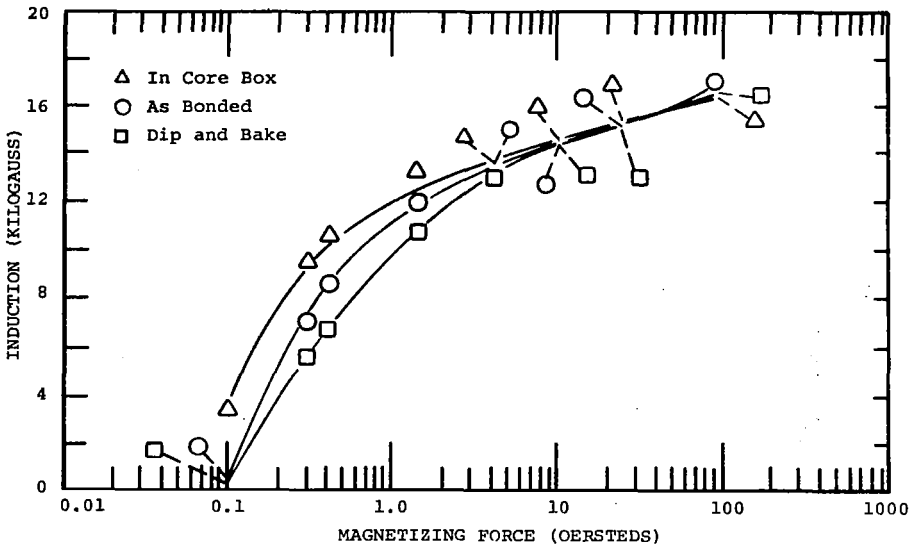

Figure 92. - Degradation Test, DC Magnetization, 0.006-Inch Doubly Grain Oriented Silicon Steel, Double Window, Magnetic Field Annealed, Core 1, Room Ambient. Processing Variables: In Core Box, As Bonded, and Dip and Bake

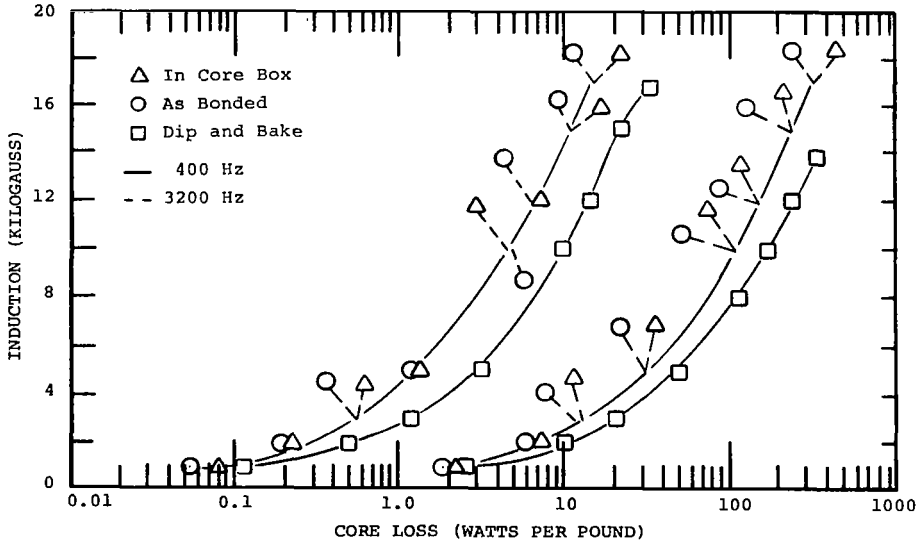

Figure 93. - Degradation Test, $P_{c,\ sq,}$ Total Core Loss, 0.006-Inch Doubly Grain Oriented Silicon Steel, Double Window, Magnetic Field Annealed, Core 1, Room Ambient. Processing Variables: In Core Box, As Bonded, and Dip and Bake

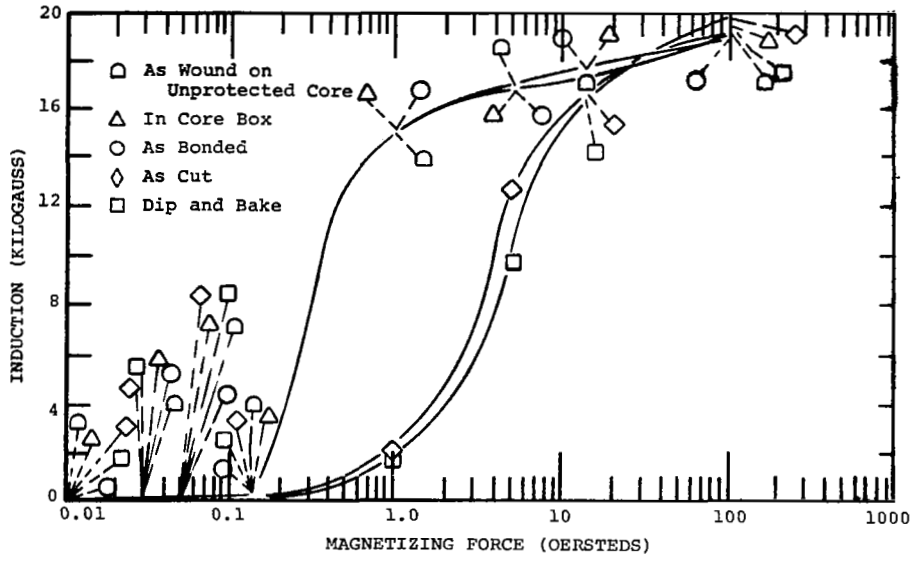

Figure 94. - Degradation Test, DC Magnetization, 0.006-Inch Singly Grain Oriented Silicon Steel, Square Toroid, Core 40, Room Ambient. Processing Variables: In Core Box, As Wound, As Bonded, As Cut and Dip and Bake

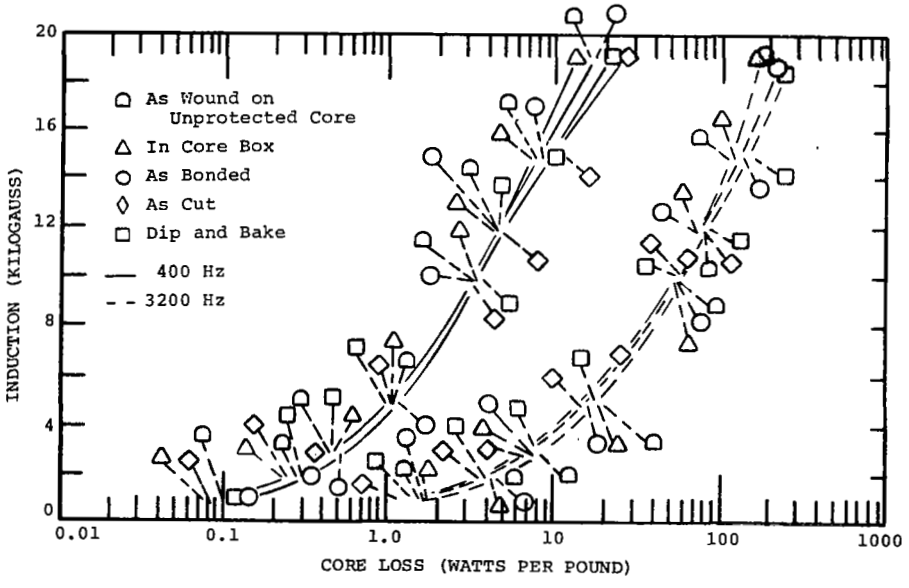

Figure 95. - Degradation Test, $P_{c,\ sq,}$ Total Core Loss, 0.006-Inch Singly Grain Oriented Silicon Steel, Square Toroid, Core 40, Room Ambient. Processing Variables: In Core Box, As Wound, As Bonded, As Cut and Dip and Bake

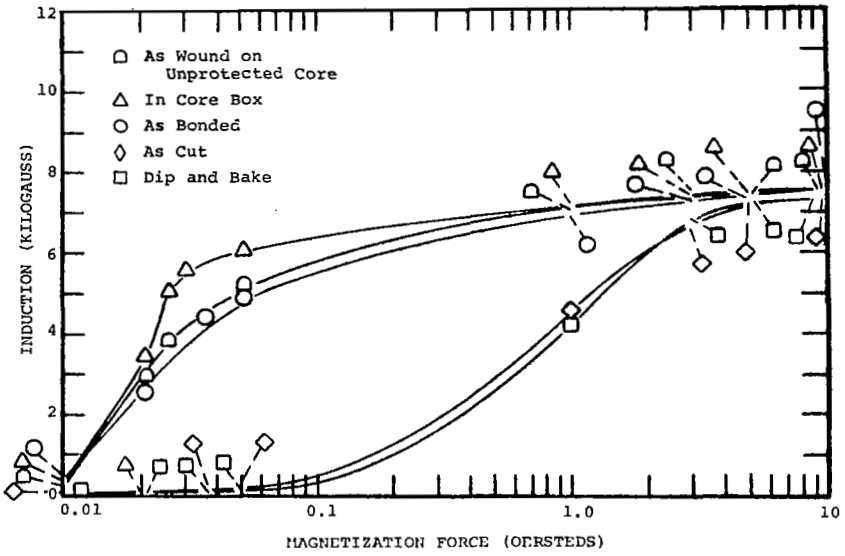

Figure 96. - Degradation Test, DC Magnetization, 0.004-Inch 4%Mo-79%Ni-17%Fe Toroid, Square Loop, Core 39, Room Ambient. Processing Variables: In Core Box, As Bonded, As cut, and Dip and Bake

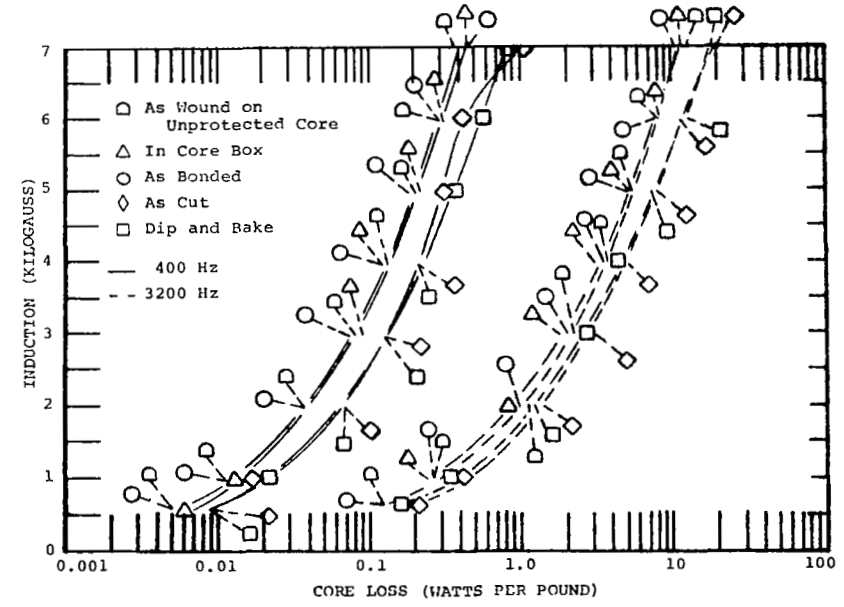

Figure 97. - Degradation Test, $P_{c, sq,}$ Total Core Loss, 0.004-Inch 4%Mo-79%Ni-17%Fe Toroid, Square Loop, Core 39, Room Ambient. Processing Variables: In Core Box, As Bonded, As Cut, and Dip and Bake

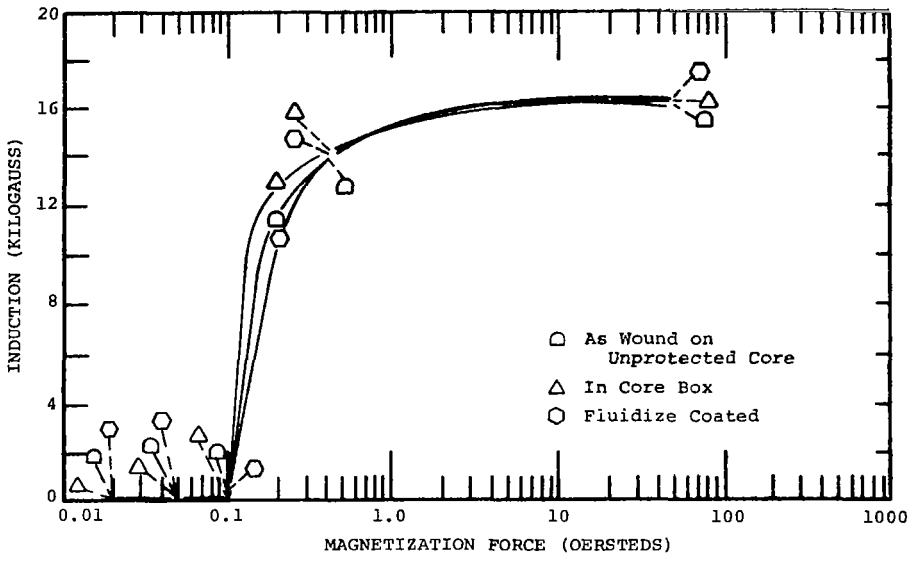

Figure 98. - Degradation Test, DC Magnetization, 0.004-Inch 50%Ni-50%Fe Toroid, Grain Oriented, Core 100, Room Ambient. Processing Variables: In Core Box, As Wound, and Fluidize Coated

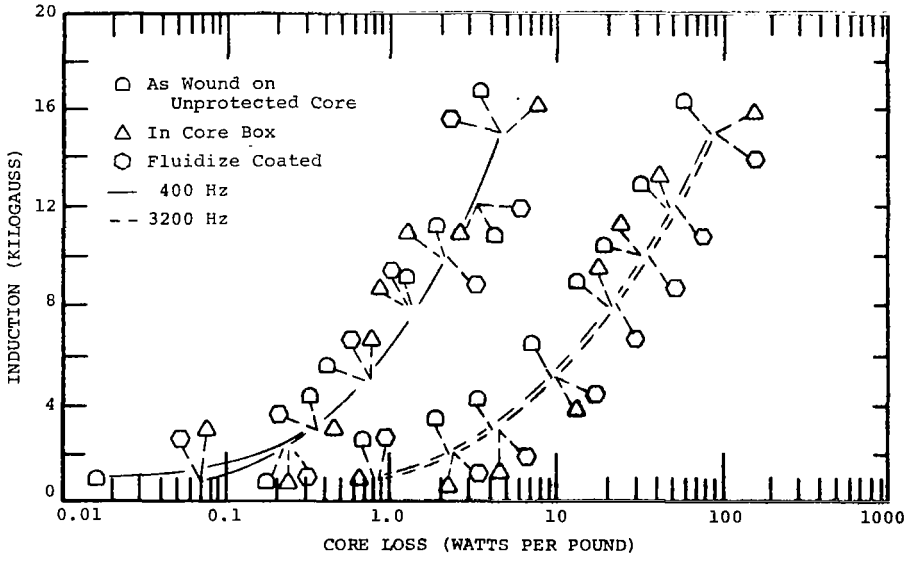

Figure 99. - Degradation Test, $P_{c,\ sq,}$ Total Core Loss, 0.004-Inch 50%Ni-50%Fe Toroid, Grain Oriented, Core 100, Room Ambient Processing Variables: In Core Box, As Wound, and Fluidize Coated

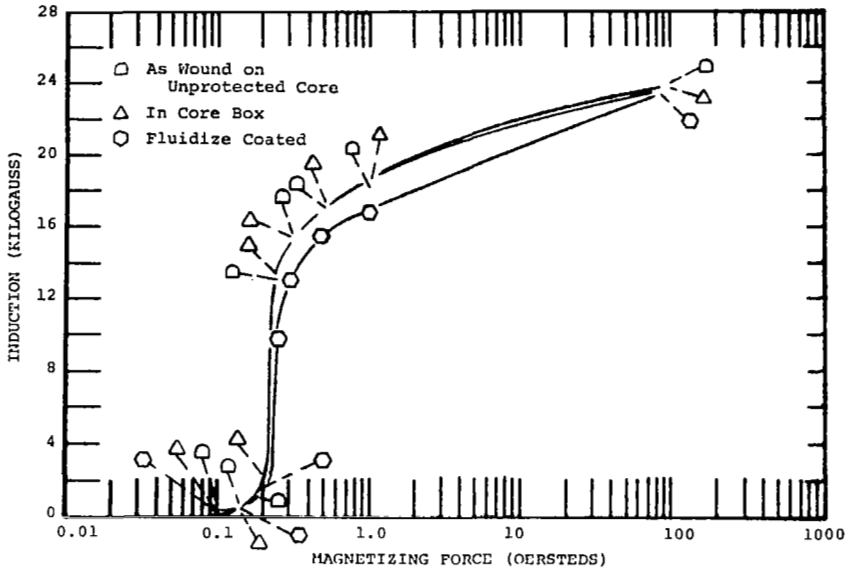

Figure 100. - Degradation Test, DC Magnetization, 0.004-Inch 49%Co-2%V-49%Fe Toroid, Magnetic Field Annealed, Core 101, Room Ambient, Processing Variables: In Core Box, As Wound, and Fluidize Coated

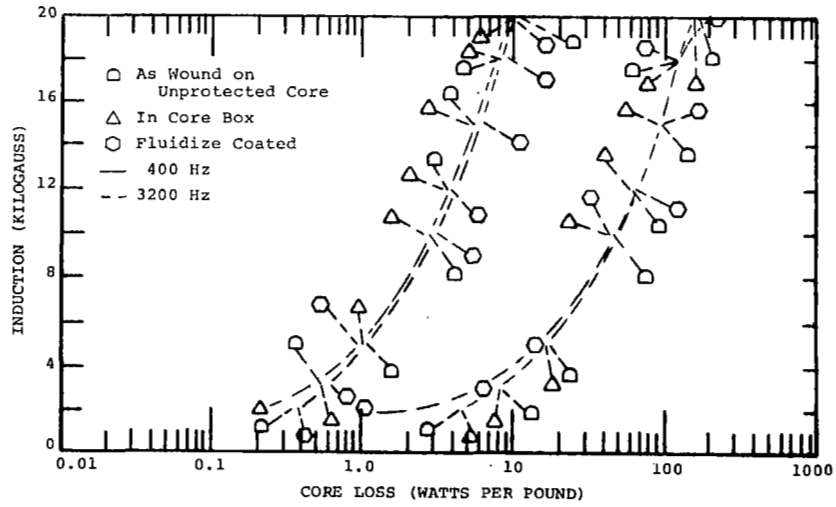

Figure 101. - Degradation Test, $P_{c,\ sq,}$ Total Core Loss, 0.004-Inch 49%Co-2%V-49%Fe Toroid, Magnetic Field Annealed, Core 101, Room Ambient Processing Variables: In Core Box, As Wound and Fluidize Coated

Vacuum Exposure Testing. - The effects of exposure to a vacuum of 10^{-6} torr for 500 and 1,000 hours at 250° C were evaluated in terms of: changes in core weight; changes in core loss; changes in interlaminar resistance; and changes in weight of interlaminar coating.

Weight Changes in Bonded Cores: The changes in weight of bonded cores (including windings) as a result of exposure are shown on table II for samples of SGO Si steel, DGO Si steel, and SHL 4Mo-79NiFe. The results show that there is practically no change in core weight for all the samples exposed to prolonged vacuum exposure at 250°C.

Core Loss Changes in Bonded Cores: The changes in total core loss as a result of exposure are shown on table III for samples of SGO Si steel, DGO Si steel and SHL 4Mo-79NiFe. The core bonding and subsequent vacuum exposure brought about an increase in core loss at high inductions of DGO Si steel MFA double window cores, resulting probably from partial loss of the magnetic annealing effect after prolonged exposure at 250° C. The core loss increase in SRA double window cores of DGO Si steel after 1000 hours exposure is unexplainable.

Core Loss Changes in Cores Not Bonded: The changes in total core loss of cores clamped but not bonded during exposure are shown on table IV for SHL 4Mo-79NiFe, GO 50NiFe, MFA 2V-CoFe, SGO Si steel, and DGO Si steel. The exposure produced only minor changes in core loss of SHL 4Mo-79NiFe and GO 50NiFe but larger core loss changes were observed in SGO Si steel and DGO Si steel.

Prolonged annealing at 250° C brought about a 10% decrease in core loss of DGO Si steel rings, SRA indicating the beneficial effect of aging on this material.

The core loss behavior of SGO Si steel appears to reflect the original core quality. The 0.006-inch rings displayed a decrease with prolonged exposure at 250° C and those of 0.004-inch rings an increase.

The rings of MFA 2V-CoFe display a decrease in core loss at both induction levels, more so in the 0.004-inch sample; this behavior may be due to a decrease in the effects of magnetic annealing with 250° C exposure.

Changes in Interlaminar Coatings: The changes in interlaminar resistance and weight observed on circular blanks as a result of exposure are shown on table V for SHL 4Mo-79NiFe, GO 50NiFe, MFA 2V-CoFe, SGO Si steel, and DGO Si steel. Changes in interlaminar insulation resistance were observed only on MFA 2V-CoFe and GO 50NiFe samples. The slight weight changes observed are not significant.

Table II. Weight of Cores, Plus Winding, Before and After Vacuum Exposure, 10^{-6} Torr, 250° C of Samples of Singly Grain Oriented Silicon Steel, Vendor No. 1; Square Hysteresis Loop, 4%Mo-79%Ni-17%Fe, Vendor No. 1; Doubly Grain Oriented Silicon Steel

Material	Core Type	Core Number	Weight of Core and Windings		
			Initial (g)	After 500 hrs at Vacuum of 10^{-6} Torr & 250° C (g)	After 1000 hrs at Vacuum of 10^{-6} Torr & 250° C (g)
0.004-inch Singly Grain Oriented Silicon Steel, Vendor No. 1, MgO Interlaminar Insulation	Square Toroid	70	657.9	655.65	655.1
0.004-Inch Square Hysteresis Loop, 4%Mo-79%Ni-17%Fe Vendor No. 1, MgO Interlaminar Insulation	Square Toroid	71	927.3	925.5	925.0
0.006-inch Doubly Grain Oriented Silicon Steel (magnetic field annealed) Aluminum orthophosphate Interlaminar Insulation	Double Window	72	636.9	635.0	635.0
0.006-inch Doubly Grain Oriented Silicon Steel (stress relief annealed) Aluminum orthophosphate Interlaminar Insulation	Double Window	73	650.0	648.45	648.45

Discussion of Test Results

Effect of Wave Form. - Schenk and Young[1] have shown that changing the excitation wave form from sine to square brings about up to 19% reduction in core loss. Favorable conditions include a high eddy-current content and a highly grain-oriented structure. This model applied probably to all of the materials tested in this program but comparable data are available only on DGO Si steel[2] and MFA 2V-CoFe cores.

In DGO Si steel, both SRA and MFA, the total core loss of square-wave and sine-wave excited samples is essentially the same at 400 Hz. As the frequency increases toward 3200 Hz, the square-wave excited samples display a less rapid increase in core loss than the sine-wave excited samples, and at 3200 Hz show a decrease of approximately 20% in the induction range 4 to 8 kG.

Table III. - $P_{c, sq}$ - Total Core Loss, Before and After Exposure, 10^6 Torr, 250° C, of Samples of Singly Grain Oriented Silicon Steel, Vendor No. 1; Square Hysteresis Loop, 4%Mo-79%Ni-17%Fe, Vendor No. 1; Doubly Grain Oriented Silicon Steel

Material	Core Type	Core Number	B, Induction (Kilogauss)	P_c, sq - Total Core Loss, 400 Hz, Room Ambient		
				After Dip & Bake Prior to Vacuum Exposure (watts/lb)	After 500 hrs at Vacuum of 10^{-6} Torr 250° C (watts/lb)	After 1000 hrs at Vacuum of 10^{-6} Torr 250° C (watts/lb)
0.004-inch Singly Grain Oriented Silicon Steel, Vendor No. 1, MgO Interlaminar Insulation	Square Toroid	70	10.0	3.2	3.69	3.91
			19.2	22.0	22.55	20.64
0.004-inch Square Hysteresis Loop, 4%Mo-79%Ni-17%Fe, Vendor No. 1, MgO Interlaminar Insulation	Square Toroid	71	4.0	0.20	0.150	0.180
			7.0	0.78	0.548	0.799
0.006-inch Doubly Grain Oriented Silicon Steel (magnetic field annealed) Aluminum Orthophosphate Interlaminar Insulation	Double Window	72	10.0	6.90	7.35	7.40
			15.4	17.0	26.15	22.8
0.006-inch Doubly Grain Oriented Silicon Steel (stress relief annealed) Aluminum Orthophosphate Interlaminar Insulation	Double Window	73	10.0	9.10	8.75	9.67
			17.0	24.0	24.2	32.95

Table IV. - Evaluation of $P_{c,sq}$ - Total Core Loss, 400 Hz, Room Ambient Temperature of Various Magnetic Materials After Heating to 250° C in a Vacuum of 10^{-6} Torr

Material[a]	Core Number	B, Induction, Kilogauss	P_c, sq - Total Core Loss at 400 Hz, Room Ambient		
			Initial Watts/lb	After 500 hours at 250°C in a Vacuum of 10-6 Torr Watts/lb	After 1000 hours at 250°C in a Vacuum of 10-6 Torr Watts/lb
0.006-Inch Square Hysteresis Loop, 4% Mo-79% Ni-17% Fe, Vendor No. 1	50	4.0 7.0	0.169 0.584	0.179 0.638	0.158 0.462
0.004-Inch Square Hysteresis Loop, 4% Mo-79% Ni-17% Fe, Vendor No. 2	66	4.0 7.0	0.195 0.453	0.222 0.569	0.210 0.505
0.004-Inch Singly Grain Oriented Silicon Steel, Vendor No. 1	52	10.0 19.2	4.01 16.8	3.83 18.2	3.72 20.6
0.004-Inch 49% Co-2% V-49% Fe, Magnetic Field Annealed	64	10.8 18.2	4.16 13.0	4.24 11.72	3.01 11.08
0.006-Inch 49% Co-2% V-49% Fe, Magnetic Field Annealed	54	10.0 18.2	4.33 12.8	3.86 11.8	4.4 12.25
0.006-Inch Doubly Grain Oriented Silicon Steel (Stress Relief Annealed)	56	10.0 17.0	5.12 17.2	5.47 14.68	4.45 15.55
0.006-Inch Singly Grain Oriented Silicon Steel, Vendor No. 2	58	10.0 19.2	4.31 20.5	3.57 17.9	3.87 18.8
0.006-Inch Grain Oriented 50% Ni-50% Fe, Vendor No. 1	60	8.0 14.8	2.11 7.25	2.21 7.08	1.95 6.19
0.004-Inch Grain Oriented 50% Ni-50% Fe, Vendor No. 2	63	8.0 14.8	1.22 4.38	1.07 4.24	1.39 4.48

[a] All cores were one inch stacks of Rowland rings coated with aluminum orthophosphate.

Table V. - Resistivity and Weights of Aluminum Orthophosphate Insulated Square Hysteresis Loop 4%Mo-79%Ni-17%Fe (Two Vendors), Grain Oriented 50%Ni-50%Fe (Two Vendors), Magnetic Field Annealed 49%Co-2%V-49%Fe, Singly Grain Oriented Silicon Steel (Two Vendors), and Doubly Grain Oriented Silicon Steel Circular Blanks Before and After Exposure to Vacuum of 10^{-6} Torr for 1000 Hours at 250° C

Material	Surface Area (sq. cm)	No. Blanks	R_S (OHMS-CM^2) (a) Average Inter-Lamination Resistance		Weight (g)		Weight Difference (g)
			Before	After	Before	After	
0.006-Inch Square Hysteresis Loop, 4%Mo-79%Ni-17%Fe, Vendor No. 1, Core No. 6	53.63	150	$>3.58\times10^6$	$>3.58\times10^6$	1094.3720	1094.3603	0.0117 (-)
0.004-Inch Square Hysteresis Loop, 4%Mo-79%Ni-17%Fe, Vendor No. 2, Core No. 1	53.63	225	$>2.38\times10^6$	$>2.38\times10^6$	994.8650	994.7744	0.0906 (-)
0.004-Inch Singly Grain Oriented Silicon Steel, Vendor No. 1, Core No. 10	53.63	225	$>2.38\times10^6$	$>2.38\times10^6$	897.7174	897.6259	0.0915 (-)
0.004-Inch 49%Co-2%V-49%Fe (Magnetic field annealed) Core No. 11	53.63	225	4.77×10^5	7.94×10^3	1086.2779	1086.2724	0.0055 (-)
0.006-Inch 49%Co-2%V-49%Fe (Magnetic field annealed) Core No. 9	53.63	150	2.53×10^2	2.99×10^2	1038.9420	1038.9546	0.0126 (+)
0.006-Inch Doubly Grain Oriented Silicon Steel, (Stress relief annealed) Core No. 3	53.63	150	$>3.58\times10^6$	$>3.58\times10^6$	975.8928	975.8025	0.0903 (-)
0.006-Inch Singly Grain Oriented Silicon Steel, Vendor No. 2, Core No. 15	53.63	150	$>3.58\times10^6$	$>3.58\times10^6$	917.8985	917.9036	0.0051 (+)
0.006-Inch Grain Oriented 50%Ni-50%Fe, Vendor No. 2, Core No. 4	53.63	150	$>3.58\times10^6$	21.4×10^4	1016.7385	1016.7404	0.0019 (+)
0.004-Inch Grain Oriented 50%Ni-50%Fe, Vendor No. 1, Core No. 17	53.63	225	$>2.3\times10^6$	5.55×10^4	1049.9020	1049.8552	0.0468 (-)

a - Preloaded at 750 psi and tested at 150 psi. Samples cycled between 750 psi and 150 psi until resistance measurement remained approximately constant. A Wheatstone bridge was used for insulation measurements, and the maximum reading was 1×10^7 ohms.

In MFA 2V-CoFe cores, the square-wave effect is based on the perfection of the domain structure. As will be discussed later in this chapter, a highly domain-oriented core, such as the 0.002-inch tape-wound toroid used in this program, has a higher total core loss at 400 Hz than a core of the same material but with a lower degree of domain orientation. An example of the latter material is the 0.004-inch MFA 2V-CoFe Rowland ring core evaluated in this program. Figures 36 and 37 show that with an increase in frequency, above 800 Hz, the toroid (figure 37) displays a smaller increase in core loss than the ring (figure 36). For higher inductions at frequencies of 1600 and 3200 Hz, the toroid displays lower losses than the ring in spite of the fact that at 400 Hz the ring showed considerably lower losses than the toroid.

Effect of Temperature. - With the exception of the MFA 2V-CoFe toroid, all the cores tested followed the same pattern in the change of dc and ac properties with temperature. This pattern of change will be discussed below.

When a single-phase magnetic material, such as grain-oriented silicon steel, is subjected to increasing temperatures (room temperature being just a temperature not a dividing line) the following changes occur: (a) the magnetization curve rises more quickly at lower fields and then flattens out and saturates at progressively lower inductions; (b) coercive force and residual induction decrease with increasing temperature; and (c) no change in room temperature magnetic properties occurs after high-temperature exposure. In addition, electrical resistivity increases with increasing temperature; for instance, the electrical resistivity of doubly grain oriented silicon steel alloy increases approximately 40% between room temperature and 250° C.[2]

The above conditions are conducive to the lowering of both hysteresis and eddy current losses, hence a decrease in core loss with increasing temperature, especially at lower inductions, can be expected. The core loss decreases gradually with increasing temperature.

Since exciting volt-amperes (apparent power) reflect competing effects of core loss and permeability, this characteristic displays a different response to an increase in temperature than the core loss. The pattern of change of exciting volt-amperes with increasing temperature displays an induction value where the competing effects of permeability and loss are at equilibrium. At this induction value the apparent power shows practically no change with temperature. Above that induction, the exciting volt-amperes increase with increasing temperature; below that induction, they decrease with increasing temperature. Futhermore, the frequency was observed to affect the position of this "dividing line", apparently displacing it toward lower induction values with increasing frequency. Depending on the material's

quality, test frequency, and core geometry, the induction at which the "dividing line" occurs for the cores tested was as follows: 12 to 14 kG for the SGO Si steel cores, 8 to 12 kG for the DGO Si steel cores, 8 to 11 kG for the GO 50NiFe cores, and 3 to 4 kG for the SHL 4Mo-79NiFe cores.

The rate of change with temperature of both dc and ac magnetic properties is primarily affected by the temperature dependence of the material's saturation magnetization. This dependence is expressed in the Is/Io versus T/T_{Curie} diagram.[3] In practical terms, this means that within the same temperature range the amount of change in the slope of the magnetization curve or in ac properties is smaller in an Fe-Co alloy (T_{Curie} 980°C) than in a 3%Si-Fe alloy (T_{Curie} 760°C); or, that the magnetic properties of Fe-Ni alloys between -55°C and 250°C display a considerably greater magnitude of change than those in Co-Fe or Fe-Si alloys.

The response of the MFA 2V-CoFe toroid to an increase in temperature was different from that of the MFA 2V-CoFe laminated ring or the other materials evaluated in this program. The MFA 2V-CoFe toroid follows a pattern in which dc and ac magnetic properties follow opposing trends with increasing temperature. The highly domain-oriented structure of this material, which brings about a rectangular dc hysteresis loop, is also conducive to a considerable "anomalous" loss. An increase in temperature, probably up to 400°C, promotes the perfection of this domain structure; this is reflected in an increase of the steepness of the magnetization loop but also in an increase in core loss. Judging by its dc properties, the laminated ring of this material has a lower degree of domain orientation and consequently, the pattern of change in both dc and ac magnetic properties of this core with temperature is similar to that of the other core materials evaluated in this program.

Effect of Grain Orientation, Domain Orientation and Gauge. - The magnetic quality of all the materials evaluated in this program depends on special treatments that these materials--or more properly their structures--were subjected to. These structure treatments will be discussed and correlated with the magnetic behavior of the core materials.

The best soft magnetic properties in a material are obtained when magnetic energies such as the magnetocrystalline energy and the magnetostrictive energy are zero. The alloys of the 4 to 5% Mo, 79%Ni-Fe family approach this condition more closely than the other materials tested in this program. As a result, 4%Mo-79%Ni-Fe cores show a very high permeability and low loss. When subjected to a special cooling treatment this material also displays a rectangular hysteresis loop. However, the saturation of this alloy family is relatively low.

When the anisotropies cannot be minimized or eliminated, the most effective way of producing favorable magnetic properties, particularly in a sheet or tape, is to either develop a suitable texture (grain orientation) or to apply magnetic annealing (domain orientation). Texture makes it possible for the easy direction of magnetization to coincide with the direction of applied field. Magnetic annealing, on the other hand, superimposes a uniaxial anisotropy in the direction of the field thus making that direction the material's easy direction of magnetization. Depending on their basic characteristics different materials respond differently to those treatments.

Si-Fe alloys and 50%Ni-50%Fe alloy respond well to texture treatments. A high degree of either "cube-on-edge" (SGO) or "cube-on-face" (DGO) texture can be produced in Si-Fe alloys (usually containing 3%Si in the DGO material and 3.25%Si in the SGO material). An even higher degree of "cube-on-face" texture can be produced in 50%Ni-50%Fe tape. In the "cube-on-edge" texture the easy direction of magnetization is aligned with the rolling direction of the sheet; in the "cube-on-face" texture the easy direction of magnetization coincides with both the rolling direction as well as with the direction perpendicular to it.

The presence of two mutually perpendicular easy directions of magnetization in the plane of the DGO Si steel sheet makes this material suitable for applications in cores of window frame design. However, this geometry has certain drawbacks; the corners of the window frame contain less-favorable directions of magnetization and cause the flux lines to congest to some extent in that area. As a result, the magnetic quality of the window frame core processed from DGO Si steel sheet is inferior to that of either grain-oriented silicon steel toroid (in which the flux travels only along the preferred direction of magnetization).

DGO Si steel toroid responds to magnetic annealing but the effect is less pronounced than in the MFA 2V-CoFe toroid. As compared with the SRA core of the same material, the MFA Si steel toroid displays higher permeabilities and improved CCFR properties but only minor improvements in ac magnetic properties. Both of these DGO Si steel toroids show higher dc permeabilities than the SGO Si steel toroid but only comparable ac properties.

The respective dc properties of both grades (toroid and laminated ring) of MFA 2V-CoFe compare favorably with published data. However, the ac properties of both the toroid and the ring show high total core losses at all four frequencies. The core losses in the toroids are twice those reported for a different batch of MFA 2V-CoFe toroids in a previous study.[2] The core losses in rings are either comparable (up to 15 kG) or higher than those reported previously for a laminated ring, 0.006-inch-lamination thickness.[2] Since the material used in both cases

has comparable dc properties, faulty interlaminar insulation was suspected to be causing excessive core losses; however resistivity checks did not confirm this assumption.

The principal effect of gauge is the one associated with the well-known decrease of eddy-current loss with diminishing sheet thickness. However, texture perfection may also change with gauge resulting in differences in magnetic quality with sheet thickness, particularly with respect to dc and the corresponding CCFR properties. For instance, DGO Si steel tape, 0.002-inch-thick, displays a better magnetic quality than the sheet, 0.006-inch-thick. The situation is different in the material with the cube-on-edge texture because SGO Si steel tape shows better magnetic quality in a thicker gauge. Although a thinner gauge is preferable in grain-oriented 50%Ni-50%Fe alloy, the difference in magnetic quality between the tapes, 0.002- and 0.004-inch-thick, is usually not as pronounced in this material as in both grain-oriented Si steels.

Effect of Frequency on CCFR Properties. - CCFR properties versus an increase in frequency of square wave excitation show a rise in AT and DAT and a decrease in gain for all the materials and core configurations tested. The drop in gain with frequency was especially pronounced in the high-gain materials -- GO 50%Ni-Fe and SHL 4%Mo-79%Ni-17%Fe. With the exception of the 0.002-inch tape-wound toroid of the latter material and the DGO Si steel double window cores, all the cores tested approach at 3200 Hz a gain value between 0.75×10^5 and 1×10^5. The SHL 4%Mo-79%Ni-17%Fe toroids show at 3200 Hz a gain of 0.55×10^5 and 2.5×10^5 for tape thicknesses of 0.004-inch and 0.002-inch respectively; the double window cores display a surprisingly high gain, 2.2×10^5, at 3200 Hz. For a given H_m, the average values of SAT, B_r, and T (squareness) show some, rather small and irregular, fluctuations with frequency except for the DGO Si steel double window cores which show a considerable decrease of these properties at 3200 Hz.

In the area of CCFR properties, no published data could be located with respect to the effects of increased frequency for either sine wave or square wave excitation. The CCFR tests performed in this program show, as expected, a progressive increase in dc reset magnetizing force (H_0, H_1, H_2) with increasing frequency and the corresponding increase in incremental magnetizing force (DAT) which in turn brings about a drop in gain. This change in properties was probably brought about through a decrease in the time period allowed for the dc current to accomplish the flux reset (further studies would be needed to confirm this model). At the higher end of the frequency range, somewhat higher excitation currents were required for most cores to maintain their B_m value in CCFR tests. The reason for this increase in excitation current requirement is that in the higher frequency

range the magnetization curve is shifted toward higher fields with an increase in frequency thus requiring a higher excitation field to maintain the same induction level.

AC Hysteresis Loops. - Both the shape and B_m of the ac hysteresis loops are in good agreement with the magnetization data. The ac hysteresis loops widened considerably with frequency as well as with the perfection of domain orientation. Some distortion at higher frequencies was noted in the ac hysteresis loop of MFA 2V-CoFe cores.

Effect of Mechanical Degradation. - Of all the strain-inducing magnetic degradation effects evaluated, core cutting is the most damaging. DC magnetization curves of cut toroids of SGO Si steel and SHL 4Mo-79NiFe flatten out at low fields and do not approach the dc magnetization curve of the uncut toroids until the latter start to approach saturation. In addition, the core loss increased 40 to 70%. Other operations such as dip and bake produce only slight degradation, the extent of which may depend on the geometry of the core or on the magnetic structure of the material or on a combination of both factors. For instance, dip and bake had a greater degradation effect on the DGO Si steel double window cores than on toroids. On the other hand, bonding stresses, which are somewhat detrimental to most cores tested raise the low-field portion of the SHL 4Mo-79NiFe magnetization curve because the magnetic structure of this material responds favorably to small tensile stresses. The stresses associated with fluidized coating appear to have a greater effect on the magnetization curve of the MFA 2V-CoFe toroid than the other similar treatments.

Magnetic degradation effects are in most cases the result of strain induced into the structure of the materials by external mechanical or chemical stresses during processing and service. The strain produces stray fields which make the magnetization process harder and generally bring about an increase in hysteresis loss and a shift of the magnetization curve toward higher fields. The effects of dip and bake, winding, bonding or fluidizing are generally based on the above mechanism. The interactions between the stress systems and the structure of the material determine the extent of damage.

The major component in the effect of core cutting is the air gap. An air gap has a powerful demagnetizing effect resulting in shearing over of the hysteresis loop and a considerable decrease in permeability of high-permeability materials. The ac excitation follows the same pattern. However, the core loss is considerably less effected by the introduction of a small air gap than the magnetization characteristics. The magnitude of the air gap effect also depends on the length of the mean magnetic path and on the characteristics of the uncut core. For the same air gap, the decrease in permeability will be less with a greater

length of the magnet flux path but more pronounced in a low coercive force, high permeability core.

Effect of Vacuum Exposure. - Vacuum exposures at 250° C for 500 hours and 1000 hours produced practically no change in the weight of core windings. However, after this vacuum exposure some decrease in average interlaminar resistance was apparent in several different cores which were coated with aluminum orthophosphate.

Long-time exposure at lower temperatures can produce chemical effects such as (a) precipitation of carbides ("aging") in certain grades of Si-Fe, (b) strain associated with atomic ordering in some Ni-Fe and Co-Fe alloys, and (c) diffusion of harmful impurities from the interlaminar insulation or gas environment into the core. Apparently, none of these effects have taken place during the 250° C exposure in a vacuum. The slight decrease in core loss is probably the result of an accompanied stress relief effect. An increase in core loss of MFA toroids of DGO Si steel resulted in all probability from the partial loss of the magnetic annealing effect after long-time exposure at 250° C.

APPLICATION OF MATERIALS EVALUATED

The materials tested in this program have many uses in devices that must be operated with square wave excitation. The materials properties shown in this report can be obtained in many production configurations but it is essential that detailed requirements be established for cores and that cores be suitably tested to assure that design requirements are achieved. In many configurations the exact properties shown in this report are not achievable and consideration must be given to packaging and manufacturing processes to be certain devices will operate as required.

Potential uses of the materials are shown on table VI and in the following discussion.

Square Hysteresis Loop 4%Mo-79%Ni-17%Fe

This material can be used in many applications as indicated by table VI. The material has very low core loss, however, its saturation flux density is approximately one half of the grain oriented 50%Ni-50%Fe material. The alloy is especially useful in apparatus such as high accuracy current transformers where losses must be kept to a minimum. It is also preferred in applications where the frequency exceeds 5000 Hz.

Table VI. Potential Application of Materials

Application	Material					
	4%Mo-79%Ni-17%Fe	50%Ni-50Fe	Magnetic Field Annealed 49%Co-2%V-49%Fe	Singly Grain Oriented Silicon Steel	Doubly Grain Oriented Silicon Steel Stress Relief Anneal	Doubly Grain Oriented Silicon Steel Magnetic Field Anneal
Power Transformers			X	X	X	X
Specialty Type Transformers	X	X	X	X	X	X
Current Transformers	X	X	X	X	X	X
Pulse Transformers	X	X	X	X	X	X
Reactors (Inductors)			X	X	X	X
Saturable Reactors	X	X	X	X	X	X
Magnetic Amplifiers	X	X	X	X	X	X
Flux Counters	X	X				
Transductors	X	X	X	X	X	X
Time Delays	X	X				
Bi-Stable Switching Devices	X	X				
Saturating Switching Devices	X	X				

Grain Oriented 50%Ni-50%Fe

The material is available in laminations and toroidal configurations. Because the material is strain sensitive it is not available in cut core form.

The material is frequently used in saturable reactors, high gain magnetic amplifiers, bi-stable switching devices and power inverter-converter applications. It is also used in applications which demand extremely rectangular hysteresis loops such as time relays, flux counters, and transductors.

Magnetic Field Annealed 49%Co-2%V-49%Fe Alloy

This material has performance characteristics similar to the oriented silicon irons. The major difference is that the saturation flux density of this material is considerably higher. If the higher flux density capability can be utilized, a weight reduction of up to 25 percent is possible. The main disadvantage of this material is its very high cost.

Grain Oriented Silicon Steels

These materials, with their high saturation flux density, high squareness, mechanical stability, relatively low core loss, and relatively low cost, are the most widely used materials for magnetic devices. The materials have a wide application in power transformers, specialty type transformers, current transformers, pulse transformers, ac and dc reactors, saturable reactors, magnetic amplifiers, and transductors.

The materials are available for use in lamination or strip wound toroidal and cut "c" cores. Because cores can have an air gap in the magnetic path they may be used readily in circuits such as inverters, where a dc component of flux may be present. With care in selecting the material thickness, to keep the hysteresis losses low, the materials may be used at relatively high frequencies. However, at higher frequencies it may not be possible to operate these materials at high flux densities, and laminations are not commercially available in thicknesses below four mils.

The oriented silicon irons all have basically the same general characteristics with there being little difference to guide a selection between singly oriented and doubly oriented stress relief annealed tape material. The doubly oriented material may be preferred in a lamination or when the special characteristics of magnetic field annealing are desired.

CONCLUSIONS

Square wave excitation as compared to sine wave excitation,[1] brings about a decrease in core loss at frequencies above 800 Hz for at least doubly grain oriented silicon steel and magnetic field annealed 49%Co-2%V-49%Fe alloy. At 3200 Hz a core loss reduction of 15% was realized for both materials. The other core materials may also be responding in the same manner to square wave excitation but no corresponding sine wave data for 800, 1600, and 3200 Hz were found in the literature for comparison.

In core loss, the magnetic field annealed doubly grain oriented Si steel toroid and the magnetic field annealed 49%Co-2%V-49%Fe alloy show optimum capabilities at high inductions. The square loop 4%Mo-79%Ni-17%Fe has the lowest core loss of all the materials tested for inductions up to 5 kG.

Temperature wise, both silicon steel toroids show the lowest change in magnetic properties between -55° C and 250° C.

In CCFR tests, highest gain values at 400 Hz are displayed by the square hysteresis loop 4%Mo-79%Ni-17%Fe toroids (4.35×10^5 to 9.5×10^5). The gain values decrease 70 to 90% in all materials with an increase in frequency to 3200 Hz. The highest squareness ratio was shown by the grain-oriented 50%Ni-50%Fe cores. In spite of some variations, there appears to be no change in squareness with increasing frequency. The same applies to the SAT values although in most cases higher H_m is required to maintain B_m at 3200 Hz.

Of all the strain-inducing magnetic degradation processes studied, core cutting is the most damaging. Some other operations such as dip and bake or a fluidized coating produce only a slight degradation the extent of which may depend on the magnetic structure of the material.

The exposure of cores to vacuum at 250° C for 10,000 hours produced only a slight change in core losses and very little change in core weight.

The grain oriented 50%Ni-50%Fe toroid has an optimum combination of overall magnetic properties for core applications within the conditions specified in this program. The magnetic field annealed doubly grain oriented silicon steel is the second most generally useful material particularly if higher flux densities and a minimum change in magnetic properties between -55° C and 250° C are required. The square hysteresis loop 4%Mo-79%Ni-17%Fe toroid is best suited for core applications requiring a high gain, the magnetic field annealed 49%Co-2%V-49%Fe toroid

for those requiring a high saturation. The singly grain-oriented silicon steel toroid is a suitable substitute for the stress relie annealed doubly grain-oriented silicon steel toroid but does not attain the magnetic quality of magnetic field annealed doubly grain-oriented silicon steel.

APPENDIX A

CONDUCTORS AND CONDUCTOR INSULATION REVIEW

Electrical conductor insulations systems and the use of aluminum foil for transformers was reviewed.

Developments in recent years have shown that aluminum foil is very useful in both commercial and aerospace applications.

The use of aluminum foil instead of copper wire has the following advantages.

(1) Conductivity-to-weight ratio is better compared to copper.

(2) Ease of winding.

(3) Better space factor with the proper insulation.

(4) Better cooling with virtual elimination of hot spots.

(5) Lower voltage stresses (turn-to-turn only).

Aluminum foil has the following disadvantages:

(1) Lower volume conductivity compared to copper.

(2) Problems with lead connections.

The electrical volume conductivity of aluminum foil (EC Alloy) is approximately 64 percent of that of copper. Aluminum with a larger volume but lower density results in a winding having about 50 percent the weight of an equivalent copper winding. Lead connections can be made adequately but the connection cost is higher and multiple connections are frequently required.

The most difficult problem to overcome in aerospace applications is turn-to-turn insulation where the conductor thickness is small. In aerospace applications, it is necessary to operate transformers at the maximum temperature possible with regard to operating conditions, reliability, and life. One of the materials used for turn-to-turn insulation is Mylar which is a Class B insulation and good only to about 150° C. An anodic coating is satisfactory in regard to operating temperature and insulation thickness but has many problems. Some of the problems of the anodic coating are poor flexibility resulting in crazing of the coating, inconsistent quality of coating, burred foil edges,

little resistance to foreign material in the winding, and high cost of coating thin gauges. Another insulation being used is a coating of ML Enamel on one side of anodized aluminum. This ML coated material has good performance but it is relatively expensive.

Commercial distribution transformer manufacturers are now using aluminum foil. Since weight is generally not critical in distribution transformers, the main goal is to utilize the other advantages of aluminum foil. Because aluminum is more ductile than copper, it forms better, creating a tightly wound unit. Aluminum strip conductor is easier to wind than copper wire, reducing manufacturing costs. Because of its better cooling properties, strip wound coils permit greater overloads. The aluminum foil is often insulated with an epoxy enamel which is limited in temperature as it is a Class B material.

Recent developments of polyimide and polyamide insulating materials have created a new possibility for turn-to-turn insulation materials. The materials are Kapton and Nomex with Kapton being available to a thickness of 0.0005-inch and Nomex to a thickness of 0.002-inch. Both materials are high temperature materials and have very good thermal, electrical, and mechanical properties. These materials can be used as interleaving insulation between turns. With these materials, it is expected that a good high temperature, lighter weight, and lower cost transformer will be possible. The interleaving eliminates the high cost of the present high temperature insulation methods, and provides an uninsulated conductor for versatility and ease of making connections.

APPENDIX B

DESIGN AND EVALUATION OF STATIC INVERTER OUTPUT TRANSFORMER UTILIZING FIELD-ANNEALED DOUBLY ORIENTED SILICON STEEL

Material Characteristics

Doubly oriented silicon steel has two easy directions of magnetization, one perpendicular to the other, rather than one as in conventional grain-oriented magnetic steels. An easy direction is defined as the direction of magnetization that results in the lowest loss for a given flux density. Most steels have direction, usually in the rolled direction. Core configurations that require flux to traverse the core in the plane of the laminations take advantage of the two-easy-directions property. A tape-wound core (toroidal) is an example of a configuration that uses only one direction of magnetization. Preliminary indications were that a technique using a magnetic field while annealing would result in lower losses for this material when the exciting frequency is 400 Hz or above.

Material characteristics of this doubly oriented steel can be used in static inverters and converters as a means of increasing efficiency and/or reducing weight. The lower loss characteristic at higher frequencies is particularly well suited to the square-wave voltages which are commonly found in inverter/converter circuits and which are rich in high harmonic frequencies. The two easy directions of magnetization make this material suitable for a variety of E-I type lamination configurations. For this type transformer construction, non-oriented materials are normally used which require higher exciting currents and have higher losses or must be operated at lower flux densities.

For this program, two identical output transformers were built using 0.011-inch singly magnetic material (3% silicon - 97% iron). These transformers were connected into static inverter models for testing. Another transformer of the same design was made using 0.006-inch doubly oriented magnetic core material. This transformer was evaluated in one of the inverter models to determine what improvement in efficiency could be realized by using this core material in an actual inverter application. A comparison of losses for these two materials with 400-Hz sinusoidal excitation is given in figure 102. Since the 0.006-inch doubly oriented steel material was not yet commercially available, the test data presented in figure 102 for this material can be considered only representative of the presently available

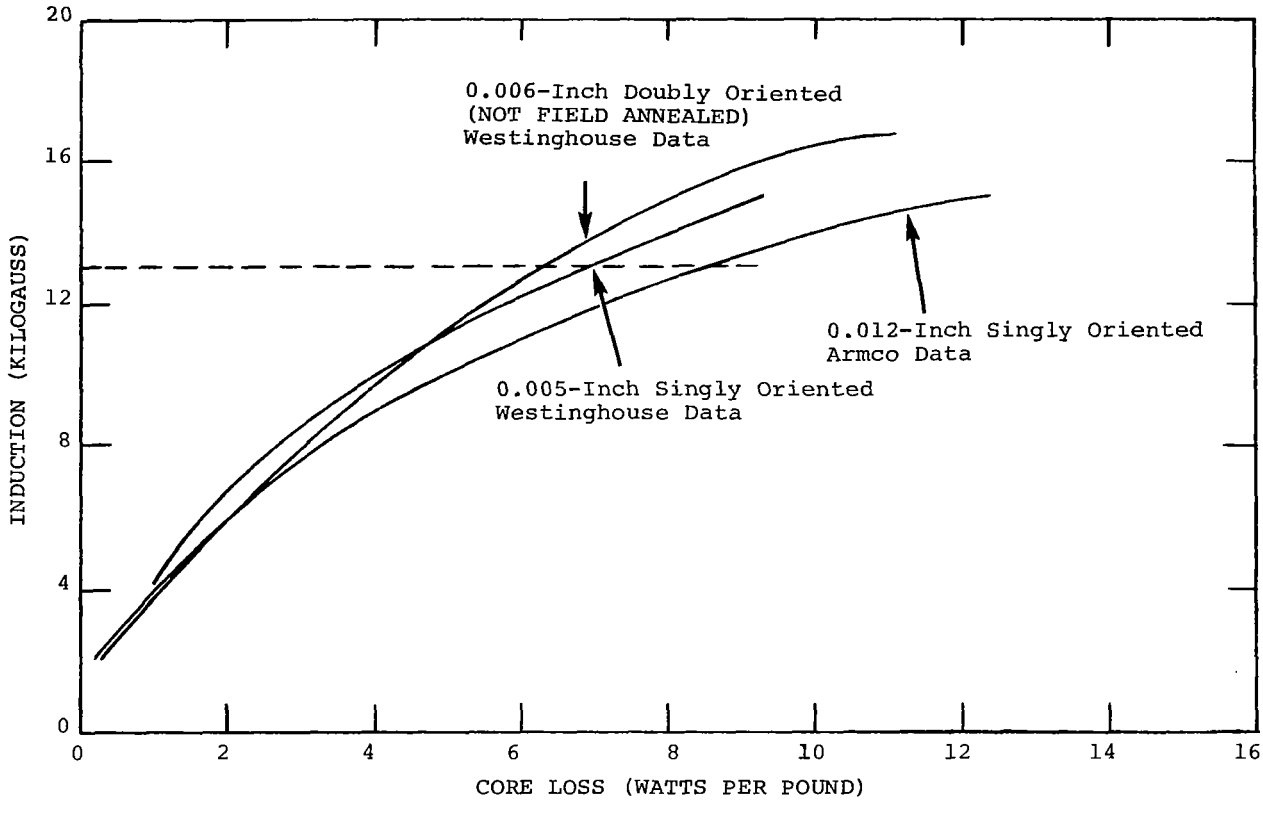

Figure 102. A Comparison of Losses for Singly and Doubly Oriented Materials with 400-Hz Sinusoidal Excitation

sample quantities. These data show that even non-field-annealed, doubly oriented steel is better than singly oriented steel at high flux densities. The 0.011-inch, singly oriented material was chosen for the two identical output transformers because it was readily available in sheet form. Material and data for 0.006-inch singly oriented material were not readily available for a more direct comparison.

Needed data were not available for 0.006-inch doubly oriented material which had been field-annealed. Such data were taken after the cores were annealed and are presented in this report.

Weight Reduction Through Lamination Configuration

"E" type cores are commonly used for three-phase sinusoidal voltage transformers and require one-third less core material than would be required for three separate single-phase transformers.

This same method of saving magnetic material weight through flux cancellation can be extended for use with a six-power-stage static inverter having six square-wave output voltages, phase-displaced 30 electrical degrees from each other.

For this program, a four-power-stage static inverter was used having four square-wave output voltages, phase-displaced 45 electrical degrees from each other. Using harmonic neutralization techniques, the secondary windings were interconnected to produce a three-step, three-phase output voltage with the first harmonic present being the seventh. The basic lamination configuration for this output transformer is shown in figure 103. Assuming a constant number of turns and wire size, this type lamination requires about 40 percent less magnetic material than would be required for four separate single-phase transformers.

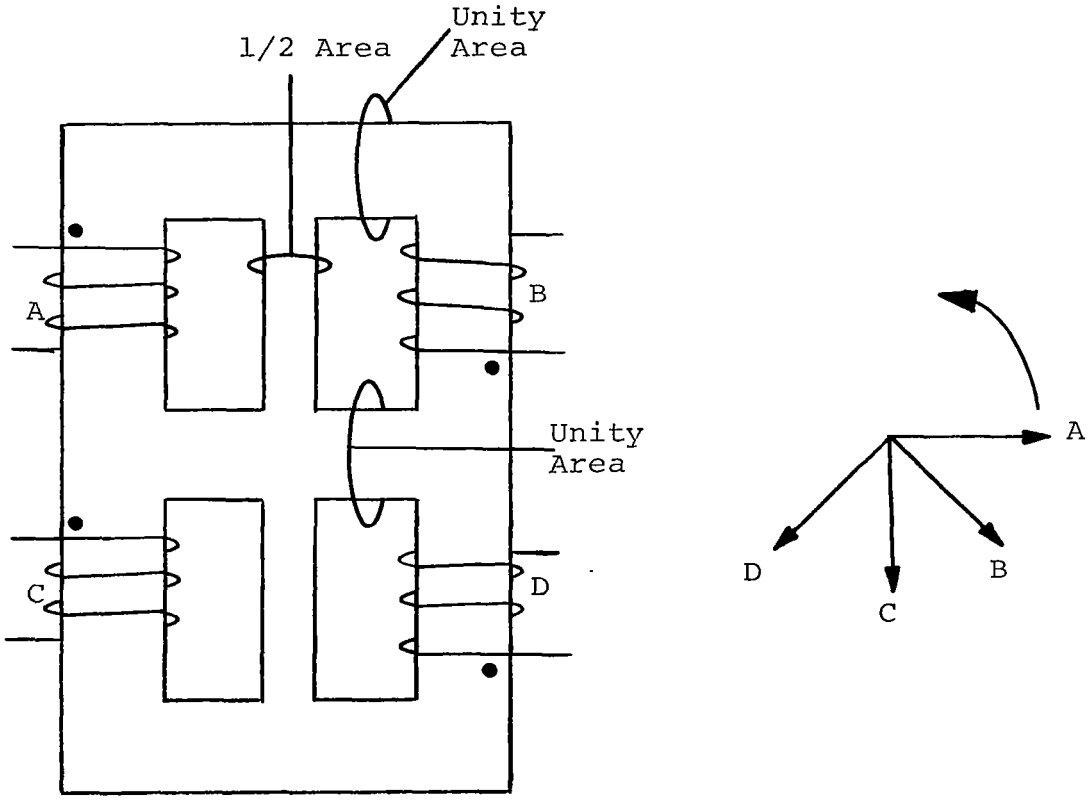

Figure 103. Basic Lamination Configuration for Output Transformer

Design of Test Transformer

The actual lamination configurations that were used to facilitate machine winding of the four transformer coils and to permit use of available tooling for punching the laminations are shown in figures 104 and 105. Placing two of the short laminations in between each layer of long laminations results in a core having the basic lamination configuration of figure 103. By alternating the gaps between ends of the short laminations from one side of the core to the other, the long laminations will carry 33 percent more flux than usual in the area of these gaps. This staggered gap accomplishes, with greater reduced loss, the effect of gapping the whole core cross-section in output transformers.

The turns and core cross-sectional area were designed to produce a maximum flux density, B_M = 13 kilogauss. With a nominal volts/turn of 0.7, the required stack height is approximately 0.95 inches. Figure 102 shows that the doubly oriented steel has a core loss of 6.3 watts per pound while 0.012-inch singly oriented steel has a core loss of 8.5 watts per pound at 13 kilogauss excitation.

The nominal rating of the transformer is 750 VA and its calculated weight was 6.9 pounds, exluding leads. Figure 106, a schematic diagram of the output transformer, shows the turns and winding interconnections required to produce a three-phase, 115-volt output with the third and fifth harmonics neutralized.

Transformer Evaluation

The effect of using doubly oriented steel in the inverter output transformer was evaluated by measuring transformer temperature rise and inverter efficiency. These measurements were made first with the singly oriented, silicon-steel core in the inverter output transformer. This output transformer was then replaced with an identical transformer having a doubly oriented steel core. Inverter efficiency and output transformer temperature rise were again measured at both zero and full load. These measurements illustrated the improved inverter efficiency caused only by changing the output transformer core material. This reduction in losses could have been traded for reduced transformer weight. This would have improved the power-to-weight ratio of the inverter without affecting efficiency.

Two inverter output transformers assembled for evaluation are shown in figure 107. As described above, one transformer uses conventional singly oriented silicon-iron core material; the other transformer uses a new, doubly oriented, field-annealed silicon-steel core material. Equal cross-sectional areas of steel

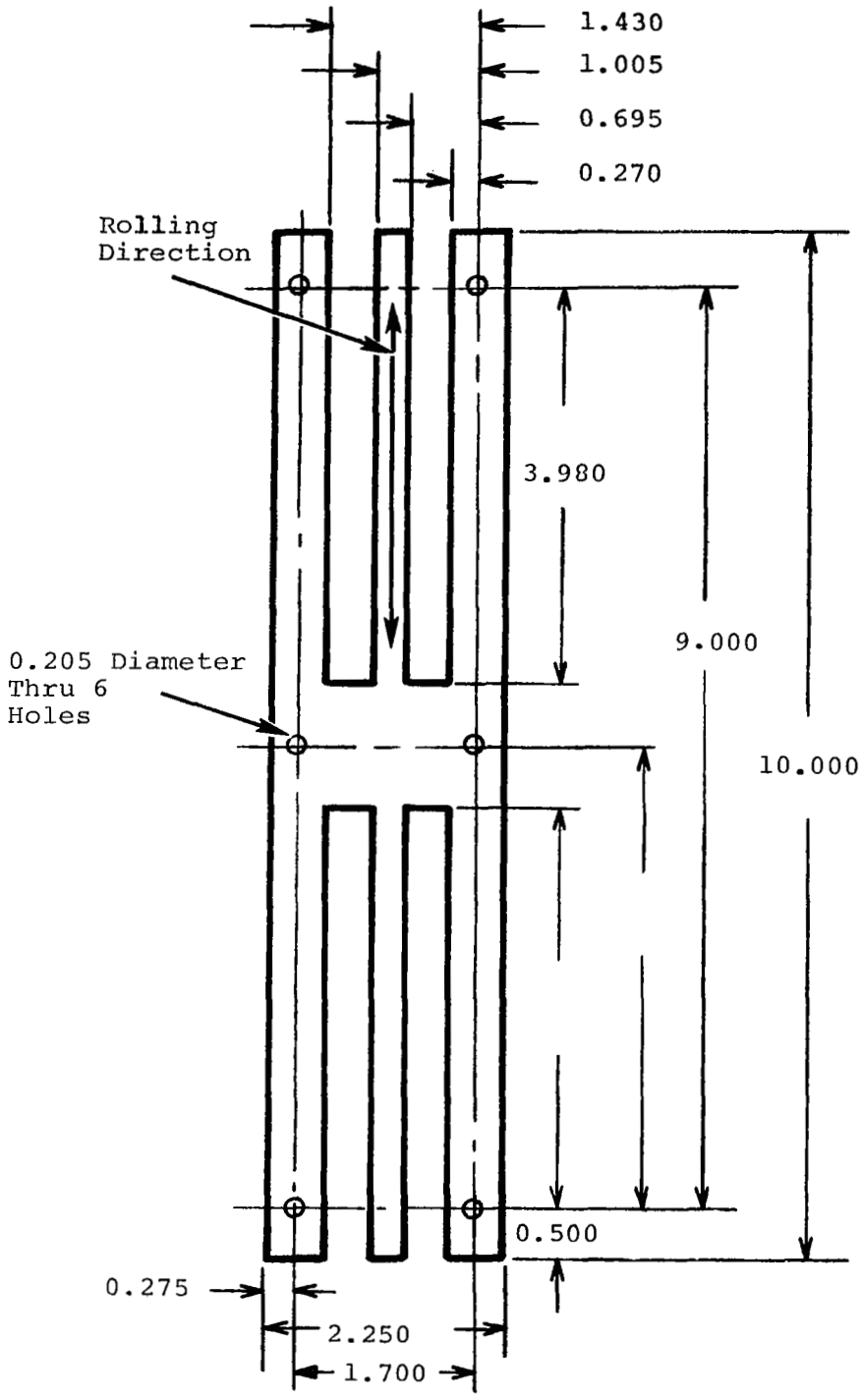

Figure 104. - Actual Output Transformer Long Lamination Dimentions

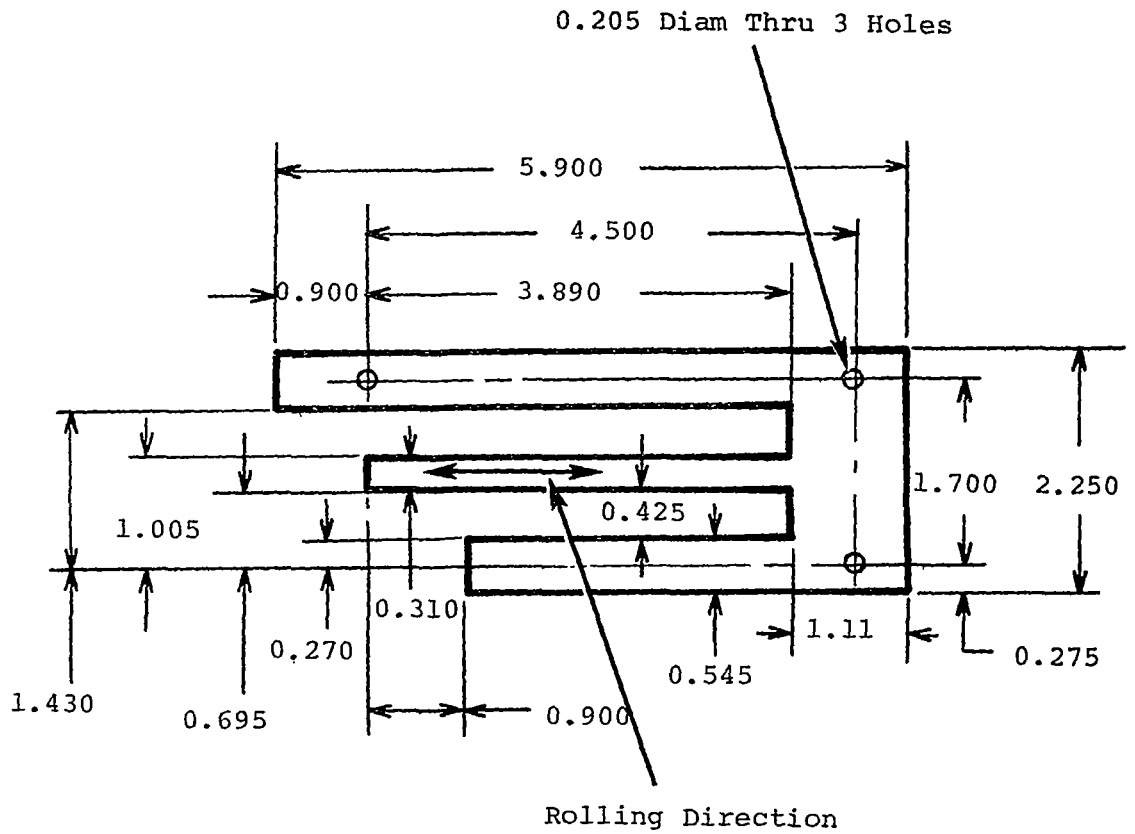

Figure 105. Actual Output Transformer Short Lamination Dimensions

were used in each transformer core. Each transformer weighs approximately 7.2 pounds with leads. The annealing processes used for both transformer laminations are described in the last section of this appendix.

These two transformers were first evaluated with sinusoidal excitation voltage and were then operated individually in the same static inverter test model.

Characteristics of Transformer Cores with 400-Hz Sinusoidal Excitation Voltage. - To obtain core loss and ac excitation data from a magnetic core material, it is desirable to have a perfectly uniform cross-sectional area throughout the entire magnetic path. This facilitates the calculation of the operating flux density and the core weight. These conditions were approached with the

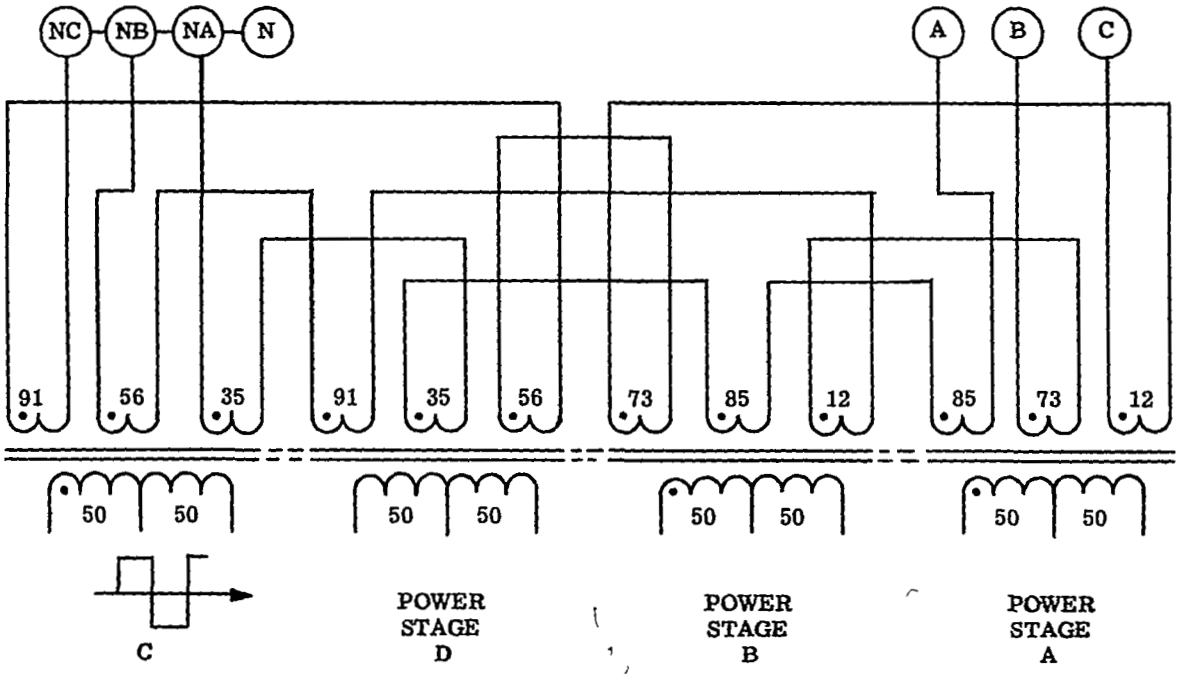

Figure 106. Output Transformer Schematic Diagram (Numbers Indicate Turns)

output transformers by placing a shorted turn around each of the four interior core legs to prevent flux from passing through these sections of the core. Then 400-Hz flux was caused to follow the outside core legs by applying 400-Hz sinusoidal voltage to the four primary windings connected in series. Voltage was applied to only half of each 90-turn primary winding, making a total effective winding of 180 turns.

The effective cross-sectional area of the outside core legs was determined by measuring the stack height on each transformer and determining the product of the stack height, known width (0.545 inches) and stacking factor. The measured stack height was 0.964 inches for the doubly oriented steel transformer and 0.909 inches for the singly oriented steel transformer while the stacking factor was 0.90 for the former and 0.95 for the latter. Therefore, the effective cross-sectional area for each core is 0.47 inches^2.

The flux density B is a function of the applied voltage according to the following equation:

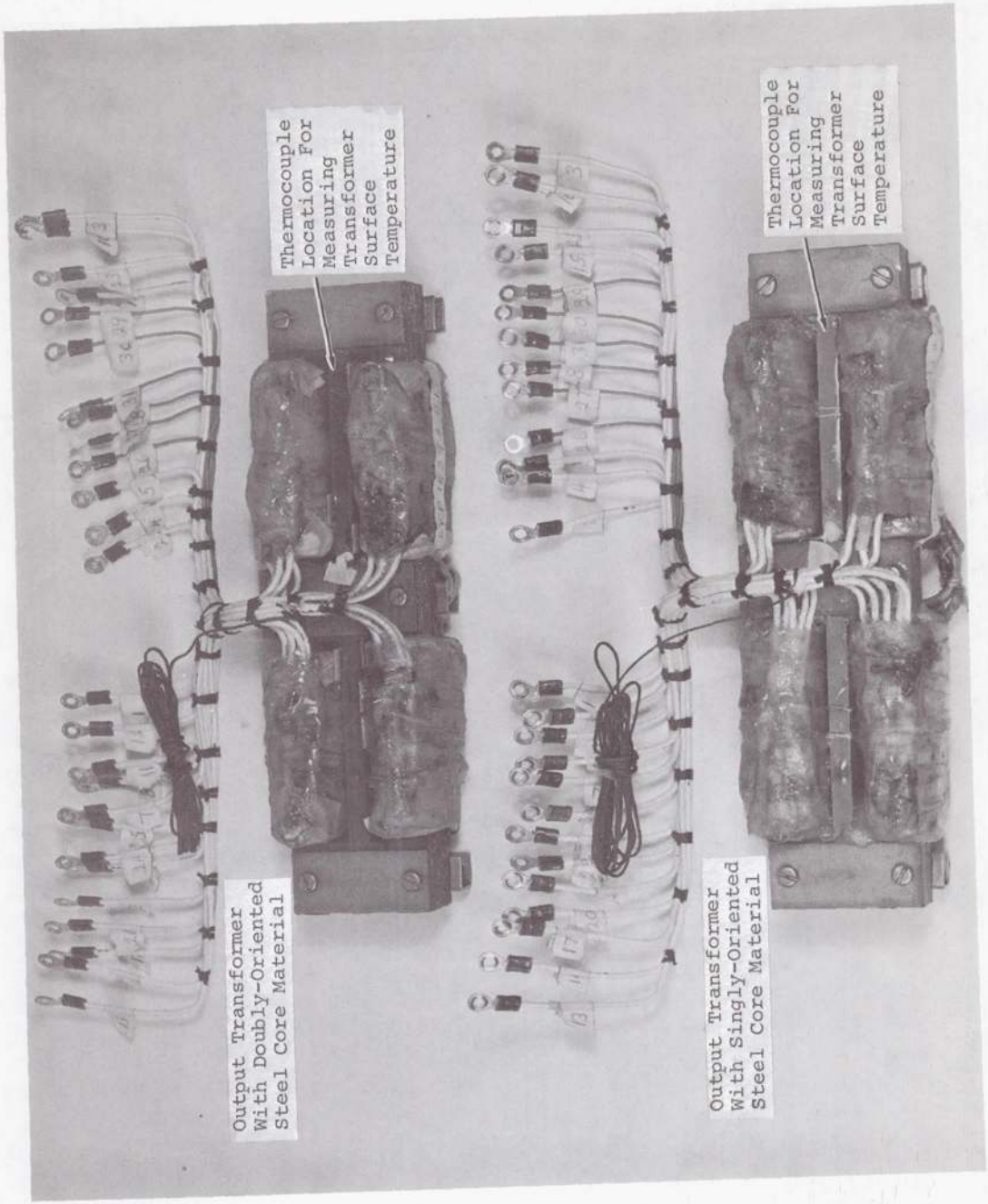

Figure 107. - Static Inverter Output Transformer Models Used In the Transformer Improvement Evaluation

$$B = \frac{3.49 \times 10^6 \, V}{Aft} \text{ gauss}$$

where

V = applied 400-Hz rms volts

A = effective core cross-sectional area; 0.47 inches^2

f = frequency of applied voltage; 400-Hz

T = 180 turns

By substitution:

$$B = \frac{V \times 3.49 \times 10^6}{0.47 \times 400 \times 180} = 103 \, V \text{ gauss}$$

By referring to the lamination dimensions in figures 104 and 105, the volume of iron in the outside core legs was calculated and found to be 10.6 cubic inches. Using the known material density of 0.255 pounds per cubic inch, the weight of the core which was excited in this test is 2.7 pounds.

The accurate measurement of core loss and ac excitation is a difficult task because the excitation current becomes non-sinusoidal as the core begins to saturate. Conventional 0.25 percent wattmeter will not give accurate indications when the applied currents have high harmonic content. To avoid these problems, test data were obtained using a VAW Meter. This meter has an accuracy of +3 percent over a frequency range of 20 to 20,000 Hz. The winding resistances were measured and the copper loss was subtracted from the measured loss to obtain the core loss for a variety of excitation levels. The core loss in watts-per-pound, the core ac excitation in apparent watts-per-pound, and the flux density in kilogauss were calculated from the test results and plotted for comparison in figures 108 and 109.

At the desired operating flux density of 13 kG, the doubly oriented steel core had a loss of 7.7 watts-per-pound compared with 11.6 watts-per-pound for the singly oriented steel core. At this same flux density, the doubly oriented steel core required 13.3 volt-amperes excitation per pound compared with 21.5 volt-amperes excitation per pound for the singly oriented steel core. The use of the 0.006-inch steel laminations represents a 33 percent reduction in core loss and a 38 percent reduction in required excitation when compared with the 0.011-inch steel laminations. This reduction is even more significant at higher flux densities.

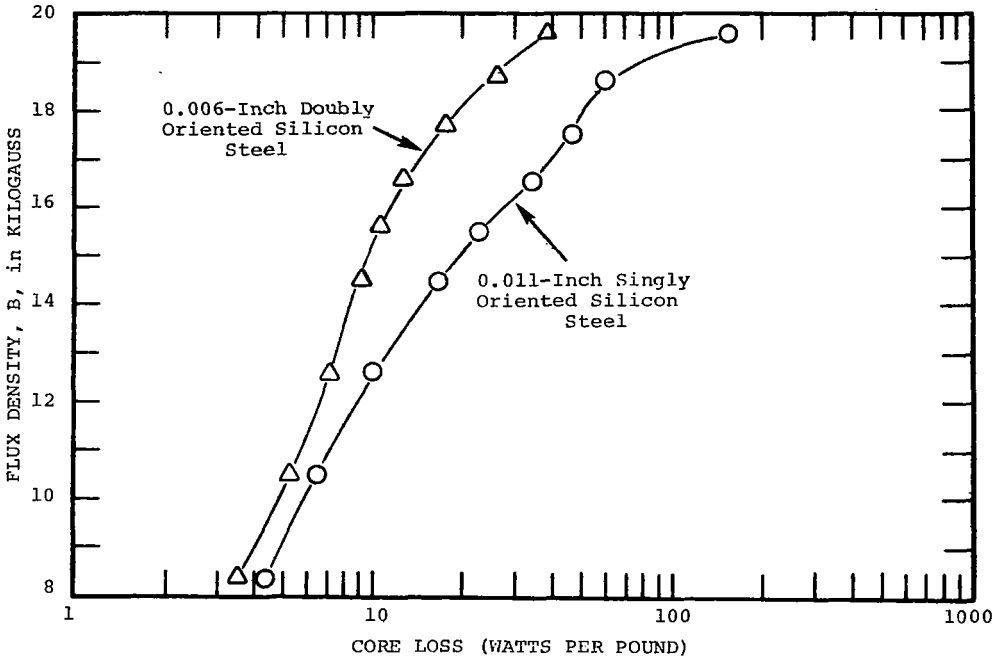

Figure 108. - A Comparison of Core Losses for Singly and Doubly Oriented Silicon Steel Transformer Cores with 400 Hz Sinusoidal Excitation Voltage

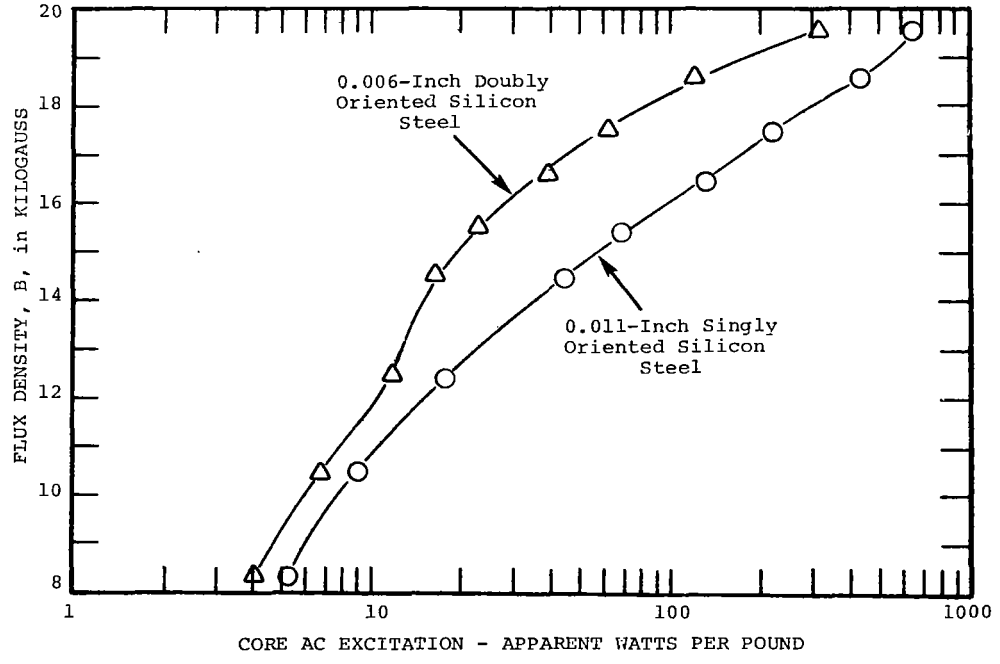

Figure 109. - A Comparison of AC Excitation for Singly and Doubly Oriented Silicon Steel Transformer Cores with 400 Hz Sinusoidal Excitation Voltage

The total core weight, including the internal core legs, is 3.3 pounds. Therefore, when the transformer is operated at 13 kG, the difference in core loss for the two materials should be (11.6 - 7.7) watts/pound x 3.3 pounds = 12.8 watts. This can be expected to change the efficiency of the 750 VA inverter model by approximately

$$\frac{12.8}{750} \times 100\% = 1.7\%.$$

It should be noted that about one half of the improvement in core material characteristics is a result of the difference in material thickness as illustrated in figure 108.

Effect of Transformer Core Material on Static Inverter Efficiency. - Tests were conducted to determine the inverter efficiency with each different transformer installed. Inverter efficiency was determined with loads ranging from 25 to 125 percent of full load and with power factors ranging from 0.75 lagging to 0.9 leading. Wattmeter and voltmeter potential coils presented an additional 12 watts load to the inverter and have been included in the efficiency calculations.

The test results plotted in figure 110 are from the 1.0 power factor tests. The inverter efficiency improved under all load conditions through the use of the doubly oriented steel transformer. Efficiency improvement at full load ranged from as low as 1.0 percent to as high as 2.6 percent. This wide range is because the transformer core flux density changes as the load power factor changes; also, the anticipated savings in core loss of 12.8 watts is 1.7 percent of full load watts at unity power factor but is 2.3 percent of full load watts at 0.75 power factor. The improved efficiency of the inverter is caused directly by the reduced core loss of the doubly oriented steel output transformer. This increase in efficiency was possible without increasing the transformer or inverter weight.

During the transformer evaluation, the surface temperature of the transformer was allowed to stabilize at zero-load and at full-load unity power factor. The surface temperature was measured at the top center portion of the core with thermocouples located as shown in figure 107. The zero- and full-load temperatures rose to 82.5° and 120° C, respectively for the singly oriented steel transformer. The zero- and full-load temperatures rose to 66° and 101° C, respectively for the doubly oriented steel transformer. Normal room temperature conditions (25° C) prevailed during the test. This lesser temperature rise adds to the life of electrical insulation and could be important on extremely long-duration applications.

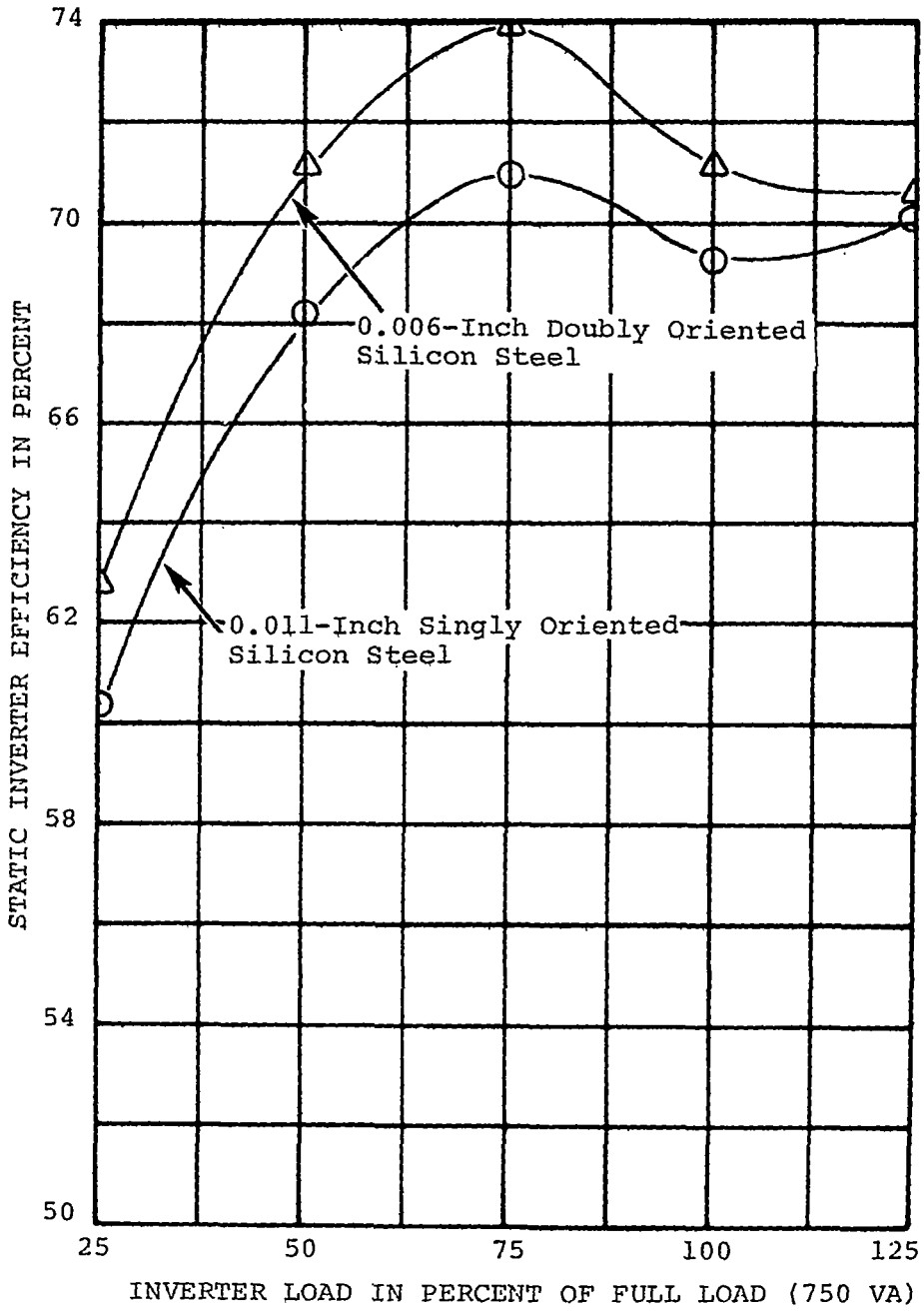

Figure 110. - The Effect of Output Transformer Core Material on Inverter Efficiency for 1.0 Power Factor Loads

Effect of Transformer Core Material on Static Inverter Weight. - In some applications it may be more desirable to reduce the weight of the static inverter than to increase efficiency. The improved magnetic characteristics of the doubly oriented steel alloy allow this.

Figure 108 illustrates the magnitude of the possible weight reduction. Based on this comparison of core losses, doubly oriented steel alloy can be operated with a flux density of 16 kG and have the same loss as singly oriented steel alloy operating at 13 kG. The ac excitation is practically the same at these two operating conditions. For example, a singly oriented steel alloy transformer will weigh approximately 13/16th as much as a doubly oriented steel transformer having equal efficiency. Each of the two transformers used in this evaluation weighs approximately 7.2 pounds. The reduction of (1-13/16) 7.2 pounds, or 1.3 pounds, represents a 19 percent reduction in transformer weight with no increase in losses.

The inverter models used in this evaluation have a packaged weight of 26 pounds. Use of a doubly oriented steel output transformer could reduce this packaged weight by 1.3 pounds without reducing efficiency. This represents a 5 percent savings in inverter weight.

Annealing of Transformer Laminations

The singly oriented steel transformer laminations were punched from 0.011-inch-thick steel sheet. These punchings were annealed in a dry hydrogen atmosphere (dew point did not exceed -20° C) at 800° C $\pm$10° C for two hours and then furnace cooled to below 150° C.

The doubly oriented steel transformer laminations were punched from 0.006-inch-thick sheet. To provide the means to establish a magnetic field in the laminations during the annealing process, a fixture was constructed and is shown in figure 111. The four plates shown were made from 3/8-inch-thick Inconel. The two coils were wound from 1/4-inch-diameter, low-oxygen copper rod. The rod was flame sprayed with alumina to insulate the conductors during the anneal.

Sufficient doubly oriented steel laminations were punched for two transformers so that two separate anneals could be made. Half of the laminations were assembled into the annealing fixture. A resistance furnace was pre-heated to 1000° C. The assembled fixture was placed in an enclosed Inconel retort. The cold retort was inserted into the furnace and raised to 900° C.

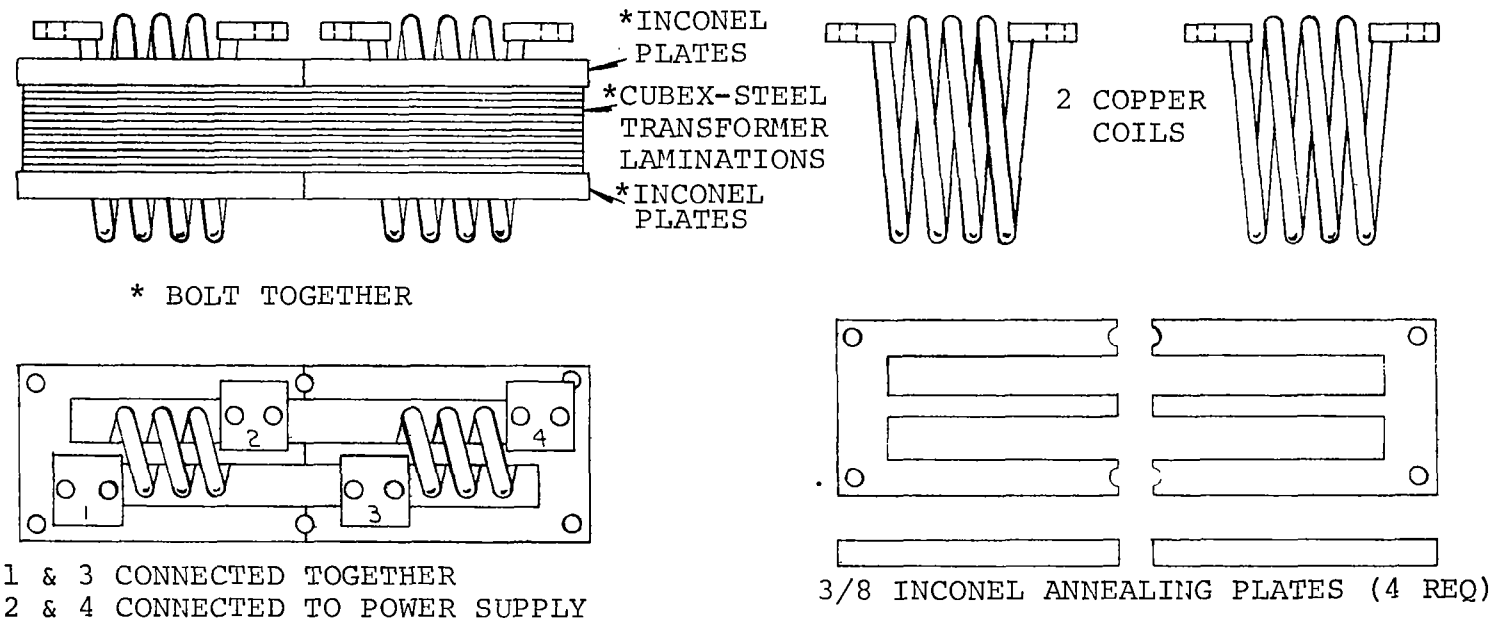

Figure 111. - Fixture Used to Establish a Magnetic Field in the Doubly-Oriented Steel Transformer Laminations During the Annealing Process

The charge was maintained at 900° C for ninety minutes. A 10-oersted field was then applied and held during the entire cooling cycle. During the entire anneal, a dry hydrogen atmosphere was present. A flow rate of 30 cubic feet per hour was accurately metered and dew points were checked at the beginning, mid-point, and end of the cycle. The entrance dew point was greater than -65° C. The exit dew points were not less than -35° C. The cooling cycle for the first anneal was programmed at 2° C per hour. The cooling cycle for the second anneal was programmed at 25° C per hour. Magnetic tests conducted after the two anneals showed that the magnetic properties were not changed by cooling rate.

APPENDIX C

TEST PROCEDURES AND TEST EQUIPMENT

Windings and Test Procedures for Core Loss and Apparent Power

The cores were wound with two windings of eight strands each. The strands were then connected in series-parallel combinations by means of a connector adapter system to provide the proper number of turns for the specified frequency of test and to maintain a constant flux-volt level at the required induction. The flux-volt level at maximum induction, with sine wave excitation, was maintained at approximately 100 volts in most cases and was proportionately reduced for the lower inductions. With square-wave excitation the voltage level was held at approximately 150 volts at the maximum inductions. These values were picked to coincide with maximum limitations of the power supply allowing for an approximate 20 volt safety factor in case higher inductions were later required.

The testing was conducted in accordance with ASTM A343-60T using the test circuit shown in figure 112.

Winding and Test Procedures for Major Hysteresis Loops

The test required a drive and pickup winding. The drive winding was the same as the primary for the 400 Hz core loss test. A one-turn winding was utilized for the pick up. The testing was conducted in accordance with ASTM A343-60T using the test circuit shown in figure 113. The loop was recorded by photographing the oscilloscope trace. The circuit was calibrated for each core and the calibration trace was photographed.

Windings and Test Procedures for DC Magnetization and DC Hysteresis Loops

The windings for dc testing were the same as used for the ac hysteresis loops. The testing was in accordance with ASTM A341-64. The test circuit for dc magnetization curves is shown in figure 114. The test circuit for dc hysteresis loops is shown in figure 115. The calibration and recording of loops was the same as for ac loops.

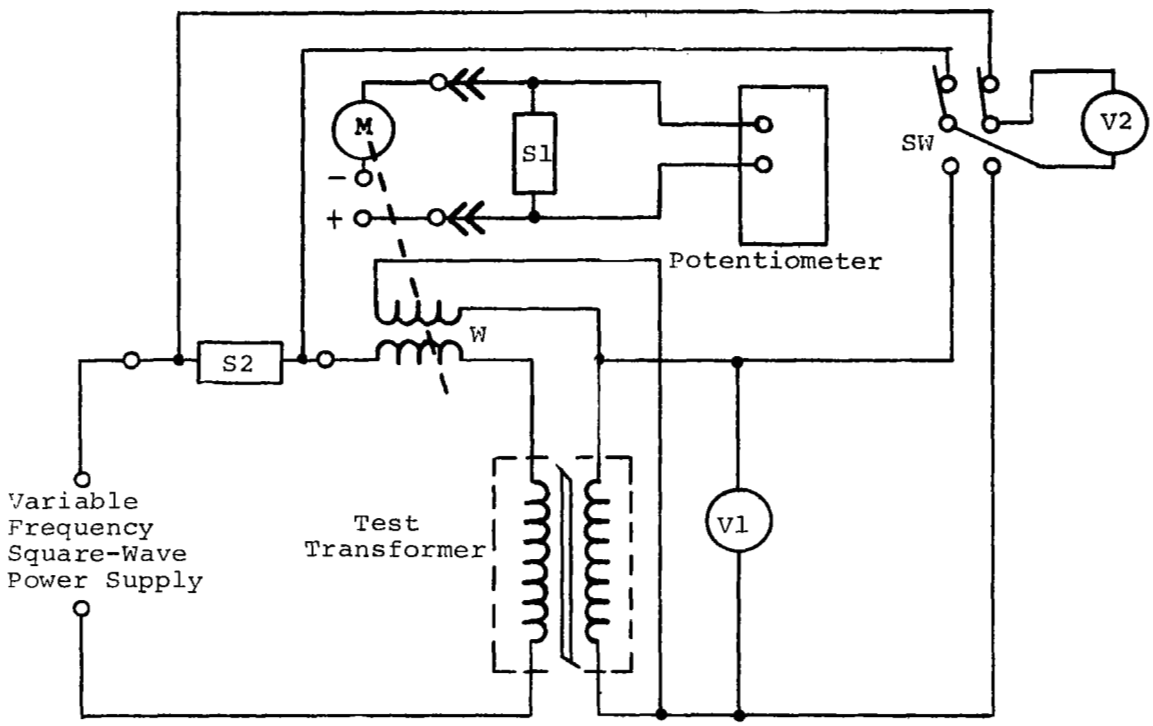

V1 - Flux Meter

V2 - Combination Meter
1 - Input I
2 - Output E
True RMS

W - Wattmeter

Potentiometer - MV Read-Out

S1 - Shunt
1K, 1W

S2 - Shunt

Figure 112. - Core Loss and Apparent Power Test Circuit

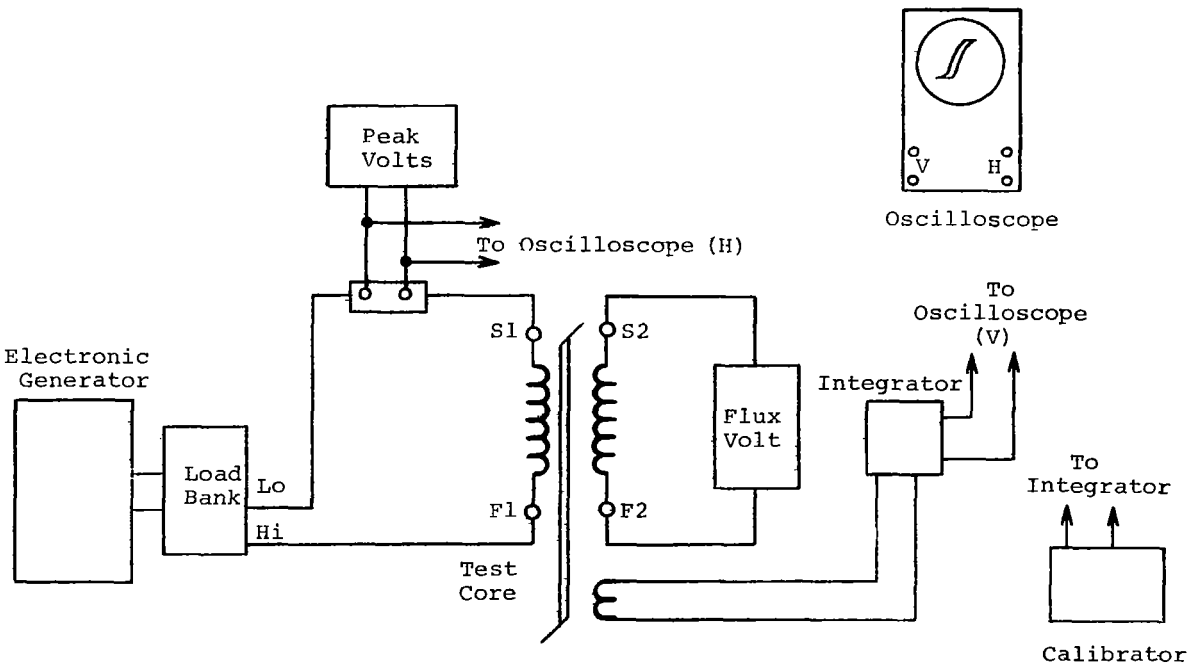

Figure 113. - Major AC Hysteresis Loop Test Circuit

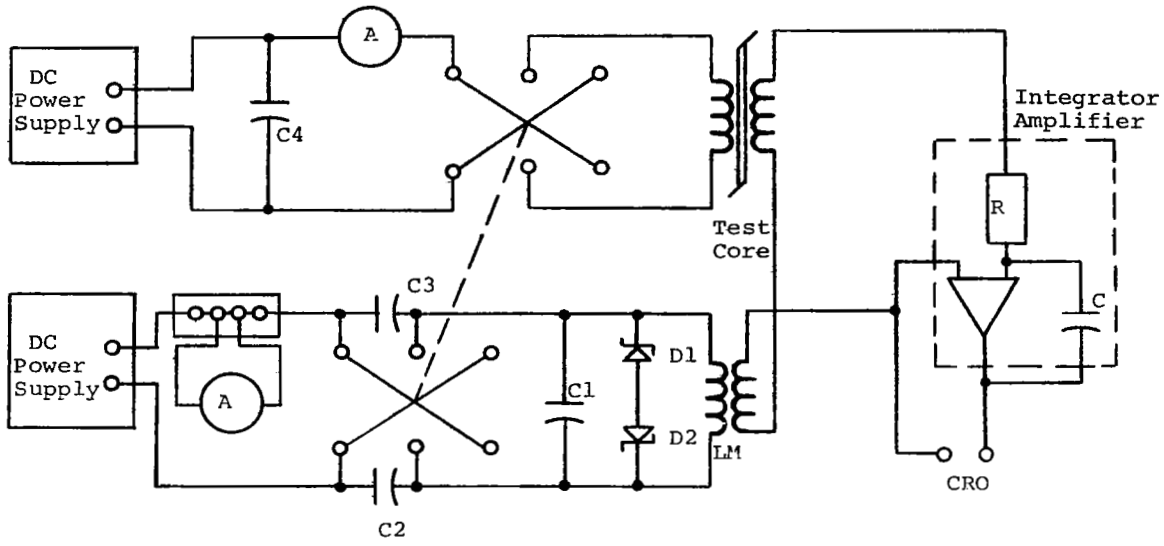

CRO = Cathode Ray Oscilloscope
C1 = 18 μf
C2,C3 = 3 μf
C4 = 700 μf
D1,D2 = 6 (IN2611 Series)
LM = Calibrating Mutual Inductor

Figure 114. - DC Magnetization Test Circuit

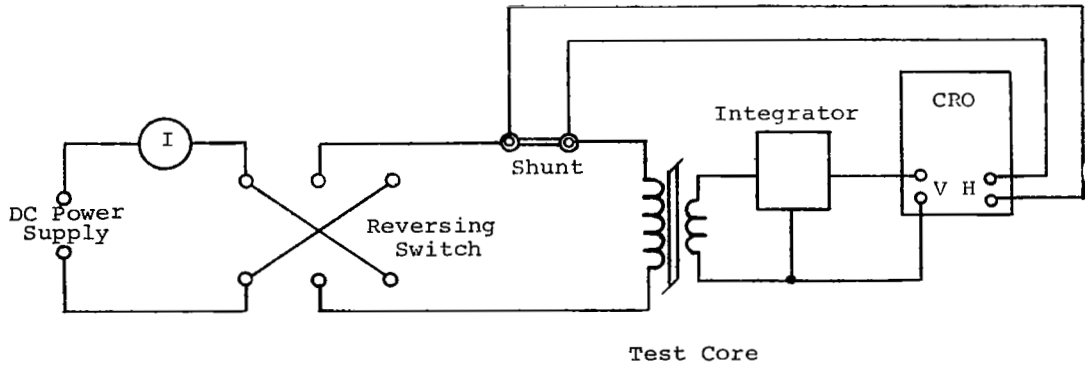

Figure 115. - Test Circuit for Display of DC Magnetization Loop

Winding and Test Procedures for CCFR Tests

For CCFR (Constant Current Flux Reset) three windings are required, drive, pickup, and reset. The pickup and reset windings consist of one turn each. The drive winding is dependent on the current limitation of the power supply and ranged from one to six turns. The testing was conducted in accordance with AEEE (now IEEE) Bulletin No. 432, Jan. 1959, Test Procedure for Toroidal Magnetic Amplifier Cores, except that square-wave excitation was used and tests were conducted at 400, 800, 1600, and 3200 Hz. The test circuit used is shown on figure 116.

Test Equipment

The following test equipment was used in this program:

1. CML Square-Wave Power Supply. - The square-wave power supply used for the testing was an Electronic Generator, made by Communications Measurement Laboratories, with square-wave frequency output of 50 to 5000 Hz. Maximum rated power level is 7000 VA on square wave. The rise time of the square wave is 15 microseconds.

A harmonic analysis of typical square-wave outputs of the generator is as follows:

Condition	Harmonic Analysis of Square Wave Output						
	Harmonic Content in % of Fundamental Amplitude						
	Harmonic No.	1	3	5	7	9	11
400 Hz No Load		100	34.55	20.84	14.65	11.40	9.31
400 Hz, Loaded to 15 kG on 0.002-inch singly grain oriented silicon steel, Vendor #1		100	33.37	20.07	14.37	11.21	9.19
3200 Hz, No Load		100	32.81	18.05	10.85	6.61	3.82
3200 Hz, Loaded to 15 kG on 0.004-inch singly grain oriented silicon steel, Vendor #1		100	31.93	16.45	9.02	4.60	2.13

2. Weston Inductronic Wattmeter, Model 1483. - This instrument was used to measure ac power by applying drive current and the induced voltage of the secondary. The dc output voltage is in direct proportion to the input and was read with an external

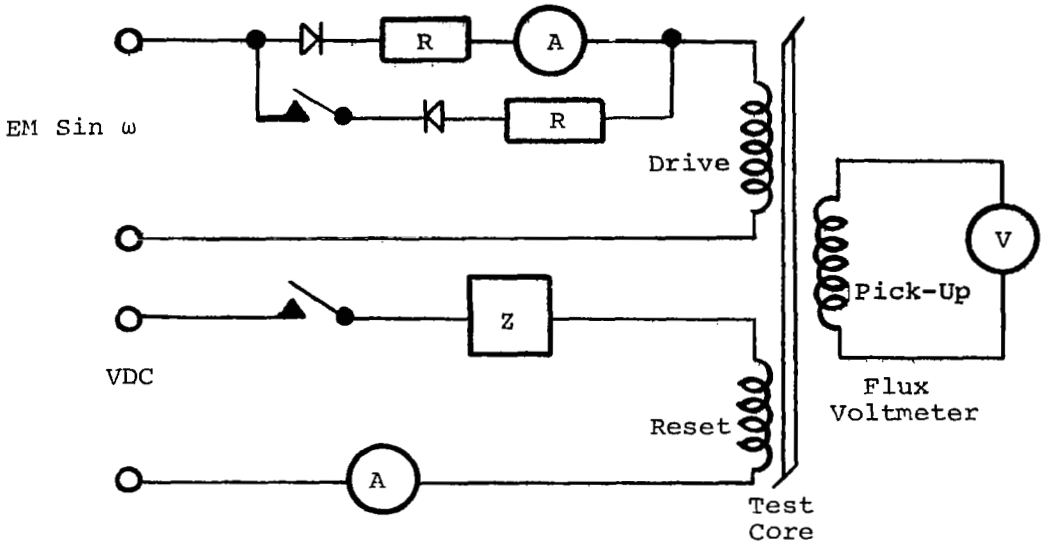

Simplified CCFR Core Tester

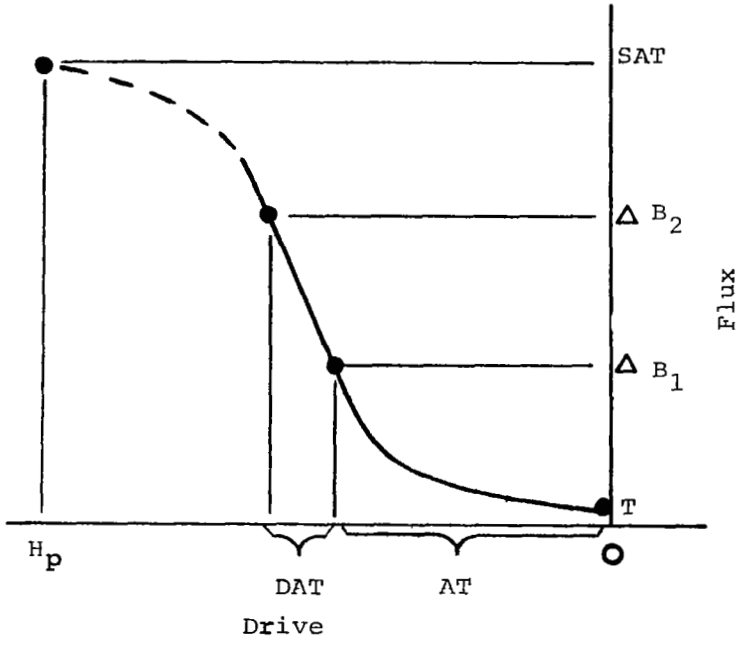

Figure 116. - Constant Current Flux Reset Core Test Circuit

potentiometer. The unit has an electrodynamometer input circuit. Due to the high burden inflicted by this instrument, it was used when testing materials at flux densities above 2 kilogauss. The ranges are as follows:

Input current:	5 A, single input
Input volt:	50 V across 471.6 ohms resistance
	100 V across 943.3 ohms resistance
	200 V across 1886.8 ohms resistance
Full scale power ranges:	250, 500, and 1000 watts
Maximum percent accuracy at full scale and unity power factor:	0.1% to 25,000 Hz, sine wave 1.0% to 10,000 Hz, sine wave 3.0% to 20,000 Hz, sine wave

Specifications above are applicable to square-wave operation, bi-directional, to 3200 Hz.

Repeatability of approximately five percent was achieved.

The output of the unit would not zero, and it was determined that a constant error was being introduced over the complete range. This error had to be deducted from each reading.

No method was available to check the accuracy of this instrument using square-wave excitation (square-wave voltage).

3. Leeds and Northrup Millivolt Potentiometer, Model 8690. - This instrument was used as a readout for the Weston Inductronic Wattmeter. The range is from -11 mV to +101 mV. The accuracy is ±0.05% of reading plus 20 mV. A typical calibration comparison is shown below:

Range	100 Millivolts		
Calibration Points	20	50	80
Standard Reading	20	50	80

4. John Fluke VAW Meter, Model 102. - This instrument was used to measure ac power when the levels were of relatively low magnitude. With an input impedance of 1 megohm, no burden was imposed. The ranges are as follows:

Voltage: 1.5, 3.5, 15, 30, 150, 300, 600 volts rms, full scale.

Current: 1.5, 3, 6, 15, 30, 60, 150, 300, 600 mA. 1.5, 3.6, 15, amperes. rms/full scale.

Power: 225 NW to 9kW.

Maximum percent accuracy at full scale:

3% (pf of 1) 20 Hz to 40 kHz sine wave

3% (pf of 0.1) 20 Hz to 20 kHz sine wave

Power measurements are without waveform error within the specified frequency range.

The repeatability of this unit varies to 20 percent. The accuracy is largely dependent on the voltage scale and the power factor scale.

A typical calibration comparison is shown below for the voltage scales, and the most used current scales at a frequency of 400 Hz:

Range	150 Volts					Volts 300	600	60	30	15	6	3	1.5
Calibration Points	30	60	90	120	150	200	400	40	20	10	4	2	1
Standard Reading	30	60	90	119	150	201	400	40	20.1	10	4	2	0.99

Calibration of Current Ranges Using a Typical Shunt			
Range	1.5 A Shunt		
Calibration Points	0.5	1	1.5
Standard Reading	0.505	1	1.5

NOTE: A check on the power scales is accomplished by taking a VA Product on a resistance load. All shunts are trimmed to produce exactly the standard reading.

5. Hewlett Packard Model 400 H Vacuum Tube Voltmeter. - This instrument was used to measure flux voltage. It actually senses the average value of the applied signal, but the scale reads average times 1.11.

The voltage ranges are from 1 mV to 300 V in 12 increments.

The frequency range is from 10 Hz to 5 mHz, with an accuracy of ±1% of full scale to 500 kHz. With the range selection provided, nearly full scale deflection can be achieved at nearly all times. Therefore, a good degree of accuracy can be maintained.

A typical calibration comparison is shown below at a frequency of 400 Hz:

Range	100 Volts					Volts							
						300	30	10	3	1	0.3	0.1	0.03
Calibration Points	20	40	60	80	100	200	20	8	2	0.8	0.2	0.08	0.02
Standard Reading	20	40	60	80	99.9	200	20	8	2	0.8	0.2	0.08	0.02

6. Hewlett Packard Model 3400 A RMS Voltmeter. - This instrument was used to measure true rms voltage in the pick-up winding and also the rms drive current, with the aid of a current shunt.

Voltage ranges are from 1 mV to 200 V in 12 increments. The frequency range is from 10 Hz to 10 mHz, with an accuracy of ±1% from 50 Hz to 1 mHz. With the range selection provided, nearly full scale deflection can be achieved at nearly all times. Therefore, a good degree of accuracy can be maintained. A typical calibration comparison is shown below at a frequency of 400 Hz:

Range	100 Volts					Volts							
						300	30	10	3	1	0.3	0.1	0.03
Calibration Points	20	40	60	80	100	200	20	8	2	0.8	0.2	0.08	0.02
Standard Readings	20.8	40.2	60	80	100	200	20	7.99	1.99	0.8	0.201	0.08	0.02

7. Ballantine Peak Responding Electronic Voltmeter Model 305A. - This instrument was used to measure peak driving current

for both CCFR and core loss tests. It indicates peak-to-peak or peak amplitudes of repetitive waveforms including sine, square, triangular and complex waves. The measurement is indicated on logarithmic voltage scales which allows for high accuracy at all points. The voltage range is from 1 mV to 1000 V in 12 increments. The frequency range is from 5 Hz to 500 Hz to 500 kHz sine wave and 200 Hz to 300 kHz square wave. Accuracy is ±2% from 20 Hz to 200 kHz sine wave and ±3% from 200 Hz to 300 kHz square wave. A typical calibration comparison is shown below at a frequency of 400 Hz:

Range	1 V Peak-to-Peak					Volts Peak-to-Peak						Millivolts Peak-to-Peak			
						1000	350	100	35	10	3.5	350	100	35	10
Calibration Points	0.3	0.4	0.6	0.8	1	800	200	80	20	8	2	200	80	20	8
Standard Reading	0.298	0.399	0.599	0.8	1	799.9	199	80.2	20	8	1.995	199	80.5	19.9	9

8. Ballantine AC/DC Precision Calibrator Model 421. - This instrument was used as the source for calibration of a comparator when CCFR and hysteresis loop data were taken. It was always used to the peak-to-peak mode at 400 Hz. The output voltage range is 1.11 mV to 111 volts full scale. The full range accuracy is ±0.1% with a linearity of controls at ±0.05% of setting. A typical calibration comparison is shown below:

Range Setting	Peak-to-Peak Reading at 400 Hz
100 V	100.01
10 V	10.002
1 V	0.9999
100 mV	99.98
10 mV	10.002
1 mV	1.0004

The accuracy of this calibration is ±0.05% mV.

9. Moseley DC Voltmeter Model 22. - This instrument was used exclusively in conjunction with current shunts in the determination of reset currents and dc magnetization induction levels. The voltage ranges are from 3 mV to 300 V in 11 increments with an accuracy of 0.2% of full scale on all ranges. A typical calibation comparison is shown on the following page:

Range	100 mV					Millivolts				Volts					
						3	10	30	300	1	3	10	30	100	300
Calibration Points	20	40	60	80	100	2	8	20	200	0.8	2	8	20	80	200
Standard Reading	20	40	60	80	100	1.99	7.97	20	199	0.8	2	7.97	19.94	79.7	199

APPENDIX D

EXPERIMENTAL PROBLEMS

Core Box Sealing

The core boxes were sealed with a silicone epoxy which failed after two hours at a temperature of 250° C. The elastomeric properties of the silicone epoxy deteriorated at this temperature sufficiently to allow the seal to be broken and the silicone oil to leak out. The mechanical seal between the aluminum core box and the silicone glass insert also failed due to the difference in expansion between the two materials.

This failure indicated that state-of-the-art core box materials would not withstand a short exposure at 250° C although vendors believed that their core box construction would be satisfactory.

Core Coating

Cores of 3% silicon steel; 50% nickel-50% iron; and 4% molybdenum, 79% nickel, 17% iron were coated with aluminum orthophosphate (aluminum oxide, orthophosphoric acid, and water solution). The coating was very thick (~1 mil) and broke down in the presence of dry electrolytic hydrogen and the elevated stress relief annealing temperatures 800° to 1175° C. The cores were badly distorted and stuck together.

Phosphorus pentoxide reacts with water in the following manner:

$$P_2O_5+3H_2O \qquad 2H_3PO_4$$

The addition of aluminum oxide along with phosphorus pentoxide in water causes the following reaction:

$$2P_2O_5+Al_2O_3+4H_2O \qquad 2H_3PO_4+AlPO_4+H_2O$$

The aluminum orthophosphate is formed in the above reaction as well as orthosphoric acid which attacks the metal cores to form complex phosphates which bond the aluminum orthophosphate to the surface. Upon heating the following reaction takes place:

$$2O_2+H_2O+2AlPO_4$$

The presence of dry electrolytic hydrogen changes the above reaction so that Al H P_2O_7 could be formed and also some further chemical reaction with the base material could take place, causing a severe attack of the metal tape.

This experiment showed that aluminum orthophosphate was not suitable as a high temperature inorganic insulation for magnetic tape wound cores, since the magnetic properties would be adversely affected by the stresses set up by the distortion and sticking of the cores.

Aluminum orthophosphate was selected because magnesium oxide, presently used by most commercial manufacturers for tape insulation except doubly oriented silicon steel, is applied as the hydroxide, Mg $(OH)_2$, milk of magnesia. The amorphous MgO used is hygroscopic.

The magnesium hydroxide when heated during annealing converts to MgO and upon cooling will pickup moisture again.

MgO when heated to a temperature such as 1200° C reacts with a steel surface such as silicon steel to form a complex iron-magnesium silicate.

A sintered magnesium oxide, sintered at ~1775° C, is available that does not hydrolyze readily, but is harder to apply, since the application requires electrostatic attraction and a critical particle size.

REFERENCES

1. Schenk, H. L. and Young, F. J.: Waveform of the time rate of change of total flux for minimum core loss. Journal of Applied Physics, Vol. 33, March, 1962, p. 1281.

2. Kueser, P. E.; Pavlovic, D. M.; Lane, D. H.; Clark, J. J.; and Spewock, M.: Properties of Magnetic Materials for Use in High-Temperature Space Power Systems. NASA SP-3043, 1967.

3. Bozorth, R. M.: Ferromagnetism. D. Van Nostrand Co., 1951, p. 431.

NASA-Langley, 1969 — 3 E-4673